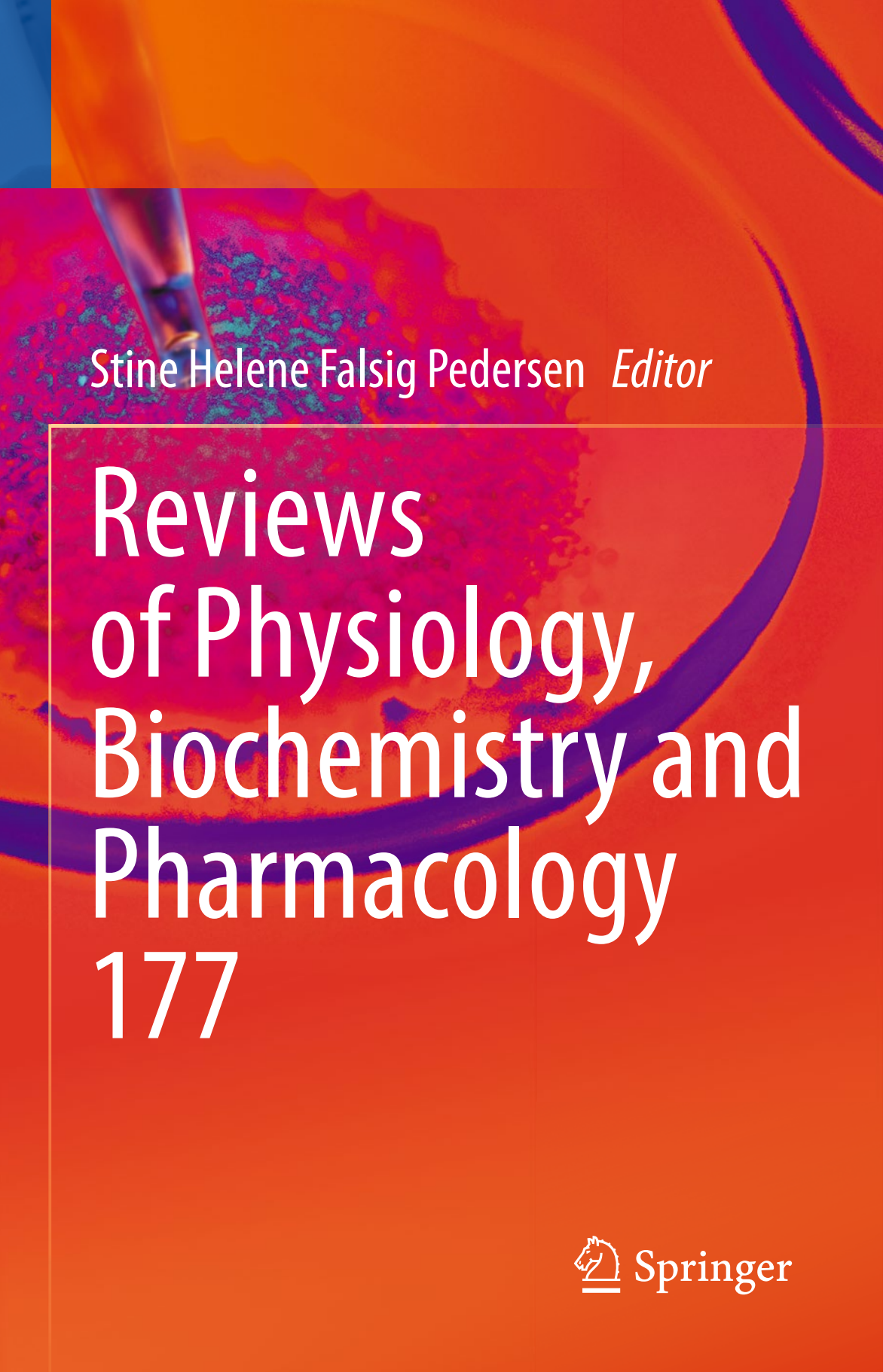
Stine Helene Falsig Pedersen Editor
Reviews of Physiology, Biochemistry and Pharmacology 177
Springer

Reviews of Physiology, Biochemistry and Pharmacology

Volume 177

The highly successful Reviews of Physiology, Biochemistry and Pharmacology continue to offer high-quality, in-depth reviews covering the full range of modern physiology, biochemistry and pharmacology. Leading researchers are specially invited to provide a complete understanding of the key topics in these archetypal multidisciplinary fields. In a form immediately useful to scientists, this periodical aims to filter, highlight and review the latest developments in these rapidly advancing fields.
2016 Impact Factor: 4.769, 5-Year Impact Factor 4.893
2019 Eigenfaktor Score: 0.00067, Article Influence Score: 1.570

More information about this series at http://www.springer.com/series/112

Stine Helene Falsig Pedersen
Editor

Reviews of Physiology, Biochemistry and Pharmacology

Springer

Editor
Stine Helene Falsig Pedersen
Department of Biology
University of Copenhagen
Copenhagen, Denmark

ISSN 0303-4240 ISSN 1617-5786 (electronic)
Reviews of Physiology, Biochemistry and Pharmacology
ISBN 978-3-030-61494-2 ISBN 978-3-030-61495-9 (eBook)
https://doi.org/10.1007/978-3-030-61495-9

This Springer imprint is published by the registered company Springer Nature Switzerland AG.
The registered company address is: Gewerbestrasse 11, 6330 Cham, Switzerland

Acknowledgements

Contributions to this volume have partly been personally invited, with kind support of the series editors D.L. Barber, E. Cordat, J. Leipziger, M.E. O'Donnell, L. Pardo, N. Schmitt, C. Stock.

Contents

Rev Physiol Biochem Pharmacol (2020) 177: 1–24
https://doi.org/10.1007/112_2020_21

Published online: 9 August 2020

The Role of Chemokine Receptors in Renal Fibrosis

Fenglei Wu, Chi Sun, and Jianquan Lu

Contents

Abstract Renal fibrosis is the final pathological process common to any ongoing, chronic kidney injury or maladaptive repair. Renal fibrosis is considered to be closely related to various cell types, such as fibroblasts, myofibroblasts, T cells, and other inflammatory cells. Multiple types of cells regulate renal fibrosis through the recruitment, proliferation, and activation of fibroblasts, and the production of the extracellular matrix. Cell trafficking is orchestrated by a family of small proteins called chemokines. Chemokines are cytokines with chemotactic properties, which are classified into 4 groups: CXCL, CCL, CX3CL, and XCL. Similarly, chemokine receptors are G protein-coupled seven-transmembrane receptors classified into

Fenglei Wu and Chi Sun contributed equally to this work.

F. Wu and J. Lu (✉)
Department of Nephrology, Qidong People's Hospital, Nantong, Jiangsu Province, China

C. Sun
Department of Pain, Affiliated Hospital of Nantong University, Nantong, Jiangsu Province, China

4 groups: XCR, CCR, CXCR, and CX3CR. Chemokine receptors are also implicated in the infiltration, differentiation, and survival of functional cells, triggering inflammation that leads to fibrosis development. In this review, we summarize the different chemokine receptors involved in the processes of fibrosis in different cell types. Further studies are required to identify the molecular mechanisms of chemokine signaling that contribute to renal fibrosis.

Keywords Chemokine receptors · Macrophages · Myofibroblasts · Renal fibrosis · T cells

1 Introduction

Renal fibrosis is widely regarded as a common pathway contributing to end-stage renal disease, characterized by aberrant activation and the development of renal fibroblasts and overproduction of proteins of extracellular matrix (ECM) (Meng et al. 2014). During fibrosis, the kidney is stimulated by various pathogenic factors in diverse diseases including trauma, infection, inflammation, blood circulation disorder, and immune response. Fibrosis can be viewed as an aberrant wound healing, in which there is progression rather than scar recovery following damage, and fibroblasts are central to this process. Fibrosis is closely related to tissue regeneration and inflammation, which is mediated by specific types of cells, including epithelial, endothelial, fibroblast, pericyte, myofibroblast, and inflammatory cells (Duffield 2014). Pathogenic factors such as drug poisoning, high blood pressure, diabetes, and infection can cause damage to the intrinsic cells which can release some cytokines. These cytokines attract a series of inflammatory cells in blood to infiltrate the mesangial, vascular, and interstitial areas. In response to inflammatory mediators, the intrinsic cells release nephrotoxic cytokines and growth factors, causing the proliferation of fibroblasts and further differentiation to myofibroblasts in the renal interstitium. With the constant stimulation of cytokines and growth factors, fibroblasts continue to proliferate and synthesize extracellular matrix (ECM) components. Kidney-derived cells, such as mesangial cells, glomerular epithelial cells, and renal tubular epithelial cells, can also be differentiated into myofibroblasts. More than half of the renal myofibroblasts have been confirmed to be derived from local fibroblasts, while most of the remainder are derived from bone marrow, endothelial-to-mesenchymal transition program, and epithelial-to-mesenchymal transition program (LeBleu et al. 2013). The impaired imbalance in the synthesis and degradation of ECM components promotes the formation of fibrous tissue, eventually leading to glomerular sclerosis, renal fibrosis, and formation of persistent scars.

Abundant evidences have shown that most chemokines and their receptors are crucial participants in the progression of renal fibrosis. Chemokines are chemotactically categorized into four groups of cytokines based on the location of two

cysteine residues in their sequence: XCL, CCL, CXCL, and CX3CL (Griffith et al. 2014). Chemokine receptors are G protein-coupled seven-transmembrane receptors classified into four groups: XCR, CCR, CXCR, and CX3CR. Chemokine receptors are expressed in various leukocytes and immune cells. Chemokines and their receptors play an essential role in various physiological and pathological processes (Griffith et al. 2014).

The change of chemokine expression at the lesion site is also an important part of renal fibrosis. High expression of CCL2 in kidney has a very strong association with the progression of renal disease, and the blockade of CCL2 receptor (CCR2) reduces interstitial fibrosis (Kitagawa et al. 2004). High expression levels of CXCL10 and CXCL9 have been reported in glomerular cells in kidney biopsies of patients with membranoproliferative and crescentic glomerulonephritis (Romagnani et al. 2002). CCL18 is also identified as one of the central chemokines in glomerulonephritis (Brix et al. 2015). In hypertension mice, significantly CX3CL1 mRNA expression increases in whole kidney, and the protein localizes to tubular epithelial and vascular endothelial cells (Shimizu et al. 2011).

Chemokines are involved in the development of inflammatory cells in pathological and physiological processes. CXCR2 regulates neutrophils recruitment in response to CXCL1 (Drummond et al. 2019). CXCL8, as another ligand of CXCR1/2, can also modulate neutrophil migration (Zuniga-Traslavina et al. 2017). CXCR3 mainly expresses on activated Th1 cells, NK cells, macrophages, and other immune cells which may play an important role in renal fibrosis (Campanella et al. 2008). CXCR4 participates macrophages differentiation (Ding et al. 2019) and T cells recruitment, so as CXCL16/CXCR6 (Seo et al. 2019; Wehr et al. 2013; Zhang et al. 2009). CCL3 and CCL5 can interact with CCR1 to attract macrophages and T cells (Olszewski et al. 2000) (Fig. 1).

Myeloid cells and organ-resident cells are also involved in the process of tissue fibrosis. Circulating bone marrow-derived fibroblast precursors were chemotactic and differentiated under the control of CXCL16/CXCR6 and CCL2/CCR2 (Chen et al. 2011; Xia et al. 2013). CXCR4 is well known for its role in the homing of progenitor cells into the bone marrow (Doring et al. 2014) (Table 1).

Some fibrosis-related molecule productions are also directly or indirectly regulated by chemokines. CXCL8 was a potent suppressor of MMPs which acted their proteolytic activity in tissue fibrosis (Milovanovic et al. 2017). CXCR4 could induce pro-fibrotic collagen in some diseases such as cancer (Dong et al. 2019). CXCR4 induced platelet-derived growth factor-β to promote pulmonary fibrosis by trafficking of circulating fibrocytes (Aono et al. 2014). Th17-derived cytokines were related to fibrosis and could be induced by CCR2 (Gurczynski et al. 2019). CXCR6 could activate human pulmonary fibroblasts to produce collagen production (Ma et al. 2019).

Accumulating evidences indicate that chemokine receptors are key regulators of renal fibrosis in diseased kidneys. Therefore, the purpose of this summary is to provide a succinct overview of recent progress in the pathogenesis of renal fibrosis on chemokine receptors.

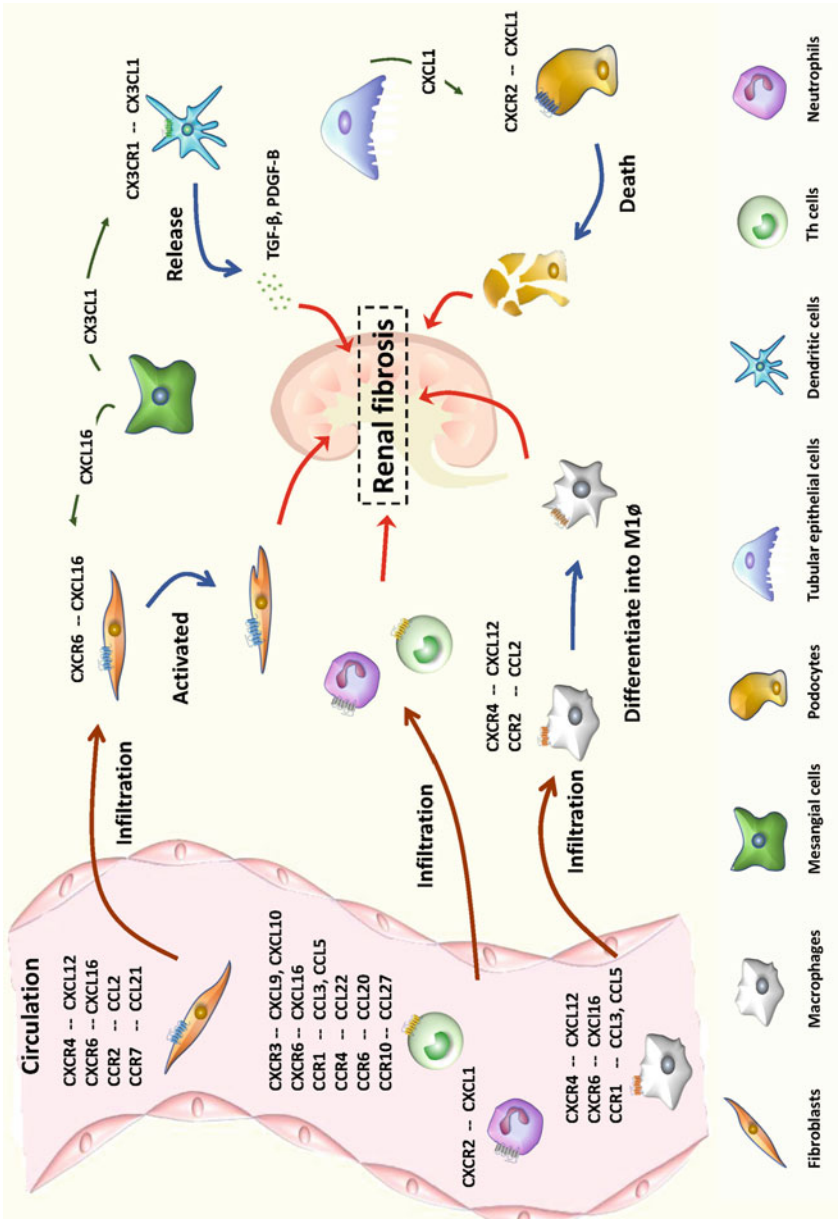

Fig.1 The role of chemokine receptors in renal fibrosis. Bone marrow-derived fibroblasts infiltrated into kidney by CXCR4, CXCR6, CCR2, and CCR7. Fibroblasts in kidney could be activated by CXCL16/CXCR6. Helper T cells in circulation expressed CXCR3, CXCR6, *CCR1* CCR4, CCR6, and CCR10 while

Fig.1 (continued) neutrophils expressed CXCR2. They could be attracted into fibrosis site by corresponding ligands. Macrophages were appealed to CXCR4, CXCR6, and *CCR1* and differentiated into M1 macrophages through CXCL12/CXCR4 and CCL2/CCR2. CX3CR1+ dendritic cells could release pro-fibrotic factors such as TGF-β and PDGF-β. CXCL2 combined with CXCR2 to facilitate podocytes loss. Tubular epithelial cells were considered as the source of CXCL2

Table 1 The role of chemokine receptors in renal fibrosis

Chemokine receptors	Ligands	Pro-fibrosis	Anti-fibrosis
CXCR1/ CXCR2	CXCL8, CXCL1, CXCL2	CXCL8 increased in both urinary and serum levels (Wong et al. 2007) G31P, an antagonist of CXCL8, inhibited fibrotic factor upregulation in human renal mesangial cells through JAK2/ STAT3 and ERK1/2 pathways (Cui et al. 2017) The GP31 improved kidney fibrosis by reduction in ECM (Cui et al. 2017; Ye et al. 2018) CXCL1 induced podocyte death and adhesion dysfunction in podocytes via CXCR2 (Zhu et al. 2013) TLR4 on intrinsic renal cells contributes to the induction of antibody-mediated glomerulonephritis via CXCL1 and CXCL2 (Brown et al. 2007) MiR-146a prevented the development of inflammation and fibrosis by targeting CXCL8 in ischemia-reperfusion injury (Amrouche et al. 2017) CXCL1 levels were positively associated with fibrosis in IgA nephropathy (Zhao et al. 2015; Zhu et al. 2013)	
CXCR3	CXCL9, CXCL10, CXCL11	CXCL9/CXCL10 in macrophages was induced by biglycan via TLR/TRIF/MyD88-signaling (Nastase et al. 2018) CXCR3+ Th1 and Th17 cells can be recruited into the kidney in fibrosis progress (Nastase et al. 2018; Steinmetz et al. 2009)	CXCL10 prevented fibrosis in diabetic kidney disease in mice (Zhang et al. 2018) Blockade of CXCL10 via CXCR3 contributes to renal fibrosis by upregulation of TGF-β1 (Nakaya et al. 2007)
CXCR4	CXCL12	CXCR4 was overexpressed in renal fibrosis samples (Maluf et al. 2008; Togel et al. 2005) Administration of AMD3100, the CXCR4 inhibitor, reduced renal fibrosis in oxidative stress-induced podocyte injury (Mo et al. 2017) CXCR4 antagonist blunts the increase in classic indicators of	Continuous AMD3100 treatment exacerbates the renal fibrosis by attracting T cell in unilateral ureteral obstruction mice (Yang et al. 2016)

(continued)

Table 1 (continued)

Chemokine receptors	Ligands	Pro-fibrosis	Anti-fibrosis
		fibrosis and fibroblast activation (Yuan et al. 2015)	
CXCR6	CXCL16	CXCL16/CXCR6 promoted the recruitment, activation, and differentiation of bone marrow-derived fibroblasts precursors and contribute to the pathogenesis of renal fibrosis (Chen et al. 2011; Xia et al. 2014b) CXCL16 deficiency impaired myeloid fibroblast accumulation and myofibroblasts formation (Ma et al. 2016a, b) CXCR6 regulated the infiltration of macrophage and T cell in renal fibrosis (Xia et al. 2014a)	
CCR1	CCL3, CCL5	CCR1 was expressed on infiltrating macrophages and T cells in the development of renal fibrosis (Vielhauer et al. 2001) CCR1 antagonist BX471 treatment significantly reduced markers of renal fibrosis (Vielhauer et al. 2004)	
CCR2	CCL2	CCL2/CCR2 accelerated renal fibrosis through bone marrow-derived myofibroblast infiltration (Xia et al. 2013) CCL2/CCR2 blockage improves renal fibrosis by inhibiting pro-fibrotic M1 macrophage (Saito et al. 2018)	
CCR7	CCL21	CCL21/CCR7 induced the trafficking of circulating fibrocytes, contributing to the pathogenesis of renal fibrosis (Wada et al. 2007; Habiel and Hogaboam 2014)	
CX3CR1	CX3CL1	CX3CR1 regulates macrophage infiltration and led to increased expression of α-SMA, TGF-β, and PDGF-B (Furuichi et al. 2006)	CX3CR1 attenuated renal fibrosis with accumulation of macrophages in UUO model (Engel et al. 2015)

2 CXC Chemokine Receptors

2.1 CXCR1/CXCR2

CXCR1and CXCR2 share 76% of their sequence homology and bind to CXCL8 with similar affinity (Holmes et al. 1991; Kunsch and Rosen 1993). Interleukin (IL)-8 (CXCL8) and granulocyte chemotactic protein 2 (GCP-2, CXCL6) are known to be ligands of both CXCR1 and CXCR2 (Wuyts et al. 1998; Ha et al. 2017). CXCL8 is commonly expressed in activated monocytes and macrophages, epithelial and endothelial cells, fibroblasts and neutrophils (Wolff et al. 1998). Growing evidences have shown that CXCL8 participates in the pathological processes of fibrosis, angiogenesis, arteriosclerosis, infection, and tumor growth (Kormann et al. 2012; Higurashi et al. 2009). In diabetic nephropathy patients, CXCL8 was seen to increase both urinary and serum levels (Wong et al. 2007). G31P is a mutant protein of CXCL8, which can selectively bind to CXCR1 and CXCR2 without agonist activity (Li et al. 2002). Recent studies have revealed that G31P can effectively improve renal fibrosis (Svensson et al. 2011). In diabetic nephropathy mice, G31P treatment reduced phosphorylation of ERK1/2, JAK2, and STAT3. Meanwhile, G31P treatment inactivated JAK2/STAT3 and ERK1/2 pathways in high-glucose-treated mesangial cells (Cui et al. 2017). Also, JAK2/STAT3 and ERK1/2 pathways were implicated in the pathogenesis of progressive diabetic nephropathy (Chuang and He 2010). JAK2/STAT3 pathways were reported to participate in the fibrosis in dermis, lung, and liver (Li et al. 2018; Zehender et al. 2018). ERK1/2 pathways were also demonstrated to be directly involved in renal fibrosis (Andrikopoulos et al. 2019). Furthermore, the administration of G31P improved kidney fibrosis as confirmed by reduction in ECM. In the diseased kidney observed in another study, the extracellular matrix degradation-related protein matrix metalloproteinases (MMP)-9 decreased while TIMP-1, known as an inhibitor of metalloproteinase, was upregulated. However, G31P treatment reversed their altered expression (Ye et al. 2018). G31P treatment was also associated with improvement in MMP-2 (Cui et al. 2017). MMPs are believed to suppress fibrosis because of their proteolytic activity (Giannandrea and Parks 2014). It has been reported that miR-146a is most induced in tubular cells in response to ischemia-reperfusion, thereby preventing the development of inflammation and fibrosis by targeting CXCL8 (Amrouche et al. 2017).

CXCL1, known as a ligand of CXCR2, has been positively associated with interstitial fibrosis in IgA nephropathy (IgAN) progression (Zhao et al. 2015). Both clinical samples and cell experiments showed the elevated expression of CXCL1 (Zhu et al. 2013). It was reported that toll-like receptor 4 in kidney-resident cells induced the antibody-mediated glomerulonephritis via CXCL1 which promotes glomerular neutrophil infiltration (Brown et al. 2007). Additionally, mesangial-induced CXCL1 and TGF-β1 synergistically increased podocyte death and decreased podocyte adhesion via CXCR2 (Zhu et al. 2013). Studies have proven that podocytes loss can impair the glomerular filtration barrier which leads to proteinuria and glomerulosclerosis in IgAN (Wharram et al. 2005).

2.2 CXCR3

CXCR3 is widely expressed in different subtypes of T and NK cells. The ligands are CXCL9, CXCL10, and CXCL11, and their secretion is predominantly driven by IFN-γ (Sallusto et al. 1998). IFN-γ, known as aa Th1-related cytokine, has been proposed to be an antifibrotic effector that inhibits fibroblast activation and proliferation and reduces collagen synthesis (Gao et al. 2007).

It was reported that increased levels of IFN-γ and IFN-γ-responsive genes (CXCL9 and CXCL10) in Sphk2$^{-/-}$ (sphingosine kinase 2) mice inhibited the progression to fibrosis (Bajwa et al. 2017). TGF-β and high glucose contributed to the development of fibrosis in diabetes. CXCL10 attenuated both high glucose and TGF-β-induced collagen synthesis (Zhang et al. 2018). CXCR3 ligands are a potent chemoattractant for activated Th1 cells, NK cells, macrophages, and other immune cells (Campanella et al. 2008). The ureter is ligated in the case of unilateral ureteral obstruction (UUO), leading to hydronephrosis and interstitial inflammatory infiltration, myofibroblast activation, and extracellular matrix deposition, ultimately leading to renal fibrosis (Verbeke et al. 2016). Although CXCL10 and CXCR3 were observed to be upregulated in the progressive renal fibrosis in UUO mice (Nakaya et al. 2007), CXCL10 blockade affected neither macrophage nor T cell infiltration. Despite this, CXCL10 blockade was also shown to promote renal interstitial fibrosis in the kidney via hepatocyte growth factor (HGF) which is a potent antifibrogenic factor (Nakaya et al. 2007). HGF created by mesangial cells prevents peritubular capillaries (PTCs) from decreasing, preserves renal blood flow, and effectively suppresses myofibroblast progression induction and collagen synthesis (Oka et al. 2019). In addition, CXCL10 blockage has also been demonstrated to reduce transcripts of CXCL9 and CXCL11 in diseased kidneys (Nakaya et al. 2007).

The results in diabetic nephropathy and lupus nephritis are controversial. Biglycan, a class I member of the small leucine-rich proteoglycans, was found to be upregulated in diabetic nephropathy and lupus nephritis. Meanwhile, CXCL9/CXCL10 in macrophages was induced by biglycan via TLR/TRIF/MyD88-signaling and then recruited CXCR3^{+} Th1 and Th17 cells into the kidney (Nastase et al. 2018). Another study showed that CXCR3 deficiency in lupus-prone mice improved the renal damage by decreasing the numbers of Th1 cells and Th17 cells in the inflamed kidneys (Steinmetz et al. 2009). Th1 and Th17 cells have been shown to play an important role in the development and progression of inflammatory and autoimmune diseases (Zheng and Zheng 2016; Stockinger and Omenetti 2017). Th1 and Th17 cells, which are Th subtypes, are key inducers of renal fibrosis (Wen et al. 2017).

2.3 CXCR4

CXCR4 is mainly expressed in hematopoietic and immune cells. CXCR4 is highly expressed in embryonic kidneys but the expression is significantly low in adult

kidneys (Takabatake et al. 2009). In tubular atrophy and interstitial fibrosis samples, however, CXCR4 genes were found to be overexpressed compared with normal allografts and normal kidneys (Maluf et al. 2008). Increased CXCR4 expression has also been observed in tubular segments after renal ischemia-reperfusion injury (IRI) (Togel et al. 2005). Thus, increased CXCR4 expression seems to be closely associated with kidney disease. Another report showed that the stimulation of CXCR4 in macrophages activated STAT and NF-κB pathways which acted as important roles in macrophage activation. Meanwhile, the administration of AMD3100, a CXCR4 inhibitor, reduced renal fibrosis in mice and was accompanied by a significant reduction in macrophage infiltration (Mo et al. 2017). In a UUO model, a lack of CXCR4 protected against renal fibrosis by suppressing macrophage activation. AMD3100 treatment downregulated the mRNA levels of multiple pro-fibrotic molecules including collagen-1a1 (Col1a1), collagen-3a1 (Col3a1), and collagen-4a1 (Col4a1) by inhibiting downstream signaling and fibroblast activation (Yuan et al. 2015).

In another study, AMD3100 treatment did not mitigate renal fibrosis but promoted tissue damage and renal fibrosis by increasing pro-fibrotic molecules expression, such as α-SMA, PDGFR-β, and collagen-IV (Yang et al. 2016). α-SMA was found to be a marker of activated fibroblasts. PDGF-β and collagen-IV is the well-characterized factor that promotes fibrosis in many diseases and organs, including the kidney (Border and Noble 1994; Hugo 2003; Li et al. 2019). This difference may be attributed to the mechanism of AMD3100 and the chemotaxis of CXCR4 ligands. The factor-1-derived chemokine stromal cell (SDF-1, also known as CXCL12) is constitutively expressed in pro-angiogenic cells and regulates embryonic development and homeostasis of the organ (Ratajczak et al. 2006). Evidence indicates that continuous AMD3100 treatment disrupts SDF-1-CXCR4 binding leading to a decrease in bone marrow-derived pro-angiogenic cell homing. Besides, the infusion of pro-angiogenic cells not only decreases vascular rarefaction but also reduces damage to the tissue and the invasion of inflammatory cells. A few studies have shown that bone marrow-derived pro-angiogenic cells participate in renal fibrosis controlled by the SDF-1/CXCR4 system (Shen et al. 2011; Petit et al. 2007). CXCR4 is also highly expressed in T cells which are major inducers of fibrosis (Arieta Kuksin et al. 2015). In Kuksin's study, AMD3100 administration increased renal T cell infiltration. This result may due to AMD3100 redistributing T cells from the bone marrow and thymus to the blood and peripheral tissues in mice (Liu et al. 2015). It suggests that AMD3100 should be more cautiously used in patients with renal disease and additional studies should be performed on this issue in the future.

2.4 CXCR6

CXCL16 has been described as a CXCR6 ligand consisting of a molecular domain accompanied by a glycosylated mucin-like stalk, a long transmembrane helix, and a short cytoplasmic tail (Matloubian et al. 2000). The CXCL16/CXCR6 pathway is

involved in tissue injury and inflammation (Wang et al. 2017). CXCL16 protein has been documented to be expressed at low levels in normal kidney epithelial cells while being upregulated in obstructive injury (Okamura et al. 2007). Recent studies have shown that precursors of fibroblasts originating from bone marrow contribute significantly to the pathogenesis of renal fibrosis. In response to kidney injury, bone marrow-derived fibroblast precursors in the circulation are recruited to the site of injury to participate in a wound healing response (Yan et al. 2016). Bone marrow-derived fibroblast precursors will differentiate into myofibroblasts that have been implicated in fibrosis pathogenesis (Gerarduzzi and Di Battista 2017). Circulating CXCR6-positive fibroblast precursors have been found in injured kidneys, with CD45 and α-SMA dual-positive myofibroblasts accumulating in the injured kidney in a CXCL16-dependent manner. Meanwhile, CXCL16 has been significantly implicated in the activation and differentiation of bone marrow-derived fibroblasts (Chen et al. 2011). In a renal artery stenosis study, CXCL16 protein was mainly distributed in tubular epithelial cells. They also found that CXCL16 deficiency impaired myeloid fibroblasts accumulation and myofibroblasts formation. Furthermore, CXCL16 deficiency inhibited the infiltration of $F4/80^+$ macrophages and $CD3^+$ T cells (Ma et al. 2016b). In Ang II-induced renal injury and fibrosis, CXCR6 plays a pivotal role in the regulation of macrophage and T cell infiltration and bone marrow-derived fibroblast accumulation (Xia et al. 2014a). In deoxycorticosterone acetate/salt hypertension, CXCR6 deficiency inhibited the accumulation of bone marrow-derived fibroblasts and myofibroblasts in the kidney (Wu et al. 2020). Given the evidence above, CXCL16/CXCR6 may play important roles in the recruitment into the kidney of bone marrow-derived fibroblast precursors, which contribute to renal fibrosis pathogenesis (Xia et al. 2014b).

3 C-C Chemokine Receptors

3.1 CCR1

CCR1 was found in the peripheral blood of mice and humans in the circulation of macrophages and lymphocytes (Murphy et al. 2000), and one of the symptoms of interstitial fibrosis was found to be the aggregation of macrophages and lymphocytes that lead to ECM development and renal fibrosis (Yan et al. 2016). Studies on UUO mice have shown that, in tandem with the growth of renal fibrosis, the CCR1 was expressed in infiltrating macrophages and T cells. Furthermore, the mRNA expression of CCR1 ligands CCL3 (MIP-1a) and CCL5 (RANTES) was revealed to be upregulated in diseased kidneys (Zeisberg et al. 2000; Ratajczak et al. 2006; Vielhauer et al. 2004). In UUO mice, loss of CCR1 decreased macrophage and lymphocyte infiltration in the obstructed kidney and the associated interstitial fibrosis had diminished renal production of TGF-β1 mRNA (Eis et al. 2004). In a murine model of Adriamycin-induced focal segmental glomerulosclerosis, the small-molecule CCR1 antagonist BX471 treatment significantly reduced markers of

renal fibrosis including interstitial fibroblasts and interstitial volume (Vielhauer et al. 2004). BX471 prevents the binding of MIP-1α/CCL3 to murine CCR1 but not CCR5 and blocks the activation of receptors as determined by the mobilization of Ca2+.

3.2 CCR2

CCL2 is a member of the CC chemokine subfamily that controls recruitment of monocytes through CCR2 (Gerard and Rollins 2001). It has been demonstrated that CCL2 and CCR2 are positively correlated with kidney fibrosis. Similar to CXCR6, CCR2 was shown to be expressed in bone marrow-derived fibroblasts expressing CD45 and procollagen I or PDGFR-β. And CCR2 deficiency could impair myeloid fibroblast accumulation and myofibroblast formation (Xia et al. 2013). Meanwhile, it was demonstrated that CCR2-knockout mice could be shielded from bone marrow-derived myofibroblast infiltration in the kidneys (Xia et al. 2013). CCR2 deficiency also affects CCL2, CCL5, CCL7, CCL8, and CXCL16 gene expression, and the M2 macrophage marker CD206 also being affected (Xia et al. 2013). CCL2/CCR2 may promote the activation of NF-κβ and AP-1 which increases the expression of inflammatory factors including MCP-1 production in diseased kidneys (Kitagawa et al. 2004). Activation of Notch pathway has been described in many human chronic renal diseases. M1 macrophages have been reported to play a pro-fibrotic function in renal fibrosis, whereas M2 macrophages are antifibrotic. Notch signaling is critically involved in macrophage differentiation and activation. Studies have revealed that Notch signaling regulates renal fibrosis mainly through $CD11b^{+}F4/80^{+}CCR2^{+}$ monocytes-derived macrophages in UUO mice with monocytes being recruited through CCL2-CCR2 chemotaxis (Jiang et al. 2019). In unilateral IRI mice, CCR2 inhibition was observed reducing the mRNA expression of M1 macrophages, while the blockade of the CCL2/CCR2 signaling improved fibrosis (Saito et al. 2018). Meanwhile, CCR2 deficiency has been found to lead to a decrease of Th17-related cytokine production and VEGF production with both processes being directly related to renal fibrosis (Braga et al. 2018). These findings suggest that the therapeutic strategy of blocking CCR2 might prove beneficial for progressive fibrosis in the diseased kidneys.

3.3 CCR7

Accumulated evidences suggest a strong candidate for tissue fibrosis activity with fibrocytes (Schmidt et al. 2003; Yoneyama et al. 2001). Recent studies indicated that the CCL21 and CCR7 signaling pathways induced the trafficking of circulating fibrocytes (Wada et al. 2007; Habiel and Hogaboam 2014). CCR7-positive fibrocytes infiltrated the kidney via CCL21-positive vessels, contributing to the

pathogenesis of renal fibrosis. Blockade of CCL21/CCR7 signaling reduced the number of CCR7-expressing fibrocytes as well as CCR2-expressing fibrocytes. Thus, the CCL21/CCR7 signaling of fibrocytes may provide therapeutic targets for combating renal fibrosis (Sakai et al. 2006).

4 CX3C Chemokine Receptor

4.1 CX3CR1

CX3CR1 was shown to be an important mediator in both acute and chronic kidney injury (Furuichi et al. 2009; Zhuang et al. 2017). In an IRI model, CX3CR1 regulated the macrophage infiltration and led to increased expression of α-SMA, TGF-β, and PDGF-B (Furuichi et al. 2006). Furthermore, α-SMA was found to be a marker of activated fibroblasts. TGF-β and PDGF-B are well-characterized factors that promote fibrosis in many diseases and organs, including the kidney (Border and Noble 1994; Hugo 2003). Meanwhile, dendritic cells (DCs) and macrophages were identified as key sources of TGF-β in renal tissue (Kassianos et al. 2013). It was also found that CX3CL1 expressed on activated proximal tubular epithelial cells (PTECs) could chemoattract $CX3CR1^+$ dendritic cells and subsequently promote adhesion of human DCs to PTECs (Kassianos et al. 2015). Given this evidence, it was hypothesized that CX3CR1 may promote renal fibrosis. However, renal fibrosis is promoted in the absence of CX3CR1 with the accumulation of macrophages and more TGF-β production in a UUO model (Engel et al. 2015). In this study, CX3CR1 was considered eligible to inhibit local macrophage proliferation (Engel et al. 2015). In contrast, another study showed that CX3CL1-CX3CR1 increased the population of macrophages contributing to UUO-induced fibrosis (Peng et al. 2015). Also, although CX3CR1 deficiency was not seen to affect monocyte trafficking or macrophage differentiation in vivo, CX3CR1 deficiency reduces renal fibrosis by inhibiting macrophage survival and extracellular matrix deposition in the obstructed kidney (Peng et al. 2015). Later research proposed that this inconsistency could be explained by the different methods for evaluating fibrosis. However, this does not account for the different outcomes of macrophages. We found that the above study had used different markers to identify the macrophages, which might be the cause of the discrepant results. Thus, further investigation is needed to clarify the role of CX3CR1 in renal fibrosis.

5 Other Chemokine Receptors

Data suggests that Th22 cells might be recruited into the kidneys via the CCL20-CCR6, CCL22-CCR4, and/or CCL27-CCR10 axes by mesangial cells and tubular epithelial cells in infection-related IgAN. Th22 cell overrepresentation has been

attributed to increases in levels of IL-1, IL-6, and TNF-α (Gan et al. 2018), thereby contributing to renal fibrosis. XCL1, the ligand of XCR1, was found to have a slight but significant increase (Vielhauer et al. 2001). Atypical chemokine receptor 2 (ACKR2) is also known as CCR10. It was reported that CCL2 levels and leukocyte counts increased in peripheral blood in Ackr2-deficient mice. Meanwhile, ACKR2 promoted renal leukocyte recruitment, the expression of inflammatory markers and fibrosis, and proinflammatory chemokine levels in autologous nephrotoxic nephritis (Bideak et al. 2018).

6 Discussion

Renal fibrosis is not a particular process, but a concept that describes various fibrotic processes of cellular and molecular structure in specific renal compartments. Throughout fibrogenesis, various chemokines and their receptors have been identified. Given the many obstacles that lie ahead, targeting chemokines remains one of the most promising ways to improve renal fibrosis treatment.

Renal fibrosis is characterized by excessive ECM deposition, which is primarily caused by myofibroblasts. Myofibroblasts are responsible for synthesizing and storing interstitial ECM components such as collagen type I and III and fibronectin during wound healing and at scar and fibrosis sites (Meran and Steadman 2011). Myofibroblasts also synthesize various ECM-degrading proteases known as MMPs, which control the turnover and remodeling of collagen and other ECM proteins (Pardo and Selman 2006). Differentiation of fibroblasts to myofibroblasts is regarded as a critical event in the pathogenesis of renal fibrosis (Strutz and Muller 2006). Myofibroblasts traditionally originate from resident renal fibroblasts and were recently found to also arise from bone marrow-derived cells (Broekema et al. 2007; Li et al. 2007). CXCL16 deficiency has been shown to impair aggregation and myofibroblast production of bone marrow-derived fibroblasts in the kidney and renal fibrosis development (Ma et al. 2016b), while CCR2 deficiency significantly reduced bone marrow-derived myofibroblasts formation by decreasing the protein expression levels of α-SMA and FSP-1 in fibroblasts (Xia et al. 2013).

T cells accumulate in glomerular and tubulointerstitial compartments that can trigger kidney damage by immune-mediated mechanisms (Zohar et al. 2018). CXCR3 ligands are chemotactic for both leukocytes and have been found activating Th1 phenotype T lymphocytes expressing CXCR3 (Bonecchi et al. 1998). In another study, CXCL10/CXCR3 interactions promoted effector Th1 polarization via STAT1, STAT4, and STAT5 phosphorylation (Karin et al. 2016). Additionally, Th17 cells have been demonstrated to play an essential role in causing renal inflammation and tissue damage by secreting IL-17, IL-21, IL-22, and other cytokines (Paust et al. 2009). Several studies have revealed the significance of cytokine IL-17 in the end-stage aggravation of renal disease. Th17 cells are suspected to be able to transdifferentiate into regulatory T cells by modifying their transcription profile, further stressing their prominent role in inflammation and pro-fibrotic disease

resolution (Gagliani et al. 2015). Our review found that proinflammatory Th1 and Th17 lymphocytes were primarily drawn by the CXCR3 receptor to the location of inflammation in the diseased kidney (Nastase et al. 2018). Finally, CXCR3 has been reported to promote $CD4^+$ T cell polarization toward Th1/Th17 effector cells by binding CXCL9/CXCL10 (Zohar et al. 2014).

Macrophage infiltration, derived from circulating monocytes, occurs early after renal injury and plays a critical role in the initial inflammatory response and induction of fibrogenesis. Macrophages can be categorized into two phenotypes: M1 (activated classically) and M2 (activated alternatively). M1 macrophages are considered proinflammatory, releasing cytokines such as IL-1, IL-6, and TNF-α, whereas M2 macrophages are thought primarily to be anti-inflammatory, pro-fibrotic, and produce arginase. Research has found that in the initial stages, proinflammatory macrophages are present in damaged tissues, whereas in the chronic period of renal disease, the population of pro-resolving macrophages increases (Braga et al. 2016). The penetration of the macrophage is caused by induction and local blood monocyte proliferation, while both the level of renal injury and the extent of renal fibrosis are associated with the degree of macrophage infiltration. M2 macrophages can release insulin-like growth factor-1, fibroblast growth factor 2, and PDGF, which promote myofibroblast proliferation and survival (Wynes et al. 2004; Floege et al. 2008). Mouse monocytes have been reported to be divided into 2 populations marked by CX3CR1 expression. In this regard, it appears that kidney IRI induces several factors (perhaps fractalkine itself) that may selectively recruit the CX3CR1 + subset (Geissmann et al. 2003). CX3CR1, CXCR6, CCR1, and CCR2 play a vital role in macrophage infiltration. Thus, chemokine receptors can be considered as targets to inhibit macrophage function in renal fibrosis.

Dendritic cells, together with macrophages, form the axis of the kidney's mononuclear phagocytic network. Monocyte-derived dendritic cells are responsible for glomerular disease invasion and recruitment of T cells, thereby increasing the frequency of the kidney injury (Ma et al. 2013). Evidence in mice has shown that CX3CR1 contributes to the entry of DCs into the inflamed kidney and the adhesion to ECs (Inoue et al. 2005).

Recently, several chemokine receptor antagonists have been studied in human trials. CCX140-B is a small-molecule CCR2 antagonist that inhibits CCR2 and prevents the activation and chemotaxis of MCP-1-dependent monocytes. In a randomized, double-blind, placebo-controlled clinical trial, although eGFR was not significantly changed between the placebo group and the CCX140-B treatment group, it exhibited significant protective effects on patients with diabetic kidneys (de Zeeuw et al. 2015). Moreover, CCX140-B showed no side-effects like hyperkalemia or cardiovascular events after a 1-year-treatment of 5 mg CCX140-B (de Zeeuw et al. 2015). Reparixin is a non-competitive CXCR1 and CXCR2 allosteric blocker that has been studied in breast cancer patients (Schott et al. 2017) and pancreatic islet transplant patients with type 1 diabetes (Citro et al. 2012). Another study showed that sorafenib inhibited renal fibrosis via macrophage with CXCR3/CXCL11 pathway (Ma et al. 2016a). In a pilot study, reparixin

attenuated IRI and inflammation after on-pump coronary artery bypass graft surgery (Opfermann et al. 2015). Although reparixin has not been trialed in patients with renal diseases, it can effectively prevent granulocyte infiltration and renal function impairment in animal experiments (Cugini et al. 2005). Finally, TAK-779 is a synthetic, non-peptide CCR5 and CXCR3 antagonist which is used to cure HIV-1 (Takama et al. 2011). In IRI animal models, TAK-779 suppressed the infiltration of T cells and NK T cells and attenuated the kidney injury (Tsutahara et al. 2012). Cenicriviroc (CVC) is an oral, dual CCR2/CCR5 antagonist with nanomolar potency against both receptors. It showed antifibrotic effects with significant reductions in collagen deposition by significantly reducing monocyte/macrophage recruitment (Lefebvre et al. 2016).

In summary, these data suggest that chemokine receptors and their ligand signaling could constitute a novel therapeutic approach for renal fibrosis.

References

Amrouche L, Desbuissons G, Rabant M, Sauvaget V, Nguyen C, Benon A, Barre P, Rabate C, Lebreton X, Gallazzini M, Legendre C, Terzi F, Anglicheau D (2017) MicroRNA-146a in human and experimental ischemic AKI: CXCL8-dependent mechanism of action. J Am Soc Nephrol 28(2):479–493. https://doi.org/10.1681/ASN.2016010045

Andrikopoulos P, Kieswich J, Pacheco S, Nadarajah L, Harwood SM, O'Riordan CE, Thiemermann C, Yaqoob MM (2019) The MEK inhibitor trametinib ameliorates kidney fibrosis by suppressing ERK1/2 and mTORC1 signaling. J Am Soc Nephrol 30(1):33–49. https://doi.org/10.1681/ASN.2018020209

Aono Y, Kishi M, Yokota Y, Azuma M, Kinoshita K, Takezaki A, Sato S, Kawano H, Kishi J, Goto H, Uehara H, Izumi K, Nishioka Y (2014) Role of platelet-derived growth factor/platelet-derived growth factor receptor axis in the trafficking of circulating fibrocytes in pulmonary fibrosis. Am J Respir Cell Mol Biol 51(6):793–801. https://doi.org/10.1165/rcmb.2013-0455OC

Arieta Kuksin C, Gonzalez-Perez G, Minter LM (2015) CXCR4 expression on pathogenic T cells facilitates their bone marrow infiltration in a mouse model of aplastic anemia. Blood 125 (13):2087–2094. https://doi.org/10.1182/blood-2014-08-594796

Bajwa A, Huang L, Kurmaeva E, Ye H, Dondeti KR, Chroscicki P, Foley LS, Balogun ZA, Alexander KJ, Park H, Lynch KR, Rosin DL, Okusa MD (2017) Sphingosine kinase 2 deficiency attenuates kidney fibrosis via IFN-gamma. J Am Soc Nephrol 28(4):1145–1161. https://doi.org/10.1681/ASN.2016030306

Bideak A, Blaut A, Hoppe JM, Muller MB, Federico G, Eltrich N, Grone HJ, Locati M, Vielhauer V (2018) The atypical chemokine receptor 2 limits renal inflammation and fibrosis in murine progressive immune complex glomerulonephritis. Kidney Int 93(4):826–841. https://doi.org/10.1016/j.kint.2017.11.013

Bonecchi R, Bianchi G, Bordignon PP, D'Ambrosio D, Lang R, Borsatti A, Sozzani S, Allavena P, Gray PA, Mantovani A, Sinigaglia F (1998) Differential expression of chemokine receptors and chemotactic responsiveness of type 1 T helper cells (Th1s) and Th2s. J Exp Med 187 (1):129–134

Border WA, Noble NA (1994) Transforming growth factor beta in tissue fibrosis. N Engl J Med 331 (19):1286–1292. https://doi.org/10.1056/NEJM199411103311907

Braga TT, Correa-Costa M, Azevedo H, Silva RC, Cruz MC, Almeida ME, Hiyane MI, Moreira-Filho CA, Santos MF, Perez KR, Cuccovia IM, Camara NO (2016) Early infiltration of p40IL12

(+)CCR7(+)CD11b(+) cells is critical for fibrosis development. Immun Inflamm Dis 4 (3):300–314. https://doi.org/10.1002/iid3.114

Braga TT, Correa-Costa M, Silva RC, Cruz MC, Hiyane MI, da Silva JS, Perez KR, Cuccovia IM, Camara NOS (2018) CCR2 contributes to the recruitment of monocytes and leads to kidney inflammation and fibrosis development. Inflammopharmacology 26(2):403–411. https://doi.org/10.1007/s10787-017-0317-4

Brix SR, Stege G, Disteldorf E, Hoxha E, Krebs C, Krohn S, Otto B, Klatschke K, Herden E, Heymann F, Lira SA, Tacke F, Wolf G, Busch M, Jabs WJ, Ozcan F, Keller F, Beige J, Wagner K, Helmchen U, Noriega M, Wiech T, Panzer U, Stahl RA (2015) CC chemokine ligand 18 in ANCA-associated crescentic GN. J Am Soc Nephrol 26(9):2105–2117. https://doi.org/10.1681/ASN.2014040407

Broekema M, Harmsen MC, van Luyn MJ, Koerts JA, Petersen AH, van Kooten TG, van Goor H, Navis G, Popa ER (2007) Bone marrow-derived myofibroblasts contribute to the renal interstitial myofibroblast population and produce procollagen I after ischemia/reperfusion in rats. J Am Soc Nephrol 18(1):165–175. https://doi.org/10.1681/ASN.2005070730

Brown HJ, Lock HR, Wolfs TG, Buurman WA, Sacks SH, Robson MG (2007) Toll-like receptor 4 ligation on intrinsic renal cells contributes to the induction of antibody-mediated glomerulonephritis via CXCL1 and CXCL2. J Am Soc Nephrol 18(6):1732–1739. https://doi.org/10.1681/ASN.2006060634

Campanella GS, Medoff BD, Manice LA, Colvin RA, Luster AD (2008) Development of a novel chemokine-mediated in vivo T cell recruitment assay. J Immunol Methods 331(1–2):127–139. https://doi.org/10.1016/j.jim.2007.12.002

Chen G, Lin SC, Chen J, He L, Dong F, Xu J, Han S, Du J, Entman ML, Wang Y (2011) CXCL16 recruits bone marrow-derived fibroblast precursors in renal fibrosis. J Am Soc Nephrol 22 (10):1876–1886. https://doi.org/10.1681/ASN.2010080881

Chuang PY, He JC (2010) JAK/STAT signaling in renal diseases. Kidney Int 78(3):231–234. https://doi.org/10.1038/ki.2010.158

Citro A, Cantarelli E, Maffi P, Nano R, Melzi R, Mercalli A, Dugnani E, Sordi V, Magistretti P, Daffonchio L, Ruffini PA, Allegretti M, Secchi A, Bonifacio E, Piemonti L (2012) CXCR1/2 inhibition enhances pancreatic islet survival after transplantation. J Clin Invest 122 (10):3647–3651. https://doi.org/10.1172/JCI63089

Cugini D, Azzollini N, Gagliardini E, Cassis P, Bertini R, Colotta F, Noris M, Remuzzi G, Benigni A (2005) Inhibition of the chemokine receptor CXCR2 prevents kidney graft function deterioration due to ischemia/reperfusion. Kidney Int 67(5):1753–1761. https://doi.org/10.1111/j.1523-1755.2005.00272.x

Cui S, Zhu Y, Du J, Khan MN, Wang B, Wei J, Cheng JW, Gordon JR, Mu Y, Li F (2017) CXCL8 antagonist improves diabetic nephropathy in male mice with diabetes and attenuates high glucose-induced Mesangial injury. Endocrinology 158(6):1671–1684. https://doi.org/10.1210/en.2016-1781

de Zeeuw D, Bekker P, Henkel E, Hasslacher C, Gouni-Berthold I, Mehling H, Potarca A, Tesar V, Heerspink HJ, Schall TJ, Group CBDNS (2015) The effect of CCR2 inhibitor CCX140-B on residual albuminuria in patients with type 2 diabetes and nephropathy: a randomised trial. Lancet Diabetes Endocrinol 3(9):687–696. https://doi.org/10.1016/S2213-8587(15)00261-2

Ding Q, Sun J, Xie W, Zhang M, Zhang C, Xu X (2019) Stemona alkaloids suppress the positive feedback loop between M2 polarization and fibroblast differentiation by inhibiting JAK2/STAT3 pathway in fibroblasts and CXCR4/PI3K/AKT1 pathway in macrophages. Int Immunopharmacol 72:385–394. https://doi.org/10.1016/j.intimp.2019.04.030

Dong XZ, Zhao ZR, Hu Y, Lu YP, Liu P, Zhang L (2019) LncRNA COL1A1-014 is involved in the progression of gastric cancer via regulating CXCL12-CXCR4 axis. Gastric Cancer 23:260. https://doi.org/10.1007/s10120-019-01011-0

Doring Y, Pawig L, Weber C, Noels H (2014) The CXCL12/CXCR4 chemokine ligand/receptor axis in cardiovascular disease. Front Physiol 5:212. https://doi.org/10.3389/fphys.2014.00212

Drummond RA, Swamydas M, Oikonomou V, Zhai B, Dambuza IM, Schaefer BC, Bohrer AC, Mayer-Barber KD, Lira SA, Iwakura Y, Filler SG, Brown GD, Hube B, Naglik JR, Hohl TM, Lionakis MS (2019) CARD9(+) microglia promote antifungal immunity via IL-1beta- and CXCL1-mediated neutrophil recruitment. Nat Immunol 20(5):559–570. https://doi.org/10.1038/s41590-019-0377-2

Duffield JS (2014) Cellular and molecular mechanisms in kidney fibrosis. J Clin Invest 124 (6):2299–2306. https://doi.org/10.1172/JCI72267

Eis V, Luckow B, Vielhauer V, Siveke JT, Linde Y, Segerer S, Perez De Lema G, Cohen CD, Kretzler M, Mack M, Horuk R, Murphy PM, Gao JL, Hudkins KL, Alpers CE, Grone HJ, Schlondorff D, Anders HJ (2004) Chemokine receptor CCR1 but not CCR5 mediates leukocyte recruitment and subsequent renal fibrosis after unilateral ureteral obstruction. J Am Soc Nephrol 15(2):337–347

Engel DR, Krause TA, Snelgrove SL, Thiebes S, Hickey MJ, Boor P, Kitching AR, Kurts C (2015) CX3CR1 reduces kidney fibrosis by inhibiting local proliferation of profibrotic macrophages. J Immunol 194(4):1628–1638. https://doi.org/10.4049/jimmunol.1402149

Floege J, Eitner F, Alpers CE (2008) A new look at platelet-derived growth factor in renal disease. J Am Soc Nephrol 19(1):12–23. https://doi.org/10.1681/ASN.2007050532

Furuichi K, Gao JL, Murphy PM (2006) Chemokine receptor CX3CR1 regulates renal interstitial fibrosis after ischemia-reperfusion injury. Am J Pathol 169(2):372–387. https://doi.org/10.2353/ajpath.2006.060043

Furuichi K, Kaneko S, Wada T (2009) Chemokine/chemokine receptor-mediated inflammation regulates pathologic changes from acute kidney injury to chronic kidney disease. Clin Exp Nephrol 13(1):9–14. https://doi.org/10.1007/s10157-008-0119-5

Gagliani N, Amezcua Vesely MC, Iseppon A, Brockmann L, Xu H, Palm NW, de Zoete MR, Licona-Limon P, Paiva RS, Ching T, Weaver C, Zi X, Pan X, Fan R, Garmire LX, Cotton MJ, Drier Y, Bernstein B, Geginat J, Stockinger B, Esplugues E, Huber S, Flavell RA (2015) Th17 cells transdifferentiate into regulatory T cells during resolution of inflammation. Nature 523 (7559):221–225. https://doi.org/10.1038/nature14452

Gan L, Zhou Q, Li X, Chen C, Meng T, Pu J, Zhu M, Xiao C (2018) Intrinsic renal cells induce lymphocytosis of Th22 cells from IgA nephropathy patients through B7-CTLA-4 and CCL-CCR pathways. Mol Cell Biochem 441(1–2):191–199. https://doi.org/10.1007/s11010-017-3185-8

Gao B, Radaeva S, Jeong WI (2007) Activation of natural killer cells inhibits liver fibrosis: a novel strategy to treat liver fibrosis. Expert Rev Gastroenterol Hepatol 1(1):173–180. https://doi.org/10.1586/17474124.1.1.173

Geissmann F, Jung S, Littman DR (2003) Blood monocytes consist of two principal subsets with distinct migratory properties. Immunity 19(1):71–82

Gerard C, Rollins BJ (2001) Chemokines and disease. Nat Immunol 2(2):108–115. https://doi.org/10.1038/84209

Gerarduzzi C, Di Battista JA (2017) Myofibroblast repair mechanisms post-inflammatory response: a fibrotic perspective. Inflamm Res 66(6):451–465. https://doi.org/10.1007/s00011-016-1019-x

Giannandrea M, Parks WC (2014) Diverse functions of matrix metalloproteinases during fibrosis. Dis Model Mech 7(2):193–203. https://doi.org/10.1242/dmm.012062

Griffith JW, Sokol CL, Luster AD (2014) Chemokines and chemokine receptors: positioning cells for host defense and immunity. Annu Rev Immunol 32:659–702. https://doi.org/10.1146/annurev-immunol-032713-120145

Gurczynski SJ, Nathani N, Warheit-Niemi HI, Hult EM, Podsiad A, Deng J, Zemans RL, Bhan U, Moore BB (2019) CCR2 mediates increased susceptibility to post-H1N1 bacterial pneumonia by limiting dendritic cell induction of IL-17. Mucosal Immunol 12(2):518–530. https://doi.org/10.1038/s41385-018-0106-4

Ha H, Debnath B, Neamati N (2017) Role of the CXCL8-CXCR1/2 Axis in cancer and inflammatory diseases. Theranostics 7(6):1543–1588. https://doi.org/10.7150/thno.15625

Habiel DM, Hogaboam C (2014) Heterogeneity in fibroblast proliferation and survival in idiopathic pulmonary fibrosis. Front Pharmacol 5:2. https://doi.org/10.3389/fphar.2014.00002

Higurashi M, Ohya Y, Joh K, Muraguchi M, Nishimura M, Terawaki H, Yagui K, Hashimoto N, Saito Y, Yamada K (2009) Increased urinary levels of CXCL5, CXCL8 and CXCL9 in patients with type 2 diabetic nephropathy. J Diabetes Complicat 23(3):178–184. https://doi.org/10.1016/j.jdiacomp.2007.12.001

Holmes WE, Lee J, Kuang WJ, Rice GC, Wood WI (1991) Structure and functional expression of a human interleukin-8 receptor. Science 253(5025):1278–1280

Hugo C (2003) The thrombospondin 1-TGF-beta axis in fibrotic renal disease. Nephrol Dial Transplant 18(7):1241–1245

Inoue A, Hasegawa H, Kohno M, Ito MR, Terada M, Imai T, Yoshie O, Nose M, Fujita S (2005) Antagonist of fractalkine (CX3CL1) delays the initiation and ameliorates the progression of lupus nephritis in MRL/lpr mice. Arthritis Rheum 52(5):1522–1533. https://doi.org/10.1002/art.21007

Jiang Y, Wang Y, Ma P, An D, Zhao J, Liang S, Ye Y, Lu Y, Zhang P, Liu X, Han H, Qin H (2019) Myeloid-specific targeting of notch ameliorates murine renal fibrosis via reduced infiltration and activation of bone marrow-derived macrophage. Protein Cell 10(3):196–210. https://doi.org/10.1007/s13238-018-0527-6

Karin N, Wildbaum G, Thelen M (2016) Biased signaling pathways via CXCR3 control the development and function of CD4+ T cell subsets. J Leukoc Biol 99(6):857–862. https://doi.org/10.1189/jlb.2MR0915-441R

Kassianos AJ, Wang X, Sampangi S, Muczynski K, Healy H, Wilkinson R (2013) Increased tubulointerstitial recruitment of human CD141(hi) CLEC9A(+) and CD1c(+) myeloid dendritic cell subsets in renal fibrosis and chronic kidney disease. Am J Physiol Renal Physiol 305(10):F1391–F1401. https://doi.org/10.1152/ajprenal.00318.2013

Kassianos AJ, Wang X, Sampangi S, Afrin S, Wilkinson R, Healy H (2015) Fractalkine-CX3CR1-dependent recruitment and retention of human CD1c+ myeloid dendritic cells by in vitro-activated proximal tubular epithelial cells. Kidney Int 87(6):1153–1163. https://doi.org/10.1038/ki.2014.407

Kitagawa K, Wada T, Furuichi K, Hashimoto H, Ishiwata Y, Asano M, Takeya M, Kuziel WA, Matsushima K, Mukaida N, Yokoyama H (2004) Blockade of CCR2 ameliorates progressive fibrosis in kidney. Am J Pathol 165(1):237–246. https://doi.org/10.1016/S0002-9440(10)63292-0

Kormann MS, Hector A, Marcos V, Mays LE, Kappler M, Illig T, Klopp N, Zeilinger S, Carevic M, Rieber N, Eickmeier O, Zielen S, Gaggar A, Moepps B, Griese M, Hartl D (2012) CXCR1 and CXCR2 haplotypes synergistically modulate cystic fibrosis lung disease. Eur Respir J 39(6):1385–1390. https://doi.org/10.1183/09031936.00130011

Kunsch C, Rosen CA (1993) NF-kappa B subunit-specific regulation of the interleukin-8 promoter. Mol Cell Biol 13(10):6137–6146

LeBleu VS, Taduri G, O'Connell J, Teng Y, Cooke VG, Woda C, Sugimoto H, Kalluri R (2013) Origin and function of myofibroblasts in kidney fibrosis. Nat Med 19(8):1047–1053. https://doi.org/10.1038/nm.3218

Lefebvre E, Moyle G, Reshef R, Richman LP, Thompson M, Hong F, Chou HL, Hashiguchi T, Plato C, Poulin D, Richards T, Yoneyama H, Jenkins H, Wolfgang G, Friedman SL (2016) Antifibrotic effects of the dual CCR2/CCR5 antagonist Cenicriviroc in animal models of liver and kidney fibrosis. PLoS One 11(6):e0158156. https://doi.org/10.1371/journal.pone.0158156

Li F, Zhang X, Gordon JR (2002) CXCL8((3-73))K11R/G31P antagonizes ligand binding to the neutrophil CXCR1 and CXCR2 receptors and cellular responses to CXCL8/IL-8. Biochem Biophys Res Commun 293(3):939–944. https://doi.org/10.1016/S0006-291X(02)00318-2

Li J, Deane JA, Campanale NV, Bertram JF, Ricardo SD (2007) The contribution of bone marrow-derived cells to the development of renal interstitial fibrosis. Stem Cells 25(3):697–706. https://doi.org/10.1634/stemcells.2006-0133

Li XY, Ban GF, Al-Shameri B, He X, Liang DZ, Chen WX (2018) High-temperature requirement protein A1 regulates Odontoblastic differentiation of dental pulp cells via the transforming growth factor Beta 1/Smad signaling pathway. J Endod 44(5):765–772. https://doi.org/10.1016/j.joen.2018.02.003

Li L, Wang C, Gu Y (2019) Collagen IV, a promising serum biomarker for evaluating the prognosis of revascularization in a 2-kidney, 1-clip hypertensive rat model. Interact Cardiovasc Thorac Surg 30:483. https://doi.org/10.1093/icvts/ivz275

Liu Q, Li Z, Gao JL, Wan W, Ganesan S, McDermott DH, Murphy PM (2015) CXCR4 antagonist AMD3100 redistributes leukocytes from primary immune organs to secondary immune organs, lung, and blood in mice. Eur J Immunol 45(6):1855–1867. https://doi.org/10.1002/eji.201445245

Ma FY, Woodman N, Mulley WR, Kanellis J, Nikolic-Paterson DJ (2013) Macrophages contribute to cellular but not humoral mechanisms of acute rejection in rat renal allografts. Transplantation 96(11):949–957. https://doi.org/10.1097/TP.0b013e3182a4befa

Ma W, Tao L, Wang X, Liu Q, Zhang W, Li Q, He C, Xue D, Zhang J, Liu C (2016a) Sorafenib inhibits renal fibrosis induced by unilateral ureteral obstruction via inhibition of macrophage infiltration. Cell Physiol Biochem 39(5):1837–1849. https://doi.org/10.1159/000447883

Ma Z, Jin X, He L, Wang Y (2016b) CXCL16 regulates renal injury and fibrosis in experimental renal artery stenosis. Am J Phys Heart Circ Phys 311(3):H815–H821. https://doi.org/10.1152/ajpheart.00948.2015

Ma Z, Yu R, Zhu Q, Sun L, Jian L, Wang X, Zhao J, Li C, Liu X (2019) CXCL16/CXCR6 axis promotes bleomycin-induced fibrotic process in MRC-5 cells via the PI3K/AKT/FOXO3a pathway. IntImmunopharmacol:106035. https://doi.org/10.1016/j.intimp.2019.106035

Maluf DG, Mas VR, Archer KJ, Yanek K, Gibney EM, King AL, Cotterell A, Fisher RA, Posner MP (2008) Molecular pathways involved in loss of kidney graft function with tubular atrophy and interstitial fibrosis. Mol Med 14(5–6):276–285. https://doi.org/10.2119/2007-00111.Maluf

Matloubian M, David A, Engel S, Ryan JE, Cyster JG (2000) A transmembrane CXC chemokine is a ligand for HIV-coreceptor Bonzo. Nat Immunol 1(4):298–304. https://doi.org/10.1038/79738

Meng XM, Nikolic-Paterson DJ, Lan HY (2014) Inflammatory processes in renal fibrosis. Nat Rev Nephrol 10(9):493–503. https://doi.org/10.1038/nrneph.2014.114

Meran S, Steadman R (2011) Fibroblasts and myofibroblasts in renal fibrosis. Int J Exp Pathol 92(3):158–167. https://doi.org/10.1111/j.1365-2613.2011.00764.x

Milovanovic J, Todorovic-Rakovic N, Abu Rabi Z (2017) The role of interleukin 8 and matrix metalloproteinases 2 and 9 in breast cancer treated with tamoxifen. J BUON 22(3):628–637

Mo H, Wu Q, Miao J, Luo C, Hong X, Wang Y, Tang L, Hou FF, Liu Y, Zhou L (2017) C-X-C chemokine receptor type 4 plays a crucial role in mediating oxidative stress-induced Podocyte injury. Antioxid Redox Signal 27(6):345–362. https://doi.org/10.1089/ars.2016.6758

Murphy PM, Baggiolini M, Charo IF, Hebert CA, Horuk R, Matsushima K, Miller LH, Oppenheim JJ, Power CA (2000) International union of pharmacology. XXII. Nomenclature for chemokine receptors. Pharmacol Rev 52(1):145–176

Nakaya I, Wada T, Furuichi K, Sakai N, Kitagawa K, Yokoyama H, Ishida Y, Kondo T, Sugaya T, Kawachi H, Shimizu F, Narumi S, Haino M, Gerard C, Matsushima K, Kaneko S (2007) Blockade of IP-10/CXCR3 promotes progressive renal fibrosis. Nephron Exp Nephrol 107(1):e12–e21. https://doi.org/10.1159/000106505

Nastase MV, Zeng-Brouwers J, Beckmann J, Tredup C, Christen U, Radeke HH, Wygrecka M, Schaefer L (2018) Biglycan, a novel trigger of Th1 and Th17 cell recruitment into the kidney. Matrix Biol 68–69:293–317. https://doi.org/10.1016/j.matbio.2017.12.002

Oka M, Sekiya S, Sakiyama R, Shimizu T, Nitta K (2019) Hepatocyte growth factor-secreting Mesothelial cell sheets suppress progressive fibrosis in a rat model of CKD. J Am Soc Nephrol 30(2):261–276. https://doi.org/10.1681/ASN.2018050556

Okamura DM, Lopez-Guisa JM, Koelsch K, Collins S, Eddy AA (2007) Atherogenic scavenger receptor modulation in the tubulointerstitium in response to chronic renal injury. Am J Physiol Renal Physiol 293(2):F575–F585. https://doi.org/10.1152/ajprenal.00063.2007

Olszewski MA, Huffnagle GB, McDonald RA, Lindell DM, Moore BB, Cook DN, Toews GB (2000) The role of macrophage inflammatory protein-1 alpha/CCL3 in regulation of T cell-mediated immunity to *Cryptococcus neoformans* infection. J Immunol 165(11):6429–6436. https://doi.org/10.4049/jimmunol.165.11.6429

Opfermann P, Derhaschnig U, Felli A, Wenisch J, Santer D, Zuckermann A, Dworschak M, Jilma B, Steinlechner B (2015) A pilot study on reparixin, a CXCR1/2 antagonist, to assess safety and efficacy in attenuating ischaemia-reperfusion injury and inflammation after on-pump coronary artery bypass graft surgery. Clin Exp Immunol 180(1):131–142. https://doi.org/10.1111/cei.12488

Pardo A, Selman M (2006) Matrix metalloproteases in aberrant fibrotic tissue remodeling. Proc Am Thorac Soc 3(4):383–388. https://doi.org/10.1513/pats.200601-012TK

Paust HJ, Turner JE, Steinmetz OM, Peters A, Heymann F, Holscher C, Wolf G, Kurts C, Mittrucker HW, Stahl RA, Panzer U (2009) The IL-23/Th17 axis contributes to renal injury in experimental glomerulonephritis. J Am Soc Nephrol 20(5):969–979. https://doi.org/10.1681/ASN.2008050556

Peng X, Zhang J, Xiao Z, Dong Y, Du J (2015) CX3CL1-CX3CR1 interaction increases the population of Ly6C(−)CX3CR1(hi) macrophages contributing to unilateral ureteral obstruction-induced fibrosis. J Immunol 195(6):2797–2805. https://doi.org/10.4049/jimmunol.1403209

Petit I, Jin D, Rafii S (2007) The SDF-1-CXCR4 signaling pathway: a molecular hub modulating neo-angiogenesis. Trends Immunol 28(7):299–307. https://doi.org/10.1016/j.it.2007.05.007

Ratajczak MZ, Zuba-Surma E, Kucia M, Reca R, Wojakowski W, Ratajczak J (2006) The pleiotropic effects of the SDF-1-CXCR4 axis in organogenesis, regeneration and tumorigenesis. Leukemia 20(11):1915–1924. https://doi.org/10.1038/sj.leu.2404357

Romagnani P, Lazzeri E, Lasagni L, Mavilia C, Beltrame C, Francalanci M, Rotondi M, Annunziato F, Maurenzig L, Cosmi L, Galli G, Salvadori M, Maggi E, Serio M (2002) IP-10 and Mig production by glomerular cells in human proliferative glomerulonephritis and regulation by nitric oxide. J Am Soc Nephrol 13(1):53–64

Saito H, Tanaka T, Tanaka S, Higashijima Y, Yamaguchi J, Sugahara M, Ito M, Uchida L, Hasegawa S, Wakashima T, Fukui K, Nangaku M (2018) Persistent expression of neutrophil gelatinase-associated lipocalin and M2 macrophage markers and chronic fibrosis after acute kidney injury. Physiol Rep 6(10):e13707. https://doi.org/10.14814/phy2.13707

Sakai N, Wada T, Yokoyama H, Lipp M, Ueha S, Matsushima K, Kaneko S (2006) Secondary lymphoid tissue chemokine (SLC/CCL21)/CCR7 signaling regulates fibrocytes in renal fibrosis. Proc Natl Acad Sci U S A 103(38):14098–14103. https://doi.org/10.1073/pnas.0511200103

Sallusto F, Lenig D, Mackay CR, Lanzavecchia A (1998) Flexible programs of chemokine receptor expression on human polarized T helper 1 and 2 lymphocytes. J Exp Med 187(6):875–883

Schmidt M, Sun G, Stacey MA, Mori L, Mattoli S (2003) Identification of circulating fibrocytes as precursors of bronchial myofibroblasts in asthma. J Immunol 171(1):380–389

Schott AF, Goldstein LJ, Cristofanilli M, Ruffini PA, McCanna S, Reuben JM, Perez RP, Kato G, Wicha M (2017) Phase Ib pilot study to evaluate Reparixin in combination with weekly paclitaxel in patients with HER-2-negative metastatic breast cancer. Clin Cancer Res 23(18):5358–5365. https://doi.org/10.1158/1078-0432.CCR-16-2748

Seo YD, Jiang X, Sullivan KM, Jalikis FG, Smythe KS, Abbasi A, Vignali M, Park JO, Daniel SK, Pollack SM, Kim TS, Yeung R, Crispe IN, Pierce RH, Robins H, Pillarisetty VG (2019) Mobilization of CD8(+) T cells via CXCR4 blockade facilitates PD-1 checkpoint therapy in human pancreatic cancer. Clin Cancer Res 25(13):3934–3945. https://doi.org/10.1158/1078-0432.CCR-19-0081

Shen L, Gao Y, Qian J, Sun A, Ge J (2011) A novel mechanism for endothelial progenitor cells homing: the SDF-1/CXCR4-Rac pathway may regulate endothelial progenitor cells homing through cellular polarization. Med Hypotheses 76(2):256–258. https://doi.org/10.1016/j.mehy.2010.10.014

Shimizu K, Furuichi K, Sakai N, Kitagawa K, Matsushima K, Mukaida N, Kaneko S, Wada T (2011) Fractalkine and its receptor, CX3CR1, promote hypertensive interstitial fibrosis in the kidney. Hypertens Res 34(6):747–752. https://doi.org/10.1038/hr.2011.23

Steinmetz OM, Turner JE, Paust HJ, Lindner M, Peters A, Heiss K, Velden J, Hopfer H, Fehr S, Krieger T, Meyer-Schwesinger C, Meyer TN, Helmchen U, Mittrucker HW, Stahl RA, Panzer U (2009) CXCR3 mediates renal Th1 and Th17 immune response in murine lupus nephritis. J Immunol 183(7):4693–4704. https://doi.org/10.4049/jimmunol.0802626

Stockinger B, Omenetti S (2017) The dichotomous nature of T helper 17 cells. Nat Rev Immunol 17 (9):535–544. https://doi.org/10.1038/nri.2017.50

Strutz F, Muller GA (2006) Renal fibrosis and the origin of the renal fibroblast. Nephrol Dial Transplant 21(12):3368–3370. https://doi.org/10.1093/ndt/gfl199

Svensson M, Yadav M, Holmqvist B, Lutay N, Svanborg C, Godaly G (2011) Acute pyelonephritis and renal scarring are caused by dysfunctional innate immunity in mCxcr2 heterozygous mice. Kidney Int 80(10):1064–1072. https://doi.org/10.1038/ki.2011.257

Takabatake Y, Sugiyama T, Kohara H, Matsusaka T, Kurihara H, Koni PA, Nagasawa Y, Hamano T, Matsui I, Kawada N, Imai E, Nagasawa T, Rakugi H, Isaka Y (2009) The CXCL12 (SDF-1)/CXCR4 axis is essential for the development of renal vasculature. J Am Soc Nephrol 20(8):1714–1723. https://doi.org/10.1681/ASN.2008060640

Takama Y, Miyagawa S, Yamamoto A, Firdawes S, Ueno T, Ihara Y, Kondo A, Matsunami K, Otsuka H, Fukuzawa M (2011) Effects of a calcineurin inhibitor, FK506, and a CCR5/CXCR3 antagonist, TAK-779, in a rat small intestinal transplantation model. Transpl Immunol 25 (1):49–55. https://doi.org/10.1016/j.trim.2011.04.003

Togel F, Isaac J, Hu Z, Weiss K, Westenfelder C (2005) Renal SDF-1 signals mobilization and homing of CXCR4-positive cells to the kidney after ischemic injury. Kidney Int 67 (5):1772–1784. https://doi.org/10.1111/j.1523-1755.2005.00275.x

Tsutahara K, Okumi M, Kakuta Y, Abe T, Yazawa K, Miyagawa S, Matsunami K, Otsuka H, Kaimori J, Takahara S, Nonomura N (2012) The blocking of CXCR3 and CCR5 suppresses the infiltration of T lymphocytes in rat renal ischemia reperfusion. NephrolDialTransplant 27 (10):3799–3806. https://doi.org/10.1093/ndt/gfs360

Verbeke L, Mannaerts I, Schierwagen R, Govaere O, Klein S, Vander Elst I, Windmolders P, Farre R, Wenes M, Mazzone M, Nevens F, van Grunsven LA, Trebicka J, Laleman W (2016) FXR agonist obeticholic acid reduces hepatic inflammation and fibrosis in a rat model of toxic cirrhosis. Sci Rep 6:33453. https://doi.org/10.1038/srep33453

Vielhauer V, Anders HJ, Mack M, Cihak J, Strutz F, Stangassinger M, Luckow B, Grone HJ, Schlondorff D (2001) Obstructive nephropathy in the mouse: progressive fibrosis correlates with tubulointerstitial chemokine expression and accumulation of CC chemokine receptor 2- and 5-positive leukocytes. J Am Soc Nephrol 12(6):1173–1187

Vielhauer V, Berning E, Eis V, Kretzler M, Segerer S, Strutz F, Horuk R, Grone HJ, Schlondorff D, Anders HJ (2004) CCR1 blockade reduces interstitial inflammation and fibrosis in mice with glomerulosclerosis and nephrotic syndrome. Kidney Int 66(6):2264–2278. https://doi.org/10.1111/j.1523-1755.2004.66038.x

Wada T, Sakai N, Matsushima K, Kaneko S (2007) Fibrocytes: a new insight into kidney fibrosis. Kidney Int 72(3):269–273. https://doi.org/10.1038/sj.ki.5002325

Wang H, Shao Y, Zhang S, Xie A, Ye Y, Shi L, Jin L, Pan X, Lin Z, Li X, Yang S (2017) CXCL16 deficiency attenuates acetaminophen-induced hepatotoxicity through decreasing hepatic oxidative stress and inflammation in mice. Acta Biochim Biophys Sin 49(6):541–549. https://doi.org/10.1093/abbs/gmx040

Wehr A, Baeck C, Heymann F, Niemietz PM, Hammerich L, Martin C, Zimmermann HW, Pack O, Gassler N, Hittatiya K, Ludwig A, Luedde T, Trautwein C, Tacke F (2013) Chemokine receptor CXCR6-dependent hepatic NK T cell accumulation promotes inflammation and liver fibrosis. J Immunol 190(10):5226–5236. https://doi.org/10.4049/jimmunol.1202909

Wen J, Zhou Y, Wang J, Chen J, Yan W, Wu J, Yan J, Zhou K, Xiao Y, Wang Y, Xia Q, Cai W (2017) Interactions between Th1 cells and Tregs affect regulation of hepatic fibrosis in biliary

atresia through the IFN-gamma/STAT1 pathway. Cell Death Differ 24(6):997–1006. https://doi.org/10.1038/cdd.2017.31

Wharram BL, Goyal M, Wiggins JE, Sanden SK, Hussain S, Filipiak WE, Saunders TL, Dysko RC, Kohno K, Holzman LB, Wiggins RC (2005) Podocyte depletion causes glomerulosclerosis: diphtheria toxin-induced podocyte depletion in rats expressing human diphtheria toxin receptor transgene. J Am Soc Nephrol 16(10):2941–2952. https://doi.org/10.1681/ASN.2005010055

Wolff B, Burns AR, Middleton J, Rot A (1998) Endothelial cell "memory" of inflammatory stimulation: human venular endothelial cells store interleukin 8 in Weibel-Palade bodies. J Exp Med 188(9):1757–1762

Wong CK, Ho AW, Tong PC, Yeung CY, Kong AP, Lun SW, Chan JC, Lam CW (2007) Aberrant activation profile of cytokines and mitogen-activated protein kinases in type 2 diabetic patients with nephropathy. Clin Exp Immunol 149(1):123–131. https://doi.org/10.1111/j.1365-2249.2007.03389.x

Wu Y, An C, Jin X, Hu Z, Wang Y (2020) Disruption of CXCR6 ameliorates kidney inflammation and fibrosis in Deoxycorticosterone acetate/salt hypertension. Sci Rep 10(1):133. https://doi.org/10.1038/s41598-019-56933-7

Wuyts A, Proost P, Lenaerts JP, Ben-Baruch A, Van Damme J, Wang JM (1998) Differential usage of the CXC chemokine receptors 1 and 2 by interleukin-8, granulocyte chemotactic protein-2 and epithelial-cell-derived neutrophil attractant-78. Eur J Biochem 255(1):67–73

Wynes MW, Frankel SK, Riches DW (2004) IL-4-induced macrophage-derived IGF-I protects myofibroblasts from apoptosis following growth factor withdrawal. J Leukoc Biol 76 (5):1019–1027. https://doi.org/10.1189/jlb.0504288

Xia Y, Entman ML, Wang Y (2013) CCR2 regulates the uptake of bone marrow-derived fibroblasts in renal fibrosis. PLoS One 8(10):e77493. https://doi.org/10.1371/journal.pone.0077493

Xia Y, Jin X, Yan J, Entman ML, Wang Y (2014a) CXCR6 plays a critical role in angiotensin II-induced renal injury and fibrosis. Arterioscler Thromb Vasc Biol 34(7):1422–1428. https://doi.org/10.1161/ATVBAHA.113.303172

Xia Y, Yan J, Jin X, Entman ML, Wang Y (2014b) The chemokine receptor CXCR6 contributes to recruitment of bone marrow-derived fibroblast precursors in renal fibrosis. Kidney Int 86 (2):327–337. https://doi.org/10.1038/ki.2014.64

Yan J, Zhang Z, Jia L, Wang Y (2016) Role of bone marrow-derived fibroblasts in renal fibrosis. Front Physiol 7:61. https://doi.org/10.3389/fphys.2016.00061

Yang J, Zhu F, Wang X, Yao W, Wang M, Pei G, Hu Z, Guo Y, Zhao Z, Wang P, Mou J, Sun J, Zeng R, Xu G, Liao W, Yao Y (2016) Continuous AMD3100 treatment worsens renal fibrosis through regulation of bone marrow derived pro-Angiogenic cells homing and T-cell-related inflammation. PLoS One 11(2):e0149926. https://doi.org/10.1371/journal.pone.0149926

Ye Y, Zhang Y, Wang B, Walana W, Wei J, Gordon JR, Li F (2018) CXCR1/CXCR2 antagonist G31P inhibits nephritis in a mouse model of uric acid nephropathy. Biomed Pharmacother 107:1142–1150. https://doi.org/10.1016/j.biopha.2018.07.077

Yoneyama H, Matsuno K, Zhang Y, Murai M, Itakura M, Ishikawa S, Hasegawa G, Naito M, Asakura H, Matsushima K (2001) Regulation by chemokines of circulating dendritic cell precursors, and the formation of portal tract-associated lymphoid tissue, in a granulomatous liver disease. J Exp Med 193(1):35–49

Yuan A, Lee Y, Choi U, Moeckel G, Karihaloo A (2015) Chemokine receptor Cxcr4 contributes to kidney fibrosis via multiple effectors. Am J Physiol Renal Physiol 308(5):F459–F472. https://doi.org/10.1152/ajprenal.00146.2014

Zehender A, Huang J, Gyorfi AH, Matei AE, Trinh-Minh T, Xu X, Li YN, Chen CW, Lin J, Dees C, Beyer C, Gelse K, Zhang ZY, Bergmann C, Ramming A, Birchmeier W, Distler O, Schett G, Distler JHW (2018) The tyrosine phosphatase SHP2 controls TGFbeta-induced STAT3 signaling to regulate fibroblast activation and fibrosis. Nat Commun 9(1):3259. https://doi.org/10.1038/s41467-018-05768-3

Zeisberg M, Strutz F, Muller GA (2000) Role of fibroblast activation in inducing interstitial fibrosis. J Nephrol 13(Suppl 3):S111–S120

Zhang L, Ran L, Garcia GE, Wang XH, Han S, Du J, Mitch WE (2009) Chemokine CXCL16 regulates neutrophil and macrophage infiltration into injured muscle, promoting muscle regeneration. Am J Pathol 175(6):2518–2527. https://doi.org/10.2353/ajpath.2009.090275

Zhang Y, Thai K, Kepecs DM, Winer D, Gilbert RE (2018) Reversing CXCL10 deficiency ameliorates kidney disease in diabetic mice. Am J Pathol 188(12):2763–2773. https://doi.org/10.1016/j.ajpath.2018.08.017

Zhao Y, Zhu L, Zhou T, Zhang Q, Shi S, Liu L, Lv J, Zhang H (2015) Urinary CXCL1: a novel predictor of IgA nephropathy progression. PLoS One 10(3):e0119033. https://doi.org/10.1371/journal.pone.0119033

Zheng Z, Zheng F (2016) Immune cells and inflammation in diabetic nephropathy. J Diabetes Res 2016:1841690. https://doi.org/10.1155/2016/1841690

Zhu L, Zhang Q, Shi S, Liu L, Lv J, Zhang H (2013) Synergistic effect of mesangial cell-induced CXCL1 and TGF-beta1 in promoting podocyte loss in IgA nephropathy. PLoS One 8(8):e73425. https://doi.org/10.1371/journal.pone.0073425

Zhuang Q, Cheng K, Ming Y (2017) CX3CL1/CX3CR1 Axis, as the therapeutic potential in renal diseases: friend or foe? Curr Gene Ther 17(6):442–452. https://doi.org/10.2174/1566523218666180214092536

Zohar Y, Wildbaum G, Novak R, Salzman AL, Thelen M, Alon R, Barsheshet Y, Karp CL, Karin N (2014) CXCL11-dependent induction of FOXP3-negative regulatory T cells suppresses autoimmune encephalomyelitis. J Clin Invest 124(5):2009–2022. https://doi.org/10.1172/JCI71951

Zohar Y, Wildbaum G, Novak R, Salzman AL, Thelen M, Alon R, Barsheshet Y, Karp CL, Karin N (2018) CXCL11-dependent induction of FOXP3-negative regulatory T cells suppresses autoimmune encephalomyelitis. J Clin Invest 128(3):1200–1201. https://doi.org/10.1172/JCI120358

Zuniga-Traslavina C, Bravo K, Reyes AE, Feijoo CG (2017) Cxcl8b and Cxcr2 regulate neutrophil migration through bloodstream in Zebrafish. J Immunol Res 2017:6530531. https://doi.org/10.1155/2017/6530531

Rev Physiol Biochem Pharmacol (2020) 177: 25–52
https://doi.org/10.1007/112_2020_26

Published online: 21 July 2020

Inflammatory Biomarkers for Cardiovascular Risk Stratification in Familial Hypercholesterolemia

Afsane Bahrami, Luca Liberale, Željko Reiner, Federico Carbone, Fabrizio Montecucco, and Amirhossein Sahebkar

Afsane Bahrami and Luca Liberale contributed equally to this work.

A. Bahrami
Cellular and Molecular Research Center, Birjand University of Medical Sciences, Birjand, Iran

L. Liberale
First Clinic of Internal Medicine, Department of Internal Medicine, University of Genoa, Genoa, Italy

Center for Molecular Cardiology, University of Zurich, Schlieren, Switzerland

Ž. Reiner
University Hospital Centre Zagreb, School of Medicine University of Zagreb, Department of Internal Medicine, Zagreb, Croatia

F. Carbone
First Clinic of Internal Medicine, Department of Internal Medicine, University of Genoa, Genoa, Italy

IRCCS Ospedale Policlinico San Martino Genoa – Italian Cardiovascular Network, Genoa, Italy

F. Montecucco
IRCCS Ospedale Policlinico San Martino Genoa – Italian Cardiovascular Network, Genoa, Italy

First Clinic of Internal Medicine, Department of Internal Medicine, and Centre of Excellence for Biomedical Research (CEBR), University of Genoa, Genoa, Italy

A. Sahebkar (✉)
Halal Research Center of IRI, FDA, Tehran, Iran

Biotechnology Research Center, Pharmaceutical Technology Institute, Mashhad University of Medical Sciences, Mashhad, Iran

Neurogenic Inflammation Research Center, Mashhad University of Medical Sciences, Mashhad, Iran

School of Pharmacy, Mashhad University of Medical Sciences, Mashhad, Iran
e-mail: sahebkara@mums.ac.ir

Contents

Abstract Familial hypercholesterolemia (FH) is a frequent autosomal genetic disease characterized by elevated concentrations of low-density lipoprotein cholesterol (LDL) from birth with increased risk of premature atherosclerotic complications. Accumulating evidence has shown enhanced inflammation in patients with FH. In vessels, the deposition of modified cholesterol lipoproteins triggers local inflammation. Then, inflammation facilitates fatty streak formation by activating the endothelium to produce chemokines and adhesion molecules. This process eventually results in the uptake of vascular oxidized LDL (OxLDL) by scavenger receptors in monocyte-derived macrophages and formation of foam cells. Further leukocyte recruitment into the sub-endothelial space leads to plaque progression and activation of smooth muscle cells proliferation. Several inflammatory biomarkers have been reported in this setting which can be directly synthetized by activated inflammatory/vascular cells or can be indirectly produced by organs other than vessels, e.g., liver. Of note, inflammation is boosted in FH patients. Inflammatory biomarkers might improve the risk stratification for coronary heart disease and predict atherosclerotic events in FH patients. This review aims at summarizing the current knowledge about the role of inflammation in FH and the potential application of inflammatory biomarkers for cardiovascular risk estimation in these patients.

Keywords Cardiovascular risk · CRP · Familial hypercholesterolemia, inflammation · Markers · Oxidized LDL · TNF-α

Abbreviations

ALCAM	Activated leukocyte cell adhesion molecule
apoB	Apolipoprotein B
BAFF	B cell activating factor receptor
baPWV	Brachial-ankle pulse wave velocity

CAC	Coronary artery calcifications
CHD	Coronary heart disease
CV	Cardiovascular
CVD	CV disease
CYS	Cholesterol-year score
ELAM-1	Endothelial-leukocyte adhesion molecule-1
FCH	Combined familiar hypercholesterolemia
FFAs	Free fatty acids
FH	Familial hypercholesterolemia
GTP	Guanosine triphosphate
HDL	High-density lipoprotein cholesterol
He	Heterozygous
Ho	Homozygous
hs-CRP	High sensitivity C-reactive protein levels
IFN-γ	Interferon gamma
IL	Interleukin
IL-RA	IL-1 receptor antagonist
IMT	Intima-media thickness
LDL	Low-density lipoprotein cholesterol
LDLR	LDL receptor
LOX-1	Lectin-like oxidized low-density lipoprotein receptor-1
Lp	Lipoprotein
Lp-PLA2	Lipoprotein-associated phospholipase A2
MCP-1	Monocyte chemoattractive protein
M-CSF	Macrophage colony stimulating factor
MI	Myocardial infarction
MIP	Macrophage inflammatory protein
MMPs	Metalloproteinases
MPV	Mean platelet volume
OxLDL	Oxidized LDL
PAI-1	Plasminogen activatorinhibitor-1
PBMCs	Peripheral blood mononuclear cells
PON1	Paraoxonase type 1
PPAR	Peroxisome proliferator-activated receptor
PWV	Pulse wave velocity
RANK	Receptor activator of NF-κB
ROS	Reactive oxygen species
RUC	Related unaffected relatives
sICAM − 1	Soluble intercellular adhesion molecule-1
sVCAM − 1	Soluble vascular adhesion molecule-1
Th	T helper cells
TLR	Toll-like receptor
TNF	Tumor necrosis factor
TNFRSF	TNF receptor superfamily

TNFSF	TNF superfamily
TRAIL	TNF-related apoptosis-inducing ligand
XO	Xanthine oxidase

1 Introduction

Familial hypercholesterolemia (FH) is a common autosomal inherited disorder of lipoprotein metabolism characterized by high levels of total and low-density lipoprotein cholesterol (LDL) from birth, increased risk for early onset cardiovascular (CV) diseases (CVDs) and pathologic cholesterol accumulations often found in tendons (i.e., xanthomas), eyelids (i.e., xanthelasmas), and corneas (i.e., corneal arcus). In FH, defects in LDL receptor (LDLR) functionality or metabolism affect the uptake/handling of LDL by the liver resulting in increased circulating cholesterol levels (McNeely et al. 2001). Familial hypercholesterolemia is further defined based on the number of mutated alleles and severity of the disease as (1) heterozygous (HeFH), the common milder form with nearly two-fold elevation in LDL levels (Goldstein and Brown 2009) or (2) homozygous (HoFH) a rare more severe pattern with LDL levels above 500 mg/dL and as high as 1,000 mg/dL. FH is a silent disease which becomes clinically evident only after the early development of its cardiovascular complications (i.e., coronary heart disease) (Soutar and Naoumova 2007; Gidding et al. 2015; Benn et al. 2012; Reiner 2015). In the case FH would remain untreated, 85% of men and 50% of women are thought to suffer a premature coronary event (Civeira 2004). Accordingly, about 5% of the patients with HeFH suffer from myocardial infarction (MI) before the age of 60 years (Goldstein and Brown 2009). Although CV risk is increased in all FH patients, the onset of clinically manifested CVD may vary among patients even when they carry identical mutation (Jansen et al. 2002; Ferrieres et al. 1995). Traditional risk factors account only for a part (~20%) of this variability (Ferrieres et al. 1995; Moorjani et al. 1993). Accordingly, it has been hypothesized that other factors such as levels of inflammation may influence the susceptibility of FH patients to cardiac disease and explain the variability in phenotypic expression (Sharifi et al. 2016).

Atherosclerosis is a multi-step process characterized by both accumulation and retention of atherogenic lipoproteins into the sub-endothelial space and chronic arterial wall inflammation with activation of resident cells and recruitment of circulating leukocytes (Montecucco et al. 2017; Mawhin 2017; Hansson et al. 2015; Hansson and Libby 2006; Iwata and Nagai 2012). Recently, clinical trials targeting inflammation confirmed the causative role of this process in atherosclerosis by showing reduced rate of secondary CV events in post-myocardial infarction patients (Ridker et al. 2017; Tardif et al. 2019). Several lines of evidence suggest enhanced chronic low-grade inflammation in patients with FH (Narverud et al. 2011a; Real et al. 2010a) and this is thought to account for part of their increased CV risk (Cheng et al. 2007a; Kastelein et al. 2003).

Given that atherosclerotic complications are major causes of morbidity in individuals diagnosed with FH, the improvement in risk stratification assessment in those patients who are at higher CV risk is important, since they could benefit from earlier and more intensive treatment. In view of the above mentioned, this review aims at dissecting the interplay between hyperlipidemia and inflammation in the determination of CV risk in FH population and analyzing the potential application of inflammatory biomarkers in the CV risk estimation of these patients.

2 Lipids and Inflammation: A Deadly Combination in FH Patients

Both lipids (either modified or in their canonical isoform) and inflammation are deeply involved in the regulation of early atherogenesis (Libby 2002). Specifically, hypercholesterolemia induces the expression of leukocyte adhesion molecules by arterial endothelium while LDL penetrates and is selectively retained at susceptible sites where it undergoes oxidative modification to OxLDL (Bergheanu et al. 2017). Circulating leukocytes invade the vessel wall driven by high levels of chemotactic factors, such as OxLDL and monocyte chemoattractive protein (MCP-1) (Montecucco et al. 2017; Bonaventura et al. 2018; Liberale et al. 2017). Besides enhancing monocyte recruitment, OxLDL also triggers their differentiation into macrophages and the expression of scavenger receptors which mediate lipids internalization and foam cell formation (Tekin et al. 2013). This sets a vicious circle since macrophages can oxidize LDL and OxLDL can directly and indirectly stimulate monocyte recruitment. Accordingly, different clinical studies report hypercholesterolemia, oxidative stress, and inflammation to be closely related (Karbiner et al. 2013; Narverud et al. 2014; Real et al. 2010b). Of interest, biomarkers of such deleterious processes are upregulated in patients with FH (Van Tits et al. 2003; Rahman et al. 2017).

Not only lipids and inflammatory molecules collaborate to initiate atherosclerotic lesions in FH (Fig. 1), these mediators are also promoters of plaque progression and culprit mediators of sudden atherosclerotic complications, including myocardial infarction. Indeed, fibrous cap fissuring and formation of thrombi are closely associated with inflammatory products that are released from endothelial cells, monocytes, and neutrophils such as tissue factor, adhesion molecules, cytokines [e.g., IL-1β, tumor necrosis factor (TNF)-α], and metalloproteinases (MMPs) (Mawhin 2017; Hansson et al. 2015). Furthermore, OxLDL increases the production of prothrombotic plasminogen activator inhibitor-1 (PAI-1) while suppressing the secretion of tissue plasminogen activator, thus reducing the fibrinolytic activity in endothelial cells (Kugiyama et al. 1993). As a result, OxLDL level predicts both carotid plaque progression and major adverse cardiovascular events in different populations (Wallenfeldt et al. 2004; Tsimikas et al. 2012; Johnston et al. 2006; Lee et al. 2005). Specific contributions of each inflammatory mediator to

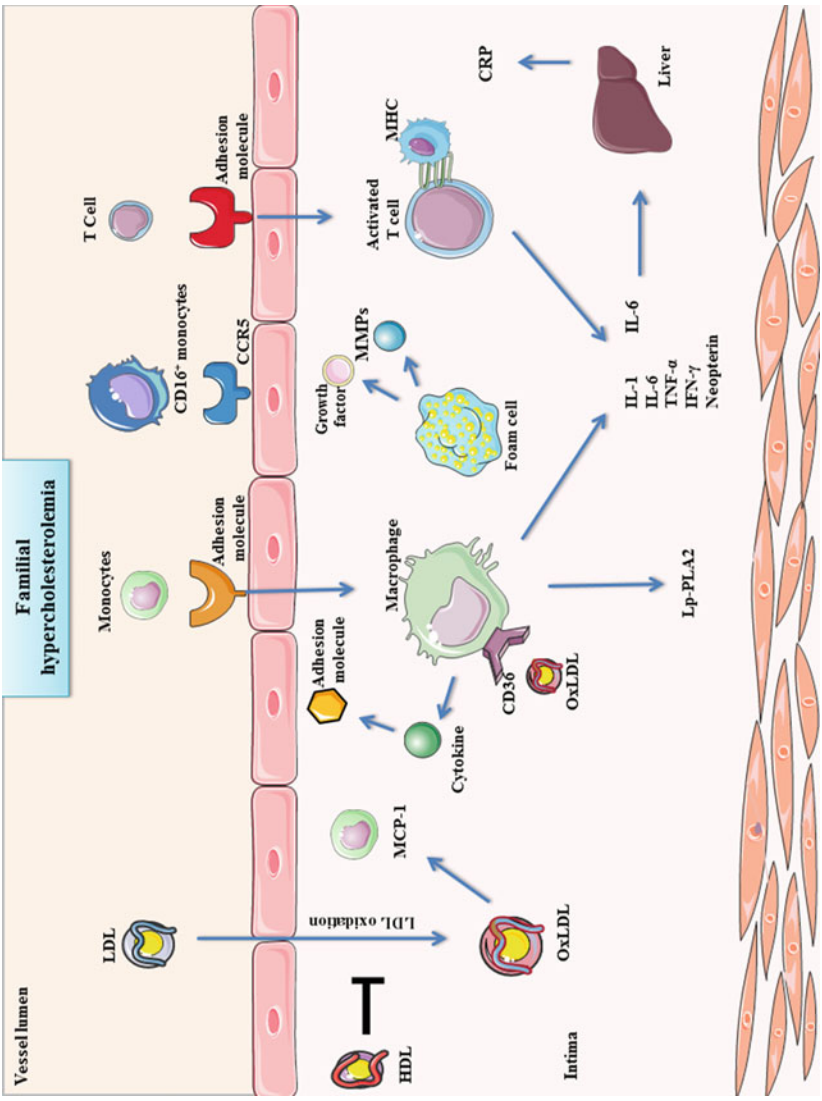

Fig. 1 Inflammation influences atherogenesis in familial hypercholesterolemia. *CCR5* C-C chemokine receptor type 5, *CRP* C-reactive protein, *ICAM-1* intercellular adhesion molecule-1, *IFN-γ* interferon gamma, *IL* interleukin, *HDL* high-density lipoprotein cholesterol, *LDL* low-density lipoprotein cholesterol, *MCP-1* monocyte chemo-attractant protein 1, *Lp-PLA2* lipoprotein-associated phospholipase A2, *MMPs* matrix metalloproteinases, *OxLDL* oxidized LDL, *TNF-α* tumor necrosis factor-alpha

atherosclerosis in FH setting and their potential role as predictor of CV risk in these patients will be dissected in the following paragraphs.

3 Inflammatory Biomarkers in FH

Biomarkers obtained from blood, plasma, and urine specimens can offer valuable details on inflammatory phenomena (Kinlay and Selwyn 2003; Packard and Libby 2008). Inflammatory biomarkers in atherosclerotic patients can be generated either directly due to activation of inflammatory/vascular cells in the plaque or indirectly in other organs, e.g., the liver (Table 1). Also, we should consider that inflammation is a non-specific phenomenon and other processes such as infection, autoimmune diseases, and traumas can induce the expression of a broad spectrum of inflammatory biomarkers and lead to misinterpretation of results in cardiovascular studies.

4 C-Reactive Protein (CRP)

High sensitivity-CRP (hs-CRP) is widely used as a biomarker of systemic inflammation in different settings (Tabatabaeizadeh et al. 2017; Zannad et al. 2012). Together with routine lipid screening test, levels of hs-CRP were shown to predict the presence of subclinical atherosclerosis in healthy men (Ridker et al. 1997). Hs-CRP is increased in adults with FH (Real et al. 2010a; Toutouzas et al. 2018). El Messal et al. assessed hs-CRP levels in FH patients with homozygous (HoFH) or heterozygous disease never treated with any lipid-lowering drug and compared to those with controls without FH (El Messal et al. 2006). Of interest, HoFH and HeFH patients had higher mean hs-CRP levels when compared to controls (five- and two-fold, respectively). Furthermore, in patients with HoFH direct relationships were reported between hs-CRP and total cholesterol, apoB and IL-18 (El Messal et al. 2006). Altogether, never-treated HoFH and HeFH patients had increased hs-CRP and higher risk for coronary heart disease (CHD) (El Messal et al. 2006). Similarly, plasma levels of hs-CRP were reported to directly correlate to those of NF-κB—a transcription factor modulating the synthesis of several inflammatory mediators—and to those of xanthine oxidase [(XO), an enzyme involved in production of reactive oxygen species (ROS)] in both FH patients and controls (Real et al. 2010a). Of interest, it has been recently reported that lectin-like oxidized low-density lipoprotein receptor-1 [LOX-1, initially identified as the major receptor for oxidized LDL (OxLDL)] also mediates CRP signaling, thus further evidencing the close interplay between inflammation and modified lipids in the setting of atherogenesis (Pothineni et al. 2017; Xu et al. 2013). Cheng et al. further analyzed the association between atherogenesis, arterial stiffness, and circulating CRP in patient with HeFH. In another study, cholesterol-year score (CYS) was used to assess the exposure to high cholesterol and brachial-ankle pulse wave velocity (baPWV) was used to

Table 1 Inflammatory biomarkers in familial hypercholesterolemia and suggested pathogenic mechanisms

Biomarker	Main mechanism	References
CRP	Negatively influences the atherogenesis at endothelium level directly by stimulating MCP-1 secretion and indirectly by enhancing the uptake of OxLDL via macrophages	Pasceri et al. (2000, 2001)
ICAM-1	Allows adhesion of monocytes/lymphocytes to the activated endothelium Participates to transendothelial migration	Santos et al. (2018)
E-selectin	Facilitates adherence of leucocytes to vascular endothelium and stimulates the cascade of pathogenic events	Rahman et al. (2017); Ley (2002)
TNF-α	Promotes the attachment of leucocytes to endothelium by stimulating adhesion molecule expression, facilitates foam cell formation and T-lymphocyte and monocyte/macrophage activation	Enayati et al. (2015)
IL-10	Prevents atherogenesis through inhibition of macrophage activation and decreases the expression of MMPs, cytokines, and cyclooxygenase-2	Hansson (2001)
CD40/CD40L	Induces the expression of different pro-atherogenic substances, such as adhesion molecules, cytokines, chemokines, growth factors, and MMPs	Gissler et al. (2016); Yuan et al. (2015)
NF-Kb	Regulates gene involved in endothelial cell activation as well as transcription of different chemokines, adhesion molecules, and other inflammatory mediators	Zernecke and Weber (2009); Monaco et al. (2004)
MCP-1	Is responsible for the recruitment of monocytes within the atherosclerotic lesion	França et al. (2017)
OxLDL	Is internalized by macrophage via the scavenger receptors, causing foam cell formation LDL oxidation process within vascular wall induces cascades of immunogenic and pro-inflammatory consequences which initiate atherogenesis	Linton and Fazio (2001); Navab et al. (2004)
Lp-PLA2	Has pro-inflammatory and pro-oxidant properties By hydrolyzing oxidized phospholipids, it produces bioactive fat compounds including lysophosphatidylcholine and oxidized non-esterified FFAs which stimulate inflammation, oxidative stress, and atherogenesis Induces in endothelial dysfunction, aortic wall inflammation, and injury	Stafforini (2009); Caslake et al. (2000); Yang et al. (2006); Weintraub (2008); Tsimikas et al. (2007)

(continued)

Table 1 (continued)

Biomarker	Main mechanism	References
$CD16^{+}$monocytes	Shows increased phagocytosis and higher tendency to adhere to the endothelium in response to native LDL/OxLDL Expresses and generates inflammatory mediators which are involved in atherosclerotic process	Belge et al. (2002); Mosig et al. (2009); Ancuta et al. (2003); Tacke et al. (2007)
MPV	High volume characterizes excessively reactive platelets with more metabolic, enzymatic, and coagulation potential Reactive platelets are associated with prothrombotic molecules, such as thromboxane	Kamath et al. (2001); Park et al. (2002); Vizioli et al. (2009)
Neopterin	Inflammatory mediator General marker of boosted cellular immunity Reflects activation of monocyte in response to IFN-γ	Murr et al. (2002)

CRP C-reactive protein, *FFAs* free fatty acids, *ICAM-1* intercellular adhesion molecule-1, *IL* interleukin, *MCP-1* monocyte chemo-attractant protein 1, *Lp-PLA2* lipoprotein-associated phospholipase A2, *MMPs* matrix metalloproteinases, *MPV* mean platelet volume, *OxLDL* oxidized LDL, *Th* T helper cell, *TNF-α* tumor necrosis factor-alpha, *NF-κB* transcription nuclear factor-kappa B

estimate arterial stiffness in FH patients (Cheng et al. 2007b). HeFH patients showed increased value of total cholesterol, LDL, as well as carotid intima-media thickness (IMT) as compared to controls. Interestingly, in patients with HeFH carotid IMT and baPWV were higher in those with long-time cholesterol exposure and in those with modestly increased hs-CRP level (>1 mg/L) (Cheng et al. 2007b). Furthermore, a multivariate regression analysis indicated both CYS and hs-CRP as strong independent predictors of IMT and baPWV in HeFH patients (Cheng et al. 2007b). This evidence implies that the pro-inflammatory vascular state is not only linked with atherosclerosis, but it also plays an important role in the progression of arterial stiffness in FH (Cheng et al. 2007b). Interestingly, in another recent report, serum concentrations of hs-CRP were significantly elevated in patients with combined familiar hypercholesterolemia (FCH) and with HeFH with respect to controls, while mean hs-CRP levels did not differ between HeFH and FCH patients (Toutouzas et al. 2018). Of importance, this is among the few studies assessing vascular inflammation in patients with FH by the mean of fluorodeoxyglucose-positron emission tomography (FDG-PET), showing a directly correlation between vascular inflammatory activity and circulating levels of hs-CRP in this population (Toutouzas et al. 2018; Iosif et al. 2017). On the other hand, another study showed no differences in CRP values between FH adult patients ($n = 89$, diagnosis based on clinical criteria with no genetic confirmation) and normal healthy controls ($n = 31$) (Martinez et al. 2008). In addition, no correlation was reported between CRP levels and atherosclerosis imaging variables, such as coronary artery calcifications (CAC) and carotid-femoral pulse wave velocity (PWV). On the other hand, a modest association between CRP levels and carotid IMT was demonstrated (Martinez et al. 2008). These results are in partial contrast with previous studies, showing

associations between CRP and IMT or CAC in the general population (Lakoski et al. 2007; Khera et al. 2005).

Although many data are available from FH adults, evidence from children is still limited and discordant. Among different studies assessing hs-CRP circulating levels in children with FH, only four articles showed significantly increased hs-CRP concentrations in FH children versus normal matched controls (Ueland et al. 2006; Ryu et al. 2011; Guardamagna et al. 2009), while five reported no difference (Narverud et al. 2011a, 2013a, 2013b; Stübiger et al. 2012; Charakida et al. 2009; Holven et al. 2006). Altogether these reports suggest that hs-CRP might be a less reliable indicator of endothelial activation and atherosclerotic progression in FH children than in adults. Of interest, Uelend et al. also demonstrated that 2-year pravastatin treatment did not affect hs-CRP levels in children with HeFH concluding that the anti-inflammatory impact of statins might be less important in children with FH than in adults (Ueland et al. 2006).

5 Soluble Adhesion Molecules

The results of several studies have supported a pivotal role of endothelial activation in atherogenesis, showing robust associations between circulating levels of adhesion molecules [i.e., E-selectin, soluble intercellular adhesion molecule-1 (sICAM-1), soluble vascular adhesion molecule-1 (sVCAM-1), and activated leukocyte cell adhesion molecule (ALCAM)] and atherosclerosis (Blankenberg et al. 2003; Galkina and Ley 2007). Indeed, the activated endothelium releases soluble adhesion molecules and thus, quantification of these molecules might be a potential indicator of endothelial dysfunction (Galkina and Ley 2007). Of interest, inflammatory molecules (i.e., CRP) can induce endothelial dysfunction and are associated with expression of different adhesion molecules (Pasceri et al. 2000; Hein et al. 2009). ICAM-1 is a transmembrane protein synthesized by leucocytes and endothelial cells which mediates adhesion of monocytes and lymphocytes to activated endothelium and participates to their transendothelial migration (Santos et al. 2018). E-selectin [also known as endothelial-leukocyte adhesion molecule-1 (ELAM-1)] is a carbohydrate-binding protein found on endothelial surface which facilitates adherence of leucocytes to the endothelium and is again implicated in the regulation of leukocyte migration (Rahman et al. 2017; Ley 2002). Much of the recent findings concerning adhesion molecules in FH derive from a case-control study on FH patients and their unaffected family members, which however based FH diagnosis only on clinical criteria without genetic confirmation thus requiring particular caution in interpretation of data (Rahman et al. 2017). In this study, both sICAM-1 and E-selectin were higher in FH patients when compared to healthy controls, while only sICAM-1 concentration was higher in unaffected family members with respect to controls. Van Haelst et al. confirmed higher ICAM-1 plasma levels in FH individuals (van Haelst et al. 2003). These results have been further confirmed in children with clinically diagnosed FH, thus suggesting an important role for

leukocyte-endothelial cell interactions also at early stages of endothelial dysfunction and atherogenesis (Charakida et al. 2009).

6 Cytokines

Cytokines are central players of cell–cell communication deeply regulating immune system function in both positive and negative fashions. Increasing evidence supports the contribution of major pro-inflammatory cytokines, namely IL-1, IL-6, and TNF-α in atherogenesis (Tousoulis et al. 2016). TNF-α is a multifunctional circulating cytokine which is nowadays accepted to be one of the main mediators of atherogenesis through promotion of leucocytes adhesion to the endothelium, foam cell formation, T-lymphocytes, and monocyte/macrophages activation (Enayati et al. 2015). TNF-α is produced by macrophages, mast cells, endothelial and smooth muscle cells and is found in vulnerable sites of atherosclerotic plaques (e.g., plaque shoulder) (Soeki and Sata 2016; Pasterkamp et al. 1999). In addition to TNF-α, other important members of the TNF superfamily (TNFSF) and TNF receptor superfamily (TNFRSF) are involved in atherosclerosis pathophysiology including Tκα, OX40 (CD134)/TNFRSF4 and its ligand (OX40L)/TNFSF4, CD40/TNFRSF5 and its ligand (CD40L,CD154)/TNFSF5, TNF-related apoptosis-inducing ligand (TRAIL or Apo2L)/TNFSF10, as well as receptor activator of NF-κB (RANK)/TNFRSF11A and its ligand (RANKL)/TNFSF11A (Dostert et al. 2018). In addition, two other pro-inflammatory pleiotropic cytokines, IL-1 and IL-6, have many humoral and cellular immune properties connecting them to inflammation and enhanced atherosclerosis as also outlined by the recent CANTOS trial (Ridker et al. 2017, 2018; Tousoulis et al. 2016). Also, CD40 and its counterpart ligand (CD40L) collaborate to enhance atherosclerosis, thromboembolism, and inflammation by inducing the expression of different pro-atherogenic substances such as adhesion molecules, cytokines, chemokines, growth factors, and MMPs in different cell types (Gissler et al. 2016; Yuan et al. 2015). ECs and smooth muscle cells amplify MCP-1 (also known as CCL2) in response to different cytokines and to OxLDL (Deshmane et al. 2009). Circulating levels of both CCL2 and its receptor CCR2 have been directly associated with enhanced atherogenesis and increased CV risk due to higher macrophage infiltration (França et al. 2017). Oppositely anti-inflammatory cytokines, such as IL-10, negatively modulate atherogenesis by favoring resolution of inflammation and are downregulated in patients with atherosclerosis and at higher risk of CV events (Mallat et al. 1999; Han and Boisvert 2015). TNFα/IL-10 ratio is emerging as an interesting marker to estimate the imbalance between pro- and anti-inflammatory cytokines and assess the CV risk (Goswami et al. 2009; Kumari et al. 2018; Narverud et al. 2011b).

Supporting the role of inflammatory cytokines in FH patients, the expression of the inflammatory gene-regulating transcription factor NF-kB in mononuclear cells of FH patients was significantly associated with plasma levels of OxLDL, xanthine oxidase, hs-CPR, apoB, and LDL (Real et al. 2010a). Increased TNF-α levels and

TNF-α/sTNFRs ratio have been reported in FH children, while no difference was reported in adults with and without FH (Narverud et al. 2011a). Of interest, FH children had lower circulating levels of IL-10 resulting in increased TNF-α/IL-10 ratios (Narverud et al. 2011a). In another similar investigation, mRNA transcription levels of TNFSF/TNFRSF genes in peripheral blood mononuclear cells (PBMCs) of children and young people with FH before and after statin therapy were measured (Narverud et al. 2013a). Baseline expression of OX40L, B cell activating factor receptor (BAFF) receptor, and TRAILR1 were significantly increased, while TRAIL and TRAILR3 were considerably reduced in FH patients when compared to controls (Narverud et al. 2013a). After statin administration, expression levels of OX40L and TRAILR1 decreased while BAFF, TRAIL, and TRAILR3 increased (Narverud et al. 2013a). Altogether these findings suggest FH children to have an impaired balance between anti- and pro-inflammatory signaling which may play an important role in the increased CV risk of these patients. In adults, the evidence is less clear, a study reported increased level of TNF-α in patients with HoFH as compared to normocholesterolemic controls (Gokalp et al. 2009). Oppositely, in the general FH population under optimal therapy no difference in terms of circulating inflammatory markers such as TNF-α, IL-1β, IL-1 receptor antagonist (IL-RA), IL-6, IL-10, and MCP-1 has been reported when compared to healthy controls (Real et al. 2010a; Hovland et al. 2010). In contrast, both HoFH and HeFH patients who were never treated with lipid-lowering agents have high or very high CHD risk and increased levels of MMP-9, TIMP-1, and IL-18 (El Messal et al. 2006). At the cellular level, monocytes from FH patients show a pro-inflammatory phenotype characterized by increased expression of CCR2, resulting in enhanced migratory capacity—a feature strongly associated with atherosclerosis development (Bernelot Moens et al. 2017). Accordingly, PBMCs from FH patients release a substantial amount of macrophage inflammatory protein (MIP)-1α, −1β, and IL-8 as compared to controls (Holven et al.2003, 2006). In young FH patients, main inflammatory mediators might differ as PBMCs from HeFH children have increased transcription of RANTES/CCL5, but not MIP-1α (Holven et al. 2006). Suggesting that during the early inflammatory phase of atherosclerosis, the crucial mediator might be leukocyte-derived RANTES (Holven et al. 2006). Lipid-lowering drugs have been hypothesized to impact inflammatory biomarkers in FH patients. A study by Semb et al demonstrated that FH patients have increased serum levels of sCD40L (about 27-folds) as compared to normal controls, while 2-year-long statin treatment reduced sCD40 levels by 40% (Semb et al. 2003). In another study, PBMCs obtained from FH patients and treated with statins for a long time (median 17 years) displayed higher expression levels of 4-1BB (CD137), CD40, TNFR1, TNFR2, and TRAIL when compared with control subjects (Holven et al. 2014). However, serum concentrations of CD40L and CD137 were similar between FH patients and controls (Holven et al. 2014). This is in accordance with a previous report from a cohort of FH children in which serum sCD40L levels were comparable to those of healthy siblings and pravastatin treatment did not modify them (Ueland et al. 2006). Also, Hovland et al. reported no significant alterations in inflammatory state among statin-treated FH patients and healthy controls (Hovland et al. 2010). Considering the pathophysiological

involvement of TNF-related molecules in FH, the use of novel anti-inflammatory treatments on top of lipid-lowering agents in highest tolerable doses in FH patients could be also suggested. For instance, the use of PCSK9 monoclonal antibodies in FH patients did not only affect plasma values of LDL, but significantly reduced the expression of CCR2 mRNA in PBMCs, monocyte migratory ability, and intracellular lipid content (Bernelot Moens et al. 2017; Pecin et al. 2017; Reiner 2018). These data suggest a pro-inflammatory role for LDL on peripheral monocytes in FH patients, which can be reversed by cholesterol-lowering therapies.

7 OxLDL

OxLDL particles are produced by lipid peroxidation due to the action of oxygen-derived free radicals on native LDL. OxLDL are thought to be key mediators in the context of atherosclerosis as previously discussed. Previous studies showed that FH patients have higher OxLDL levels when compared to those without FH (Real et al. 2010a). Increased OxLDL levels were also observed in FH children when compared to non-FH children. Of interest, OxLDL values are significantly correlated with the expression of OX40L, TRAILR1, and BAFF-receptor, deeply involved in inflammation (Narverud et al. 2013a; Jehlička et al. 2009). In PBMCs from FH patients, OxLDL induces gene expression of TRAILR1, TRAILR4, and BAFF-receptor (Narverud et al. 2013a). Moreover, in vitro experiments revealed that OX40L promotes OxLDL-induced expression of MMP-9 in human monocytes (Narverud et al. 2013a). Furthermore, higher OxLDL have been reported in patients with HeFH particularly when showing Achilles tendon xanthoma (Nielsen et al. 2015). In this population, regression analysis demonstrated that OxLDL is a strong predictor of MMP levels and regulates monocyte expression of pro-atherosclerotic and pro-inflammatory genes by interaction with its scavenger receptor CD36 (Nielsen et al. 2015). Modified LDL epitopes including OxLDL are found within macrophages of FH patients with tendon xanthoma (Sugiyama et al. 1992). Interestingly, macrophages of FH patients with Achilles tendon xanthoma have greater intracellular cholesterol ester pooling and a unique gene expression pattern as compared to those of patients without tendon lesion (Sugiyama et al. 1992). Accordingly, the occurrence of xanthomas in FH patients could be explained by distinctive gene expression profile (including several pro-inflammatory chemokines), which enhances the transformation of macrophages into foam cells (Artieda et al. 2005).

OxLDL is associated with and predicts acute CVD events in apparently healthy subjects and is thought to be a promising risk marker for CV events (Holvoet et al. 2004; Tsimikas et al. 2003; Nordin Fredrikson et al. 2003; Meisinger et al. 2005; Gao and Liu 2017). This evidence still needs specific validation in FH patients. Being modified self-lipoprotein, OxLDLs can trigger an adaptive immune response eventually leading to formation of anti-OxLDL autoantibodies (Zhang et al. 2015). Based on the existing evidence, IgG autoantibodies might be directly associated with CVD events, while IgM autoantibodies seem to have a protective profile (Shoenfeld

et al. 2004; Karvonen et al. 2003). Of interest, when compared to unaffected siblings, FH children are characterized by elevated levels of total immune complex per apoB and malondialdehyde-LDL autoantibodies (Rodenburg et al. 2006). Lipid-lowering therapy was able to reduce circulating autoantibodies in the same cohort (Rodenburg et al. 2006). Interference due to lipid-lowering therapy might account for some apparent discordant findings in this field (Barros et al. 2006). Further investigations are needed to confirm the role of autoantibodies against modified LDL in atherosclerosis and dissect their potential function as CV risk biomarkers in the specific FH setting.

Paraoxonase type 1 (PON1) is a HDL-related enzyme capable of hydrolyzing different substrates among which are oxidative pro-oxidant species (van den Berg et al. 2019). For this reason, PON1 was hypothesized to protect against atherosclerosis. Despite this, in FH patients no association was found between peripheral concentration of PON1 and carotid IMT, levels of OxLDL and hs-CRP (van Himbergen et al. 2005). More recently, PON1 esterase activity was found to be reduced in FH patients as compared to healthy relatives (Idrees et al. 2018). These results are still very preliminary and should be interpreted with caution; more evidence is needed to assess the potential role of PON1 in FH-related atherosclerosis.

8 Lipoprotein-Associated Phospholipase A2

Lipoprotein-associated phospholipase A2 (Lp-PLA2) is a calcium-independent catalytic enzyme predominantly synthetized in macrophages (De Stefano et al. 2019). Lp-PLA2 is thought to hold pro-atherogenic function by its pro-inflammatory and pro-oxidant activity (Stafforini 2009). Through hydrolysis of oxidized phos pholipid molecules, Lp-PLA2 produces bioactive substances including lysophosphatidylcholine and oxidized non-esterified free fatty acids (FFAs) and modifies OxLDL (Caslake et al. 2000). Also, Lp-PLA2 participates in endothelial dysfunction (Yang et al. 2006), aortic wall inflammation and affects vulnerability of plaques with thin caps (Weintraub 2008; Tsimikas et al. 2007). Lp-PLA2 circulates together with Lp(a) and apoB-100 containing lipoproteins, mainly LDL (~80%) and HDL (~20%) (Tsimikas et al. 2007; Saougos et al. 2007; Blencowe et al. 1995). A considerable amount of evidence supports the idea that increased concentrations of Lp-PLA2 are associated with higher risk of coronary heart disease, stroke, and general vascular morbidity and mortality (Collaboration L-PS 2010; Wallentin et al. 2016; Tibuakuu et al. 2018; Garg et al. 2015, 2016).

It has been reported that hypercholesterolemic patients without FH have lower Lp-PLA2 activity when compared with patients with clinically confirmed FH diagnosis independently of circulating lipoprotein values (Mattina et al. 2018). The increased Lp-PLA2 activity might account for the enhanced arterial inflammation as reported in FH patients and participate in premature onset of CV events (Mattina et al. 2018). In children with FH, Lp-PLA2 mass and activity were also considerably

higher in comparison with unaffected siblings, but Lp(a) levels and carotid IMT were not (Ryu et al. 2011). In addition, after 2 years of statin therapy Lp-PLA2 mass and activity were significantly decreased and net-changes in Lp-PLA2 activity positively correlated with the changes in LDL-C levels (Ryu et al. 2011). Summarizing, the predictive role of Lp-PLA2 on CV events in FH patients still requires further investigations.

HDL particles have several athero- and vasculo-protective features such as reverse cholesterol transport, anti-oxidant and anti-inflammatory properties (Ganjali et al. 2017, 2018; Chapman et al. 2011). A specific sub-fraction, HDL3 particles in normolipidemic subjects effectively prevent vascular injury caused by LDL. In FH patients, anti-oxidative and anti-inflammation properties of HDL3, which prevent deposition of OxLDL in vessels, are decreased by up to three-fold (Hussein et al. 2016). Moreover, surface lipids of HDL are decreased, while the amount of core lipids is increased in FH. This ratio is directly associated with the anti-oxidant and anti-inflammatory characteristics of HDL which are suboptimal in FH patients (Hussein et al. 2016).

9 $CD16^{+}$Monocytes

Peripheral monocytes are heterogeneous and two main subsets have been described according to surface expression of CD14 and CD16 (Ghattas et al. 2013; Ziegler-Heitbrock 1996). It is well known that in early reversible stage of atherosclerotic process, inflammatory lesions are mainly consisting of monocyte-derived macrophages with high CD16 and low CD14 expression (Häkkinen et al. 2000). At this stage, the activation of $CD16^{pos}$ monocytes by the Toll-like receptor (TLR)-4/-2 ligands leads to increased TNF-α and decreased IL-10 mRNA transcription levels. Thus, $CD16^{pos}$ monocytes are generally thought to be pro-inflammatory cells (Belge et al. 2002). Also, $CD16^{pos}$ monocytes have elevated phagocytosis capability and higher tendency to adhere to the endothelium as a result of LDL and OxLDL infiltration (Mosig et al. 2009). $CD16^{pos}$ monocytes express and generate inflammatory mediators and chemokine receptors, which are involved in atherosclerotic process (Ancuta et al. 2003; Tacke et al. 2007). Uptake of OxLDL via CD36 in monocytes results in over-expression of this scavenger receptor via induction of transcription factors NF-κB and peroxisome proliferator-activated receptor (PPAR)-γ. As a result of this vicious circle, macrophages undergo phenotypic alteration and become atherogenic foam cells (Gurnell 2003; Tak and Firestein 2001). Yet, all monocyte subsets have been described in advanced atherosclerotic plaques (Hansson 2005).

FH patients have increased amount of intermediate $CD14^{++}CD16^{+}$ monocytes (Nielsen et al. 2015). Additionally, their transcription of pro-atherosclerotic and pro-inflammatory genes in response to OxLDL–CD36 interaction is significantly elevated, particularly in patients with Achilles tendon xanthoma (Nielsen et al. 2015). Also, $CD16^{pos}$ monocytes from FH patients show an increased uptake of

OxLDL-C via the scavenger receptor CD36, while $CD16^{neg}$ monocytes from FH subjects preferentially uptake native LDL particles (Mosig et al. 2009). $CD16^{pos}$ monocytes of FH patients are more mature as compared to $CD16^{pos}$ of healthy persons. It has been speculated that $CD16^{pos}$ monocytes evolve and more quickly transform into macrophages as a reaction to OxLDL which also stimulates cell apoptosis (Wintergerst et al. 2000; Kashiwakura et al. 2004). The potential role of monocyte and their subset as predictive markers of CV disease in the setting of FH still requires further investigations.

10 Mean Platelet Volume

Platelets from clinically diagnosed FH patients are highly active, easy to activate, and show reduced circulating life (Blaha et al. 2004; Betteridge et al. 1994). Platelet activation plays an important role in both early and advanced atherogenesis in patients with FH (Heidari-Bakavoli et al. 2018). Among many platelet parameters, mean platelet volume (MPV) as a marker of platelet activity appears to be promising (Heidari-Bakavoli et al. 2018). Indeed, an increased MPV is associated with larger and excessive reactive platelets with more metabolic, enzymatic, and coagulation potential (Kamath et al. 2001; Park et al. 2002). Reactive platelets are associated with higher levels of prothrombotic substances, thromboxane, and glycoproteins which enhance their aggregability (Vizioli et al. 2009). Many data have demonstrated increased prothrombotic tendency and activity in platelets from dyslipidemia patients (Georgieva et al. 2004; Khemka and Kulkarni 2014). Also, it has been shown that FH patients have remarkably increased MPV levels, but lower platelet count when compared to controls (Icli et al. 2016). Of interest, MPV is independently correlated with total cholesterol in clinically diagnosed FH patients (Icli et al. 2016).

11 Neopterin

Activated blood-derived macrophages contribute throughout the whole atherogenesis process (Liberale et al. 2017; Ross 1999; Robbie and Libby 2001). Neopterin is produced in macrophages stimulated with interferon gamma (IFN-γ) as a result of guanosine triphosphate (GTP) catabolism. Accordingly, neopterin is an inflammation product considered to be a general marker of cellular immunity (Murr et al. 2002) as well as an indicator of activation of T helper cells (Th) type 1 (Wachter et al. 1989), whose main product is IFN-γ.

Two comparable studies reported increased levels of neopterin in HeFH children as compared to controls or unaffected siblings. Furthermore, BMI and HDL-C were independent predictors of neopterin in these subjects (Ueland et al. 2006; Holven et al. 2006). However, the first reports suggest such a difference not to be conserved

in adult HeFH patients (Holven et al. 2006). Although this observation may be due to the rather low number of adults enrolled, it may also indicate a unique pattern of macrophage activation in HeFH adults and children (Holven et al. 2006). Although IFN-γ activates the pathways responsible for elevation of neopterin concentrations in different pathologic states, no significant differences were found on IFN-γ expression in stimulated T-cells from children with HeFH and healthy controls (Holven et al. 2006). This observation might be explained by the fact that neopterin is not only regulated through IFN-γ (Holven et al. 2006). Indeed several cytokines such as IL-1, IL-6, and TNF-α modulate monocyte activation and thus might modulate neopterin levels, and some of these cytokines possibly have an important role in low-grade inflammation in FH children (Holven et al. 2006). Despite very preliminary, these findings might suggest the important role of chronic Th1-induced monocyte/macrophage over-activation in the early onset of atherosclerosis (Ueland et al. 2006; Holven et al. 2006).

12 CV Risk Assessment in Patients with FH

Differences in incidence of CV events remain a major unsolved issue for patients with FH and this is reflected by the availability of different CV risk scores. Different studies demonstrated that traditional CV risk factors are not totally overwhelmed by the high LDL levels in FH patients and they still hold important predictive value also in such a particular population (Kramer et al. 2006; et al. 2019). In the SAFEHEART-Risk Equation, CV risk in FH is estimated based on age, sex, BMI, levels of LDL and Lp(a), history of CV disease, hypertension, or smoking (et al. 2019; Mata and Alonso 2018). An expert consensus from the International Atherosclerosis Society (IAS) suggests to further define FH patients in severe and non-severe FH with the former being characterized by severely elevated levels of LDL (>400 mg/dL) or milder elevation of LDL (>310 mg/dL or>190 mg/dL) with respectively one or high-risk features (Santos et al. 2016). These supplementary risk factors include those listed for the SAFEHEART-Risk Equation while also taking into consideration low HDL levels or presence of diabetes mellitus, chronic kidney disease, and familial history of early CV afflictions (Santos et al. 2016). Interestingly, the IAS risk stratification also includes the diagnosis of advanced coronary disease as assessed by coronary artery calcium score or degree of obstruction at CT angiography. In this sense, CV imaging techniques are thought to provide crucial information to guide the prognostic assessment of patients with FH and are fundamental for providing an adequate CV assessment in studies investigating potential novel risk biomarkers. With particular reference to potential inflammatory risk biomarkers, FDG-PET may represent an important additional value providing direct evidence of inflammatory activity of the vessel/plaque and allowing direct correlation with circulating markers (Joshi et al. 2018; Duivenvoorden et al. 2013). None of the previously mentioned inflammatory biomarkers has so far provided enough sensitivity and specificity to be included in any CV risk prediction algorithms for

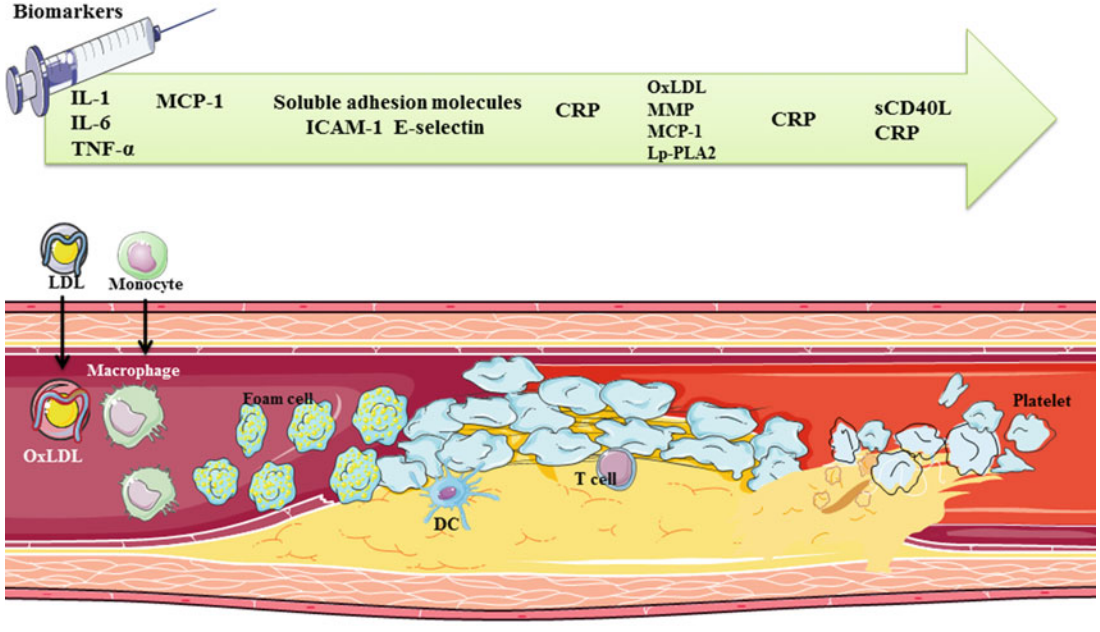

Fig. 2 Promising inflammatory biomarkers in familial hypercholesterolemia. *CRP* C-reactive protein, *DC* dendritic cell, *ICAM-1* intercellular adhesion molecule-1, *IL* interleukin, *MCP-1* monocyte chemo-attractant protein 1, *Lp-PLA2* Lipoprotein-associated phospholipase A2, *MMPs* matrix metalloproteinases, *OxLDL* oxidized LDL, *TNF-α* tumor necrosis factor-alpha

FH patients. This is likely due to many reasons including different limitations of studies so far investigating this hypothesis. Some of them enrolled heterogeneous cohorts of FH patients without genetic characterization which are likely to include patients with familial combined hyperlipidemia and metabolic syndrome. Also, patients with FH are often affected by metabolic syndrome which associates with increased levels of inflammatory biomarkers on its own thus adding even more variability to the literature. Solid large, longitudinal data from registry cohorts enrolling patients with definite disease diagnosis and optimal patient characterization—including comorbidities and imaging characterization of the coronary three—are needed to investigate whether inflammatory biomarkers might provide additional value to CV risk stratification in FH.

13 Conclusion

Atherosclerotic complications are leading causes of mortality in FH patients. In the last decades, our understanding of atherosclerosis pathophysiology revealed a previously unexpected pivotal role for inflammation in this process. Accordingly, inflammatory mediators became interesting markers of disease as well as therapeutic targets to counteract plaque initiation and progression. In FH patients, the enhanced inflammation may account for part of the increased CV risk and anti-inflammatory interventions on top of optimal lipid-lowering therapy may effectively reduce the incidence of major CV events. Yet, whether inflammatory biomarkers may be of help in stratifying the risk of this highly heterogenic population remains to be fully assessed (Fig. 2). Available evidence suggests that the predictive role of each inflammatory mediator may vary depending on the age of FH subjects and the stage of the atherosclerotic disease. Further prospective studies are needed to elucidate whether measurements of these inflammatory biomarkers, alone or in combination, will provide added value in the identification of those patients at higher CV risk who will benefit from more intense pharmacological interventions.

Conflict of Interest None.

Funding None.

References

Ancuta P, Rao R, Moses A, Mehle A, Shaw SK, Luscinskas FW et al (2003) Fractalkine preferentially mediates arrest and migration of CD16+ monocytes. J Exp Med 197(12):1701–1707

Artieda M, Cenarro A, Junquera C, Lasierra P, Martínez-Lorenzo MJ, Pocoví M et al (2005) Tendon xanthomas in familial hypercholesterolemia are associated with a differential inflammatory response of macrophages to oxidized LDL. FEBS Lett 579(20):4503–4512

Barros MRAC, Bertolami MC, Abdalla DSP, Ferreira WP (2006) Identification of mildly oxidized low-density lipoprotein (electronegative LDL) and its auto-antibodies IgG in children and adolescents hypercholesterolemic offsprings. Atherosclerosis 184(1):103–107

Belge K-U, Dayyani F, Horelt A, Siedlar M, Frankenberger M, Frankenberger B et al (2002) The proinflammatory CD14+ CD16+ DR++ monocytes are a major source of TNF. J Immunol 168 (7):3536–3542

Benn M, Watts GF, Tybjaerg-Hansen A, Nordestgaard BG (2012) Familial hypercholesterolemia in the Danish general population: prevalence, coronary artery disease, and cholesterol-lowering medication. J Clin Endocrinol Metabol 97(11):3956–3964

Bergheanu SC, Bodde MC, Jukema JW (2017) Pathophysiology and treatment of atherosclerosis: current view and future perspective on lipoprotein modification treatment. Neth Heart J 25 (4):231–242

Bernelot Moens SJ, Neele AE, Kroon J, van der Valk FM, Van den Bossche J, Hoeksema MA et al (2017) PCSK9 monoclonal antibodies reverse the pro-inflammatory profile of monocytes in familial hypercholesterolaemia. Eur Heart J 38(20):1584–1593

Betteridge D, Cooper M, Saggerson E, Prichard B, Tan K, Ling E et al (1994) Platelet function in patients with hypercholesterolaemia. Eur J Clin Investig 24(S1):30–33

Blaha M, Pecka M, Urbankova J, Blaha V, Maly J, Zadak Z et al (2004) Activity of thrombocytes as a marker of sufficient intensity of LDL-apheresis in familial hypercholesterolaemia. Transfus Apher Sci 30(2):83–87

Blankenberg S, Barbaux S, Tiret L (2003) Adhesion molecules and atherosclerosis. Atherosclerosis 170(2):191–203

Blencowe C, Hermetter A, Kostner GM, Deigner HP (1995) Enhanced association of platelet-activating factor acetylhydrolase with lipoprotein (a) in comparison with low density lipoprotein. J Biol Chem 270(52):31151–31157

Bonaventura A, Liberale L, Carbone F, Vecchie A, Diaz-Canestro C, Camici GG et al (2018) The pathophysiological role of neutrophil extracellular traps in inflammatory diseases. Thromb Haemost 118(1):6–27

Caslake MJ, Packard CJ, Suckling KE, Holmes SD, Chamberlain P, Macphee CH (2000) Lipoprotein-associated phospholipase A2, platelet-activating factor acetylhydrolase: a potential new risk factor for coronary artery disease. Atherosclerosis 150(2):413–419

Chapman MJ, Ginsberg HN, Amarenco P, Andreotti F, Boren J, Catapano AL et al (2011) Triglyceride-rich lipoproteins and high-density lipoprotein cholesterol in patients at high risk of cardiovascular disease: evidence and guidance for management. Eur Heart J 32 (11):1345–1361

Charakida M, Tousoulis D, Skoumas I, Pitsavos C, Vasiliadou C, Stefanadi E et al (2009) Inflammatory and thrombotic processes are associated with vascular dysfunction in children with familial hypercholesterolemia. Atherosclerosis 204(2):532–537

Cheng H, Ye Z, Chiou K, Lin S, Charng M (2007a) Vascular stiffness in familial hypercholesterolaemia is associated with C-reactive protein and cholesterol burden. Eur J Clin Investig 37(3):197–206

Cheng HM, Ye ZX, Chiou KR, Lin SJ, Charng MJ (2007b) Vascular stiffness in familial hypercholesterolaemia is associated with C-reactive protein and cholesterol burden. Eur J Clin Investig 37(3):197–206

Civeira F (2004) Hypercholesterolemia IPoMoF. Guidelines for the diagnosis and management of heterozygous familial hypercholesterolemia. Atherosclerosis 173(1):55–68

Collaboration L-PS (2010) Lipoprotein-associated phospholipase A2 and risk of coronary disease, stroke, and mortality: collaborative analysis of 32 prospective studies. Lancet 375 (9725):1536–1544

De Stefano A, Mannucci L, Tamburi F, Cardillo C, Schinzari F, Rovella V et al (2019) Lp-PLA2, a new biomarker of vascular disorders in metabolic diseases. Int J Immunopathol Pharmacol 33:2058738419827154

Deshmane SL, Kremlev S, Amini S, Sawaya BE (2009) Monocyte chemoattractant protein-1 (MCP-1): an overview. J Interf Cytokine Res 29(6):313–326

Dostert C, Grusdat M, Letellier E, Brenner D (2018) The TNF family of ligands and receptors: communication modules in the immune system and beyond. Physiol Rev 99(1):115–160

Duivenvoorden R, Mani V, Woodward M, Kallend D, Suchankova G, Fuster V et al (2013) Relationship of serum inflammatory biomarkers with plaque inflammation assessed by FDG PET/CT: the dal-PLAQUE study. JACC Cardiovasc Imaging 6(10):1087–1094

El Messal M, Beaudeux J-L, Drissi A, Giral P, Chater R, Bruckert E et al (2006) Elevated serum levels of proinflammatory cytokines and biomarkers of matrix remodeling in never-treated patients with familial hypercholesterolemia. Clin Chim Acta 366(1–2):185–189

Enayati S, Seifirad S, Amiri P, Abolhalaj M, Mohammad-Amoli M (2015) Interleukin-1 beta, interferon-gamma, and tumor necrosis factor-alpha gene expression in peripheral blood mononuclear cells of patients with coronary artery disease. ARYA Atherosclerosis 11(5):267

Ferrieres J, Lambert J, Lussier-Cacan S, Davignon J (1995) Coronary artery disease in heterozygous familial hypercholesterolemia patients with the same LDL receptor gene mutation. Circulation 92(3):290–295

França CN, Izar MC, Hortêncio MN, do Amaral JB, Ferreira CE, Tuleta ID et al (2017) Monocyte subtypes and the CCR2 chemokine receptor in cardiovascular disease. Clin Sci 131 (12):1215–1224

Galkina E, Ley K (2007) Vascular adhesion molecules in atherosclerosis. Arterioscler Thromb Vasc Biol 27(11):2292–2301

Ganjali S, Momtazi AA, Banach M, Kovanen PT, Stein EA, Sahebkar A (2017) HDL abnormalities in familial hypercholesterolemia: focus on biological functions. Prog Lipid Res 67:16–26

Ganjali S, Momtazi-Borojeni AA, Banach M, Kovanen PT, Gotto AM Jr, Sahebkar A (2018) HDL functionality in familial hypercholesterolemia: effects of treatment modalities and pharmacological interventions. Drug Discov Today 23(1):171–180

Gao S, Liu J (2017) Association between circulating oxidized low-density lipoprotein and atherosclerotic cardiovascular disease. Chronic Dis Trans Med 3(2):89–94

Garg PK, McClelland RL, Jenny NS, Criqui MH, Greenland P, Rosenson RS et al (2015) Lipoprotein-associated phospholipase A2 and risk of incident cardiovascular disease in a multi-ethnic cohort: the multi ethnic study of atherosclerosis. Atherosclerosis 241(1):176–182

Garg PK, Arnold AM, Hinckley Stukovsky KD, Koro C, Jenny NS, Mukamal KJ et al (2016) Lipoprotein-associated phospholipase A2 and incident peripheral arterial disease in older adults: the cardiovascular health study. Arterioscler Thromb Vasc Biol 36(4):750–756

Georgieva AM, Ten Cate H, Keulen ET, van Oerle R, Govers-Riemslag JW, Hamulyák K et al (2004) Prothrombotic markers in familial combined hyperlipidemia: evidence of endothelial cell activation and relation to metabolic syndrome. Atherosclerosis 175(2):345–351

Ghattas A, Griffiths HR, Devitt A, Lip GY, Shantsila E (2013) Monocytes in coronary artery disease and atherosclerosis: where are we now? J Am Coll Cardiol 62(17):1541–1551

Gidding SS, Ann Champagne M, de Ferranti SD, Defesche J, Ito MK, Knowles JW et al (2015) The agenda for familial hypercholesterolemia: a scientific statement from the American Heart Association. Circulation 132(22):2167–2192

Gissler MC, Willecke F, Anto Michel N, Härtner C, Hilgendorf I, Wolf D et al (2016) The role of CD40 in endothelial and smooth muscle cells in atherosclerosis. Circulation 134(Suppl_1): A18410-A

Gokalp D, Tuzcu A, Bahceci M, Arikan S, Pirinccioglu AG, Bahceci S (2009) Levels of proinflammatory cytokines and hs-CRP in patients with homozygous familial hypercholesterolaemia. Acta Cardiol 64(5):603–609

Goldstein JL, Brown MS (2009) The LDL receptor. Arterioscler Thromb Vasc Biol 29(4):431–438

Goswami B, Rajappa M, Mallika V, Shukla DK, Kumar S (2009) TNF-alpha/IL-10 ratio and C-reactive protein as markers of the inflammatory response in CAD-prone north Indian patients with acute myocardial infarction. Clin Chim Acta 408(1–2):14–18

Guardamagna O, Abello F, Saracco P, Baracco V, Rolfo E, Pirro M (2009) Endothelial activation, inflammation and premature atherosclerosis in children with familial dyslipidemia. Atherosclerosis 207(2):471–475
Gurnell M (2003) PPARγ and metabolism: insights from the study of human genetic variants. Clin Endocrinol 59(3):267–277
Häkkinen T, Karkola K, Ylä-Herttuala S (2000) Macrophages, smooth muscle cells, endothelial cells, and T-cells express CD40 and CD40L in fatty streaks and more advanced human atherosclerotic lesions. Virchows Arch 437(4):396–405
Han X, Boisvert WA (2015) Interleukin-10 protects against atherosclerosis by modulating multiple atherogenic macrophage function. Thromb Haemost 113(3):505–512
Hansson GK (2001) Immune mechanisms in atherosclerosis. Arterioscler Thromb Vasc Biol 21 (12):1876–1890
Hansson GK (2005) Inflammation, atherosclerosis, and coronary artery disease. N Engl J Med 352 (16):1685–1695
Hansson GK, Libby P (2006) The immune response in atherosclerosis: a double-edged sword. Nat Rev Immunol 6(7):508
Hansson GK, Libby P, Tabas I (2015) Inflammation and plaque vulnerability. J Intern Med 278 (5):483–493
Heidari-Bakavoli A, Hassanian SM, Avan A, Shafiee M, Bahrami A, Tayefi M et al (2018) Hypertriglyceridemia is associated with white blood cell count and red cell distribution width: a gender stratified analysis in a population-based study. Acta MedIran 56(10):645
Hein TW, Singh U, Vasquez-Vivar J, Devaraj S, Kuo L, Jialal I (2009) Human C-reactive protein induces endothelial dysfunction and uncoupling of eNOS in vivo. Atherosclerosis 206(1):61–68
Holven KB, Myhre AM, Aukrust P, Hagve TA, Ose L, Nenseter MS (2003) Patients with familial hypercholesterolaemia show enhanced spontaneous chemokine release from peripheral blood mononuclear cells ex vivo: dependency of xanthomas/xanthelasms, smoking and gender. Eur Heart J 24(19):1756–1762
Holven KB, Damås JK, Yndestad A, Wæhre T, Ueland T, Halvorsen B et al (2006) Chemokines in children with heterozygous familiar hypercholesterolemia: selective upregulation of RANTES. Arterioscler Thromb Vasc Biol 26(1):200–205
Holven KB, Narverud I, Lindvig HW, Halvorsen B, Langslet G, Nenseter MS et al (2014) Subjects with familial hypercholesterolemia are characterized by an inflammatory phenotype despite long-term intensive cholesterol lowering treatment. Atherosclerosis 233(2):561–567
Holvoet P, Kritchevsky SB, Tracy RP, Mertens A, Rubin SM, Butler J et al (2004) The metabolic syndrome, circulating oxidized LDL, and risk of myocardial infarction in well-functioning elderly people in the health, aging, and body composition cohort. Diabetes 53(4):1068–1073
Hovland A, Aagnes I, Brekke O-L, Flage JH, Lappegård KT (2010) No evidence of impaired endothelial function or altered inflammatory state in patients with familial hypercholesterolemia treated with statins. J Clin Lipidol 4(4):288–292
Hussein H, Saheb S, Couturier M, Atassi M, Orsoni A, Carrié A et al (2016) Small, dense high-density lipoprotein 3 particles exhibit defective antioxidative and anti-inflammatory function in familial hypercholesterolemia: partial correction by low-density lipoprotein apheresis. J Clin Lipidol 10(1):124–133
Icli A, Aksoy F, Nar G, Kaymaz H, Alpay MF, Nar R et al (2016) Increased mean platelet volume in familial hypercholesterolemia. Angiology 67(2):146–150
Idrees M, Siddiq AR, Ajmal M, Akram M, Khalid RR, Hussain A et al (2018) Decreased serum PON1 arylesterase activity in familial hypercholesterolemia patients with a mutated LDLR gene. Genet Mol Biol 41(3):570–577
Iosif KP, Toutouzas K, Benetos G, Skoumas I, Kafouris P, Georgakopoulos A et al (2017) Increased subclinical systemic and vascular inflammation in familial combined hyperlipidemia compared to heterozygous hypercholesterolemia: insights from a positron emission tomography study. J Am College Cardiol 69(11):1519

Iwata H, Nagai R (2012) Novel immune signals and atherosclerosis. Curr Atheroscler Rep 14 (5):484–490

Jansen AC, van Wissen S, Defesche JC, Kastelein JJ (2002) Phenotypic variability in familial hypercholesterolaemia: an update. Curr Opin Lipidol 13(2):165–171

Jehlička P, Stožický F, Mayer O Jr, Varvařovská J, Racek J, Trefil L et al (2009) Asymmetric dimethylarginine and the effect of folate substitution in children with familial hypercholesterolemia and diabetes mellitus type 1. Physiol Res 58(2)

Johnston N, Jernberg T, Lagerqvist B, Siegbahn A, Wallentin L (2006) Oxidized low-density lipoprotein as a predictor of outcome in patients with unstable coronary artery disease. Int J Cardiol 113(2):167–173

Joshi AA, Lerman JB, Dey AK, Sajja AP, Belur AD, Elnabawi YA et al (2018) Association between aortic vascular inflammation and coronary artery plaque characteristics in psoriasis. JAMA Cardiol 3(10):949–956

Kamath S, Blann A, Lip G (2001) Platelet activation: assessment and quantification. Eur Heart J 22 (17):1561–1571

Karbiner MS, Sierra L, Minahk C, Fonio MC, Bruno MP, Jerez S (2013) The role of oxidative stress in alterations of hematological parameters and inflammatory markers induced by early hypercholesterolemia. Life Sci 93(15):503–508

Karvonen J, Paivansalo M, Kesaniemi YA, Horkko S (2003) Immunoglobulin M type of autoantibodies to oxidized low-density lipoprotein has an inverse relation to carotid artery atherosclerosis. Circulation 108(17):2107–2112

Kashiwakura Y, Watanabe M, Kusumi N, Sumiyoshi K, Nasu Y, Yamada H et al (2004) Dynamin-2 regulates oxidized low-density lipoprotein–induced apoptosis of vascular smooth muscle cell. Circulation 110(21):3329–3334

Kastelein JJ, Wiegman A, de Groot E (2003) Surrogate markers of atherosclerosis: impact of statins. Atheroscler Suppl 4(1):31–36

Khemka R, Kulkarni K (2014) Study of relationship between platelet volume indices and hyperlipidemia. Ann Pathol Lab Med 1(1):8–14

Khera A, de Lemos JA, Peshock R, Lo SH, Stanek GH, Murphy SA et al (2005) Relationship between C-reactive protein and subclinical atherosclerosis. The Dallas heart study. Circulation 113:38–43

Kinlay S, Selwyn AP (2003) Effects of statins on inflammation in patients with acute and chronic coronary syndromes. Am J Cardiol 91(4):9–13

Kramer A, Jansen AC, van Aalst-Cohen ES, Tanck MW, Kastelein JJ, Zwinderman AH (2006) Relative risk for cardiovascular atherosclerotic events after smoking cessation: 6-9 years excess risk in individuals with familial hypercholesterolemia. BMC Public Health 6:262

Kugiyama K, Sakamoto T, Misumi I, Sugiyama S, Ohgushi M, Ogawa H et al (1993) Transferable lipids in oxidized low-density lipoprotein stimulate plasminogen activator inhibitor-1 and inhibit tissue-type plasminogen activator release from endothelial cells. Circ Res 73(2):335–343

Kumari R, Kumar S, Ahmad MK, Singh R, Pradhan A, Chandra S et al (2018) TNF-alpha/IL-10 ratio: an independent predictor for coronary artery disease in north Indian population. Diabetes Metab Syndr 12(3):221–225

Lakoski SG, Cushman M, Blumenthal RS, Kronmal R, Arnett D, D'Agostino RB Jr et al (2007) Implications of C-reactive protein or coronary artery calcium score as an adjunct to global risk assessment for primary prevention of CHD. Atherosclerosis 193(2):401–407

Lee IM, Cook NR, Gaziano JM, Gordon D, Ridker PM, Manson JE et al (2005) Vitamin E in the primary prevention of cardiovascular disease and cancer: the Women's health study: a randomized controlled trial. JAMA 294(1):56–65

Ley K (2002) Integration of inflammatory signals by rolling neutrophils. Immunol Rev 186(1):8–18

Libby P (2002) Inflammation in atherosclerosis. Nature 420(6917):868–874

Liberale L, Dallegri F, Montecucco F, Carbone F (2017) Pathophysiological relevance of macrophage subsets in atherogenesis. Thromb Haemost 117(1):7–18

Linton MF, Fazio S (2001) Class A scavenger receptors, macrophages, and atherosclerosis. Curr Opin Lipidol 12(5):489–495

Mallat Z, Besnard S, Duriez M, Deleuze V, Emmanuel F, Bureau MF et al (1999) Protective role of interleukin-10 in atherosclerosis. Circ Res 85(8):e17–e24

Martinez LR, Miname MH, Bortolotto LA, Chacra AP, Rochitte CE, Sposito AC et al (2008) No correlation and low agreement of imaging and inflammatory atherosclerosis' markers in familial hypercholesterolemia. Atherosclerosis 200(1):83–88

Mata P, Alonso R, Perez de Isla L (2018) Atherosclerotic cardiovascular disease risk assessment in familial hypercholesterolemia: does one size fit all? Curr Opin Lipidol 29(6):445–452

Mattina A, Rosenbaum D, Bittar R, Bonnefont-Rousselot D, Noto D, Averna M et al (2018) Lipoprotein-associated phospholipase A2 activity is increased in patients with definite familial hypercholesterolemia compared with other forms of hypercholesterolemia. Nutr Metab Cardiovasc Dis 28(5):517–523

Mawhin M-A (2017) Role of neutrophils and leukotrienes in atherosclerotic plaque destabilisation: implication of endotoxemia. Strasbourg

McNeely MJ, Edwards KL, Marcovina SM, Brunzell JD, Motulsky AG, Austin MA (2001) Lipoprotein and apolipoprotein abnormalities in familial combined hyperlipidemia: a 20-year prospective study. Atherosclerosis 159(2):471–481

Meisinger C, Baumert J, Khuseyinova N, Loewel H, Koenig W (2005) Plasma oxidized low-density lipoprotein, a strong predictor for acute coronary heart disease events in apparently healthy, middle-aged men from the general population. Circulation 112(5):651–657

Monaco C, Andreakos E, Kiriakidis S, Mauri C, Bicknell C, Foxwell B et al (2004) Canonical pathway of nuclear factor κB activation selectively regulates proinflammatory and prothrombotic responses in human atherosclerosis. Proc Natl Acad Sci 101(15):5634–5639

Montecucco F, Liberale L, Bonaventura A, Vecchie A, Dallegri F, Carbone F (2017) The role of inflammation in cardiovascular outcome. Curr Atheroscler Rep 19(3):11

Moorjani S, Torres A, Gagn C, Brun D, Lupien P, Roy M et al (1993) Mutations of low-density-lipoprotein-receptor gene, variation in plasma cholesterol, and expression of coronary heart disease in homozygous familial hypercholesterolaemia. Lancet 341(8856):1303–1306

Mosig S, Rennert K, Krause S, Kzhyshkowska J, Neunübel K, Heller R et al (2009) Different functions of monocyte subsets in familial hypercholesterolemia: potential function of CD14+ CD16+ monocytes in detoxification of oxidized LDL. FASEB J 23(3):866–874

Murr C, Widner B, Wirleitner B, Fuchs D (2002) Neopterin as a marker for immune system activation. Curr Drug Metab 3(2):175–187

Narverud I, Ueland T, Nenseter MS, Retterstøl K, Telle-Hansen VH, Halvorsen B et al (2011a) Children with familial hypercholesterolemia are characterized by an inflammatory imbalance between the tumor necrosis factor α system and interleukin-10. Atherosclerosis 214(1):163–168

Narverud I, Ueland T, Nenseter MS, Retterstol K, Telle-Hansen VH, Halvorsen B et al (2011b) Children with familial hypercholesterolemia are characterized by an inflammatory imbalance between the tumor necrosis factor alpha system and interleukin-10. Atherosclerosis 214 (1):163–168

Narverud I, Halvorsen B, Nenseter M, Retterstøl K, Yndestad A, Dahl T et al (2013a) Oxidized LDL level is related to gene expression of tumour necrosis factor super family members in children and young adults with familial hypercholesterolaemia. J Intern Med 273(1):69–78

Narverud I, Iversen PO, Aukrust P, Halvorsen B, Ueland T, Johansen SG et al (2013b) Maternal familial hypercholesterolaemia (FH) confers altered haemostatic profile in offspring with and without FH. Thromb Res 131(2):178–182

Narverud I, Retterstol K, Iversen PO, Halvorsen B, Ueland T, Ulven SM et al (2014) Markers of atherosclerotic development in children with familial hypercholesterolemia: a literature review. Atherosclerosis 235(2):299–309

Navab M, Ananthramaiah GM, Reddy ST, Van Lenten BJ, Ansell BJ, Fonarow GC et al (2004) The oxidation hypothesis of atherogenesis: the role of oxidized phospholipids and HDL. J Lipid Res 45(6):993–1007

Nielsen MH, Irvine H, Vedel S, Raungaard B, Beck-Nielsen H, Handberg A (2015) Elevated atherosclerosis-related gene expression, monocyte activation and microparticle-release are related to increased lipoprotein-associated oxidative stress in familial hypercholesterolemia. PLoS One 10(4):e0121516

Nordin Fredrikson G, Hedblad B, Berglund G, Nilsson J (2003) Plasma oxidized LDL: a predictor for acute myocardial infarction? J Intern Med 253(4):425–429

Packard RR, Libby P (2008) Inflammation in atherosclerosis: from vascular biology to biomarker discovery and risk prediction. Clin Chem 54(1):24–38

Park Y, Schoene N, Harris W (2002) Mean platelet volume as an indicator of platelet activation: methodological issues. Platelets 13(5–6):301–306

Pasceri V, Willerson JT, Yeh ET (2000) Direct proinflammatory effect of C-reactive protein on human endothelial cells. Circulation 102(18):2165–2168

Pasceri V, Chang J, Willerson JT, Yeh ET (2001) Modulation of C-reactive protein–mediated monocyte chemoattractant protein-1 induction in human endothelial cells by anti-atherosclerosis drugs. Circulation 103(21):2531–2534

Pasterkamp G, Schoneveld AH, van der Wal AC, Hijnen DJ, van Wolveren WJ, Plomp S et al (1999) Inflammation of the atherosclerotic cap and shoulder of the plaque is a common and locally observed feature in unruptured plaques of femoral and coronary arteries. Arterioscler Thromb Vasc Biol 19(1):54–58

Pecin I, Hartgers ML, Hovingh GK, Dent R, Reiner Z (2017) Prevention of cardiovascular disease in patients with familial hypercholesterolaemia: the role of PCSK9 inhibitors. Eur J Prev Cardiol 24(13):1383–1401

Perez de Isla L, Ray KK, Watts GF, Santos RD, Alonso R, Muniz-Grijalvo O et al (2019) Potential utility of the SAFEHEART risk equation for rationalising the use of PCSK9 monoclonal antibodies in adults with heterozygous familial hypercholesterolemia. Atherosclerosis 286:40–45

Pothineni NVK, Karathanasis SK, Ding Z, Arulandu A, Varughese KI, Mehta JL (2017) LOX-1 in atherosclerosis and myocardial ischemia: biology, genetics, and modulation. J Am Coll Cardiol 69(22):2759–2768

Rahman T, Hamzan NS, Mokhsin A, Rahmat R, Ibrahim ZO, Razali R et al (2017) Enhanced status of inflammation and endothelial activation in subjects with familial hypercholesterolaemia and their related unaffected family members: a case control study. Lipids Health Dis 16(1):81

Real J, Martínez-Hervás S, García-García A, Civera M, Pallardó F, Ascaso J et al (2010a) Circulating mononuclear cells nuclear factor-kappa B activity, plasma xanthine oxidase, and low grade inflammatory markers in adult patients with familial hypercholesterolaemia. Eur J Clin Investig 40(2):89–94

Real JT, Martinez-Hervas S, Garcia-Garcia AB, Civera M, Pallardo FV, Ascaso JF et al (2010b) Circulating mononuclear cells nuclear factor-kappa B activity, plasma xanthine oxidase, and low grade inflammatory markers in adult patients with familial hypercholesterolaemia. Eur J Clin Investig 40(2):89–94

Reiner Z (2015) Management of patients with familial hypercholesterolaemia. Nat Rev Cardiol 12 (10):565–575

Reiner Z (2018) PCSK9 inhibitors in clinical practice: expectations and reality. Atherosclerosis 270:187–188

Ridker PM, Cushman M, Stampfer MJ, Tracy RP, Hennekens CH (1997) Inflammation, aspirin, and the risk of cardiovascular disease in apparently healthy men. N Engl J Med 336 (14):973–979

Ridker PM, Everett BM, Thuren T, MacFadyen JG, Chang WH, Ballantyne C et al (2017) Antiinflammatory therapy with Canakinumab for atherosclerotic disease. N Engl J Med 377 (12):1119–1131

Ridker PM, Libby P, MacFadyen JG, Thuren T, Ballantyne C, Fonseca F et al (2018) Modulation of the interleukin-6 signalling pathway and incidence rates of atherosclerotic events and all-cause

mortality: analyses from the Canakinumab anti-inflammatory thrombosis outcomes study (CANTOS). Eur Heart J 39(38):3499–3507
Robbie L, Libby P (2001) Inflammation and atherothrombosis. Ann N Y Acad Sci 947(1):167–180
Rodenburg J, Vissers MN, Wiegman A, Miller ER, Ridker PM, Witztum JL et al (2006) Oxidized low-density lipoprotein in children with familial hypercholesterolemia and unaffected siblings: effect of pravastatin. J Am Coll Cardiol 47(9):1803–1810
Ross R (1999) Atherosclerosis—an inflammatory disease. N Engl J Med 340(2):115–126
Ryu SK, Hutten BA, Vissers MN, Wiegman A, Kastelein JJ, Tsimikas S (2011) Lipoprotein-associated phospholipase A2 mass and activity in children with heterozygous familial hypercholesterolemia and unaffected siblings: effect of pravastatin. J Clin Lipidol 5(1):50–56
Santos RD, Gidding SS, Hegele RA, Cuchel MA, Barter PJ, Watts GF et al (2016) Defining severe familial hypercholesterolaemia and the implications for clinical management: a consensus statement from the international atherosclerosis society severe familial hypercholesterolemia panel. Lancet Diabetes Endocrinol 4(10):850–861
Santos JCD, Cruz MS, Bortolin RH, Oliveira KM, Araujo JNG, Duarte VHR et al (2018) Relationship between circulating VCAM-1, ICAM-1, E-selectin and MMP9 and the extent of coronary lesions. Clinics (Sao Paulo, Brazil) 73:e203
Saougos VG, Tambaki AP, Kalogirou M, Kostapanos M, Gazi IF, Wolfert RL et al (2007) Differential effect of hypolipidemic drugs on lipoprotein-associated phospholipase A2. Arterioscler Thromb Vasc Biol 27(10):2236–2243
Semb AG, van Wissen S, Ueland T, Smilde T, Waehre T, Tripp MD et al (2003) Raised serum levels of soluble CD40 ligand in patients with familial hypercholesterolemia: downregulatory effect of statin therapy. J Am Coll Cardiol 41(2):275–279
Sharifi M, Rakhit RD, Humphries SE, Nair D (2016) Cardiovascular risk stratification in familial hypercholesterolaemia. Heart 102(13):1003–1008
Shoenfeld Y, Wu R, Dearing LD, Matsuura E (2004) Are anti-oxidized low-density lipoprotein antibodies pathogenic or protective? Circulation 110(17):2552–2558
Soeki T, Sata M (2016) Inflammatory biomarkers and atherosclerosis. Int Heart J 57(2):134–139
Soutar AK, Naoumova RP (2007) Mechanisms of disease: genetic causes of familial hypercholesterolemia. Nat Rev Cardiol 4(4):214
Stafforini DM (2009) Biology of platelet-activating factor acetylhydrolase (PAF-AH, lipoprotein associated phospholipase A 2). Cardiovasc Drugs Ther 23(1):73–83
Stübiger G, Aldover-Macasaet E, Bicker W, Sobal G, Willfort-Ehringer A, Pock K et al (2012) Targeted profiling of atherogenic phospholipids in human plasma and lipoproteins of hyperlipidemic patients using MALDI-QIT-TOF-MS/MS. Atherosclerosis 224(1):177–186
Sugiyama N, Marcovina S, Gown AM, Seftel H, Joffe B, Chait A (1992) Immunohistochemical distribution of lipoprotein epitopes in xanthomata from patients with familial hypercholesterolemia. Am J Pathol 141(1):99–106
Tabatabaeizadeh SA, Avan A, Bahrami A, Khodashenas E, Esmaeili H, Ferns GA et al (2017) High dose supplementation of vitamin D affects measures of systemic inflammation: reductions in high sensitivity C-reactive protein level and neutrophil to lymphocyte ratio (NLR) distribution. J Cell Biochem 118(12):4317–4322
Tacke F, Alvarez D, Kaplan TJ, Jakubzick C, Spanbroek R, Llodra J et al (2007) Monocyte subsets differentially employ CCR2, CCR5, and CX3CR1 to accumulate within atherosclerotic plaques. J Clin Invest 117(1):185–194
Tak PP, Firestein GS (2001) NF-κB: a key role in inflammatory diseases. J Clin Invest 107(1):7–11
Tardif JC, Kouz S, Waters DD, Bertrand OF, Diaz R, Maggioni AP et al (2019) Efficacy and safety of low-dose colchicine after myocardial infarction. N Engl J Med
Tekin IO, Orem A, Shiri-Sverdlov R (2013) Oxidized LDL in inflammation: from bench to bedside. Mediat Inflamm 2013:762759
Tibuakuu M, Kianoush S, DeFilippis AP, McEvoy JW, Zhao D, Guallar E et al (2018) Usefulness of lipoprotein-associated phospholipase A2 activity and C-reactive protein in identifying high-

risk smokers for atherosclerotic cardiovascular disease (from the atherosclerosis risk in communities study). Am J Cardiol 121(9):1056–1064

Tousoulis D, Oikonomou E, Economou EK, Crea F, Kaski JC (2016) Inflammatory cytokines in atherosclerosis: current therapeutic approaches. Eur Heart J 37(22):1723–1732

Toutouzas K, Skoumas J, Koutagiar I, Benetos G, Pianou N, Georgakopoulos A et al (2018) Vascular inflammation and metabolic activity in hematopoietic organs and liver in familial combined hyperlipidemia and heterozygous familial hypercholesterolemia. J Clin Lipidol 12 (1):33–43

Tsimikas S, Bergmark C, Beyer RW, Patel R, Pattison J, Miller E et al (2003) Temporal increases in plasma markers of oxidized low-density lipoprotein strongly reflect the presence of acute coronary syndromes. J Am Coll Cardiol 41(3):360–370

Tsimikas S, Tsironis LD, Tselepis AD (2007) New insights into the role of lipoprotein (a)-associated lipoprotein-associated phospholipase A2 in atherosclerosis and cardiovascular disease. Arterioscler Thromb Vasc Biol 27(10):2094–2099

Tsimikas S, Willeit P, Willeit J, Santer P, Mayr M, Xu Q et al (2012) Oxidation-specific biomarkers, prospective 15-year cardiovascular and stroke outcomes, and net reclassification of cardiovascular events. J Am Coll Cardiol 60(21):2218–2229

Ueland T, Vissers M, Wiegman A, Rodenburg J, Hutten B, Gullestad L et al (2006) Increased inflammatory markers in children with familial hypercholesterolaemia. Eur J Clin Investig 36 (3):147–152

van den Berg EH, Gruppen EG, James RW, Bakker SJ, Dullaart RP (2019) Serum paraoxonase 1 activity is paradoxically maintained in nonalcoholic fatty liver disease despite low HDL cholesterol. J Lipid Res 60(1):168–175

van Haelst PL, van Doormaal JJ, Asselbergs FW, Veeger NJ, Henneman MM, Tervaert JWC et al (2003) Correlates of endothelial function and their relationship with inflammation in patients with familial hypercholesterolaemia. Clin Sci 104(6):627–632

van Himbergen TM, Roest M, de Graaf J, Jansen EH, Hattori H, Kastelein JJ et al (2005) Indications that paraoxonase-1 contributes to plasma high density lipoprotein levels in familial hypercholesterolemia. J Lipid Res 46(3):445–451

Van Tits L, De Graaf J, Hak-Lemmers H, Bredie S, Demacker P, Holvoet P et al (2003) Increased levels of low-density lipoprotein oxidation in patients with familial hypercholesterolemia and in end-stage renal disease patients on hemodialysis. Lab Investig 83(1):13–21

Vizioli L, Muscari S, Muscari A (2009) The relationship of mean platelet volume with the risk and prognosis of cardiovascular diseases. Int J Clin Pract 63(10):1509–1515

Wachter H, Fuchs D, Hausen A, Reibnegger G, Werner ER (1989) Neopterin as marker for activation of cellular immunity: immunologic basis and clinical application. Adv Clin Chem 27:81–141

Wallenfeldt K, Fagerberg B, Wikstrand J, Hulthe J (2004) Oxidized low-density lipoprotein in plasma is a prognostic marker of subclinical atherosclerosis development in clinically healthy men. J Intern Med 256(5):413–420

Wallentin L, Held C, Armstrong PW, Cannon CP, Davies RY, Granger CB et al (2016) Lipoprotein-associated phospholipase A2 activity is a marker of risk but not a useful target for treatment in patients with stable coronary heart disease. J Am Heart Assoc 5(6):e003407

Weintraub HS (2008) Identifying the vulnerable patient with rupture-prone plaque. Am J Cardiol 101(12):S3–S10

Wintergerst ES, Jelk J, Rahner C, Asmis R (2000) Apoptosis induced by oxidized low density lipoprotein in human monocyte-derived macrophages involves CD36 and activation of caspase-3. Eur J Biochem 267(19):6050–6059

Xu S, Ogura S, Chen J, Little PJ, Moss J, Liu P (2013) LOX-1 in atherosclerosis: biological functions and pharmacological modifiers. Cell Mol Life Sci 70(16):2859–2872

Yang EH, McConnell JP, Lennon RJ, Barsness GW, Pumper G, Hartman SJ et al (2006) Lipoprotein-associated phospholipase A2 is an independent marker for coronary endothelial dysfunction in humans. Arterioscler Thromb Vasc Biol 26(1):106–111

Yuan M, Fu H, Ren L, Wang H, Guo W (2015) Soluble CD40 ligand promotes macrophage foam cell formation in the etiology of atherosclerosis. Cardiology 131(1):1–12

Zannad F, De Backer G, Graham I, Lorenz M, Mancia G, Morrow DA et al (2012) Risk stratification in cardiovascular disease primary prevention - scoring systems, novel markers, and imaging techniques. Fundam Clin Pharmacol 26(2):163–174

Zernecke A, Weber C (2009) Chemokines in the vascular inflammatory response of atherosclerosis. Cardiovasc Res 86(2):192–201

Zhang J, Wang D, He S (2015) Roles of antibody against oxygenized low density lipoprotein in atherosclerosis: recent advances. Int J Clin Exp Med 8(8):11922–11929

Ziegler-Heitbrock H (1996) Heterogeneity of human blood monocytes: the CD14+ CD16+ subpopulation. Immunol Today 17(9):424–428

Rev Physiol Biochem Pharmacol (2020) 177: 53–82
https://doi.org/10.1007/112_2020_27

Published online: 21 July 2020

Beyond the Paradigm: Novel Functions of Renin-Producing Cells

Anne Steglich, Linda Hickmann, Andreas Linkermann, Stefan Bornstein, Christian Hugo, and Vladimir T. Todorov

Contents

Abstract The juxtaglomerular renin-producing cells (RPC) of the kidney are referred to as the major source of circulating renin. Renin is the limiting factor in renin-angiotensin system (RAS), which represents a proteolytic cascade in blood plasma that plays a central role in the regulation of blood pressure. Further cells disseminated in the entire organism express renin at a low level as part of tissue RASs, which are thought to locally modulate the effects of systemic RAS. In recent years, it became increasingly clear that the renal RPC are involved in developmental, physiological, and pathophysiological processes outside RAS. Based on recent experimental evidence, a novel concept emerges postulating that next to their traditional role, the RPC have non-canonical RAS-independent progenitor and renoprotective functions. Moreover, the RPC are part of a widespread renin lineage population, which may act as a global stem cell pool coordinating homeostatic, stress, and regenerative responses throughout the organism. This review focuses on

Christian Hugo and Vladimir T. Todorov contributed equally to this work.

A. Steglich, L. Hickmann, A. Linkermann, S. Bornstein, C. Hugo, and V. T. Todorov (✉)
Experimental Nephrology, Division of Nephrology, Department of Internal Medicine III, University Hospital Carl Gustav Carus, TU Dresden, Dresden, Germany
e-mail: anne.steglich2@uniklinikum-dresden.de; linda.hickmann@ukdd.de; andreas.linkermann@ukdd.de; stefan.bornstein@uniklinikum-dresden.de; christian.hugo@ukdd.de; vladimir.todorov@ukdd.de

the RAS-unrelated functions of RPC – a dynamic research area that increasingly attracts attention.

Keywords Juxtaglomerular cells · Progenitor cells · Regeneration · Renin lineage · Tissue injury

Abbreviations

AA	Afferent arteriole
ACE	Angiotensin-converting enzyme
Akr1b7	Aldo-keto reductase family 1 member B7
Ang	Angiotensin
ArcA	Arcuate artery
AT1	Angiotensin II type 1 receptors
AT2	Angiotensin II type 2 receptors
BrdU	Bromdesoxyuridin
cAMP	3′,5′-Cyclic adenosine monophosphate
Cre	Cre-recombinase
DAMPs	Damage-associated molecular patterns
DNA	Deoxyribonucleic acid
EP	Prostaglandin EP receptor
EPO	Erythropoietin
FoxD1	Forkhead box D1
G	Glomerulus
GFR	Glomerular filtration rate
Gs	G-protein stimulatory subunit
GTPases	Guanosine-5′-triphosphate hydrolases
IA	Interlobular artery
IP	Prostacyclin I2 receptor
JG	Juxtaglomerular
JGA	JG apparatus
loxP	Locus of X-over P1
MC	Mesangial cell
NB	Nota bene
NF-kappa B	Nuclear factor “kappa-light-chain-enhancer” of activated B-cells
PE	Parietal epithelial
PT	Proximal tubule
RAS	Renin-angiotensin system
Rb	Retinoblastoma protein
RBP-J	Recombination signal binding protein for immunoglobulin kappa J region
RLC	Renin lineage cells
RNA	Ribonucleic acid
RPC	Renin-producing cells

SISC	Stress-inducible stem cells
STAT	Signal transducers and activators of transcription
tet	Tetracycline
TGF	Transforming growth factor
Thy1	Thymocyte antigen 1
VEGF	Vascular endothelial growth factor
VSMC	Vascular smooth muscle cells
WT1	Wilms' tumor suppressor 1

1 Background: The Classical View on Renal Renin-Producing Cells (RPC) Within Renin-Angiotensin System (RAS)

Circulating renin-angiotensin system (RAS) is a major endocrine factor that governs arterial blood pressure acting both in a short-term scale on vascular tone and in a long-term scale on salt, water, and volume homeostasis. Within RAS, the proteases renin and angiotensin-converting enzyme (ACE) sequentially cleave the plasma protein angiotensinogen to angiotensin (Ang) I and then to Ang II. Ang II is the main effector hormone of the system. Acting primarily through Ang II type 1 (AT1) receptors, it induces strong vasoconstriction and maintains sodium and water balance by regulating the production of aldosterone and antidiuretic hormone, respectively. The multifaceted activity of Ang II results in complex cross talk between its different modes of action. Particularly in the kidney, the functional integrity between Ang II effects on afferent/efferent arteriole tone and tubular reabsorption is decisive for the maintenance of glomerular (as well as renal) hemodynamics and water/electrolyte excretion. In fact, RAS is more complicated because it also includes AT2 receptor, prorenin, and its receptor, as well as a protective arm with ACE2, Ang 1–7, and Mas receptor. These further members are responsible for the fine-tuning of RAS under physiological conditions. They acquire a substantial role in patients with cardiovascular diseases in particular when the AT1-mediated Ang II effects of RAS are pharmacologically inhibited. The detailed description of RAS is beyond the scope of this review. Recent reviews summarizing the state of the art on the intricate RAS aspects in health and disease are available elsewhere (Ames et al. 2019; Arendse et al. 2019; Fournier et al. 2012; Santos et al. 2018; Sparks et al. 2014).

The renin-producing cells (RPC) of the adult mammalian kidney are located in the wall of the afferent arterioles next to the glomerular vascular poles. Therefore, the RPC are also dubbed juxtaglomerular (JG) cells. The JG cells are very few – they amount to only 4–8 cells per afferent arteriole. Renin is the rate-limiting factor of circulating systemic RAS since it primarily determines the rate of generated Ang II and thus the overall biological activity of the system. The reason for the key regulatory status of renin in RAS is the tight control of renin synthesis and secretion by systemic and local factors including perfusion pressure, renal sympathetic nerve

activity, macula densa mechanism, and autocrine cues (nitric oxide, prostanoids, and adenosine). The function of renal RPC in steering RAS activity under physiological and pathophysiological conditions has been characterized very well and elucidated in excellent reviews (Castrop et al. 2010; Damkjaer et al. 2013; Friis et al. 2013; Schweda and Kurtz 2011; Sparks et al. 2014).

2 RPC Beyond RAS

For about 10 years, we have being interested whether the renal RPC might be more than a mere source of renin. Initially, there were two lines of evidence justifying this hypothesis. First, the number of RPC in the afferent arterioles of the adult kidney is not constant but changes in response to homeostatic fluctuations in salt intake, intravascular volume, arterial tone, or adrenergic input. Therein, the RPC do not seem to proliferate. Instead, the renin gene is switched on upstream in the afferent arterioles in some vascular smooth muscle cells (VSMC) thus changing their phenotype from contractile to secretory (Cantin et al. 1977; Dominick et al. 1990). This process is reversible and known as recruitment or metaplastic transformation (Gomez et al. 1988, 1990). The latter term, however, is confusing because it implies pathology when in fact it represents a physiological process. The phenotype plasticity of the RPC in adult life is particularly interesting with regard to the localization of these cells within the JG apparatus (JGA), which includes macula densa and the vascular glomerular pole with the adherent parts of the afferent and efferent arterioles. JGA essentially coordinates renal perfusion, glomerular filtration rate (GFR), and tubular reabsorption into integrative mechanistic responses to provide optimal kidney function. While modulation of RAS activity is part of these responses, it was worth arguing that the phenotypic flexibility of the RPC is of further functional and structural importance for the kidney. Second, the prevalence of RPC in the renal vasculature during kidney development (nephrogenesis) is higher than in adult life (Gomez et al. 1986; Sauter et al. 2008). In addition, knockout of renin in mice leads to kidney malformations and perinatal death (Takahashi et al. 2005; Yanai et al. 2000). Importantly, an identical phenotype has been reported in human fetuses with inactivating mutations in the renin gene (Michaud et al. 2011; Zivna et al. 2009). These observations provided a crucial hint that the RPC should be important for the normal development of the kidney. Based on these findings, a role of RPC as a progenitor cell pool during nephrogenesis was originally proposed. However, experimental evidence in rats and frogs suggested a fundamental role of RAS activity in terms of Ang II effects on kidney morphogenesis and vascular development (Tufro-McReddie et al. 1995). In line with these initial findings, studies in mice and humans demonstrated that the very same detrimental renal phenotype is observed when RAS is inactivated by genetic mutations not only in renin gene but also in its further key component genes, namely, angiotensinogen, ACE, and AT1 (Gribouval et al. 2005, 2012; Gubler and Antignac 2010; Hibino et al. 2015; Hilgers et al. 1997; Kim et al. 1995; Krege et al. 1995; Oliverio et al. 1998; Takahashi et al. 2005; Yanai et al.

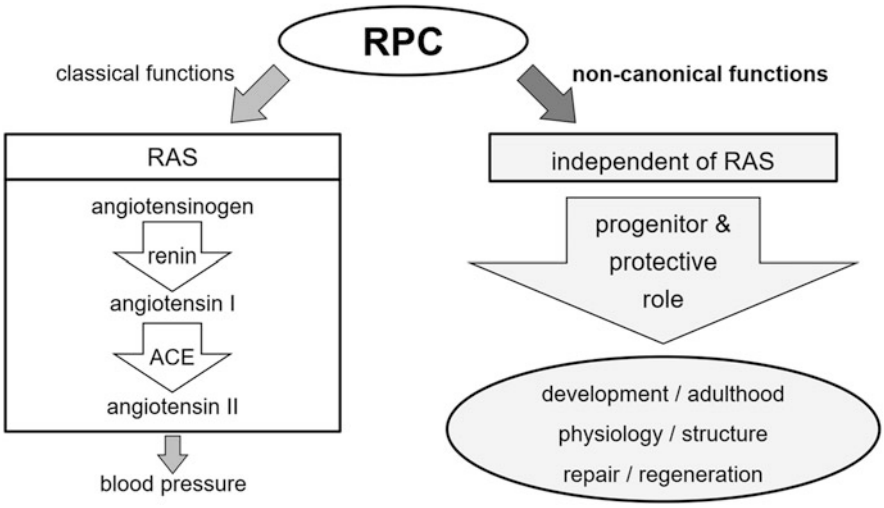

Fig. 1 Novel concept on the dual role of the renin-producing cells (RPC) in kidney highlighting their new RAS-independent functions. *RAS* renin-angiotensin system, *ACE* angiotensin-converting enzyme

2000). Moreover, antihypertensive treatment with RAS inhibitors (ACE inhibitors, AT1 blockers, etc.) is counter-indicated during pregnancy because they cause fetal malformations (Broughton Pipkin et al. 1982; Daikha-Dahmane et al. 2006; Friberg et al. 1994; Grove et al. 1995; Knott et al. 1989; Landing et al. 1994; McCausland et al. 1997; Polifka 2012). RAS is believed to be important in embryonic life for not only maintaining blood pressure and organ perfusion but also because Ang II exerts growth factor-like effects in the developing kidney (Chen et al. 2004; Iosipiv and Schroeder 2003; Madsen et al. 2010; McCausland et al. 1997; Niimura et al. 1995; Tufro-McReddie et al. 1995). Altogether, these findings indicated that active RAS is necessary for normal ontogenesis and nephrogenesis, in particular, thus questioning the role of RPC themselves as progenitors.

Starting from these initial observations, experimental evidence accumulated to favor a concept where RPC do have RAS independent functions (Fig. 1). These non-canonical RAS functions will be discussed in more detail below. Notwithstanding, modern transgenic animal models provided decisive evidence that independently from RAS, the RPC do serve as a progenitor niche in embryonic and adult kidney.

2.1 Progenitor Cell Pool

2.1.1 Nephrogenesis

The original observations that the RPC population is spread throughout the growing renal arterial tree during nephrogenesis before shrinking to the glomerular proximity of the adult kidney came out more than 30 years ago (Gomez et al. 1986; Robillard and Nakamura 1988). This distribution has been demonstrated in multiple studies with mice, rats, pigs, and humans (Celio et al. 1985; Egerer et al. 1984; Gomez et al. 1991; Graham et al. 1992; Molteni et al. 1974). The high interspecies similarity of renal RPC ontogenesis legitimated the widespread use of transgenic animals, mostly mice, as experimental models with high translational capacity and potential clinical relevance. RPC appear in the fetal kidney around embryonic day 16 in mice (gestational week 6 in humans) shortly after the onset of renal vascular development (Celio et al. 1985; Hickmann et al. 2017; Sauter et al. 2008). The renin production is first detected in arcuate arteries and moves next to interlobular arteries and then to the afferent arterioles, i.e., proximal to distal in the growing vascular tree (Fig. 2a). The classic RPC position close to the glomeruli within the wall of terminal afferent arterioles is patterned at the end of nephrogenesis around postpartal day 10 in rodents and gestational week 35 in humans (Graham et al. 1992; Sauter et al. 2008; Sequeira Lopez and Gomez 2011). The RPC in the kidney vessels originate from a subset of cells in the stroma of the metanephric mesenchyme that expresses transcription factor FoxD1 (Pierrou et al. 1994; Lin et al. 2014). In general, the FoxD1 stromal progenitors give rise to intramural and interstitial cells (Hatini et al. 1996; Humphreys et al. 2010; Sequeira Lopez and Gomez 2011). Next to the RPC, renal VSMC, pericytes, and fibroblast-like cells are also of FoxD1 lineage. Therein, cell fate tracing experiments revealed interesting relations (Fig. 2b).

The RPC appear to be exclusively of FoxD1 descent (Gomez and Sequeira-Lopez 2018; Sequeira-Lopez et al. 2015a, b). Within the FoxD1 lineage, the RPC serve as a more differentiated precursor pool giving rise to the JG cells as well as to subpopulations of VSMC and pericytes (Sequeira Lopez et al. 2004). Pericytes are mural cells that stabilize the microvascular tree (Birbrair et al. 2015). In the kidney, mesangial cells of the glomerular capillary tuft and peritubular interstitial cells are regarded as specialized pericyte populations (Stefanska et al. 2013). Thus, in the adult mammalian kidney, a considerable part of the vasculature originates from fetal RPC progenitors. Consistent with the function of RPC as a progenitor pool during kidney development, interference with their intracellular regulatory networks such as Gs-alpha/cAMP, Notch signaling, or micro-RNA leads to adverse renal phenotype (Castellanos Rivera et al. 2011, 2015; Chen et al. 2010a, 2007; Gomez et al. 2009; Medrano et al. 2012; Neubauer et al. 2009; Sequeira-Lopez et al. 2010). As a rule, intervening in these cellular signaling pathways derails the renin production in RPC. Therefore, it remains difficult to completely separate RAS-specific and RAS-independent aspects of RPC in nephrogenesis. Importantly, two lines of recent experimental data shed light on this issue. First, renin cell ablation and renin

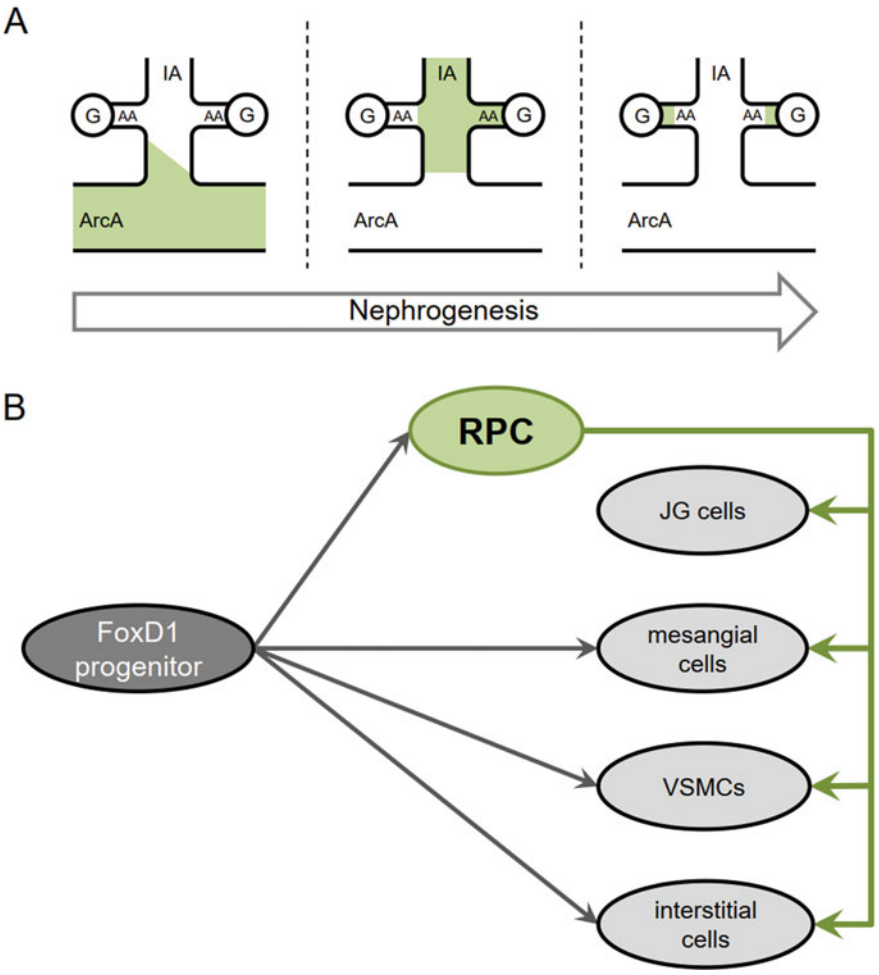

Fig. 2 Renin-producing cells (RPC) in kidney development. (**a**) Localization of RPC (green) in the renal vascular tree at different developmental stages of the maturing kidney. (**b**) RPC as a progenitor niche in nephrogenesis. *AA* afferent arteriole, *IA* interlobular artery, *ArcA* arcuate artery, *G* glomerulus, *JG* juxtaglomerular, *VSMCs* vascular smooth muscle cells

deficiency (renin gene "knockout") during ontogenesis result in different kidney phenotypes (Oka et al. 2017; Pentz et al. 2004; Sequeira Lopez and Gomez 2011; Takahashi et al. 2005). The most striking difference has been observed in the renal arterioles, which in "classical" renin knockout mice are with narrowed lumen due to hyperplasia of mural cells. Interestingly, these cells represent RPC descendants depleted of renin (Oka et al. 2017). On the other hand, the renal arterioles in mice with embryonic ablation of RPC have a thin vascular wall and perivascular fibrosis (Pentz et al. 2004). Second, activating molecular hypoxic signaling by conditional deletion of von Hippel-Lindau protein in RPC converts them into renin-negative

fibroblast-like erythropoietin (EPO)-producing cells without leading to any further major kidney phenotype (Kurt et al. 2013, 2015). EPO is the master hormone regulating erythropoiesis. In adult mammals, it is produced almost exclusively by interstitial cells in the renal cortex (Bachmann et al. 1993; Kurtz 2017, 2019; Maxwell et al. 1997). The surprising finding that RPC could transform into EPO-expressing cells implicates that during nephrogenesis, at least part of the EPO-producing peritubular pericytes may derive from RPC. This exciting possibility awaits definitive experimental confirmation. Importantly, activating hypoxic molecular pathways in the entire FoxD1 lineage cell pool resulted in renal malformations, indicating that intact oxygen signaling in early embryonic life (before the emergence of renal RPC) is essential for the normal development of the stromal compartment of the adult kidney (Gerl et al. 2017).

Altogether, these findings demonstrated a role of RPC as a progenitor pool during ontogenesis irrespective of renin and RAS activity. At the same time, fine-tuning of the complex functions of RPC is indispensable for proper nephrogenesis.

2.1.2 Adult Kidney

The role of RPC as a progenitor niche during fetal life inspired us to address the possibility if these cells have a similar function in the adult kidney. To this end, we used reversible injury models such as intravenous infusion of anti-mesangial cell serum or renal artery perfusion with concanavalin A/anti-concanavalin A antibody to target primarily the glomeruli in the kidney (Hohenstein et al. 2008; Sradnick et al. 2016; Yo et al. 2003). We concentrated our studies on the regenerative phase after the initial acute damage. This approach was based on the general paradigm that developmental cellular mechanisms, which are active during embryogenesis, may be reenacted to regenerate damaged organs in adulthood. Since RPC serve as progenitors for glomerular cells during nephrogenesis (e.g., mesangial cells; see Sect. 2.1.1) and since glomerulopathies are a primary cause for end-stage renal disease (Jha et al. 2013), we have been focusing on glomerular injury models. We also developed a novel transgenic mouse model by combining Cre-loxP recombination with tet-on system (Schonig et al. 2002; Urlinger et al. 2000) to pulse-label and fate-trace RPC in adulthood (Kessel et al. 2019; Lachmann et al. 2017; Ruhnke et al. 2018; Starke et al. 2015; Steglich et al. 2019).

We first found that during the regenerative phase after initial damage induced by anti-mesangial cell serum, the RPC migrate away from their classical JG position into the diseased glomerulus (Starke et al. 2015). Thereby, the migrating cells differentiate in a way that they lose the renin expression and acquire alpha-8-integrin as well as platelet-derived growth factor receptor-beta proteins which are specific for mesangial cells in the glomerulus. Hence, our hypothesis received experimental confirmation because RPC transdifferentiation in the mature kidney recapitulated nephrogenesis, where mesangial cells originate from RPC (Gomez and Sequeira-Lopez 2018; Sequeira Lopez et al. 2004). However, in adult life, this is a regenerative process observed only after organ damage with cell loss and not under

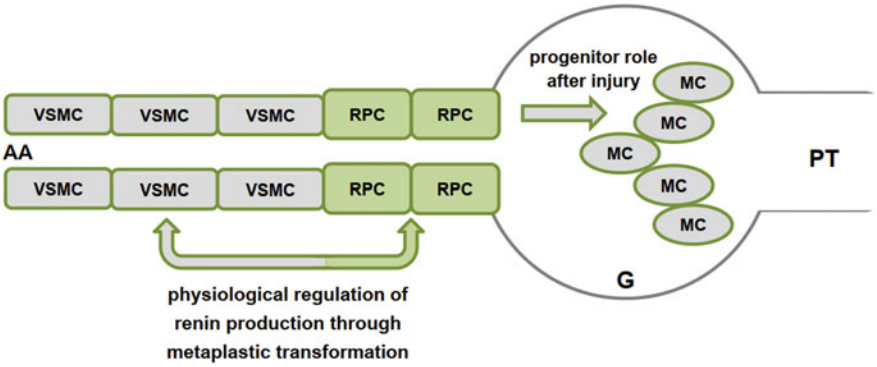

Fig. 3 Plasticity (transdifferentiation) of the renin-producing cells (RPC) in adult kidney recapitulates embryonic patterns. RPC serve as progenitors, which repopulate the glomerulus to replace damaged mesangial cells after injury. RPC could also reversibly switch between secretory and contractile phenotype to regulate renin production under physiological conditions through metaplastic transformation. See also Sects. 2, 2.1.1, and 2.2 and Figs. 2 and 4. *AA* afferent arteriole, *G* glomerulus, *VSMC* vascular smooth muscle cell, *MC* mesangial cell, *PT* proximal tubule

physiological conditions. Throughout development and adulthood, the RPC progenitors maintain cell-specific plasticity, i.e., they transdifferentiate to the very same cell types (Fig. 3). Moreover, RPC descendants did not regenerate the endothelium after depletion of glomerular endothelial cells in reversible endothelial cell injury model induced by renal artery perfusion with concanavalin A/anti-concanavalin A antibody (Ruhnke et al. 2018). Instead, RPC transdifferentiated to exclusively replace glomerular mesangial cells, which seemed to be damaged secondary to the endothelial injury.

Other investigators used an alternative transgenic mouse model for inducible labeling and tracing of RPC in a model of focal segmental glomerulosclerosis (Kaverina et al. 2017b; Lichtnekert et al. 2016; Pippin et al. 2015). They found that RPC repopulate the glomerular Bowman's capsule and differentiate not only to mesangial cells but also to podocytes and parietal epithelial (PE) cells. The reasons for the partial discrepancy compared to our results lay most probably on the different animal or injury models used. For instance, the experimental setups we used do not lead to podocyte depletion (Ruhnke et al. 2018). In any case, it is somewhat counterintuitive that RPC could replace damaged podocytes or PE cells because these are not of FoxD1 origin and thus do not belong to the RPC stromal mesenchyme descendants in the adult kidney (see Sect. 3). Therefore, it is plausible to conclude that after severe glomerular injury the progenitor potential of RPC is utilized beyond the developmentally based transdifferentiation programs of cell type-specific regeneration. Thus, the RPC seem to universally protect damaged tissue as a part of integrative stress response of the organism. Anyway, more experimental support is needed to utterly validate this hypothesis.

The communication modes between RPC and (damaged) intraglomerular cells in the mature kidney are still poorly understood. With this regard, it is unlikely that

soluble messenger molecules are transported with blood flow because the RPC are upstream to the glomerulus. Cell-cell contacts are important for the physiological signaling within the JGA, and therefore they may be involved in regenerative signaling (Just et al. 2009; Kurtz 2015; Wagner et al. 2007). Moreover, the RPC are featured by a specific gap junction protein expression signature where connexin 40 is central for their function and morphology (Kurtz et al. 2009; Wagner and Kurtz 2013). Hence, future studies on the role of cell-cell contacts in transmitting signals from damaged glomeruli to the precursor RPC niche in the afferent arterioles are an attractive perspective. However, the advancements in this strategic area of interest are hampered by a deficit of appropriate experimental models. For instance, efforts to identify mesangial-specific gene(s) fail until now, thus making the generation of transgenic animals with selectively targeted mesangial cells impossible.

Immune cells could also be considered as paramount players mediating cues from injured and regenerating glomeruli to RPC. According to the modern concept of necroinflammation, necrotic organ damage inevitably goes together with an inflammatory component (Linkermann 2019; Sarhan et al. 2018). Conversely, inflammation and release of damage-associated molecular patterns (DAMPs) do not only augment tissue damage but also initiate regenerative reactions (Sarhan et al. 2018). These processes are mediated by resident cells of innate immunity like macrophages, dendritic cells, and natural killer cells that orchestrate local and systemic mechanisms with adaptive relevance in host-pathogen interactions, metabolic responses to tissue injury and degeneration, or allogeneic transplantation. Importantly, we and others have demonstrated that the RPC are equipped with the molecular machinery (including tumor necrosis factor receptors, functional NF-kappa B and STAT signaling, etc.) necessary for acquisition and transduction of innate immunity signals like inflammatory cytokines (Baumann et al. 2000; Desch et al. 2012; Liu et al. 2006; Petrovic et al. 1997; Todorov et al. 2002, 2005, 2004). Therefore, we favor the immune-mediated processes as the most feasible mechanism(s) responsible for signal delivery from damaged glomeruli to RPC and vice versa. There is already indirect evidence in support of such an assumption. Thus, both necroinflammation and RPC progenitor function in adulthood are specific for pathophysiological conditions (Linkermann 2019; Ruhnke et al. 2018; Starke et al. 2015).

At present, little is known about how RPC set up to differentiate and migrate upon glomerular damage. First data from us demonstrated that when renin is switched off by interfering with Gs-alpha/cAMP signaling, the RPC descendants produce increased amounts of tissue remodeling factors (Steglich et al. 2019). The latter could loosen cells and potentiate their migration (see also Sect. 2.3). With this regard, proteins involved in the control of cellular mechanics like small GTPases are particularly interesting targets for future studies, since cytoskeleton rearrangement generally accompanies cell motility and differentiation. The transcription factor Wilms' tumor suppressor 1 (WT1), which belongs to this group of proteins and is expressed in RPC, has already been reported to affect their transformation and glomerular migration after podocyte depletion (Kaverina et al. 2017a).

Collectively, although it is now established that the RPC operate as a progenitor cell niche in the adult mammalian kidney, we are still at the onset of exciting findings

that should elaborate the understanding of underlying molecular mechanisms and pathophysiological relevance. Therein large-scale "omics" analyses of the global transcriptional/translational landscape of RPC would be of exceptional importance (Martinez et al. 2018; Steglich et al. 2019; Wang et al. 2018).

2.2 Neogenesis and Recruitment

The discovery of a progenitor function of RPC inspired studies on their maintenance as a stable population in adulthood. This issue is also critical with regard to the classical role of RPC in RAS – if upon glomerular injury all JG cells differentiate to renin-negative descendants, RAS would be switched off, thus disturbing the general control of circulation and overall homeostasis. Moreover, (self)renewal is an archetypal feature of stem cell niches (Seaberg and van der Kooy 2003). Therefore, it is somewhat surprising that there is no conclusive data demonstrating proliferation of RPC. Early pulse labeling studies with DNA intercalating agents in the rat anti-Thy1 model indicated that repopulation of the glomerulus during repair after mesangial injury involves migration and proliferation of precursors from the JGA (Hugo et al. 1996, 1997). Recent findings did not show prominent RPC proliferation in an equivalent mouse model (Starke et al. 2015). This is consistent with other studies (Cantin et al. 1977; R. Ariel Gomez, personal communication). In contrast, proliferating RPC have been detected after continuous loading with the DNA intercalating agent bromdesoxyuridin (BrdU) for lineage tracing of dividing cells for up to 27 days (Lichtnekert et al. 2016; Owen et al. 1994). Altogether, these findings inferred that mechanisms beyond proliferation are necessary to maintain the RPC precursor niche, particularly after injury when the JG cells transdifferentiate to replace damaged glomerular cells. Progenitor cell niches (such as the RPC) could also be filled up by differentiating pluripotent stem cells through a process termed neogenesis or de novo differentiation. For RPC (and renin lineage cells in general; see Sect. 3), neogenesis is the process where a cell that is not related to the renin lineage (i.e., never expressed renin before and does not originate from cells that express/ed renin) starts to express renin for a very first time (Hickmann et al. 2017). We were lucky to make use of a versatile transgenic mouse model for neogenesis tracing (Muzumdar et al. 2007; Xiao et al. 2013), which was modified for RPC targeting. During nephrogenesis, RPC emerge almost exclusively via neogenesis (Hickmann et al. 2017). Although proliferation should also play a role in the establishment of the RPC population in the developing kidney, de novo differentiation seems to be the superior mechanism. In adulthood, the RPC neogenesis is featured by three hallmarks: it is intrarenal, lifelong, and regulated (Hickmann et al. 2017). Thus, the kidney appears to be able to effectively preserve and renew a local progenitor cell population. Moreover, the process of RPC neogenesis is counteracted by rate-matched apoptotic cell death, which explains why the adult kidney is not overfilled with RPC (Hickmann et al. 2017). Even more important is the fact that RPC neogenesis is stress-inducible. During injury when RPC repopulate damaged

glomeruli, de novo differentiation is upregulated, leading to a moderate increase in RPC number (Hickmann et al. 2017). This mechanism safeguards not only the RPC precursor pool, which is primed to replace the depleted glomerular cells, but also the RAS activity. This is an important aspect demonstrating that the RPC act as a progenitor niche without impeding their classical role within RAS. The origin of the de novo differentiated RPC in the adult kidney remains open. We experimentally excluded the option that the renal RPC are bone marrow-derived (Hickmann et al. 2017). FoxD1-positive precursors are the source for RPC during development (see Sect. 2.1.1), but FoxD1 is not expressed in the mature kidney (Humphreys et al. 2010). Preliminary observations from us suggest a pericyte origin for new RPC after nephrogenesis is finished, but more studies are needed to identify the adult precursor renal niche for RPC.

Increased de novo differentiation of RPC has also been observed in a physiological model of decreased blood pressure (Hickmann et al. 2017). Arterial hypotension is the main stimulus for renin production, and the renin production is scaled up and down by changing the number of RPC, rather than the renin expression rate in the single cell (Castrop et al. 2010; Hackenthal et al. 1990; Rasch et al. 1998). The adjustment of RPC number to the functional status of the organism is a versatile process termed recruitment or metaplastic transformation (see Sect. 2). Recruitment is one of the early described physiological manifestations of RPC plasticity in the adult mammalian kidney (Cantin et al. 1977). It represents a reversible phenotypic switch between VSMC and RPC in the wall of the afferent arterioles upstream to their JG parts. Lineage tracing revealed that the switching VSMC in the afferent arterioles originate from RPC during nephrogenesis meaning that the recruitment is a recapitulation of a developmental process (Gomez et al. 2014; Kurt and Kurtz 2015; Martini and Danser 2017; Sequeira Lopez et al. 2004) in adulthood (see Sect. 2.1.1). It should be emphasized that recruitment is not to be mixed up with neogenesis although both are hallmarks of RPC plasticity. Recruitment (metaplastic transformation) is a reversible phenotype change of a cell within the developmental RPC pool (referred also in Figs. 2 and 3), while neogenesis (de novo differentiation) is the differentiation of a cell to join the renin lineage (Fig. 4a; see the definition of neogenesis above in this section). In addition, neogenesis is involved primarily in RPC renewal and progenitor function after injury, whereas recruitment is responsible for the physiological control of renin production and RAS activity (Fig. 4b; see also Fig. 3).

Thus, the RPC are not only featured by plasticity but also represent a dynamic population predestined to be involved in complex physiological and pathophysiological processes.

Antihypertensive drugs and particularly RAS inhibitors boost the renin production and the RPC count (due to negative feedback within RAS linking blood pressure to renin expression) demonstrating that recruitment and neogenesis could be targeted by therapeutic strategies (Azizi and Menard 2004; Hickmann et al. 2017; Mooser et al. 1990; Nussberger et al. 2007; Pugh et al. 2019). Although an increased number of RPC correlates with the renoprotective effect of the RAS inhibitors, it is still

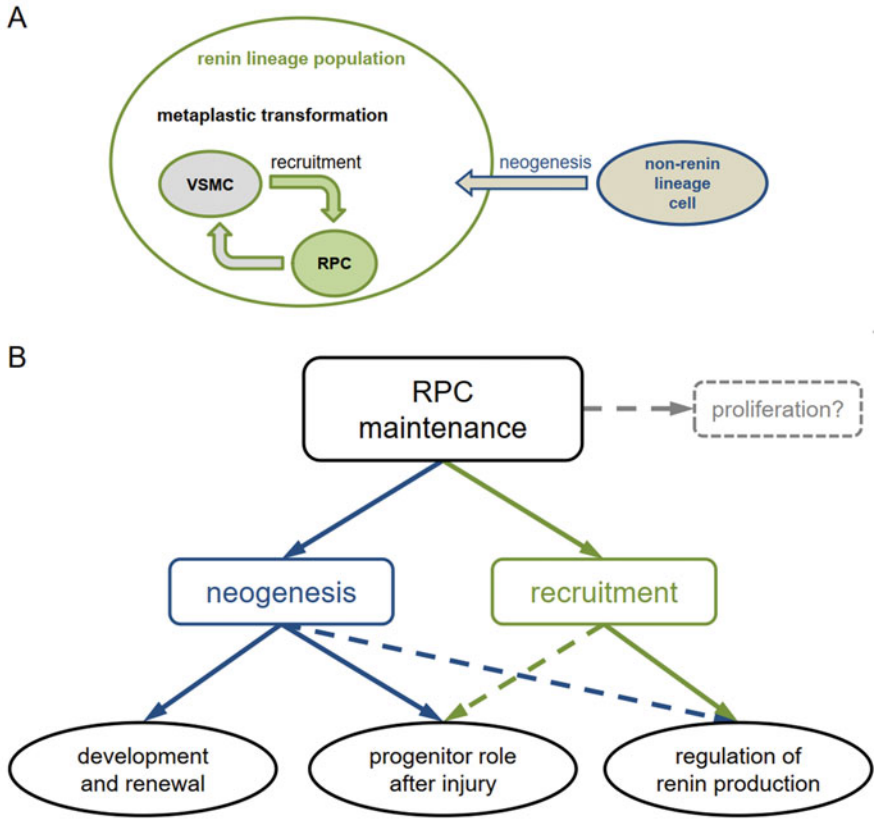

Fig. 4 Recruitment and neogenesis of renin-producing cells (RPC). (**a**) Schematic presentation of the difference between recruitment and neogenesis. Metaplastic transformation is a phenotype switch within the developmental RPC pool (see also Fig. 2) where recruitment specifically refers to the transformation of VSMC into RPC. In neogenesis, an unrelated cell enters the renin lineage population by starting to express renin for the first time (see also Sect. 3). (**b**) Role of recruitment and neogenesis in the maintenance of the RPC population. The role of proliferation therein is not well understood. Dashed arrows represent secondary role. *VSMC* vascular smooth muscle cell

controversial whether this increase might be beneficial (NB! only when RAS activity is inhibited in terms of AT1-dependent Ang II effects) or not (Moniwa et al. 2013).

2.3 Protection of Renal Microvascular Endothelium

Lately, our studies revealed that RPC are quite surprisingly involved in the maintenance of renal capillary endothelium in adulthood. This novel function of RPC has been discovered when characterizing an inducible transgenic model with compromised Gs-alpha/cAMP signaling pathway (Lachmann et al. 2017).

Gs-alpha is the stimulatory subunit of membrane receptor coupled trimeric G-proteins (Spiegel et al. 1992; Weinstein et al. 2001). It catalyzes the generation of cAMP upon ligand binding to the associated receptor. The RPC are equipped with Gs-alpha coupled IP/EP2/EP4 and beta-adrenergic receptors mediating effects of prostanoids and catecholamines, respectively (Boivin et al. 2001; Churchill et al. 1983; Facemire et al. 2011; Friis et al. 2005; Jensen et al. 1996; Karger et al. 2018; Kim et al. 2007; Schweda et al. 2004). Blood pressure fluctuations seem to modulate renal prostanoid production and sympathetic nerve activity to regulate renin production by adjusting the RPC number (Chen et al. 2010b; Kim et al. 2012). Therefore, Gs-alpha/cAMP signaling is central for renin synthesis and secretion, thus essentially determining the RPC phenotype (see also Sect. 2.1.1). It was predictable that the induction of Gs-alpha knockout in RPC of adult mice would result in renin deficiency and arterial hypotension (Kessel et al. 2019; Lachmann et al. 2017). However, these changes were transient because the drop in blood pressure served as a stimulus to recruit RPC in upstream parts of the afferent arterioles (see Sect. 2.2) that were not affected by the pulse induction of the Gs-alpha knockout. Although normal renin production and blood pressure persisted after these initial fluctuations, the JG-specific Gs-alpha-deficient mice developed chronic kidney disease. The adverse renal phenotype most unexpectedly included microvascular endothelial damage featured by morphological and systemic signs of thrombotic microangiopathy (Benz and Amann 2010; Lachmann et al. 2017). Remarkably, kidney injury developed on the background of normalized renin production, indicating that RPC exhibit protective effects on renal microvascular endothelium-independent on their role in the control of RAS activity (Lachmann et al. 2017). The mode of action of RPC on endothelial cells is multifaceted, and the implicated interactions are just beginning to be unraveled. One mechanism involves the production of angiogenic factors by RPC, which has been displayed in several studies (Brunskill et al. 2011; Haltia et al. 1996; Lachmann et al. 2017; Sequeira Lopez and Gomez 2011). Within the RPC-derived proangiogenic cues, vascular endothelial growth factor (VEGF) appears to be particularly relevant for two reasons. First, both pharmacological inhibition and genetically induced intrarenal deficiency of VEGF result in thrombotic microangiopathy (Eremina et al. 2008; Sison et al. 2010). Second, VEGF is a cAMP-regulated gene and its expression in RPC is induced by cAMP (Bradbury et al. 2005; Han et al. 2013; Lachmann et al. 2017). Another factor contributing to the proangiogenic capacity of RPC appears to be their secretory phenotype per se. This conclusion is also based on findings in adult RPC-specific Gs-alpha-deficient mice, where the RPC have been found to persist after Gs-alpha knockout as renin-negative cells (Steglich et al. 2019). In the persisting RPC progeny, a pool of 16 genes involved in tissue remodeling with vascular damage and fibrosis including collagens and TGF-beta were upregulated. Simultaneously, genes conferring the identity of RPC such as renin itself, connexin 40, and aldo-keto reductase family 1 member B7 (Akr1b7) was downregulated. Ablation of RPC resulted in renin deficiency but failed to produce any sign of endothelial injury (Steglich et al. 2019). This observation additionally confirmed that Gs-alpha-negative RPC descendants are necessary for the development of endothelial dysfunction.

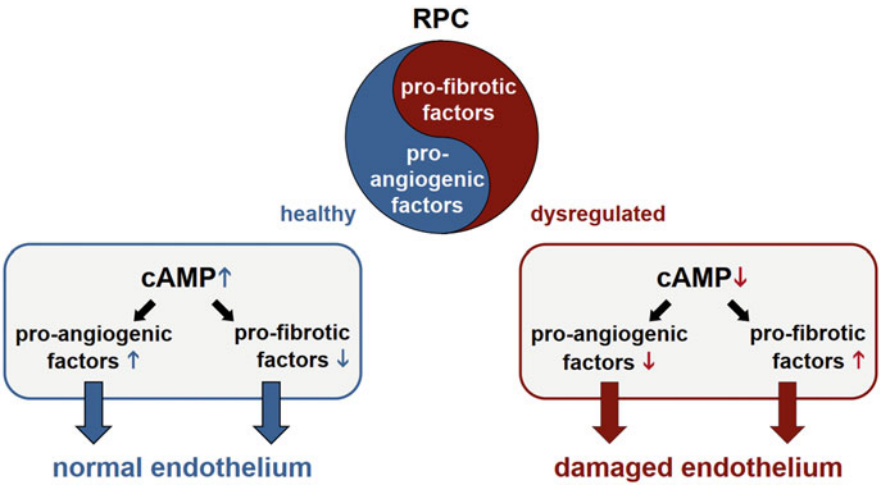

Fig. 5 Current view on the non-canonical effects of renin-producing cells (RPC) on renal microvascular endothelium

In total, the inactivation of Gs-alpha/cAMP signaling seems to switch the RPC phenotype from "protective/secretory" to "damaging/profibrotic" (Fig. 5).

The discovery of a protective role of RPC on renal microvasculature elicits some very exciting questions to be addressed in the future. As discussed above in this section, RPC recruitment is a cAMP-regulated process. Therefore, it would be interesting to know whether the recruitable VSMC in the afferent arterioles may exert profibrotic remodeling effects when not switched to the renin-producing phenotype. It is now established that renal VSMC are of heterogeneous embryonic origin (see Sect. 2.1.1) implying that RPC-derived and non-RPC-derived VSMC may have different functional characteristics. Vice versa, a decrease of RPC number when renin production is suppressed, for instance, in some forms of arterial hypertension, could be an independent risk factor for renal damage. Extrapolating these considerations would suggest that the renoprotective effects of pharmacological RAS inhibitors rely on cAMP-dependent RPC recruitment on top of the Ang II antagonism. Therefore, discoveries of further mechanisms involved in the complex interactions between RPC and kidney microvasculature with potential pathophysiological and therapeutic significance are anticipated.

3 Renin Lineage Cells

Studies in adult mice, rats, and humans unequivocally demonstrated that many organs and specialized tissues express renin mRNA albeit to a much lesser level than the JG cells. The non-JG renin-expressing cells are part of local or tissue-specific RASs (Paul et al. 2006). However, the JG cells appear to be the sole source

for plasma renin because circulating renin disappears after bilateral nephrectomy (Fordis et al. 1983; Hannon et al. 1969; Katz et al. 1997). The generation of renin from its inactive precursor prorenin upon binding to the prorenin receptor does not essentially contribute to the plasma renin activity (Nguyen et al. 2014, 2002; Rosendahl et al. 2014).

Systemic and local RASs functionally integrate into concerted Ang II-mediated effects in a way that the local RASs modulate the action of systemic RAS (Paul et al. 2006). Accordingly, fate-tracing experiments demonstrated that a marked number of cells in kidneys, spleen, bone marrow, and endocrine pancreas of the adult organism could be attributed to the renin lineage (Belyea et al. 2014; Desch et al. 2011; Glenn et al. 2014; Hickmann et al. 2017; Sequeira Lopez et al. 2004). These findings prompted the definition of a renin lineage cell (RLC) population which comprises all cells collectively featured by the expression of renin gene and/or the presence of a renin-expressing cell in their ancestry (Hickmann et al. 2017). The existence of local RAS infers that RLC build a huge population spread throughout the whole body. Such a conclusion appears to diverge from the paradigm that the JG cells are the sole RPC niche in adulthood. Indeed, there is still some controversy on the systemic availability of renin from source(s) other than the JG cells. The current view is a kind of reasonable compromise postulating that in certain diseases such as diabetes mellitus, high-grade obesity, or some subsets of arterial hypertension, renin from non-JG origin would be of pathophysiological relevance. The major issue provoking conflicting interpretations is that with very few exceptions such as pituitary, adrenal glands, or testes (Lee et al. 2005; Naruse et al. 1985), renin protein is detectable exclusively in JG cells of the kidney. The JG cells are the only cell type in the adult organism equipped with molecular machinery to store renin in secretory vesicles, which greatly facilitates their identification as renin-positive cells (Hackenthal et al. 1990; Lacasse et al. 1985; Mendez 2014; Taugner et al. 1984, 1985). In all other renin-expressing cell types, the translated (pro)renin protein is constitutively sequestered to the extracellular compartment. Thus, the lack of secretory granules together with the much lower renin mRNA expression provides a reasonable explanation for why renin is hardly observed in non-JG cells.

What about RAS independent functions for RLC? As already discussed in Sect. 2.1.1, the progenitor RPC in the kidney, which should be regarded as a subpopulation within the RLC pool, give rise not only to JG cells but also to further mural cells in the mature kidney. However, lineage-tracing experiments reproducibly demonstrated that cells in the Bowman's capsule (PE cells), proximal tubules, and collecting ducts of the adult kidney are also mapped to the renin lineage (Hickmann et al. 2017; Sequeira-Lopez et al. 2004, 2015b). Altogether, the renal RLC represent around 10% of the renal cell mass in adult mice, and it is feasible to extrapolate this data to humans. Similar to RPC, the RLC are also maintained by neogenesis balanced by apoptosis, and thus they represent a dynamic population persisting throughout adult life (Hickmann et al. 2017). Therefore, RLC appear to be fundamental for the morphological architecture of the adult mammalian kidney. On the other hand, the renal RLC are not a homogeneous population with regard to their embryonic origin. RPC and their descendants originate from FoxD1-expressing cells

in the stromal compartment of the metanephric mesenchyme (see Fig. 2b and Sect. 2.1), PE cells and proximal tubules from the core layer of the metanephric mesenchyme (known as cap mesenchyme), and collecting ducts from the ureteric bud (Humphreys et al. 2010; Kobayashi et al. 2008; Kress et al. 1990; Nelson et al. 1998; Srinivas et al. 1999). The most probable scenario for the development of FoxD1-unrelated renal RLC is that the renin gene is switched on in their transcriptional programs at some time point of embryonic differentiation. The functional importance of this event remains elusive. Tubular renin is dispensable during nephrogenesis (Sequeira-Lopez et al. 2015b). The role of collecting duct as a source of renin in diabetes mellitus and hypertensive disease is disputed (Gonzalez et al. 2011; Liu et al. 2011; Prieto-Carrasquero et al. 2004, 2005, 2009; Ramkumar et al. 2014; Song et al. 2016; Tang et al. 2019).

Taking into account that local RAS are ubiquitous, extrarenal RLC are still extremely underrepresented in current research. Such status-quo is quite amazing because the few available studies on non-kidney RLC yielded very exciting results. Brain RLC seem to protect from arterial hypertension. The mechanistic explanation is that in brain RLC a specific renin isoform is transcribed from an alternative start codon producing a truncated protein, which remains intracellularly and controls neurotransmitter release (Shinohara et al. 2016). Unfortunately, there are no studies focusing on a putative role of brain RLC after injury in the central nervous system.

RLC are detectable in the bone marrow, peripheral blood, and spleen (Belyea et al. 2014), where they are also maintained by neogenesis (Hickmann et al. 2017). The majority of the immune system RLC are B-lymphocytes. Defects in the developmental transcriptional program induced by RLC-specific knockout of the Notch pathway transcriptional effector RBP-J (recombination signal binding protein for immunoglobulin kappa J region) or p53 and retinoblastoma protein (Rb) result in B-cell leukemia or pancreatic neuroendocrine carcinoma, respectively (Belyea et al. 2014; Glenn et al. 2014). These findings imply that the embryonic differentiation of extrarenal RLC is under tight control to ensure proper organogenesis. At present, further roles for RLC in adulthood are not known.

4 Future Perspectives

This review tells a story where after entering the textbooks in the context of RAS, nowadays the renal RPC revive as a hot topic in research for their novel RAS-independent functions. Progenitor and protective features are the main aspects delineating the new non-canonical profile of RPC (see also Fig. 1). While already expanding the paradigm, the novel insights on RPC summarized above provide also an inspiration for future work. The questions to be addressed could be grouped into three prospective experimental pipelines:

1. Deciphering the molecular “motors” driving the complex protective activity of renal RPC in health and in response to tissue injury

2. Characterization of the RPC niche as a dynamic population with regard to origin, refilling and cell death
3. Unravelling the role of RLC beyond RAS

The last group includes several independent intriguing aspects. One is the role of renin in RLC – is it simply an eponymous marker or it has some non-conventional function(s)? Since renin is a protease, we hypothesize that it might be involved in the remodeling of neighboring tissue by cleavage of extracellular matrix proteins, which is a fundamental process in organ growth and regeneration. Support for RAS-unrelated protease activity of renin provided the recent observation that it activates the complement cascade by triggering C3 proteolysis (Bekassy et al. 2018). Another aspect is the idea that RLC represent stress-inducible stem cells (SISC). SISC have been recently defined as a subpopulation of progenitor cells that are particularly prone to stress-related signals (Bornstein et al. 2019). SISC are featured by coordinated signaling pathways and transcriptional signature, which enable them to be an efficient integrative part of general adaptive stress responses in the entire organism. Accordingly, in distress situations, SISC function would be dysregulated leading to maladaptive reactions and disease. It has been postulated that SISC are ubiquitous and should be present in virtually any organ and specialized tissue. Nestin and Notch1 serve as general markers of SISC populations. RLC fulfill all these criteria thus perfectly fitting into the definition for SISC (Hanner et al. 2008) (see also this section above). Stress signals influencing RLC and particularly renal RPC include acute drop in arterial blood pressure (e.g., due to hemorrhage), chronic salt depletion, extreme dehydration, hyperactivation of the sympathetic nervous system by environmental natural and social factors, etc. Therefore, it is feasible to assume that RLC build at least part of the SISC niche and that the renin lineage might be one further universal SISC marker. Being an attractive unifying concept, the presence of interrelated organ- and tissue-specific RLC (including RPC) with coordinated stress-regulated functions during development and adulthood awaits empirical support. Since transgenic animal models applicable in experiments addressing the issues formulated above already exist, a further expansion of our knowledge on renal RPC and RLC is pending.

Acknowledgments We are greatly indebted to all present and past members of the Experimental Nephrology for their devoted scientific work.

We would also like to thank Armin Kurtz from the University of Regensburg and Maria Luisa Sequeira Lopez and R. Ariel Gomez from the University of Virginia for the inspiring discussions.

The authors' work is continuously supported by Deutsche Forschungsgemeinschaft (DFG) Projects SFB 699/B1, TO 679/1-1, TO 679/2-1, TO 679/3-1 (to V.T.T.), HU 600/6-1, HU 600/8-1, HU 600/11-1, HU 600/12-1, HU 600/13-1 (to C.H.). A.L. is supported by the DFG Heisenberg-Professorship Programme (Project number 324141047). A. S. received grant from the Graduate Academy of the Technical University, Dresden.

References

Ames MK, Atkins CE, Pitt B (2019) The renin-angiotensin-aldosterone system and its suppression. J Vet Intern Med 33(2):363–382. https://doi.org/10.1111/jvim.15454

Arendse LB, Danser AHJ, Poglitsch M, Touyz RM, Burnett JC Jr, Llorens-Cortes C, Ehlers MR, Sturrock ED (2019) Novel therapeutic approaches targeting the renin-angiotensin system and associated peptides in hypertension and heart failure. Pharmacol Rev 71(4):539–570. https://doi.org/10.1124/pr.118.017129

Azizi M, Menard J (2004) Combined blockade of the renin-angiotensin system with angiotensin-converting enzyme inhibitors and angiotensin II type 1 receptor antagonists. Circulation 109 (21):2492–2499. https://doi.org/10.1161/01.CIR.0000131449.94713.AD

Bachmann S, Le Hir M, Eckardt KU (1993) Co-localization of erythropoietin mRNA and ecto-5′-nucleotidase immunoreactivity in peritubular cells of rat renal cortex indicates that fibroblasts produce erythropoietin. J Histochem Cytochem 41(3):335–341. https://doi.org/10.1177/41.3.8429197

Baumann H, Wang Y, Richards CD, Jones CA, Black TA, Gross KW (2000) Endotoxin-induced renal inflammatory response. Oncostatin M as a major mediator of suppressed renin expression. J Biol Chem 275(29):22014–22019. https://doi.org/10.1074/jbc.M002830200

Bekassy ZD, Kristoffersson AC, Rebetz J, Tati R, Olin AI, Karpman D (2018) Aliskiren inhibits renin-mediated complement activation. Kidney Int 94(4):689–700. https://doi.org/10.1016/j.kint.2018.04.004

Belyea BC, Xu F, Pentz ES, Medrano S, Li M, Hu Y, Turner S, Legallo R, Jones CA, Tario JD, Liang P, Gross KW, Sequeira-Lopez ML, Gomez RA (2014) Identification of renin progenitors in the mouse bone marrow that give rise to B-cell leukaemia. Nat Commun 5:3273. https://doi.org/10.1038/ncomms4273

Benz K, Amann K (2010) Thrombotic microangiopathy: new insights. Curr Opin Nephrol Hypertens 19(3):242–247. https://doi.org/10.1097/MNH.0b013e3283378f25

Birbrair A, Zhang T, Wang ZM, Messi ML, Mintz A, Delbono O (2015) Pericytes at the intersection between tissue regeneration and pathology. Clin Sci 128(2):81–93. https://doi.org/10.1042/CS20140278

Boivin V, Jahns R, Gambaryan S, Ness W, Boege F, Lohse MJ (2001) Immunofluorescent imaging of beta 1- and beta 2-adrenergic receptors in rat kidney. Kidney Int 59(2):515–531. https://doi.org/10.1046/j.1523-1755.2001.059002515.x

Bornstein SR, Steenblock C, Chrousos GP, Schally AV, Beuschlein F, Kline G, Krone NP, Licinio J, Wong ML, Ullmann E, Ruiz-Babot G, Boehm BO, Behrens A, Brennand A, Santambrogio A, Berger I, Werdermann M, Sancho R, Linkermann A, Lenders JW, Eisenhofer G, Andoniadou CL (2019) Stress-inducible-stem cells: a new view on endocrine, metabolic and mental disease? Mol Psychiatry 24(1):2–9. https://doi.org/10.1038/s41380-018-0244-9

Bradbury D, Clarke D, Seedhouse C, Corbett L, Stocks J, Knox A (2005) Vascular endothelial growth factor induction by prostaglandin E2 in human airway smooth muscle cells is mediated by E prostanoid EP2/EP4 receptors and SP-1 transcription factor binding sites. J Biol Chem 280 (34):29993–30000. https://doi.org/10.1074/jbc.M414530200

Broughton Pipkin F, Symonds EM, Turner SR (1982) The effect of captopril (SQ14,225) upon mother and fetus in the chronically cannulated ewe and in the pregnant rabbit. J Physiol 323:415–422. https://doi.org/10.1113/jphysiol.1982.sp014081

Brunskill EW, Sequeira-Lopez ML, Pentz ES, Lin E, Yu J, Aronow BJ, Potter SS, Gomez RA (2011) Genes that confer the identity of the renin cell. J Am Soc Nephrol 22(12):2213–2225. https://doi.org/10.1681/ASN.2011040401

Cantin M, Araujo-Nascimento MD, Benchimol S, Desormeaux Y (1977) Metaplasia of smooth muscle cells into juxtaglomerular cells in the juxtaglomerular apparatus, arteries, and arterioles of the ischemic (endocrine) kidney. An ultrastructural-cytochemical and autoradiographic study. Am J Pathol 87(3):581–602

Castellanos Rivera RM, Monteagudo MC, Pentz ES, Glenn ST, Gross KW, Carretero O, Sequeira-Lopez ML, Gomez RA (2011) Transcriptional regulator RBP-J regulates the number and plasticity of renin cells. Physiol Genomics 43(17):1021–1028. https://doi.org/10.1152/physiolgenomics.00061.2011

Castellanos-Rivera RM, Pentz ES, Lin E, Gross KW, Medrano S, Yu J, Sequeira-Lopez ML, Gomez RA (2015) Recombination signal binding protein for Ig-kappaJ region regulates juxtaglomerular cell phenotype by activating the myo-endocrine program and suppressing ectopic gene expression. J Am Soc Nephrol 26(1):67–80. https://doi.org/10.1681/ASN.2013101045

Castrop H, Hocherl K, Kurtz A, Schweda F, Todorov V, Wagner C (2010) Physiology of kidney renin. Physiol Rev 90(2):607–673. https://doi.org/10.1152/physrev.00011.2009

Celio MR, Groscurth P, Inagami T (1985) Ontogeny of renin immunoreactive cells in the human kidney. Anat Embryol 173(2):149–155. https://doi.org/10.1007/bf00316297

Chen Y, Lasaitiene D, Gabrielsson BG, Carlsson LM, Billig H, Carlsson B, Marcussen N, Sun XF, Friberg P (2004) Neonatal losartan treatment suppresses renal expression of molecules involved in cell-cell and cell-matrix interactions. J Am Soc Nephrol 15(5):1232–1243. https://doi.org/10.1097/01.asn.0000123690.75029.3f

Chen L, Kim SM, Oppermann M, Faulhaber-Walter R, Huang Y, Mizel D, Chen M, Lopez ML, Weinstein LS, Gomez RA, Briggs JP, Schnermann J (2007) Regulation of renin in mice with Cre recombinase-mediated deletion of G protein Gsalpha in juxtaglomerular cells. Am J Physiol Renal Physiol 292(1):F27–F37. https://doi.org/10.1152/ajprenal.00193.2006

Chen L, Faulhaber-Walter R, Wen Y, Huang Y, Mizel D, Chen M, Sequeira Lopez ML, Weinstein LS, Gomez RA, Briggs JP, Schnermann J (2010a) Renal failure in mice with Gsalpha deletion in juxtaglomerular cells. Am J Nephrol 32(1):83–94. https://doi.org/10.1159/000314635

Chen L, Kim SM, Eisner C, Oppermann M, Huang Y, Mizel D, Li L, Chen M, Sequeira Lopez ML, Weinstein LS, Gomez RA, Schnermann J, Briggs JP (2010b) Stimulation of renin secretion by angiotensin II blockade is Gsalpha-dependent. J Am Soc Nephrol 21(6):986–992. https://doi.org/10.1681/ASN.2009030307

Churchill PC, Churchill MC, McDonald FD (1983) Evidence that beta 1-adrenoceptor activation mediates isoproterenol-stimulated renin secretion in the rat. Endocrinology 113(2):687–692. https://doi.org/10.1210/endo-113-2-687

Daikha-Dahmane F, Levy-Beff E, Jugie M, Lenclen R (2006) Foetal kidney maldevelopment in maternal use of angiotensin II type I receptor antagonists. Pediatr Nephrol 21(5):729–732. https://doi.org/10.1007/s00467-006-0070-1

Damkjaer M, Isaksson GL, Stubbe J, Jensen BL, Assersen K, Bie P (2013) Renal renin secretion as regulator of body fluid homeostasis. Pflugers Arch 465(1):153–165. https://doi.org/10.1007/s00424-012-1171-2

Desch M, Harlander S, Neubauer B, Gerl M, Germain S, Castrop H, Todorov VT (2011) cAMP target sequences enhCRE and CNRE sense low-salt intake to increase human renin gene expression in vivo. Pflugers Arch 461(5):567–577. https://doi.org/10.1007/s00424-011-0956-z

Desch M, Hackmayer G, Todorov VT (2012) Identification of ATF2 as a transcriptional regulator of renin gene. Biol Chem 393(1–2):93–100. https://doi.org/10.1515/BC-2011-157

Dominick MA, Bobrowski WF, Metz AL, Gough AW, MacDonald JR (1990) Ultrastructural juxtaglomerular cell changes in normotensive rats treated with quinapril, an inhibitor of angiotensin-converting enzyme. Toxicol Pathol 18(3):396–406. https://doi.org/10.1177/019262339001800306

Egerer G, Taugner R, Tiedemann K (1984) Renin immunohistochemistry in the mesonephros and metanephros of the pig embryo. Histochemistry 81(4):385–390. https://doi.org/10.1007/bf00514334

Eremina V, Jefferson JA, Kowalewska J, Hochster H, Haas M, Weisstuch J, Richardson C, Kopp JB, Kabir MG, Backx PH, Gerber HP, Ferrara N, Barisoni L, Alpers CE, Quaggin SE (2008) VEGF inhibition and renal thrombotic microangiopathy. N Engl J Med 358(11):1129–1136. https://doi.org/10.1056/NEJMoa0707330

Facemire CS, Nguyen M, Jania L, Beierwaltes WH, Kim HS, Koller BH, Coffman TM (2011) A major role for the EP4 receptor in regulation of renin. Am J Physiol Renal Physiol 301(5): F1035–F1041. https://doi.org/10.1152/ajprenal.00054.2011

Fordis CM, Megorden JS, Ropchak TG, Keiser HR (1983) Absence of renin-like activity in rat aorta and microvessels. Hypertension 5(5):635–641. https://doi.org/10.1161/01.hyp.5.5.635

Fournier D, Luft FC, Bader M, Ganten D, Andrade-Navarro MA (2012) Emergence and evolution of the renin-angiotensin-aldosterone system. J Mol Med 90(5):495–508. https://doi.org/10.1007/s00109-012-0894-z

Friberg P, Sundelin B, Bohman SO, Bobik A, Nilsson H, Wickman A, Gustafsson H, Petersen J, Adams MA (1994) Renin-angiotensin system in neonatal rats: induction of a renal abnormality in response to ACE inhibition or angiotensin II antagonism. Kidney Int 45(2):485–492. https://doi.org/10.1038/ki.1994.63

Friis UG, Stubbe J, Uhrenholt TR, Svenningsen P, Nusing RM, Skott O, Jensen BL (2005) Prostaglandin E2 EP2 and EP4 receptor activation mediates cAMP-dependent hyperpolarization and exocytosis of renin in juxtaglomerular cells. Am J Physiol Renal Physiol 289(5):F989–F997. https://doi.org/10.1152/ajprenal.00201.2005

Friis UG, Madsen K, Stubbe J, Hansen PB, Svenningsen P, Bie P, Skott O, Jensen BL (2013) Regulation of renin secretion by renal juxtaglomerular cells. Pflugers Arch 465(1):25–37. https://doi.org/10.1007/s00424-012-1126-7

Gerl K, Steppan D, Fuchs M, Wagner C, Willam C, Kurtz A, Kurt B (2017) Activation of hypoxia signaling in stromal progenitors impairs kidney development. Am J Pathol 187(7):1496–1511. https://doi.org/10.1016/j.ajpath.2017.03.014

Glenn ST, Jones CA, Sexton S, LeVea CM, Caraker SM, Hajduczok G, Gross KW (2014) Conditional deletion of p53 and Rb in the renin-expressing compartment of the pancreas leads to a highly penetrant metastatic pancreatic neuroendocrine carcinoma. Oncogene 33 (50):5706–5715. https://doi.org/10.1038/onc.2013.514

Gomez RA, Sequeira-Lopez MLS (2018) Renin cells in homeostasis, regeneration and immune defence mechanisms. Nat Rev Nephrol 14(4):231–245. https://doi.org/10.1038/nrneph.2017.186

Gomez RA, Chevalier RL, Sturgill BC, Johns DW, Peach MJ, Carey RM (1986) Maturation of the intrarenal renin distribution in Wistar-Kyoto rats. J Hypertens 4(Suppl. 5):S31–S33

Gomez RA, Lynch KR, Chevalier RL, Everett AD, Johns DW, Wilfong N, Peach MJ, Carey RM (1988) Renin and angiotensinogen gene expression and intrarenal renin distribution during ACE inhibition. Am J Phys 254(6 Pt 2):F900–F906. https://doi.org/10.1152/ajprenal.1988.254.6.F900

Gomez RA, Chevalier RL, Everett AD, Elwood JP, Peach MJ, Lynch KR, Carey RM (1990) Recruitment of renin gene-expressing cells in adult rat kidneys. Am J Phys 259(4 Pt 2):F660–F665. https://doi.org/10.1152/ajprenal.1990.259.4.F660

Gomez RA, Pupilli C, Everett AD (1991) Molecular and cellular aspects of renin during kidney ontogeny. Pediatr Nephrol 5(1):80–87. https://doi.org/10.1007/bf00852854

Gomez RA, Pentz ES, Jin X, Cordaillat M, Sequeira Lopez ML (2009) CBP and p300 are essential for renin cell identity and morphological integrity of the kidney. Am J Physiol Heart Circ Physiol 296(5):H1255–H1262. https://doi.org/10.1152/ajpheart.01266.2008

Gomez RA, Belyea B, Medrano S, Pentz ES, Sequeira-Lopez ML (2014) Fate and plasticity of renin precursors in development and disease. Pediatr Nephrol 29(4):721–726. https://doi.org/10.1007/s00467-013-2688-0

Gonzalez AA, Liu L, Lara LS, Seth DM, Navar LG, Prieto MC (2011) Angiotensin II stimulates renin in inner medullary collecting duct cells via protein kinase C and independent of epithelial sodium channel and mineralocorticoid receptor activity. Hypertension 57(3):594–599. https://doi.org/10.1161/HYPERTENSIONAHA.110.165902

Graham PC, Kingdom JC, Raweily EA, Gibson AA, Lindop GB (1992) Distribution of renin-containing cells in the developing human kidney: an immunocytochemical study. Br J Obstet Gynaecol 99(9):765–769. https://doi.org/10.1111/j.1471-0528.1992.tb13881.x

Gribouval O, Gonzales M, Neuhaus T, Aziza J, Bieth E, Laurent N, Bouton JM, Feuillet F, Makni S, Ben Amar H, Laube G, Delezoide AL, Bouvier R, Dijoud F, Ollagnon-Roman E, Roume J, Joubert M, Antignac C, Gubler MC (2005) Mutations in genes in the renin-angiotensin system are associated with autosomal recessive renal tubular dysgenesis. Nat Genet 37(9):964–968. https://doi.org/10.1038/ng1623

Gribouval O, Moriniere V, Pawtowski A, Arrondel C, Sallinen SL, Saloranta C, Clericuzio C, Viot G, Tantau J, Blesson S, Cloarec S, Machet MC, Chitayat D, Thauvin C, Laurent N, Sampson JR, Bernstein JA, Clemenson A, Prieur F, Daniel L, Levy-Mozziconacci A, Lachlan K, Alessandri JL, Cartault F, Riviere JP, Picard N, Baumann C, Delezoide AL, Belar Ortega M, Chassaing N, Labrune P, Yu S, Firth H, Wellesley D, Bitzan M, Alfares A, Braverman N, Krogh L, Tolmie J, Gaspar H, Doray B, Majore S, Bonneau D, Triau S, Loirat C, David A, Bartholdi D, Peleg A, Brackman D, Stone R, DeBerardinis R, Corvol P, Michaud A, Antignac C, Gubler MC (2012) Spectrum of mutations in the renin-angiotensin system genes in autosomal recessive renal tubular dysgenesis. Hum Mutat 33(2):316–326. https://doi.org/10.1002/humu.21661

Grove KL, Mayo RJ, Forsyth CS, Frank AA, Speth RC (1995) Fosinopril treatment of pregnant rats: developmental toxicity, fetal angiotensin-converting enzyme inhibition, and fetal angiotensin II receptor regulation. Toxicol Lett 80(1–3):85–95. https://doi.org/10.1016/0378-4274(95)03346-m

Gubler MC, Antignac C (2010) Renin-angiotensin system in kidney development: renal tubular dysgenesis. Kidney Int 77(5):400–406. https://doi.org/10.1038/ki.2009.423

Hackenthal E, Paul M, Ganten D, Taugner R (1990) Morphology, physiology, and molecular biology of renin secretion. Physiol Rev 70(4):1067–1116. https://doi.org/10.1152/physrev.1990.70.4.1067

Haltia A, Solin ML, Jalanko H, Holmberg C, Miettinen A, Holthofer H (1996) Mechanisms of proteinuria: vascular permeability factor in congenital nephrotic syndrome of the Finnish type. Pediatr Res 40(5):652–657. https://doi.org/10.1203/00006450-199611000-00002

Han DY, Cho JS, Moon YM, Lee HR, Lee HM, Lee BD, Baek BJ (2013) Effect of prostaglandin e2 on vascular endothelial growth factor production in nasal polyp fibroblasts. Allergy Asthma Immunol Res 5(4):224–231. https://doi.org/10.4168/aair.2013.5.4.224

Hanner F, von Maltzahn J, Maxeiner S, Toma I, Sipos A, Kruger O, Willecke K, Peti-Peterdi J (2008) Connexin45 is expressed in the juxtaglomerular apparatus and is involved in the regulation of renin secretion and blood pressure. Am J Physiol Regul Integr Comp Physiol 295(2):R371–R380. https://doi.org/10.1152/ajpregu.00468.2007

Hannon RC, Deruyck RP, Joossens JV, Ameryak AK (1969) Disappearance rate of endogenous renin from the plasma after bilateral nephrectomy in humans. J Clin Endocrinol Metab 29(11):1420–1424. https://doi.org/10.1210/jcem-29-11-1420

Hatini V, Huh SO, Herzlinger D, Soares VC, Lai E (1996) Essential role of stromal mesenchyme in kidney morphogenesis revealed by targeted disruption of Winged Helix transcription factor BF-2. Genes Dev 10(12):1467–1478. https://doi.org/10.1101/gad.10.12.1467

Hibino S, Sasaki H, Abe Y, Hojo A, Uematsu M, Sekine T, Itabashi K (2015) Renal function in angiotensinogen gene-mutated renal tubular dysgenesis with glomerular cysts. Pediatr Nephrol 30(2):357–360. https://doi.org/10.1007/s00467-014-3007-0

Hickmann L, Steglich A, Gerlach M, Al-Mekhlafi M, Sradnick J, Lachmann P, Sequeira-Lopez MLS, Gomez RA, Hohenstein B, Hugo C, Todorov VT (2017) Persistent and inducible neogenesis repopulates progenitor renin lineage cells in the kidney. Kidney Int 92(6):1419–1432. https://doi.org/10.1016/j.kint.2017.04.014

Hilgers KF, Reddi V, Krege JH, Smithies O, Gomez RA (1997) Aberrant renal vascular morphology and renin expression in mutant mice lacking angiotensin-converting enzyme. Hypertension 29(1 Pt 2):216–221. https://doi.org/10.1161/01.hyp.29.1.216

Hohenstein B, Braun A, Amann KU, Johnson RJ, Hugo CP (2008) A murine model of site-specific renal microvascular endothelial injury and thrombotic microangiopathy. Nephrol Dial Transplant 23(4):1144–1156. https://doi.org/10.1093/ndt/gfm774

Hugo C, Hugo C, Pichler R, Gordon K, Schmidt R, Amieva M, Couser WG, Furthmayr H, Johnson RJ (1996) The cytoskeletal linking proteins, moesin and radixin, are upregulated by platelet-derived growth factor, but not basic fibroblast growth factor in experimental mesangial proliferative glomerulonephritis. J Clin Invest 97(11):2499–2508. https://doi.org/10.1172/JCI118697

Hugo C, Shankland SJ, Bowen-Pope DF, Couser WG, Johnson RJ (1997) Extraglomerular origin of the mesangial cell after injury. A new role of the juxtaglomerular apparatus. J Clin Invest 100 (4):786–794. https://doi.org/10.1172/JCI119592

Humphreys BD, Lin SL, Kobayashi A, Hudson TE, Nowlin BT, Bonventre JV, Valerius MT, McMahon AP, Duffield JS (2010) Fate tracing reveals the pericyte and not epithelial origin of myofibroblasts in kidney fibrosis. Am J Pathol 176(1):85–97. https://doi.org/10.2353/ajpath.2010.090517

Iosipiv IV, Schroeder M (2003) A role for angiotensin II AT1 receptors in ureteric bud cell branching. Am J Physiol Renal Physiol 285(2):F199–F207. https://doi.org/10.1152/ajprenal.00401.2002

Jensen BL, Schmid C, Kurtz A (1996) Prostaglandins stimulate renin secretion and renin mRNA in mouse renal juxtaglomerular cells. Am J Phys 271(3 Pt 2):F659–F669. https://doi.org/10.1152/ajprenal.1996.271.3.F659

Jha V, Garcia-Garcia G, Iseki K, Li Z, Naicker S, Plattner B, Saran R, Wang AY, Yang CW (2013) Chronic kidney disease: global dimension and perspectives. Lancet 382(9888):260–272. https://doi.org/10.1016/S0140-6736(13)60687-X

Just A, Kurtz L, de Wit C, Wagner C, Kurtz A, Arendshorst WJ (2009) Connexin 40 mediates the tubuloglomerular feedback contribution to renal blood flow autoregulation. J Am Soc Nephrol 20(7):1577–1585. https://doi.org/10.1681/ASN.2008090943

Karger C, Machura K, Schneider A, Hugo C, Todorov VT, Kurtz A (2018) COX-2-derived PGE2 triggers hyperplastic renin expression and hyperreninemia in aldosterone synthase-deficient mice. Pflugers Arch 470(7):1127–1137. https://doi.org/10.1007/s00424-018-2118-z

Katz SA, Opsahl JA, Lunzer MM, Forbis LM, Hirsch AT (1997) Effect of bilateral nephrectomy on active renin, angiotensinogen, and renin glycoforms in plasma and myocardium. Hypertension 30(2 Pt 1):259–266. https://doi.org/10.1161/01.hyp.30.2.259

Kaverina NV, Eng DG, Largent AD, Daehn I, Chang A, Gross KW, Pippin JW, Hohenstein P, Shankland SJ (2017a) WT1 is necessary for the proliferation and migration of cells of renin lineage following kidney podocyte depletion. Stem Cell Rep 9(4):1152–1166. https://doi.org/10.1016/j.stemcr.2017.08.020

Kaverina NV, Kadoya H, Eng DG, Rusiniak ME, Sequeira-Lopez ML, Gomez RA, Pippin JW, Gross KW, Peti-Peterdi J, Shankland SJ (2017b) Tracking the stochastic fate of cells of the renin lineage after podocyte depletion using multicolor reporters and intravital imaging. PLoS One 12 (3):e0173891. https://doi.org/10.1371/journal.pone.0173891

Kessel F, Steglich A, Tschongov T, Gembardt F, Ruhnke L, Stumpf J, Behrendt R, Cohrs C, Kopaliani I, Todorov V, Gerlach M, Hugo C (2019) New automatic quantification method of immunofluorescence and histochemistry in whole histological sections. Cell Signal 62:109335. https://doi.org/10.1016/j.cellsig.2019.05.020

Kim HS, Krege JH, Kluckman KD, Hagaman JR, Hodgin JB, Best CF, Jennette JC, Coffman TM, Maeda N, Smithies O (1995) Genetic control of blood pressure and the angiotensinogen locus. Proc Natl Acad Sci U S A 92(7):2735–2739. https://doi.org/10.1073/pnas.92.7.2735

Kim SM, Chen L, Faulhaber-Walter R, Oppermann M, Huang Y, Mizel D, Briggs JP, Schnermann J (2007) Regulation of renin secretion and expression in mice deficient in beta1- and beta2-adrenergic receptors. Hypertension 50(1):103–109. https://doi.org/10.1161/HYPERTENSIONAHA.107.087577

Kim SM, Briggs JP, Schnermann J (2012) Convergence of major physiological stimuli for renin release on the Gs-alpha/cyclic adenosine monophosphate signaling pathway. Clin Exp Nephrol 16(1):17–24. https://doi.org/10.1007/s10157-011-0494-1

Knott PD, Thorpe SS, Lamont CA (1989) Congenital renal dysgenesis possibly due to captopril. Lancet 1(8635):451. https://doi.org/10.1016/s0140-6736(89)90058-5

Kobayashi A, Valerius MT, Mugford JW, Carroll TJ, Self M, Oliver G, McMahon AP (2008) Six2 defines and regulates a multipotent self-renewing nephron progenitor population throughout mammalian kidney development. Cell Stem Cell 3(2):169–181. https://doi.org/10.1016/j.stem.2008.05.020

Krege JH, John SW, Langenbach LL, Hodgin JB, Hagaman JR, Bachman ES, Jennette JC, O'Brien DA, Smithies O (1995) Male-female differences in fertility and blood pressure in ACE-deficient mice. Nature 375(6527):146–148. https://doi.org/10.1038/375146a0

Kress C, Vogels R, De Graaff W, Bonnerot C, Meijlink F, Nicolas JF, Deschamps J (1990) Hox-2.3 upstream sequences mediate lacZ expression in intermediate mesoderm derivatives of transgenic mice. Development 109(4):775–786

Kurt B, Kurtz A (2015) Plasticity of renal endocrine function. Am J Physiol Regul Integr Comp Physiol 308(6):R455–R466. https://doi.org/10.1152/ajpregu.00568.2013

Kurt B, Paliege A, Willam C, Schwarzensteiner I, Schucht K, Neymeyer H, Sequeira-Lopez ML, Bachmann S, Gomez RA, Eckardt KU, Kurtz A (2013) Deletion of von Hippel-Lindau protein converts renin-producing cells into erythropoietin-producing cells. J Am Soc Nephrol 24(3):433–444. https://doi.org/10.1681/ASN.2012080791

Kurt B, Gerl K, Karger C, Schwarzensteiner I, Kurtz A (2015) Chronic hypoxia-inducible transcription factor-2 activation stably transforms juxtaglomerular renin cells into fibroblast-like cells in vivo. J Am Soc Nephrol 26(3):587–596. https://doi.org/10.1681/ASN.2013111152

Kurtz A (2015) Connexins, renin cell displacement and hypertension. Curr Opin Pharmacol 21:1–6. https://doi.org/10.1016/j.coph.2014.11.009

Kurtz A (2017) Endocrine functions of the renal interstitium. Pflugers Arch 469(7–8):869–876. https://doi.org/10.1007/s00424-017-2008-9

Kurtz A (2019) Nobel prize 2019 pays tribute to translational physiology on oxygen sensing. Pflugers Arch 471(11–12):1341–1342. https://doi.org/10.1007/s00424-019-02328-6

Kurtz L, Janssen-Bienhold U, Kurtz A, Wagner C (2009) Connexin expression in renin-producing cells. J Am Soc Nephrol 20(3):506–512. https://doi.org/10.1681/ASN.2008030252

Lacasse J, Ballak M, Mercure C, Gutkowska J, Chapeau C, Foote S, Menard J, Corvol P, Cantin M, Genest J (1985) Immunocytochemical localization of renin in juxtaglomerular cells. J Histochem Cytochem 33(4):323–332. https://doi.org/10.1177/33.4.3884706

Lachmann P, Hickmann L, Steglich A, Al-Mekhlafi M, Gerlach M, Jetschin N, Jahn S, Hamann B, Wnuk M, Madsen K, Djonov V, Chen M, Weinstein LS, Hohenstein B, Hugo CPM, Todorov VT (2017) Interference with gsalpha-coupled receptor signaling in renin-producing cells leads to renal endothelial damage. J Am Soc Nephrol 28(12):3479–3489. https://doi.org/10.1681/ASN.2017020173

Landing BH, Ang SM, Herta N, Larson EF, Turner M (1994) Labeled lectin studies of renal tubular dysgenesis and renal tubular atrophy of postnatal renal ischemia and end-stage kidney disease. Pediatr Pathol 14(1):87–99. https://doi.org/10.3109/15513819409022029

Lee G, Makhanova N, Caron K, Lopez ML, Gomez RA, Smithies O, Kim HS (2005) Homeostatic responses in the adrenal cortex to the absence of aldosterone in mice. Endocrinology 146(6):2650–2656. https://doi.org/10.1210/en.2004-1102

Lichtnekert J, Kaverina NV, Eng DG, Gross KW, Kutz JN, Pippin JW, Shankland SJ (2016) Renin-angiotensin-aldosterone system inhibition increases podocyte derivation from cells of renin lineage. J Am Soc Nephrol 27(12):3611–3627. https://doi.org/10.1681/ASN.2015080877

Lin EE, Sequeira-Lopez ML, Gomez RA (2014) RBP-J in FOXD1+ renal stromal progenitors is crucial for the proper development and assembly of the kidney vasculature and glomerular mesangial cells. Am J Physiol Renal Physiol 306(2):F249–F258. https://doi.org/10.1152/ajprenal.00313.2013

Linkermann A (2019) Death and fire-the concept of necroinflammation. Cell Death Differ 26(1):1–3. https://doi.org/10.1038/s41418-018-0218-0

Liu X, Shi Q, Sigmund CD (2006) Interleukin-1beta attenuates renin gene expression via a mitogen-activated protein kinase kinase-extracellular signal-regulated kinase and signal

transducer and activator of transcription 3-dependent mechanism in As4.1 cells. Endocrinology 147(12):6011–6018. https://doi.org/10.1210/en.2006-0129

Liu L, Gonzalez AA, McCormack M, Seth DM, Kobori H, Navar LG, Prieto MC (2011) Increased renin excretion is associated with augmented urinary angiotensin II levels in chronic angiotensin II-infused hypertensive rats. Am J Physiol Renal Physiol 301(6):F1195–F1201. https://doi.org/10.1152/ajprenal.00339.2011

Madsen K, Marcussen N, Pedersen M, Kjaersgaard G, Facemire C, Coffman TM, Jensen BL (2010) Angiotensin II promotes development of the renal microcirculation through AT1 receptors. J Am Soc Nephrol 21(3):448–459. https://doi.org/10.1681/ASN.2009010045

Martinez MF, Medrano S, Brown EA, Tufan T, Shang S, Bertoncello N, Guessoum O, Adli M, Belyea BC, Sequeira-Lopez MLS, Gomez RA (2018) Super-enhancers maintain renin-expressing cell identity and memory to preserve multi-system homeostasis. J Clin Invest 128 (11):4787–4803. https://doi.org/10.1172/JCI121361

Martini AG, Danser AHJ (2017) Juxtaglomerular cell phenotypic plasticity. High Blood Press Cardiovasc Prev 24(3):231–242. https://doi.org/10.1007/s40292-017-0212-5

Maxwell PH, Ferguson DJ, Nicholls LG, Iredale JP, Pugh CW, Johnson MH, Ratcliffe PJ (1997) Sites of erythropoietin production. Kidney Int 51(2):393–401. https://doi.org/10.1038/ki.1997.52

McCausland JE, Bertram JF, Ryan GB, Alcorn D (1997) Glomerular number and size following chronic angiotensin II blockade in the postnatal rat. Exp Nephrol 5(3):201–209

Medrano S, Monteagudo MC, Sequeira-Lopez ML, Pentz ES, Gomez RA (2012) Two microRNAs, miR-330 and miR-125b-5p, mark the juxtaglomerular cell and balance its smooth muscle phenotype. Am J Physiol Renal Physiol 302(1):F29–F37. https://doi.org/10.1152/ajprenal.00460.2011

Mendez M (2014) Renin release: role of SNAREs. Am J Physiol Regul Integr Comp Physiol 307 (5):R484–R486. https://doi.org/10.1152/ajpregu.00175.2014

Michaud A, Bur D, Gribouval O, Muller L, Iturrioz X, Clemessy M, Gasc JM, Gubler MC, Corvol P (2011) Loss-of-function point mutations associated with renal tubular dysgenesis provide insights about renin function and cellular trafficking. Hum Mol Genet 20(2):301–311. https://doi.org/10.1093/hmg/ddq465

Molteni A, Rahill WJ, Koo JH (1974) Evidence for a vasopressor substance (renin) in human fetal kidneys. Lab Investig 30(2):115–118

Moniwa N, Varagic J, Ahmad S, VonCannon JL, Simington SW, Wang H, Groban L, Brosnihan KB, Nagata S, Kato J, Kitamura K, Gomez RA, Lopez ML, Ferrario CM (2013) Hemodynamic and hormonal changes to dual renin-angiotensin system inhibition in experimental hypertension. Hypertension 61(2):417–424. https://doi.org/10.1161/HYPERTENSIONAHA.112.201889

Mooser V, Nussberger J, Juillerat L, Burnier M, Waeber B, Bidiville J, Pauly N, Brunner HR (1990) Reactive hyperreninemia is a major determinant of plasma angiotensin II during ACE inhibition. J Cardiovasc Pharmacol 15(2):276–282. https://doi.org/10.1097/00005344-199002000-00015

Muzumdar MD, Tasic B, Miyamichi K, Li L, Luo L (2007) A global double-fluorescent Cre reporter mouse. Genesis 45(9):593–605. https://doi.org/10.1002/dvg.20335

Naruse K, Murakoshi M, Osamura RY, Naruse M, Toma H, Watanabe K, Demura H, Inagami T, Shizume K (1985) Immunohistological evidence for renin in human endocrine tissues. J Clin Endocrinol Metab 61(1):172–177. https://doi.org/10.1210/jcem-61-1-172

Nelson RD, Stricklett P, Gustafson C, Stevens A, Ausiello D, Brown D, Kohan DE (1998) Expression of an AQP2 Cre recombinase transgene in kidney and male reproductive system of transgenic mice. Am J Phys 275(1):C216–C226. https://doi.org/10.1152/ajpcell.1998.275.1.C216

Neubauer B, Machura K, Chen M, Weinstein LS, Oppermann M, Sequeira-Lopez ML, Gomez RA, Schnermann J, Castrop H, Kurtz A, Wagner C (2009) Development of vascular renin expression in the kidney critically depends on the cyclic AMP pathway. Am J Physiol Renal Physiol 296 (5):F1006–F1012. https://doi.org/10.1152/ajprenal.90448.2008

Nguyen G, Delarue F, Burckle C, Bouzhir L, Giller T, Sraer JD (2002) Pivotal role of the renin/prorenin receptor in angiotensin II production and cellular responses to renin. J Clin Invest 109 (11):1417–1427. https://doi.org/10.1172/JCI14276

Nguyen G, Blanchard A, Curis E, Bergerot D, Chambon Y, Hirose T, Caumont-Prim A, Tabard SB, Baron S, Frank M, Totsune K, Azizi M (2014) Plasma soluble (pro)renin receptor is independent of plasma renin, prorenin, and aldosterone concentrations but is affected by ethnicity. Hypertension 63(2):297–302. https://doi.org/10.1161/HYPERTENSIONAHA.113.02217

Niimura F, Labosky PA, Kakuchi J, Okubo S, Yoshida H, Oikawa T, Ichiki T, Naftilan AJ, Fogo A, Inagami T et al (1995) Gene targeting in mice reveals a requirement for angiotensin in the development and maintenance of kidney morphology and growth factor regulation. J Clin Invest 96(6):2947–2954. https://doi.org/10.1172/JCI118366

Nussberger J, Gradman AH, Schmieder RE, Lins RL, Chiang Y, Prescott MF (2007) Plasma renin and the antihypertensive effect of the orally active renin inhibitor aliskiren in clinical hypertension. Int J Clin Pract 61(9):1461–1468. https://doi.org/10.1111/j.1742-1241.2007.01473.x

Oka M, Medrano S, Sequeira-Lomicronpez MLS, Gomez RA (2017) Chronic stimulation of renin cells leads to vascular pathology. Hypertension 70(1):119–128. https://doi.org/10.1161/HYPERTENSIONAHA.117.09283

Oliverio MI, Kim HS, Ito M, Le T, Audoly L, Best CF, Hiller S, Kluckman K, Maeda N, Smithies O, Coffman TM (1998) Reduced growth, abnormal kidney structure, and type 2 (AT2) angiotensin receptor-mediated blood pressure regulation in mice lacking both AT1A and AT1B receptors for angiotensin II. Proc Natl Acad Sci U S A 95(26):15496–15501. https://doi.org/10.1073/pnas.95.26.15496

Owen RA, Molon-Noblot S, Hubert MF, Kindt MV, Keenan KP, Eydelloth RS (1994) The morphology of juxtaglomerular cell hyperplasia and hypertrophy in normotensive rats and monkeys given an angiotensin II receptor antagonist. Toxicol Pathol 22(6):606–619. https://doi.org/10.1177/019262339402200605

Paul M, Poyan Mehr A, Kreutz R (2006) Physiology of local renin-angiotensin systems. Physiol Rev 86(3):747–803. https://doi.org/10.1152/physrev.00036.2005

Pentz ES, Moyano MA, Thornhill BA, Sequeira Lopez ML, Gomez RA (2004) Ablation of renin-expressing juxtaglomerular cells results in a distinct kidney phenotype. Am J Physiol Regul Integr Comp Physiol 286(3):R474–R483. https://doi.org/10.1152/ajpregu.00426.2003

Petrovic N, Kane CM, Sigmund CD, Gross KW (1997) Downregulation of renin gene expression by interleukin-1. Hypertension 30(2 Pt 1):230–235. https://doi.org/10.1161/01.hyp.30.2.230

Pierrou S, Hellqvist M, Samuelsson L, Enerback S, Carlsson P (1994) Cloning and characterization of seven human forkhead proteins: binding site specificity and DNA bending. EMBO J 13 (20):5002–5012

Pippin JW, Kaverina NV, Eng DG, Krofft RD, Glenn ST, Duffield JS, Gross KW, Shankland SJ (2015) Cells of renin lineage are adult pluripotent progenitors in experimental glomerular disease. Am J Physiol Renal Physiol 309(4):F341–F358. https://doi.org/10.1152/ajprenal.00438.2014

Polifka JE (2012) Is there an embryopathy associated with first-trimester exposure to angiotensin-converting enzyme inhibitors and angiotensin receptor antagonists? A critical review of the evidence. Birth Defects Res A Clin Mol Teratol 94(8):576–598. https://doi.org/10.1002/bdra.23027

Prieto-Carrasquero MC, Harrison-Bernard LM, Kobori H, Ozawa Y, Hering-Smith KS, Hamm LL, Navar LG (2004) Enhancement of collecting duct renin in angiotensin II-dependent hypertensive rats. Hypertension 44(2):223–229. https://doi.org/10.1161/01.HYP.0000135678.20725.54

Prieto-Carrasquero MC, Kobori H, Ozawa Y, Gutierrez A, Seth D, Navar LG (2005) AT1 receptor-mediated enhancement of collecting duct renin in angiotensin II-dependent hypertensive rats. Am J Physiol Renal Physiol 289(3):F632–F637. https://doi.org/10.1152/ajprenal.00462.2004

Prieto-Carrasquero MC, Botros FT, Kobori H, Navar LG (2009) Collecting duct renin: a major player in angiotensin II-dependent hypertension. J Am Soc Hypertens 3(2):96–104. https://doi.org/10.1016/j.jash.2008.11.003

Pugh D, Gallacher PJ, Dhaun N (2019) Management of hypertension in chronic kidney disease. Drugs 79(4):365–379. https://doi.org/10.1007/s40265-019-1064-1

Ramkumar N, Stuart D, Rees S, Hoek AV, Sigmund CD, Kohan DE (2014) Collecting duct-specific knockout of renin attenuates angiotensin II-induced hypertension. Am J Physiol Renal Physiol 307(8):F931–F938. https://doi.org/10.1152/ajprenal.00367.2014

Rasch R, Jensen BL, Nyengaard JR, Skott O (1998) Quantitative changes in rat renin secretory granules after acute and chronic stimulation of the renin system. Cell Tissue Res 292 (3):563–571. https://doi.org/10.1007/s004410051085

Robillard JE, Nakamura KT (1988) Neurohormonal regulation of renal function during development. Am J Phys 254(6 Pt 2):F771–F779. https://doi.org/10.1152/ajprenal.1988.254.6.F771

Rosendahl A, Niemann G, Lange S, Ahadzadeh E, Krebs C, Contrepas A, van Goor H, Wiech T, Bader M, Schwake M, Peters J, Stahl R, Nguyen G, Wenzel UO (2014) Increased expression of (pro)renin receptor does not cause hypertension or cardiac and renal fibrosis in mice. Lab Investig 94(8):863–872. https://doi.org/10.1038/labinvest.2014.83

Ruhnke L, Sradnick J, Al-Mekhlafi M, Gerlach M, Gembardt F, Hohenstein B, Todorov VT, Hugo C (2018) Progenitor Renin Lineage Cells are not involved in the regeneration of glomerular endothelial cells during experimental renal thrombotic microangiopathy. PLoS One 13(5): e0196752. https://doi.org/10.1371/journal.pone.0196752

Santos RAS, Sampaio WO, Alzamora AC, Motta-Santos D, Alenina N, Bader M, Campagnole-Santos MJ (2018) The ACE2/angiotensin-(1-7)/MAS axis of the renin-angiotensin system: focus on angiotensin-(1-7). Physiol Rev 98(1):505–553. https://doi.org/10.1152/physrev.00023.2016

Sarhan M, Land WG, Tonnus W, Hugo CP, Linkermann A (2018) Origin and consequences of necroinflammation. Physiol Rev 98(2):727–780. https://doi.org/10.1152/physrev.00041.2016

Sauter A, Machura K, Neubauer B, Kurtz A, Wagner C (2008) Development of renin expression in the mouse kidney. Kidney Int 73(1):43–51. https://doi.org/10.1038/sj.ki.5002571

Schonig K, Schwenk F, Rajewsky K, Bujard H (2002) Stringent doxycycline dependent control of CRE recombinase in vivo. Nucleic Acids Res 30(23):e134. https://doi.org/10.1093/nar/gnf134

Schweda F, Kurtz A (2011) Regulation of renin release by local and systemic factors. Rev Physiol Biochem Pharmacol 161:1–44. https://doi.org/10.1007/112_2008_1

Schweda F, Klar J, Narumiya S, Nusing RM, Kurtz A (2004) Stimulation of renin release by prostaglandin E2 is mediated by EP2 and EP4 receptors in mouse kidneys. Am J Physiol Renal Physiol 287(3):F427–F433. https://doi.org/10.1152/ajprenal.00072.2004

Seaberg RM, van der Kooy D (2003) Stem and progenitor cells: the premature desertion of rigorous definitions. Trends Neurosci 26(3):125–131. https://doi.org/10.1016/S0166-2236(03)00031-6

Sequeira Lopez ML, Gomez RA (2011) Development of the renal arterioles. J Am Soc Nephrol 22 (12):2156–2165. https://doi.org/10.1681/ASN.2011080818

Sequeira Lopez ML, Pentz ES, Nomasa T, Smithies O, Gomez RA (2004) Renin cells are precursors for multiple cell types that switch to the renin phenotype when homeostasis is threatened. Dev Cell 6(5):719–728. https://doi.org/10.1016/s1534-5807(04)00134-0

Sequeira-Lopez ML, Weatherford ET, Borges GR, Monteagudo MC, Pentz ES, Harfe BD, Carretero O, Sigmund CD, Gomez RA (2010) The microRNA-processing enzyme dicer maintains juxtaglomerular cells. J Am Soc Nephrol 21(3):460–467. https://doi.org/10.1681/ASN.2009090964

Sequeira-Lopez ML, Lin EE, Li M, Hu Y, Sigmund CD, Gomez RA (2015a) The earliest metanephric arteriolar progenitors and their role in kidney vascular development. Am J Physiol Regul Integr Comp Physiol 308(2):R138–R149. https://doi.org/10.1152/ajpregu.00428.2014

Sequeira-Lopez ML, Nagalakshmi VK, Li M, Sigmund CD, Gomez RA (2015b) Vascular versus tubular renin: role in kidney development. Am J Physiol Regul Integr Comp Physiol 309(6): R650–R657. https://doi.org/10.1152/ajpregu.00313.2015

Shinohara K, Liu X, Morgan DA, Davis DR, Sequeira-Lopez ML, Cassell MD, Grobe JL, Rahmouni K, Sigmund CD (2016) Selective deletion of the brain-specific isoform of renin

causes neurogenic hypertension. Hypertension 68(6):1385–1392. https://doi.org/10.1161/HYPERTENSIONAHA.116.08242

Sison K, Eremina V, Baelde H, Min W, Hirashima M, Fantus IG, Quaggin SE (2010) Glomerular structure and function require paracrine, not autocrine, VEGF-VEGFR-2 signaling. J Am Soc Nephrol 21(10):1691–1701. https://doi.org/10.1681/ASN.2010030295

Song K, Stuart D, Abraham N, Wang F, Wang S, Yang T, Sigmund CD, Kohan DE, Ramkumar N (2016) Collecting duct renin does not mediate DOCA-salt hypertension or renal injury. PLoS One 11(7):e0159872. https://doi.org/10.1371/journal.pone.0159872

Sparks MA, Crowley SD, Gurley SB, Mirotsou M, Coffman TM (2014) Classical renin-angiotensin system in kidney physiology. Compr Physiol 4(3):1201–1228. https://doi.org/10.1002/cphy.c130040

Spiegel AM, Shenker A, Weinstein LS (1992) Receptor-effector coupling by G proteins: implications for normal and abnormal signal transduction. Endocr Rev 13(3):536–565. https://doi.org/10.1210/edrv-13-3-536

Sradnick J, Rong S, Luedemann A, Parmentier SP, Bartaun C, Todorov VT, Gueler F, Hugo CP, Hohenstein B (2016) Extrarenal progenitor cells do not contribute to renal endothelial repair. J Am Soc Nephrol 27(6):1714–1726. https://doi.org/10.1681/ASN.2015030321

Srinivas S, Goldberg MR, Watanabe T, D'Agati V, al-Awqati Q, Costantini F (1999) Expression of green fluorescent protein in the ureteric bud of transgenic mice: a new tool for the analysis of ureteric bud morphogenesis. Dev Genet 24(3–4):241–251. https://doi.org/10.1002/(SICI)1520-6408(1999)24:3/4<241::AID-DVG7>3.0.CO;2-R

Starke C, Betz H, Hickmann L, Lachmann P, Neubauer B, Kopp JB, Sequeira-Lopez ML, Gomez RA, Hohenstein B, Todorov VT, Hugo CP (2015) Renin lineage cells repopulate the glomerular mesangium after injury. J Am Soc Nephrol 26(1):48–54. https://doi.org/10.1681/ASN.2014030265

Stefanska A, Peault B, Mullins JJ (2013) Renal pericytes: multifunctional cells of the kidneys. Pflugers Arch 465(6):767–773. https://doi.org/10.1007/s00424-013-1263-7

Steglich A, Kessel F, Hickmann L, Gerlach M, Lachmann P, Gembardt F, Lesche M, Dahl A, Federlein A, Schweda F, Hugo CPM, Todorov VT (2019) Renin cells with defective Gsalpha/cAMP signaling contribute to renal endothelial damage. Pflugers Arch 471(9):1205–1217. https://doi.org/10.1007/s00424-019-02298-9

Takahashi N, Lopez ML, Cowhig JE Jr, Taylor MA, Hatada T, Riggs E, Lee G, Gomez RA, Kim HS, Smithies O (2005) Ren1c homozygous null mice are hypotensive and polyuric, but heterozygotes are indistinguishable from wild-type. J Am Soc Nephrol 16(1):125–132. https://doi.org/10.1681/ASN.2004060490

Tang J, Wysocki J, Ye M, Valles PG, Rein J, Shirazi M, Bader M, Gomez RA, Sequeira-Lopez MS, Afkarian M, Batlle D (2019) Urinary renin in patients and mice with diabetic kidney disease. Hypertension 74(1):83–94. https://doi.org/10.1161/HYPERTENSIONAHA.119.12873

Taugner R, Buhrle CP, Nobiling R (1984) Ultrastructural changes associated with renin secretion from the juxtaglomerular apparatus of mice. Cell Tissue Res 237(3):459–472. https://doi.org/10.1007/bf00228430

Taugner R, Whalley A, Angermuller S, Buhrle CP, Hackenthal E (1985) Are the renin-containing granules of juxtaglomerular epithelioid cells modified lysosomes? Cell Tissue Res 239(3):575–587. https://doi.org/10.1007/bf00219236

Todorov V, Muller M, Schweda F, Kurtz A (2002) Tumor necrosis factor-alpha inhibits renin gene expression. Am J Physiol Regul Integr Comp Physiol 283(5):R1046–R1051. https://doi.org/10.1152/ajpregu.00142.2002

Todorov VT, Volkl S, Muller M, Bohla A, Klar J, Kunz-Schughart LA, Hehlgans T, Kurtz A (2004) Tumor necrosis factor-alpha activates NFkappaB to inhibit renin transcription by targeting cAMP-responsive element. J Biol Chem 279(2):1458–1467. https://doi.org/10.1074/jbc.M308697200

Todorov VT, Volkl S, Friedrich J, Kunz-Schughart LA, Hehlgans T, Vermeulen L, Haegeman G, Schmitz ML, Kurtz A (2005) Role of CREB1 and NF{kappa}B-p65 in the down-regulation of

renin gene expression by tumor necrosis factor {alpha}. J Biol Chem 280(26):24356–24362. https://doi.org/10.1074/jbc.M502968200

Tufro-McReddie A, Romano LM, Harris JM, Ferder L, Gomez RA (1995) Angiotensin II regulates nephrogenesis and renal vascular development. Am J Phys 269(1 Pt 2):F110–F115. https://doi.org/10.1152/ajprenal.1995.269.1.F110

Urlinger S, Baron U, Thellmann M, Hasan MT, Bujard H, Hillen W (2000) Exploring the sequence space for tetracycline-dependent transcriptional activators: novel mutations yield expanded range and sensitivity. Proc Natl Acad Sci U S A 97(14):7963–7968. https://doi.org/10.1073/pnas.130192197

Wagner C, Kurtz A (2013) Distribution and functional relevance of connexins in renin-producing cells. Pflugers Arch 465(1):71–77. https://doi.org/10.1007/s00424-012-1134-7

Wagner C, de Wit C, Kurtz L, Grunberger C, Kurtz A, Schweda F (2007) Connexin40 is essential for the pressure control of renin synthesis and secretion. Circ Res 100(4):556–563. https://doi.org/10.1161/01.RES.0000258856.19922.45

Wang Y, Eng DG, Pippin JW, Gharib SA, McClelland A, Gross KW, Shankland SJ (2018) Sex differences in transcriptomic profiles in aged kidney cells of renin lineage. Aging 10 (4):606–621. https://doi.org/10.18632/aging.101416

Weinstein LS, Yu S, Warner DR, Liu J (2001) Endocrine manifestations of stimulatory G protein alpha-subunit mutations and the role of genomic imprinting. Endocr Rev 22(5):675–705. https://doi.org/10.1210/edrv.22.5.0439

Xiao X, Chen Z, Shiota C, Prasadan K, Guo P, El-Gohary Y, Paredes J, Welsh C, Wiersch J, Gittes GK (2013) No evidence for beta cell neogenesis in murine adult pancreas. J Clin Invest 123 (5):2207–2217. https://doi.org/10.1172/JCI66323

Yanai K, Saito T, Kakinuma Y, Kon Y, Hirota K, Taniguchi-Yanai K, Nishijo N, Shigematsu Y, Horiguchi H, Kasuya Y, Sugiyama F, Yagami K, Murakami K, Fukamizu A (2000) Renin-dependent cardiovascular functions and renin-independent blood-brain barrier functions revealed by renin-deficient mice. J Biol Chem 275(1):5–8. https://doi.org/10.1074/jbc.275.1.5

Yo Y, Braun MC, Barisoni L, Mobaraki H, Lu H, Shrivastav S, Owens J, Kopp JB (2003) Anti-mouse mesangial cell serum induces acute glomerulonephropathy in mice. Nephron Exp Nephrol 93(3):e92–e106. https://doi.org/10.1159/000069551

Zivna M, Hulkova H, Matignon M, Hodanova K, Vylet'al P, Kalbacova M, Baresova V, Sikora J, Blazkova H, Zivny J, Ivanek R, Stranecky V, Sovova J, Claes K, Lerut E, Fryns JP, Hart PS, Hart TC, Adams JN, Pawtowski A, Clemessy M, Gasc JM, Gubler MC, Antignac C, Elleder M, Kapp K, Grimbert P, Bleyer AJ, Kmoch S (2009) Dominant renin gene mutations associated with early-onset hyperuricemia, anemia, and chronic kidney failure. Am J Hum Genet 85 (2):204–213. https://doi.org/10.1016/j.ajhg.2009.07.010

Rev Physiol Biochem Pharmacol (2020) 177: 83–100
https://doi.org/10.1007/112_2020_45

Published online: 14 August 2020

Role of ASIC1a in Normal and Pathological Synaptic Plasticity

Dalila Mango and Robert Nisticò

Contents

Abstract Acid-sensing ion channels (ASICs), members of the degenerin/epithelial Na+ channel superfamily, are broadly distributed in the mammalian nervous system where they play important roles in a variety of physiological processes, including neurotransmission and memory-related behaviors. In the last few years, we and others have investigated the role of ASIC1a in different forms of synaptic plasticity especially in the CA1 area of the hippocampus. This review summarizes the latest research linking ASIC1a to synaptic function either in physiological or pathological

D. Mango (✉)
Laboratory of Pharmacology of Synaptic Plasticity, EBRI Rita Levi-Montalcini Foundation, Rome, Italy

R. Nisticò
Laboratory of Pharmacology of Synaptic Plasticity, EBRI Rita Levi-Montalcini Foundation, Rome, Italy

School of Pharmacy, University of Rome Tor Vergata, Rome, Italy
e-mail: robert.nistico@uniroma2.it

conditions. A better understanding of how these channels are regulated in brain circuitries relevant to synaptic plasticity and memory may offer novel targets for pharmacological intervention in neuropsychiatric and neurological disorders.

Keywords Acid-sensing ion channel · LTD · LTP · Synaptic transmission

Abbreviations

AD	Alzheimer's disease
ASICs	Acid-sensing ion channels
CNS	Central nervous system
EAE	Experimental autoimmune encephalomyelitis
EPSCs	Excitatory post-synaptic currents
LTD	Long-term depression
LTP	Long-term potentiation
MS	Multiple sclerosis
NAc	Nucleus accumbens
NMDA	N-methyl-D-aspartate
PcTx1	Psalmotoxin-1

1 Introduction

The first evidence that protons (H^+) act on specific receptors was observed in 1981 by Krishtal and Pidoplichko. An inward current mediated by Na^+ ions in response to rapid external pH change lower than 7.4 was recorded in sensory neurons (Krishtal and Pidoplichko 1981a, b).

In 1997 the channel was cloned for the first time by Waldmann and colleagues and has been termed acid-sensing ion channel (ASIC) (Waldmann et al. 1997).

More studies subsequently have investigated expression, structure, pharmacology, and the role of ASIC channels (ASICs) in physiology and pathology.

In the past, the presence of protons in the synaptic vesicles storing neurotransmitter was a well-known physiological condition (Anderson and Orci 1988; Liu and Edwards 1997; Miesenbock et al. 1998). During neural activity, protons, which are co-released with neurotransmitters, promote the acidification of synaptic cleft (Palmer et al. 2003; Hnasko and Edwards 2012) and this fostered the idea that protons can act as transmitters. Indeed, it is now recognized that extracellular acidification occurs in different physiological states such as basal synaptic transmission and plasticity (Chesler and Kaila 1992; Trapp et al. 1996; Chesler 2003; Kim and Trussell 2009; Magnotta et al. 2012).

However, the binding of protons to ASICs produces only a very small inward current which is difficult to detect, and this explains why proton-mediated currents

were not considered in neurotransmission for a long time (Alvarez De La Rosa et al. 2003; Du et al. 2014; Kreple et al. 2014; Mango and Nisticò 2019).

Nowadays it has been widely demonstrated that ASICs play a role in synaptic transmission, neuroplasticity, and also in learning, memory, and fear responses (Wemmie et al. 2002, 2003; Chu and Xiong 2012; Huang et al. 2015). Moreover, many studies have shown that ASICs are implicated in different pathological conditions, including ischemic stroke (Chu and Xiong 2012), epileptic seizures (Ziemann et al. 2008), autoimmune encephalomyelitis (Friese et al. 2007), and Alzheimer's disease (AD) (Mango and Nisticò 2018).

In the present work we will first provide a general overview of ASIC1a and then describe the role of ASIC1a in synaptic plasticity under normal and pathological conditions.

2 ASIC1a Structure and Location

ASICs belong to the superfamily of degenerin/epithelial sodium channel (Deg/ENaC) (Waldmann et al. 1997; Bianchi and Driscoll 2002; Krishtal 2003), which are expressed abundantly in the nervous system (Noel et al. 2010; Sluka et al. 2009).

ASICs are voltage-insensitive, chemically gated, ion channels which are blocked, non-selectively, by amiloride (Krishtal and Pidoplichko 1981a, b; Waldmann et al. 1997; Kellenberger and Schild 2015).

Six different mammalian protein subunits have been cloned (ASIC1a, ASIC1b, ASIC2a, ASIC2b, ASIC3, and ASIC4), among which, the "a" and "b" represent two splice variants for ASIC1 and ASIC2 genes (Waldmann et al. 1997; Chen et al. 1998; Bässler et al. 2001). Each ASIC subunit has two transmembrane domains. Functional ASIC channels can be assembled from either homomeric or heteromeric subunit combinations to form functional channels (Krishtal 2003; Gonzales et al. 2009; Jasti et al. 2007; Babinski et al. 1999; Baron et al. 2001; Bassilana et al. 1997; Chu et al. 2004; Hesselager et al. 2004; Voilley et al. 2001; Waldmann and Lazdunski 1998). These channels are activated by acidic pH that mediates a Na^+ or Ca^{2+} inward current that induces neuronal depolarization (Deval et al. 2003; Vukicevic and Kellenberger 2004; Poirot et al. 2006) and are sensitive to blockade with amiloride.

ASIC1a, ASIC2, and ASIC4 subunits are mainly found in the central nervous system (CNS) (Wemmie et al. 2003; Coryell et al. 2009; Price et al. 2014), while ASIC3 are more common in sensory neurons of the spinal cord and ganglia (Waldmann et al. 1997; Deval and Lingueglia 2015).

ASIC1a is the most abundant form expressed in the mammalian CNS where it is mainly found in hippocampus, amygdala, cingulate cortex, somatosensorial cortex, and striatum (Alvarez De La Rosa et al. 2003; Wemmie et al. 2003; Coryell et al. 2009).

ASIC1a localization is predominant in the soma region and in the dendritic spines of neurons where they play a role in modulating their number and density (Alvarez De La Rosa et al. 2003; Xiang-ming et al. 2006). Here, ASIC1a subunit allows Ca^{2+} influx making it of strong interest for neuronal processes in which calcium plays a key role (Waldmann et al. 1997; Bässler et al. 2001; Boillat et al. 2014) such as learning, memory, synaptic transmission, and plasticity (Wemmie et al. 2002).

3 Experimental Tools to Investigate ASIC1a

Ligands of ASIC1a were identified in the last 20 years and consist in endogenous modulators, animal toxins, and chemicals.

3.1 Endogenous Modulators

The endogenous polyamine *spermine,* which is abundantly present in the brain where it potentiates the action of N-methyl-D-aspartate (NMDA) at micromolar concentrations, is able to increase sensitization of ASIC1a-mediated currents (Babini et al. 2002; Duan et al. 2011). Notably, also *histamine* was found to potentiate ASIC1a current (Nagaeva et al. 2016). Also some ligands of histamine receptors show significant potentiation of ASIC1a currents and should therefore be considered ASIC modulators (Shteinikov et al. 2017).

3.2 Polypeptide Toxins

The first selective and potent pharmacological tool to study ASIC1a was isolated from *Psalmopoeus cambridgei* tarantula venom. Psalmotoxin-1 (PcTx1) is a polypeptide toxin that specifically inhibits homomeric ASIC1a with an IC50 of ~1 nM (Escoubas et al. 2000).

MitTx is a non-covalent heterodimeric peptide isolated from the venom of the *Micrurus tener tener* snake, whose neurotoxic venom can produce extreme pain, and even death (Bohlen et al. 2011).

The *mambalgins* are a family of peptides isolated from the venom of several *Dendroaspis* mamba snakes. Mambalgin-1 is a potent and selective blocker of ASIC1a (IC50 = 55 nM) having no effect on ASIC2a, ASIC3, ASIC1a+ASIC3, and ASIC1b+ASIC3 channels (Diochot et al. 2012).

3.3 Chemicals

Many compounds targeting ASIC have been identified so far. The first is amiloride, a classic potassium-sparing diuretic, which also acts as a reversible ASIC inhibitor with IC_{50} values in the low micromolar range (Kleyman and Cragoe 1988; Schild et al. 1997).

Several non-steroidal anti-inflammatory drugs (NSAIDs) affect ASIC1a function (Voilley et al. 2001).

Flurbiprofen and ibuprofen are not particularly potent (IC50 ~350 μM) but are selective for ASIC1a versus the other ASIC channels (Voilley et al. 2001).

Our group has demonstrated that CHF5074 (also called CSP-1103), a derivative of flurbiprofen, can also induce a potent inhibition of ASIC1a-mediated currents induced by application of pH 5.5 bath medium (IC50 ~50 nM) (Mango et al. 2014).

Diminazene, drug used to treat trypanosomiasis, was able to inhibit ASIC1a by blocking the ion pore (Krauson et al. 2018).

PPC-5650 is a novel selective antagonist of ASIC1a (IC50 500 nM) that reduces hyperalgesia in the human inflammatory model of pain (Dube et al. 2009). It is currently being tested in clinical trials for the treatment of irritable bowel syndrome, characterized by chronic abdominal pain (Olesen et al. 2015).

NS-383 is a small molecule with a potent and selective inhibitory activity on ASIC1a that has been shown to reduce neuropathic hyperalgesia in rats (IC50 ~0.44 μM) (Munro et al. 2016).

Finally, ASC06-IgG1 is a novel potent antibody with selective ASIC1a inhibitor activity (IC50 ~0.85 nM) that has been shown to protect cells from acid-mediated death (Qiang et al. 2018).

3.4 ASIC Knockout Mice

ASIC knockout mice were generated in 1996 by deleting a region of genomic DNA encoding the first 121 amino acids of ASICα (Price et al. 1996). ASIC1 null mice show normal viability, fertility, life span, motor, and behavioral activity (Wemmie et al. 2002). Recently, floxed ASIC1a mice were generated. This mice model lacks selectively ASIC1a gene in the nervous system (Wu et al. 2013) and seemingly shows a normal phenotype.

4 Role of ASIC1a in Normal Synaptic Plasticity

Synaptic plasticity refers to the ability of synapses to modify their strength in response to experience (Bliss and Collingridge 1993). ASIC1a current has been implicated in the two major forms of synaptic plasticity, namely long-term

Table 1 The table summarizes relevant data relative ASIC1a role in synaptic plasticity in different brain areas

Brain area	Tools	Synaptic plasticity			Literature
Amygdala	ASIC ko	↓ LTP	–	–	Du et al. (2014)
	ASIC ko	↓ LTP	–	–	Chiang et al. (2015)
Cortex	PcTx1/ASIC ko	↓ LTP	n.c. LTD	n.c. AMPA/ NMDA ratio	Li et al. (2019)
	PcTx/ASIC ko	n.c. LTP	↓ LTD	–	Li et al. (2016)
Hippocampus	PcTx1	–	↓ LTD	–	Mango and Nisticò (2019)
	ASIC ko	↓ LTP	–	–	Wemmie et al. (2002)
	PcTx1 + Aβ	–	↓ LTD	–	Mango and Nisticò (2018)
	PcTxl	–	↓ LTD	–	Mango et al. (2017)
	5b	↓ LTP	–	–	Buta et al. (2015)
	PcTx1/ASIC ko	↓ LTP	n.c. LTD	–	Liu et al. (2016)
Striatum	ASIC ko	–		↑ AMPA/ NMDA ratio	Yu et al. (2018)
	ASIC ko + cocaine	–		↓ AMPA/ NMDA ratio	Kreple et al. (2014)

Electrophysiological readouts include long-term potentiation (LTP), long-term depression (LTD), and AMPA/NMDA ratio. For each result, we report the principal references. *n.c.* no change

potentiation (LTP) and long-term depression (LTD). These synaptic events have been mainly investigated in discrete brain regions such as hippocampus, striatum, amygdala, and cortex. Other studies also investigated the AMPA/NMDA ratio which represents a functional measure of the relative expression of AMPAR and NMDAR at the synapse (Mango et al. 2017; Yu et al. 2018; Wang et al. 2018; Li et al. 2019) (see Table 1). This review focuses primarily on the role of ASICs in hippocampal synaptic plasticity, even though novel functions are emerging in other brain areas. In particular, in the striatum, ASIC1a facilitates excitatory synaptic function which underlies striatum-mediated plasticity and procedural learning and memory (Yu et al. 2018). Moreover, in the hippocampal-prefrontal circuitry, ASIC1a contributes to extinction-driven plasticity through the modulation of NMDA receptor function (Wang et al. 2018). Finally, in the anterior cingulate cortex, ASIC1a mediates synaptic potentiation critically modulating pain hypersensitivity, thus highlighting ASIC1a as a potential target for the treatment of chronic pain (Li et al. 2019).

4.1 Long-Term Potentiation (LTP)

Consistent with the robust expression of ASIC1a in amygdala and hippocampus (Wemmie et al. 2002, 2003; Poirot et al. 2006), mice lacking ASIC1 exhibit impairment in multiple fear-related behaviors enclosing acquisition and retention of conditioned fear (Wemmie et al. 2003; Coryell et al. 2007). On the contrary, a

transgenic mice overexpressing ASIC1 displays increased context fear conditioning (Wemmie et al. 2004). Also, Chiang and colleagues (2015) have demonstrated that fear learning requires ASIC-dependent LTP at amygdala synapses.

Controversial observations on the role of ASIC1a in hippocampal LTP are present in the literature. Indeed, Wemmie and colleagues were the first to demonstrate that ASIC1a is required for LTP (Wemmie et al. 2002). They have shown an impairment of LTP in brain slices obtained from ASIC1a KO mice. However, these results were not confirmed in a subsequent study using CRE-mediated knockout of ASIC1a mice (Wu et al. 2013).

In addition, subsequent studies using different electrophysiological approaches suggested a contribution of ASIC1a to hippocampal LTP (Buta et al. 2015; Liu et al. 2016). These different results suggest that system and experimental conditions, including electrophysiological approach, animal age, recording temperature, and concentration of the ASIC1a blocker used, are important to detect and to expose the contribution of the ASIC1a component. Indeed, the evidences on the role of ASIC1a in hippocampal LTP are still contentious and elusive.

Following these studies, it has been suggested that ASIC1a facilitates the activation of the NMDA receptor occurring in LTP induction, suggesting a functional interplay between these receptors in the regulation of hippocampal synaptic plasticity (Du et al. 2014; Wemmie et al. 2002; Buta et al. 2015; Liu et al. 2016).

It is possible to assume that ASIC1a facilitates neuronal depolarization especially during high frequency stimulation and this may promote the opening of NMDA receptors which function as the induction trigger of hippocampal LTP (Collingridge et al. 1983). However, other studies are needed to better understand the role of ASIC1a channel in hippocampal synaptic plasticity.

4.2 Long-Term Depression (LTD)

In the past years, our group has investigated the possible contribution of ASIC1a in synaptic transmission and two different forms of hippocampal LTD, the metabotropic glutamate (mGlu)- and NMDA receptor-dependent LTD (Mango and Nisticò 2019; Mango et al. 2017) (Fig. 1).

In order to assess whether ASIC1 is involved in basal excitatory transmission, we recorded excitatory post-synaptic currents (EPSCs) elicited by stimulation of the Schaffer collaterals fibers. As expected, application of the ionotropic glutamate receptor antagonists CNQX and D-AP5 strongly decreased EPSC amplitude. In this condition, the residual current was further reduced by application of PcTx1 (100 ng/ml). The amplitude of the isolated ASIC1a-mediated current is very small, yet significant (Fig. 1a).

We have also shown the role of ASIC1a in the modulation of group I mGlu receptor-dependent synaptic plasticity in juvenile and adult mice. Indeed, we demonstrated that in slices obtained from early adult mice (P30-P40), PcTx1 was able to

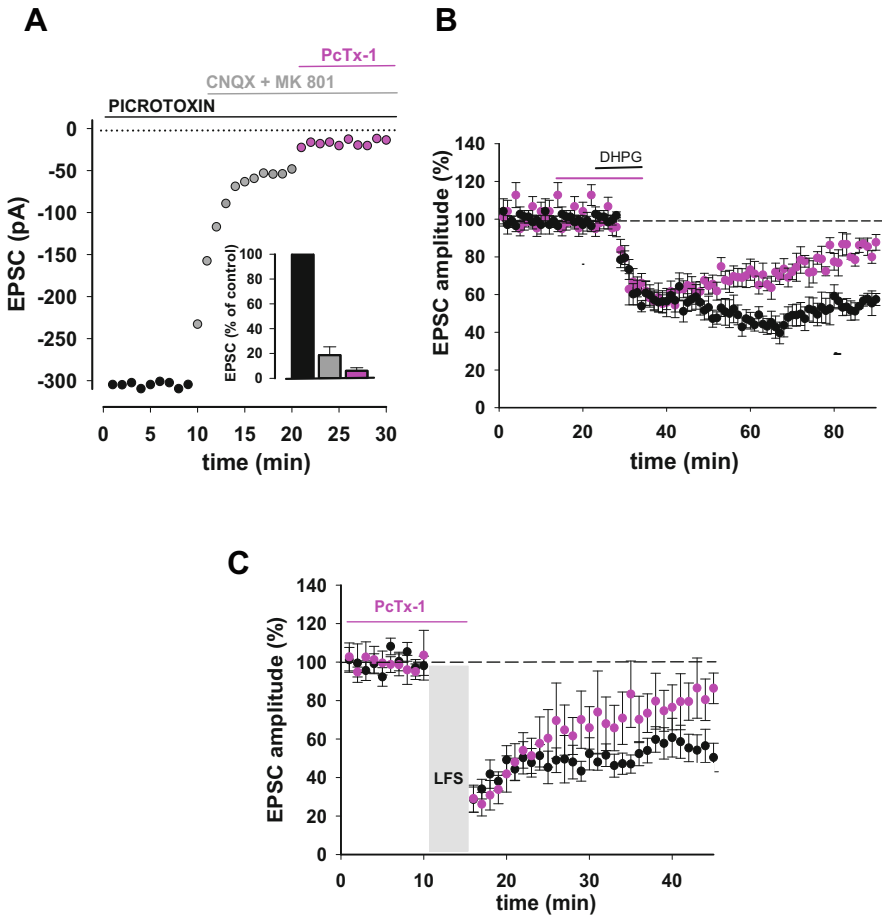

Fig. 1 ASIC1a contributes to basal excitatory transmission and modulates different forms of LTD in CA1 of hippocampus. (**a**) Isolated ASIC1a current elicited by stimulation of the Schaffer collaterals fibers in the presence of selective receptors antagonists. (**b**) Normalized pooled data showing mGlu receptor-dependent LTD in control condition and in the presence of PcTx1. (**c**) Normalized pooled data showing NMDA receptor-dependent LTD in control condition and in the presence of PcTx1

reduce, in a concentration-dependent manner, the induction of DHPG-dependent LTD (Fig. 1b).

Using a standard post-synaptic-enriched biochemical preparation, we found that the levels of p-GluA1/GluA1 ratio were significantly increased upon DHPG treatment compared to control, and that PcTx1was able to reverse the DHPG-mediated increase in phospho-GluA1/GluA1ratio (Mango et al. 2017). Overall, these results indicate ASIC1a is able to regulate post-synaptic AMPA-GluA1 subunit phosphorylation, suggesting that a functional interplay between ASIC1a and AMPA receptors

might occur during mGlu receptor LTD, even though the exact mechanisms remain to be clarified.

Next, to shed some light on the role of ASIC1a in another form of synaptic plasticity, we have performed an electrophysiological study to explore the involvement of ASIC1a in NMDA receptor-dependent LTD, in young and adult mice (Mango and Nisticò 2019). We observed that blocking ASIC1a with PcTx1 was able to decrease the magnitude of NMDA receptor LTD in both age stages (Fig. 1c), and this was confirmed by the non-selective ASIC blocker amiloride (100 μM).

Of note, Gao et al. (2005) have previously demonstrated an interaction between ASIC1a and NMDA receptor function. They show that ASIC1a activity plays a key role in facilitating the opening of NMDA receptor channel, whereas inhibition of ASIC1a impaired NMDA receptor function at physiological pH (Ma et al. 2019). Also, a recent paper has shown an increase of the NMDA receptor current following ASIC1a activation, which is mediated by the NR2 subunit (Craig 2009). Based on these results, it can be hypothesized that the opening of ASIC1a might contribute to depolarize the post-synaptic cell thus allowing Ca^{2+} influx through the NMDA receptor within the dendritic spine thereby contributing to the modulation of LTD.

On the other hand, Li et al. (2019) show that ASIC1a is involved in LTP but not in LTD in the anterior cingulate cortex, suggesting that ASIC1a plays brain region-specific roles in synaptic plasticity as previously described (Li et al. 2019). Another study investigated the role of ASIC1a in LTD in the insular cortex in which this channel subunit is highly expressed (Waldmann et al. 1997; Wemmie et al. 2003). Insular cortex is critical for cognition, sensory integration (Qiu et al. 2013), chronic pain (Qiu et al. 2014; Nieuwenhuys 2012), emotional control (Damasio et al. 2000) and processing (Qiu et al. 2013; Bermudez-Rattoni 2004), and gustatory recognition memory (Rosenblum et al. 1997). It is best known for its role in taste learning and processing aversively motivated learning (Li et al. 2016). In this brain region, ASIC1a is a critical modulator of LTD and this function is important for the extinction of the acquired taste aversion memory (Nisticò et al. 2017).

5 Role of ASIC1a in Pathological Synaptic Plasticity

Synaptic plasticity alterations occur in different pathological conditions some of which characterized by an inflammatory state such as Alzheimer's disease and multiple sclerosis (Amor et al. 2014), and also in drug-seeking behavior (Lv et al. 2011). Several studies highlighted the role of ASIC1a in other brain disorders such as ischemia, neuronal injury and epilepsy, multiple sclerosis, Huntington disease and Parkinson disease (Ziemann et al. 2008; Ma et al. 2019; Vergo et al. 2011; Arias et al. 2008; Selkoe 2001; Hu et al. 2014).

5.1 Alzheimer's Disease

Alzheimer's disease is a chronic neurodegenerative pathological condition characterized by progressive memory impairment and cognitive ability loss (Chapman et al. 1999).

Today, only one study has investigated the role of ASIC1a in experimental AD (Mango and Nisticò 2018). It is known that Aβ oligomers perturb hippocampal plasticity forms such as LTP and LTD (Chen et al. 2000; Varga et al. 2015; Mango et al. 2019; Amorini et al. 2014). In this frame, Aβ affects mGlu receptor signaling and exacerbates mGlu receptor-mediated LTD (Chen et al. 2000). Blocking ASIC1a with PcTx1, before and during LTD induction, restored the enhanced mGlu receptor-dependent LTD in slices either treated with Aβ oligomers or obtained from Tg2576, as well-known mouse model of Alzheimer disease (Mango and Nisticò 2018; Zaaraoui et al. 2010).

The significance of these results remains to be established.

5.2 Multiple Sclerosis

Multiple sclerosis (MS) is a neuroinflammatory disorder associated with prolonged acidification. Indeed, this has been demonstrated both in the experimental autoimmune encephalomyelitis (EAE) model (Friese et al. 2007) and in MS patients with high lactate concentration in serum compared to healthy subjects, which reflects the elevated concentration of lactate in the brain caused by impaired energy metabolism (Arun et al. 2013; Suman et al. 2010).

Several studies have shown an increase of ASIC1a expression in axons and an up-regulation of ASIC1a in oligodendrocytes both in the EAE model and in human MS (Wong et al. 2008; Zhang et al. 2009). Deleting or inhibiting ASIC1a reduces the EAE-induced axonal injury (Friese et al. 2007). A clinical study has previously demonstrated that oral treatment with amiloride, a non-selective ASIC1 blocker, was able to reduce brain atrophy and improve clinical score in MS patients (Zhang et al. 2009), even though the possible mechanisms underlying this effect remain to be clarified.

5.3 Cocaine Addiction

The nucleus accumbens (NAc) is a brain region that plays a crucial role in the regulation of drug-seeking behavior (Kourrich et al. 2007; Jiang et al. 2013). In medium spiny neurons of NAc, cocaine exposure alters glutamatergic transmission and receptor composition and increases the AMPA/NMDA ratio (Gutman et al. 2018). Disrupting ASIC1a in the mouse NAc increased cocaine-induced behavior;

on the other hand ASIC1a overexpression in mice reduced cocaine self-administration, overall suggesting that ASIC1a plays a role in drug addiction (Kreple et al. 2014). Accordingly, Kreple et al. (2014) demonstrated that ASIC1a null mice have increased sensitivity to cocaine. In these animals, following exposure to cocaine, glutamate receptor function and subunit composition were different to what has been found in cocaine withdrawal animals, further confirming that ASIC1a opposes cocaine-related synaptic changes and plasticity (Kreple et al. 2014). These evidences are in agreement with behavioral findings suggesting that ASIC1a ko mice show significant locomotor sensitization to chronic cocaine administration (Zha et al. 2006). Restoring ASIC1a to the NAc induced the opposite effect and reduced cocaine conditioned place preference, a model of drug reward-associated learning and memory (Kreple et al. 2014). Furthermore, the overexpression of ASIC1a in the NAc suggests a dynamic role of these channels in cocaine-taking and seeking behavior (Cho and Askwith 2008), as well as in the regulation of neuroplasticity and behavioral adaptation.

Overall, these observations indicate a role of ASIC1a in the cocaine-related changes in glutamatergic transmission which in turn may influence the addictive behavior.

6 Discussion and Conclusion

The role of ASIC1s in neuroplasticity and memory has been broadly characterized through the use of several techniques, including electrophysiology, molecular biology, biochemistry, genetics, and behavior. Protons have been found to regulate neuronal communication in several regions of the CNS being therefore considered as neurotransmitters.

It is known that ASIC1a exerts area-specific roles in modulating synaptic function and structure. Indeed, ASIC1a overexpression is associated with increased dendritic spine density (Gao et al. 2015) and the regulation of different forms of LTP and LTD in the hippocampus (Mango and Nisticò 2019; Mango et al. 2017; Liu et al. 2016). On the other hand, in the NAc MSNs, loss of ASIC1a increases dendritic spine density, whereas the overexpression of ASIC1a suppresses cocaine-evoked plasticity (Kreple et al. 2014). Also the AMPA/NMDA current ratio was differently affected in hippocampus and in NAc following ASIC1a gene ablation (Kreple et al. 2014; Zhang et al. 2020). Thus, ASICs play distinct roles in dendritic spine shape, size, and density even though the underlying mechanisms are still poorly understood.

Despite the small currents mediated by ASIC1a, it can be hypothesized that ASIC1a activation by allowing Na^+ and Ca^{2+} entry may facilitate post-synaptic depolarization required to remove Mg^{2+} block from NMDA receptors, thereby contributing to functional and structural synaptic plasticity underlying learning and memory processes.

Moreover, recent studies have shown the interplay between ASIC1a and NMDA receptors and the influence of ASICs on NMDA receptor-mediated currents (Craig 2009). Accordingly, inhibition of ASIC1a decreases post-synaptic NMDA receptor-mediated currents, while promoting ASIC1a function increases NMDA receptor activity leading to exacerbation of ischemic brain injury (Craig 2009).

The existence of this functional interaction between NMDA receptors and ASIC1a might explain why ASIC knockout mice show impaired NMDA receptor-dependent synaptic plasticity, learning and spatial memory, and a significant reduction in synapse formation (Wemmie et al. 2002; Xiang-ming et al. 2006).

Recent work by our group also highlighted that ASIC1a drives AMPA receptor plasticity. Indeed, ASIC1a regulates post-synaptic AMPA-GluA1 subunit phosphorylation following mGlu receptor-dependent synaptic plasticity (Mango et al. 2017). Notably, ASIC1a activation is necessary and sufficient to induce enhanced GluA1/GluA2 ratio associated with ischemia and excitotoxicity (Quintana et al. 2015). Overall, these observations provide additional evidence that the interplay between ASIC1a and AMPA plays a role in structural and functional synaptic plasticity in discrete regions of the brain.

On the other hand, multiple pathological processes such as inflammatory events and atherosclerosis contribute to increase proton concentration in brain (Zhang et al. 2020). Therefore, it can be hypothesized that tissue acidification occurring in neuroinflammatory, neurodegenerative conditions and during intense neuronal activity can lead to hyper-activation of ASICs which, in turn, perturb synaptic homeostasis affecting LTP and LTD expression. In line with this, blockade of ASIC1a expression has been shown to exert neuroprotective effects in AD models and in patients with multiple sclerosis. Moreover, ASIC1a is involved the synaptic and behavioral adaptation to cocaine (Fig. 2).

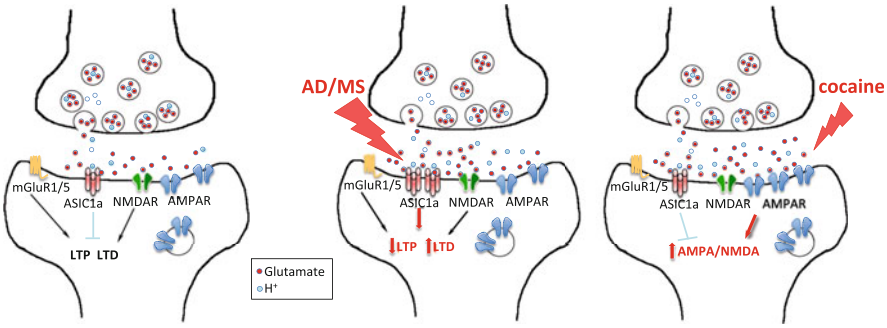

Fig. 2 Cartoon showing the proposed role of ASIC1a in the physiological and pathological synapse. In the hippocampus, ASIC1a is implicated in both LTP and LTD since PcTx1 is able to inhibit both forms of synaptic plasticity. On the other hand, in Alzheimer disease (AD) and Multiple sclerosis (MS), pathological triggers including Aβ and inflammatory mediators increase the synaptic expression of ASIC1a thereby leading to synaptic dysfunction manifested as decreased LTP and enhanced LTD. In cocaine-evoked plasticity, in which AMPA-to-NMDA ratio and glutamatergic transmission are altered, it can be hypothesized that ASIC1a activation may normalize neurotransmission thereby reducing addiction-related neuroplasticity and behavior

More effort is required to unveil new aspects of proton-mediated signaling and to validate the potential targeting of ASICs for the treatment of neuropsychiatric and neurological disorders.

Contributions DM conceived the idea and prepared the manuscript, RN prepared the manuscript and reviewed the drafts. All authors contributed to the writing and final approval of the manuscript.

Conflicts of Interest The authors declare no conflict of interest.

References

Alvarez De La Rosa D, Krueger SR, Kolar A, Shao D, Fitzsimonds RM, Canessa CM (2003) Distribution, subcellular localization and ontogeny of ASIC1 in the mammalian central nervous system. J Physiol 546:77–87

Amor S, Peferoen LA, Vogel DY, Breur M, van der Valk P, Baker D, van Noort JM (2014) Inflammation in neurodegenerative diseases – an update. Immunology 142:151–166

Amorini AM, Nociti V, Petzold A, Gasperini C, Quartuccio E, Lazzarino G, Di Pietro V, Belli A, Signoretti S, Vagnozzi R, Lazzarino G, Tavazzi B (2014) Serum lactate as a novel potential biomarker in multiple sclerosis. Biochim Biophys Acta 1842:1137–1143

Anderson RG, Orci L (1988) A view of acidic intracellular compartments. J Cell Biol 106:539–543

Arias RL, Sung MLA, Vasylyev D, Zhang MY, Albinson K, Kubek K, Kagan N, Beyer C, Lin Q, Dwyer JM, Zaleska MM, Bowlby MR, Dunlop J, Monaghan M (2008) Amiloride is neuroprotective in an MPTP model of Parkinson's disease. Neurobiol Dis 31:334–341

Arun T, Tomassini V, Sbardella E, de Ruiter MB, Matthews L, Leite MI, Gelineau-Morel R, Cavey A, Vergo S, Craner M, Fugger L, Rovira A, Jenkinson M, Palace J (2013) Targeting ASIC1 in primary progressive multiple sclerosis: evidence of neuroprotection with amiloride. Brain 136:106–115

Babini E, Paukert M, Geisler HS, Grunder S (2002) Alternative splicing and interaction with di- and polyvalent cations control the dynamic range of acid-sensing ion channel 1 (ASIC1). J Biol Chem 277:41597–41603

Babinski K, Le KT, Seguela P (1999) Molecular cloning and regional distribution of a human proton receptor subunit with biphasic functional properties. J Neurochem 72:51–57

Baron A, Schaefer L, Lingueglia E, Champigny G, Lazdunski M (2001) Zn2+ and H+ are coactivators of acid-sensing ion channels. J Biol Chem 276:35361–35367

Bassilana F, Champigny G, Waldmann R, de Weille JR, Heurteaux C, Lazdunski M (1997) The acid-sensitive ionic channel subunit ASIC and the mammalian degenerin MDEG form a heteromultimeric H+-gated Na+ channel with novel properties. J Biol Chem 272:28819–28822

Bässler EL, Ngo-Anh TJ, Geisler HS, Ruppersberg JP, Gründer S (2001) Molecular and functional characterization of acid-sensing ion channel (ASIC) 1b. J Biol Chem 276:33782–33787

Bermudez-Rattoni F (2004) Molecular mechanisms of taste-recognition memory. Nat Rev Neurosci 5:209–217

Bianchi L, Driscoll M (2002) Protons at the gate: DEG/ENaC ion channels help us feel and remember. Neuron 34:337–340

Bliss TV, Collingridge GL (1993) A synaptic model of memory: long-term potentiation in the hippocampus. Nature 361:31–39

Bohlen CJ, Chesler AT, Sharif-Naeini R, Medzihradszky KF, Zhou S, King D, Sánchez EE, Burlingame AL, Basbaum AI, Julius D (2011) A heteromeric Texas coral snake toxin targets acid-sensing ion channels to produce pain. Nature 479:410–414

Boillat A, Alijevic O, Kellenberger S (2014) Calcium entry via TRPV1 but not ASICs induces neuropeptide release from sensory neurons. Mol Cell Neurosci 61:13–22

Buta A, Maximyuk O, Kovalskyy D, Sukach V, Vovk M, Ievglevskyi O, Isaeva E, Isaev D, Savotchenko A, Krishtal O (2015) Novel potent orthosteric antagonist of ASIC1a prevents NMDAR-dependent LTP induction. J Med Chem 58:4449–4461

Chapman PF, White GL, Jones MW, Cooper-Blacketer D, Marshall VJ, Irizarry M, Younkin L, Good MA, Bliss TV, Hyman BT, Younkin SG, Hsiao KK (1999) Impaired synaptic plasticity and learning in aged amyloid precursor protein transgenic mice. Nat Neurosci 2:271–276

Chen CC, England S, Akopian AN, Wood JN (1998) A sensory neuron-specific, proton-gated ion channel. Proc Natl Acad Sci U S A 95:10240–10245

Chen QS, Kagan BL, Hirakura Y, Xie CW (2000) Impairment of hippocampal long-term potentiation by Alzheimer amyloid beta-peptides. J Neurosci Res 60:65–72

Chesler M (2003) Regulation and modulation of pH in the brain. Physiol Rev 83:1183–1221

Chesler M, Kaila K (1992) Modulation of pH by neuronal activity. Trends Neurosci 15:396–402

Chiang PH, Chien TC, Chen CC, Yanagawa Y, Lien CC (2015) ASIC-dependent LTP at multiple glutamatergic synapses in amygdala network is required for fear memory. Sci Rep 15:10143

Cho JH, Askwith CC (2008) Presynaptic release probability is increased in hippocampal neurons from ASIC1 knockout mice. J Neurophysiol 99:426–441

Chu XP, Xiong ZG (2012) Physiological and pathological functions of Acid-sensing ion channels in the central nervous system. Curr Drug Targets 13:263–271

Chu XP, Wemmie JA, Wang WZ, Zhu XM, Saugstad JA, Price MP, Simon RP, Xiong ZG (2004) Subunit-dependent high-affinity zinc inhibition of acid- sensing ion channels. J Neurosci 24:8678–8689

Collingridge GL, Kehl SJ, McLennan H (1983) Excitatory amino acids in synaptic transmission in the Schaffer collateral-commissural pathway of the rat hippocampus. J Physiol:334

Coryell MW, Ziemann AE, Westmoreland PJ, Haenfler JM, Kurjakovic Z, Zha XM, Price M, Schnizler MK, Wemmie JA (2007) Targeting ASIC1a reduces innate fear and alters neuronal activity in the fear circuit. Biol Psychiatry 62:1140–1148

Coryell MW, Wunsch AM, Haenfler JM, Allen JE, Schnizler M, Ziemann AE, Cook MN, Dunning JP, Price MP, Rainier JD, Liu Z, Light AR, Langbehn DR, Wemmie JA (2009) Acid-sensing ion channel-1a in the amygdala, a novel therapeutic target in depression-related behavior. J Neurosci 29:5381–5388

Craig AD (2009) How do you feel--now? The anterior insula and human awareness. Nat Rev Neurosci 10:59–70

Damasio AR, Grabowski TJ, Bechara A, Damasio H, Ponto LL, Parvizi J, Hichwa RD (2000) Subcortical and cortical brain activity during the feeling of self-generated emotions. Nat Neurosci 3:1049–1056

Deval E, Lingueglia E (2015) Acid-sensing ion channels and nociception in the peripheral and central nervous systems. Neuropharmacology 94:49–57

Deval E, Baron A, Lingueglia E, Mazarguil H, Zajac JM, Lazdunski M (2003) Effects of neuropeptide SF and related peptides on acid sensing ion channel 3 and sensory neuron excitability. Neuropharmacology 44:662–671

Diochot S, Baron A, Salinas M, Douguet D, Scarzello S, Dabert-Gay AS, Debayle D, Friend V, Alloui A, Lazdunski M, Lingueglia E (2012) Black mamba venom peptides target acid-sensing ion channels to abolish pain. Nature 490:552–555

Du J, Reznikov LR, Price MP, Zha XM, Lu Y, Moninger TO, Wemmie JA, Welsh MJ (2014) Protons are a neurotransmitter that regulates synaptic plasticity in the lateral amygdala. Proc Natl Acad Sci U S A 111:8961–8966

Duan B, Wang YZ, Yang T, Chu XP, Yu Y, Huang Y, Cao H, Hansen J, Simon RP, Zhu MX, Xiong ZG, Xu TL (2011) Extracellular spermine exac- erbates ischemic neuronal injury through sensitization of ASIC1a channels to extracellular acidosis. J Neurosci 31:2101–2112

Dube GR, Elagoz A, Mangat H (2009) Acid sensing ion channels and acid nociception. Curr Pharm Des 15:1750–1766

Escoubas P, De Weille JR, Lecoq A, Diochot S, Waldmann R, Champigny G, Moinier D, Ménez A, Lazdunski M (2000) Isolation of a tarantula toxin specific for a class of proton-gated Na+ channels. J Biol Chem 1275:25116–25121

Friese MA, Craner MJ, Etzensperger R, Vergo S, Wemmie JA, Welsh MJ, Vincent A, Fugger L (2007) Acid-sensing ion channel-1 contributes to axonal degeneration in autoimmune inflammation of the central nervous system. Nat Med 13:1483–1489

Gao J, Duan B, Wang DG, Deng XH, Zhang GY, Xu L, Xu TL (2005) Coupling between NMDA receptor and acid-sensing ion channel contributes to ischemic neuronal death. Neuron 48:635–646

Gao S, Yu Y, Ma ZY, Sun H, Zhang YL, Wang XT et al (2015) NMDA-mediated hippocampal neuronal death is exacerbated by activities of ASIC1a. Neurotox Res 28:122–137

Gonzales EB, Kawate T, Gouaux E (2009) Pore architecture and ion sites in acid- sensing ion channels and P2X receptors. Nature 460:599–604

Gutman AL, Cosme CV, Noterman MF, Worth WR, Wemlumie JA, LaLumiere RT (2018) Overexpression of ASIC1A in the nucleus accumbens of rats potentiates cocaine-seeking behavior. Addict Biol. https://doi.org/10.1111/adb.12690

Hesselager M, Timmermann DB, Ahring PK (2004) pH Dependency and desensitization kinetics of heterologously expressed combinations of acid-sensing ion channel subunits. J Biol Chem 279:11006–11015

Hnasko TS, Edwards RH (2012) Neurotransmitter co-release: mechanism and physiological role. Annu Rev Physiol 74:225–243

Hu NW, Nicoll AJ, Zhang D, Mably AJ, O'Malley T, Purro SA, Terry C, Collinge J, Walsh DM, Rowanm MJ (2014) Glu5 receptors and cellular prion protein mediate amyloid-β-facilitated synaptic long-term depression in vivo. Nat Commun 4:533–574

Huang Y, Jiang N, Li J, Ji YH, Xiong ZJ, Zha XM (2015) Two aspects of ASIC function: synaptic plasticity and neuronal injury. Neuropharmacology 94:42–48

Jasti J, Furukawa H, Gonzales EB, Gouaux E (2007) Structure of acid-sensing ion channel 1 at 1.9 A resolution and low pH. Nature 449:316–323

Jiang Q, Wang CM, Fibuch EE, Wang JQ, Chu XP (2013) Differential regulation of locomotor activity to acute and chronic cocaine administration by acid-sensing ion channel 1a and 2 in adult mice. Neuroscience 246:170–178

Kellenberger S, Schild L (2015) International union of basic and clinical pharmacology. XCI. structure, function, and pharmacology of acid-sensing ion channels and the epithelial Na+ channel. Pharmacol Rev 67:1–35

Kim Y, Trussell LO (2009) Negative shift in the glycine reversal potential mediated by a Ca2+- and pH-dependent mechanism in interneurons. J Neurosci 29:11495–11510

Kleyman TR, Cragoe EJ Jr (1988) Amiloride and its analogs as tools in the study of ion transport. J Membr Biol 105:1–21

Kourrich S, Rothwell PE, Klug JR, Thomas MJ (2007) Cocaine experience controls bidirectional synaptic plasticity in the nucleus accumbens. J Neurosci 27:7921–7928

Krauson AJ, Rooney JG, Carattino MD (2018) Molecular basis of inhibition of acid sensing ion channel 1A by diminazene. PLoS One 13(5):e0196894

Kreple CJ, Lu Y, Taugher RJ, Schwager-Gutman AL, Du J, Stump M, Wang Y, Ghobbeh A, Fan R, Cosme CV, Sowers LP, Welsh MJ, Radley JJ, LaLumiere RT, Wemmie JA (2014) Acid-sensing ion channels contribute to synaptic transmission and inhibit cocaine-evoked plasticity. Nat Neurosci 17:1083–1091

Krishtal O (2003) The ASICs: signaling molecules? Modulators? Trends Neurosci 26:477–483

Krishtal OA, Pidoplichko VI (1981a) Receptor for protons in the membrane of sensory neurons. Brain Res 214:150–154

Krishtal OA, Pidoplichko VI (1981b) A receptor for protons in the membrane of sensory neurons may participate in nociception. Neuroscience 6:2599–2601

Li WG, Liu MG, Deng S, Liu YM, Shang L, Ding J, Hsu TT, Jiang Q, Li Y, Li F, Zhu MX, Xu TL (2016) ASIC1a regulates insular long-term depression and is required for the extinction of conditioned taste aversion. Nat Commun 7:7–13770

Li HS, Su XY, Song XL, Qi X, Li Y, Wang RQ, Maximyuk O, Krishtal O, Wang T, Fang H, Liao L, Cao H, Zhang YQ, Zhu MX, Liu MG, Xu TL (2019) Protein kinase C lambda mediates acid-sensing ion channel 1a-dependent cortical synaptic plasticity and pain hypersensitivity. J Neurosci 39:5773–5793

Liu Y, Edwards RH (1997) The role of vesicular transport proteins in synaptic transmission and neural degeneration. Annu Rev Neurosci 20:125–156

Liu MG, Li HS, Li WG, Wu YJ, Deng SN, Huang C, Maximyuk O, Sukach V, Krishtal O, Zhu MX, Xu TL (2016) Acid-sensing ion channel 1a contributes to hippocampal LTP inducibility through multiple mechanisms. Sci Rep 21:6–23350

Lv RJ, He JS, Fu YH, Zhang YQ, Shao XQ, Wu LW, Lu Q, Jin LR, Liu H (2011) ASIC1a polymorphism is associated with temporal lobe epilepsy. Epilepsy Res 96:74–80

Ma CL, Sun H, Yang L, Wang XT, Gao S, Chen XW, Ma ZY, Wang GH, Shi Z, Zheng QY (2019) Acid-sensing ion channel 1a modulates NMDA receptor function through targeting NR1/NR2A/NR2B triheteromeric receptors. Neuroscience 406:389–404

Magnotta VA, Heo HY, Dlouhy BJ, Dahdaleh NS, Follmer RL, Thedens DR, Welsh MJ, Wemmie JA (2012) Detecting activity evoked pH changes in human brain. Proc Natl Acad Sci U S A 109:8270–8273

Mango D, Nisticò R (2018) Role of ASIC1a in Aβ-induced synaptic alterations in the hippocampus. Pharmacol Res 131:61–65

Mango D, Nisticò R (2019) Acid-sensing ion channel 1a is involved in N-methyl D-aspartate receptor-dependent long-term depression in the hippocampus. Front Pharmacol 10:555

Mango D, Barbato G, Piccirilli S, Panico MB, Feligioni M, Schepisi C, Graziani M, Porrini V, Benarese M, Lanzillotta A, Pizzi M, Pieraccini S, Sironi M, Blandini F, Nicoletti F, Mercuri NB, Imbimbo BP, Nisticò R (2014) Electrophysiological and metabolic effects of CHF5074 in the hippocampus: protection against in vitro ischemia. Pharmacol Res 81:83–90

Mango D, Braksator E, Battaglia G, Marcelli S, Mercuri NB, Feligioni M, Nicoletti F, Bashir ZI, Nisticò R (2017) Acid-sensing ion channel 1a is required for mGlu receptor dependent long-term depression in the hippocampus. Pharmacol Res 119:12–19

Mango D, Saidi A, Cisale GY, Feligioni M, Corbo M, Nisticò R (2019) Targeting synaptic plasticity in experimental models of Alzheimer's disease. Front Pharmacol 10:778

Miesenbock G, De Angelis DA, Rothman JE (1998) Visualizing secretion and synaptic transmission with pH-sensitive green fluorescent proteins. Nature 394:192–195

Munro G, Christensen JK, Erichsen HK, Dyhring T, Demnitz J, Dam E, Ahring PK (2016) NS383 selectively inhibits acid-sensing ion channels containing 1a and 3 subunits to reverse inflammatory and neuropathic hyperalgesia in rats. CNS Neurosci Ther 22:135–145

Nagaeva EI, Tikhonova TB, Magazanik LG, Tikhonov DB (**2016**) Histamine selectively potentiates acid-sensing ion channel 1a. Neurosci Lett 632:136–140

Nieuwenhuys R (2012) The insular cortex: a review. Prog Brain Res 195:123–163

Nisticò R, Salter E, Nicolas C, Feligioni M, Mango D, Bortolotto ZA, Gressens P, Collingridge GL, Peineau S (2017) Synaptoimmunology – roles in health and disease. Mol Brain 10:26

Noel J, Salinas M, Baron A, Diochot S, Deval E, Lingueglia E (2010) Current perspectives on acid-sensing ion channels: new advances and therapeutic implications. Expert Rev Clin Pharmacol 3:331–346

Olesen AE, Nielsen LM, Larsen IM, Drewes AM (2015) Randomized clinical trial: efficacy and safety of PPC-5650 on experimental esophageal pain and hyperalgesia in healthy volunteer. Scand J Gastroenterol 50:138–144

Palmer MJ, Hull C, Vigh J, von Gersdorff H (2003) Synaptic cleft acidification and modulation of short-term depression by exocytosed protons in retinal bipolar cells. J Neurosci 23:11332–11341

Poirot O, Berta T, Decosterd I, Kellenberger S (2006) Distinct ASIC currents are expressed in rat putative nociceptors and are modulated by nerve injury. J Physiol 576:215–234

Price MP, Snyder PM, Welsh MJ (1996) Cloning and expression of a novel human brain Na+ channel. J Biol Chem 271:7879–7882

Price MP, Gong H, Parsons MG, Kundert JR, Reznikov LR, Bernardinelli L, Chaloner K, Buchanan GF, Wemmie JA, Richerson GB, Cassell MD, Welsh MJ (2014) Localization and behaviors in null mice suggest that ASIC1 and ASIC2 modulate responses to aversive stimuli. Genes Brain Behav 13:179–194

Qiang M, Dong X, Zha Z, Zuo XK, Song XL, Zhao L, Yuan C, Huang C, Tao P, Hu H, Li WG, Hu W, Li J, Nie Y, Buratto D, Zonta F, Ma P, Zi Y, Liu L, Zhang Y, Yang B, Xie J, Xu TL, Qu Z, Yang G, Lerner R (2018) Selection of an ASIC1a-blocking combinatorial antibody that protects cells from ischemic death. Proc Natl Acad Sci U S A 115:7469–7477

Qiu S, Chen T, Koga K, Guo YY, Xu H, Song Q, Wang JJ, Descalzi G, Kaang BK, Luo JH, Zhuo M, Zhao MG (2013) An increase in synaptic NMDA receptors in the insular cortex contributes to neuropathic pain. Sci Signal 6:34

Qiu S, Zhang M, Liu Y, Guo Y, Zhao H, Song Q, Zhao M, Huganir RL, Luo J, Xu H, Zhuo M (2014) GluA1 phosphorylation contributes to postsynaptic amplification of neuropathic pain in the insular cortex. J Neurosci 34:13505–13515

Quintana P, Soto D, Poirot O, Zonouzi M, Kellenberger S, Muller D, Chrast R, Cull-Candy SG (2015) Acid-sensing ion channel 1a drives AMPA receptor plasticity following ischaemia and acidosis in hippocampal CA1 neurons. J Physiol 593:4373–4386

Rosenblum K, Berman DE, Hazvi S, Lamprecht R, Dudai Y (1997) NMDA receptor and the tyrosine phosphorylation of its 2B subunit in taste learning in the rat insular cortex. J Neurosci 17:5129–5135

Schild L, Schneeberger E, Gautschi I, Firsov D (1997) Identification of amino acid residues in the alpha, beta, and gamma subunits of the epithelial sodium channel (ENaC) involved in amiloride block and ion permeation. J Gen Physiol 109:15–26

Selkoe DJ (2001) Alzheimer's disease: genes, proteins, and therapy. Physiol Rev 81:741–766

Shteinikov VY, Korosteleva A, Tikhonova TB, Potapieva NN, Tikhonov DB (2017) Ligands of histamine receptors modulate acid-sensing ion channels. Biochem Biophys Res Commun 490:1314–1318

Sluka KA, Winter OC, Wemmie JA (2009) Acid-sensing ion channels: a new target for pain and CNS diseases. Curr Opin Drug Discov Devel 12:693–704

Suman A, Mehta B, Guo ML, Chu XP, Fibuch EE, Mao LM, Wang JQ (2010) Alterations in subcellular expression of acid-sensing ion channels in the rat forebrain following chronic amphetamine administration. Neurosci Res 68:1–8

Trapp S, Lückermann M, Kaila KA, Ballanyi K (1996) Acidosis of hippocampal neurones mediated by a plasmalemmal Ca2+/H+ pump. Neuroreport 7:2000–2004

Varga E, Juhász G, Bozsó Z, Penke B, Fülöp L, Szegedi V (2015) Amyloid-β1-42 disrupts synaptic plasticity by altering glutamate recycling at the synapse. J Alzheimers Dis 45:449–456

Vergo S, Craner MJ, Etzensperger R, Attfield K, Friese MA, Newcombe J, Esiri M, Fugger L (2011) Acid-sensing ion channel 1 is involved in both axonal injury and demyelination in multiple sclerosis and its animal model. Brain 5:571–584

Voilley N, de Weille J, Mamet J, Lazdunski M (2001) Nonsteroid anti-inflammatory drugs inhibit both the activity and the inflammation-induced expression of acid-sensing ion channels in nociceptors. J Neurosci 21:8026–8033

Vukicevic M, Kellenberger S (2004) Modulatory effects of acid-sensing ion channels on action potential generation in hippocampal neurons. Am J Physiol Cell Physiol 287:682–690

Waldmann R, Lazdunski M (1998) H(+)-gated cation channels: neuronal acid sensors in the NaC/DEG family of ion channels. Curr Opin Neurobiol 8:418–424

Waldmann R, Champigny G, Bassilana F, Heurteaux C, Lazdunski M (1997) A proton-gated cation channel involved in acid-sensing. Nature 386:173–177

Wang Q, Wang Q, Song XL, Jiang Q, Wu YJ, Li Y, Yuan TF, Zhang S, Xu NJ, Zhu MX, Li WJ, Xu TL (2018) Fear extinction requires ASIC1a-dependent regulation of hippocampal-prefrontal correlates. Sci Adv 4:3075

Wemmie JA, Chen J, Askwith CC, Hruska-Hageman AM, Price MP, Nolan BC, Yoder PG, Lamani E, Hoshi T, Freeman JH Jr, Welsh MJ (2002) The acid-activated ion channel ASIC contributes to synaptic plasticity, learning, and memory. Neuron 34:463–477

Wemmie JA, Askwith CC, Lamani E, Cassell MD, Freeman JH Jr, Welsh MJ (2003) Acid-sensing ion channel 1 is localized in brain regions with high synaptic density and contributes to fear conditioning. J Neurosci 23:5496–5502

Wemmie JA, Coryell MW, Askwith CC, Lamani E, Leonard AS, Sigmund CD, Welsh MJ (2004) Over- expression of acid-sensing ion channel 1a in transgenic mice increases acquired fear-related behavior. Proc Natl Acad Sci U S A 101:3621–3626

Wong HK, Bauer PO, Kurosawa M, Goswami A, Washizu C, Machida Y, Tosaki A, Yamada M, Knöpfel T, Nakamura T, Nukina N (2008) Blocking acid-sensing ion channel 1 alleviates Huntington's disease pathology via an ubiquitin-proteasome system-dependent mechanism. Hum Mol Genet 17:3223–3235

Wu PY, Huang YY, Chen CC, Hsu TT, Lin YC, Weng JY, Chien TC, Cheng IH, Lien CC (2013) Acid-sensing ion channel-1a is not required for normal hippocampal LTP and spatial memory. J Neurosci 33:1828–1832

Xiang-ming Z, Wemmie JA, Green SH, Welsh MJ (2006) Acid-sensing ion channel 1a is a postsynaptic proton receptor that affects the density of dendritic spines. Proc Natl Acad Sci U S A 103:16556–16561

Yu Z, Wu YJ, Wang YZ, Liu DS, Song XL, Jiang Q, Li Y, Zhang S, Xu NJ, Zhu MX, Li WG, Xu TL (2018) The acid-sensing ion channel ASIC1a mediates striatal synapse remodeling and procedural motor learning. Sci Signal 11:4481

Zaaraoui W, Rico A, Audoin Reuter B, Malikova I, Soulier E, Viout P, Le Fur Y, Confort-Gouny S, Cozzone PJ, Pellettier J, Ranjeva JP (2010) Unfolding the long-term pathophysiological processes following an acute inflammatory demyelinating lesion of multiple sclerosis. Magn Reson Imaging 28:477–486

Zha X-m, Wemmie JA, Green SH, Welsh MJ (2006) Acid-sensing ion channel 1a is a postsynaptic proton receptor that affects the density of dendritic spines. Proc Natl Acad Sci U S A 103:16556–16561

Zhang GC, Mao LM, Wang JQ, Chu XP (2009) Upregulation of acid-sensing ion channel 1 protein expression by chronic administration of cocaine in the mouse striatum in vivo. Neurosci Lett 459:119–122

Zhang RJ, Yin YF, Xie XJ, Gu HF (2020) Acid-sensing ion channels: linking extracellular acidification with atherosclerosis. Clin Chim Acta 502:183–190

Ziemann AE, Schnizler MK, Albert GW, Severson MA, Howard MA, Welsh MJ, Wemmie JA (2008) Seizure termination by acidosis depends on ASIC1a. Nat Neurosci 11:816–822

Rev Physiol Biochem Pharmacol (2020) 177: 101–148
DOI: 10.1007/112_2019_16

Published online: 24 May 2019

Stationary and Nonstationary Ion and Water Flux Interactions in Kidney Proximal Tubule: Mathematical Analysis of Isosmotic Transport by a Minimalistic Model

Erik Hviid Larsen and Jens Nørkær Sørensen

Contents

The original version of this chapter was revised. A correction to this chapter can be found at https://doi.org/10.1007/112_2020_40

E. H. Larsen (✉)
Department of Biology, University of Copenhagen, Copenhagen, Denmark
e-mail: ehlarsen@bio.ku.dk

J. N. Sørensen
Department of Wind Energy, Technical University of Denmark, Lyngby, Denmark
e-mail: jnso@dtu.dk

Abstract Our mathematical model of epithelial transport (Larsen et al. Acta Physiol. 195:171–186, 2009) is extended by equations for currents and conductance of apical SGLT2. With independent variables of the physiological parameter space, the model reproduces intracellular solute concentrations, ion and water fluxes, and electrophysiology of proximal convoluted tubule. The following were shown:

1. Water flux is given by active Na^+ flux into lateral spaces, while osmolarity of absorbed fluid depends on osmotic permeability of apical membranes.
2. Following aquaporin "knock-out," water uptake is not reduced but redirected to the paracellular pathway.
3. Reported decrease in epithelial water uptake in aquaporin-1 knock-out mouse is caused by downregulation of active Na^+ absorption.
4. Luminal glucose stimulates Na^+ uptake by instantaneous depolarization-induced pump activity ("cross-talk") and delayed stimulation because of slow rise in intracellular [Na^+].
5. Rate of fluid absorption and flux of active K^+ absorption would have to be attuned at epithelial cell level for the [K^+] of the absorbate being in the physiological range of interstitial [K^+].
6. Following unilateral osmotic perturbation, time course of water fluxes between intraepithelial compartments provides physical explanation for the transepithelial osmotic permeability being orders of magnitude smaller than cell membranes' osmotic permeability.
7. Fluid absorption is always hyperosmotic to bath.
8. Deviation from isosmotic absorption is increased in presence of glucose contrasting experimental studies showing isosmotic transport being independent of glucose uptake.
9. For achieving isosmotic transport, the cost of Na^+ recirculation is predicted to be but a few percent of the energy consumption of Na^+/K^+ pumps.

Keywords AQP-1 knock-out · Glucose absorption · Isosmotic transport · Kidney proximal tubule · Mathematical-modeling · Osmotic permeability · Time dependent- and stationary states of water and ion fluxes

1 Introduction

In the study from A. K. Solomon's laboratory of Necturus proximal tubule in which net flux of NaCl and water were measured over the same period of time, reabsorbed fluid was isosmotic over a wide range of water fluxes. In the phrasing of the authors (Windhager et al. 1959), "water transport in the proximal tubule depends on the

tubular NaCl concentration rather than upon the water activity," and "the driving force for water movement arises from the efflux of NaCl from tubule to plasma," which was shown to be inhibited by the Na^+/K^+-ATPase inhibitor ouabain (Schatzmann et al. 1958). Work from several groups confirmed isosmotic transport by kidney proximal tubule (Bennett et al. 1967; Kokko et al. 1971; Morel and Murayama 1970; Schafer et al. 1974) and by other low-resistance epithelia (Curran 1960; Diamond 1964). More recently, isosmotic transport was also observed in high-resistance epithelia (Gaeggeler et al. 2011; Nielsen and Larsen 2007; Schafer 1993), indicating that the ability to transport water at osmotic equilibrium energized by the Na^+/K^+-ATPase is a general feature of transporting epithelia. This may occur even against an adverse osmotic gradient, confirming that epithelia are capable of spending metabolic energy to move water (Diamond 1964; Green et al. 1991; Nielsen and Larsen 2007; Parsons and Wingate 1958). The mechanism of isosmotic transport is debated (Andreoli and Schafer 1979; Fischbarg 2010; Larsen et al. 2009; Nedergaard et al. 1999; Spring 1999; Tripathi and Boulpaep 1989; Whittembury and Reuss 1992; Zeuthen 2000; Zeuthen et al. 2001). Since Na^+/K^+ pumps are expressed in membranes lining the lateral intercellular space (DiBona and Mills 1979; Maunsbach and Boulpaep 1991; Mills et al. 1977; Padilla-Benavides et al. 2010; Stirling 1972) similarly to aquaporin water channels (Agre et al. 1993b), it is generally accepted that this space by way of osmosis couples the active Na^+ flux and the water flux and that isosmotic transport simply follows from a large water permeability (Altenberg and Reuss 2013).

Weinstein and Stephenson (1981) established tradition for applying mathematical formalisms in the analysis of steady state water and ion absorption by kidney proximal tubule (Weinstein 1986, 1992, 2013). Our steady state mathematical models of leaky epithelia (Larsen et al. 2000, 2002) have been expanded for computing time-dependent states (Larsen et al. 2009). The present analytical model comprising new apical glucose transport equations and comprehensive mathematical handling of electrical properties enables us to confront quantitatively computations with crucial experiments on kidney proximal tubule.

The present study has a dual purpose. Firstly, we present in detail complex relationships between active ion fluxes and water flows in an epithelium of extremely large membrane hydraulic permeabilities, as exemplified by mammalian proximal tubule of amplified apical and lateral plasma membrane areas (Welling and Welling 1975, 1988), which make this nephron segment one of the most water-permeable epithelia in nature (Carpi-Medina et al. 1983; Schafer 1990). This is done by quantitative analysis of a mathematical model which comprises cellular and paracellular pathways for fluxes of ions, glucose, and water. It is an important quality of our treatment that water absorption is governed by a driving force resulting from solute fluxes and intraepithelial solute solvent coupling reflecting the conditions in vivo (Gottschalk 1963) and in microperfused isolated tubules (Green et al. 1991). By including glucose and electrical properties, commonly applied laboratory protocols can be simulated for investigating the explanatory power of the model over a wide range of observations. Besides analysis of relationships between volume flows and solute fluxes, our analysis comprises time-dependent states evoked by

perturbation of, e.g., osmolarity of external solutions or "knock-out" of a specific membrane transporter providing novel insight into redistributions of water flows between cells and paracellular space.

The second purpose of the study is to analyse in the depth problems of importance for the function of vertebrate kidney that hitherto have been out of focus. Examples are the conflict between osmotic permeability of whole epithelium and that of individual membranes, with reference to the studies from Solomon's laboratory discussed above; the relative significance of sodium pump activity to aquaporin water channel osmotic permeability for the rate of water absorption; robustness of mathematical solutions giving isosmotic absorption; and the relative significance of transcellular and paracellular fluid absorption, respectively. Our analysis of every one of these problems provides novel information of definitive and general nature.

2 Description of the Minimalistic Model

2.1 Functional Organization of Proximal Tubule Epithelium

Mammalian proximal tubule is a heterocellular epithelium with three consecutive segments of individual functional and structural complexity (Maunsbach 1966; Welling and Welling 1988; Zhuo and Li 2013). All segments are engaged in isosmotic fluid absorption energized by lateral Na^+/K^+ pumps. The minimalistic model epithelium reproduces Na^+-coupled water transport in all three segments, and by having lumen-negative transepithelial potential difference and water absorption coupled predominantly to absorption of NaCl and glucose, the model epithelium has these features in common with the proximal convoluted tubule. It follows that the model discussed here does not handle acid-base transport and cannot, therefore, reproduce absorption of bicarbonate ions. However, by containing the essential module of subcellular complexity driving isosmotic transport, all conclusions of the present study apply to all three segments – and generally to other transporting epithelia.

The width of the lateral space (distance between neighbouring cells) is constant while neighbouring cells interdigitate in progressively more complicated way toward the cell base (Maunsbach 1973; Welling and Welling 1988). A quantitative stereologic study of size and shape of cells and lateral intercellular spaces (*lis*) of all three segments of proximal tubule indicated similar relatively large areas of apical membrane (comprising brush border surface and intervening membrane) and lateral membrane (Welling and Welling 1988). The area of serosal membrane contacting the basement membrane is much smaller than those of the above two membrane domains. The interspace basement membrane providing exit from the lateral intercellular space is about 10% of the area of the entire basement membrane. Morphometric analyses further indicated that the so-called basal infoldings do not stem from serosal membrane contacting the basement membrane but represent a

complex lateral-membrane arrangement of arbitrary orientation in the basal 20% region of tubule cells (Welling et al. 1987a). A fluorometric micro-assay of Na^+/K^+-ATPase (Garg et al. 1981) demonstrated highest expression of this enzyme in proximal convoluted tubule as compared to downstream segments of the nephron, and net Na^+ transport previously measured in microperfused tubule segments correlated well with their Na^+/K^+-ATPase activity. Immunocytochemical studies localized the Na^+/K^+-ATPase to lateral plasma membranes and to the abovementioned complex of lateral plasma membrane infoldings at the base of tubule cells (Kashgarian et al. 1985; Maunsbach and Boulpaep 1991). Immunochemical reaction was not observed on those areas of the basal plasma membrane directly contacting basal lamina (Kashgarian et al. 1985) nor is this transporter found on the luminal brush border (Jørgensen 1986). This agrees with studies on localization of [^{3}H]-ouabain in other transporting epithelia (DiBona and Mills 1979; Mills and DiBona 1977, 1978; Stirling 1972). In ileal intestinal mucosa, a thyroid epithelial FRT-cell line, and MDCK cells grown as a confluent monolayer on permeable filter support is the Na^+/K^+-ATPase present in lateral membranes of cells with no immunofluorescent staining neither at apical nor at serosal cell surfaces (Amerongen et al. 1989; Padilla-Benavides et al. 2010; Zurzolo and Rodriguezboulan 1993). Thus, in transporting epithelia, the lateral plasma membrane and the serosal plasma membrane constitute different functional domains implying that sodium ions transported into the cell through the apical plasma membrane are actively transported into *lis* for exiting the epithelium through the interspace basement membrane. Because the so-called "basolateral" osmotic permeability identified as AQP-1 (Agre et al. 1993a, b) is confined to the lateral membrane, the lateral intercellular space constitutes a compartment of its own with physically well-defined boundary toward the serosal (interstitial) compartment as depicted in Fig. 1a. Thus, for transepithelial osmotic equilibrium, water entering the epithelium through any membrane domain leaves the epithelium through the interspace basement membrane. This applies even if the serosal cell membrane's osmotic permeability is non-zero and follows from a slightly hyperosmotic cell water driving water into the cell not only from luminal solution but also from serosal bath. The above functional organization constitutes the prerequisite for truly isosmotic transport. Thus, quantitative analysis of water uptake by our minimalistic model provides insight into isosmotic transport by absorbing epithelia in general.

2.2 Solute Flux Equations

The computations presented in this paper do not depend on any particular assumption about the nature of luminal entrance mechanisms as long as we keep absolute ion fluxes and water flows in agreement with measured quantities. With this requirement being fulfilled, there are additional features of the minimalistic model

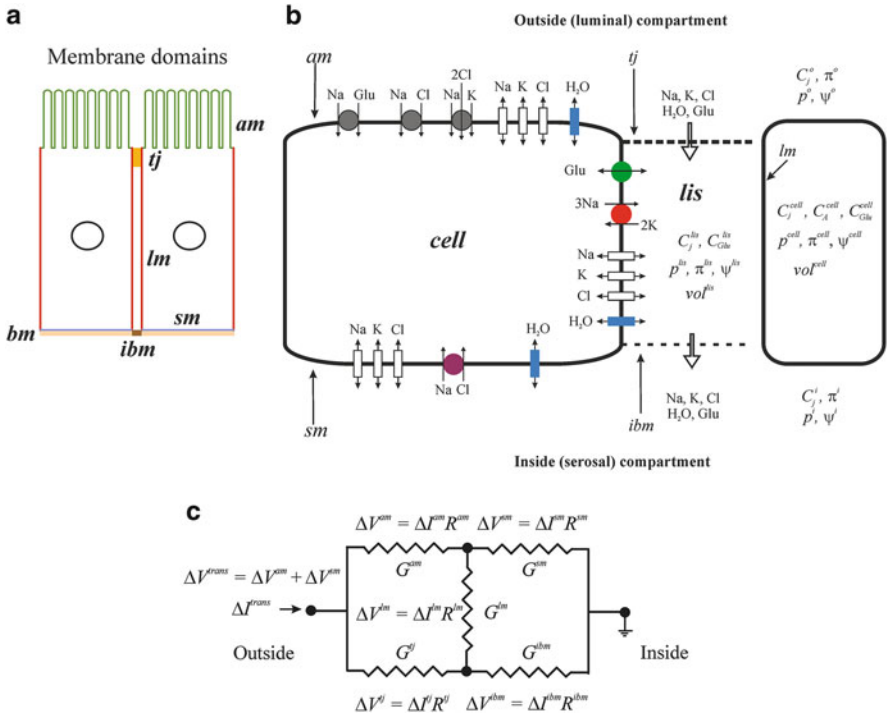

Fig. 1 (**a**) Cell membranes of transporting epithelia constitute three functionally different domains. Localization of fluorescence probes or radioactive ^{3}H-labeling of antibodies raised against transport proteins indicated that lateral and serosal membranes constitute functionally different domains; see text for references. As a consequence, the notion "basolateral membrane" would have to be avoided. *am* apical membrane with microvilli, *tj* tight junction, *lm* lateral membrane, *sm* serosal membrane, *bm* basement membrane in light brown color that includes the interspace basement membrane, *ibm* indicated by darker brown color. (**b**) Transport systems of the minimalistic epithelial model with definitions and nomenclature. Transport systems and symbols as defined in text and Appendix 1 and 2. In the investigation of conditions for obtaining truly isosmotic transport is the 1 Na^+: 1 Cl cotransporter activated for obtaining an overall isosmotic transport (see text for further explanation). (**c**) The five membranes of the epithelium constitute a bridge circuit. The solution to the mathematical problem for a given set of independent variables contains values of the five membrane resistors indicated above. The resistance of the bridge circuit, however, cannot be calculated according to rules for series and parallel resistors. Therefore, it is computed by simulating a current injection, ΔI^{trans}, and applying Kirchhoff's rules for solving the set of five current equations by the "solve routine" of *Mathematica*©. Subsequently, the five membrane currents, ΔI^{m}, are used for calculating change in membrane potentials, transepithelial resistance ($R^{trans} = \Delta V^{trans}/\Delta I^{trans}$), and fractional resistance of the apical membrane. The resistance notation in Mathematica© equations are defined as follows: $R^{am} = R_1$, $R^{sm} = R_2$, $R^{lm} = R_3$, $R^{tj} = R_4$, and $R^{ibm} = R_5$. See methods for details

that would have to be met for our purpose. In the absence of glucose and amino acids, Frömter's seminal study reported a fairly large apical membrane conductance of about 4 mS cm^{-2} with a ratio of the resistance of the luminal membrane to the transcellular resistance of 0.8 (Frömter 1982). In the cell, both K^+ and Cl^- are above

thermodynamic equilibrium (Cassola et al. 1983; Edelman et al. 1978; Windhager 1979). Since neither is secreted into the luminal solution, the above electrical conductance is governed predominantly by a Na^+ conductance. A Na^+ conductance is associated with the 3 Na^+:1HPO_4^{2-} cotransporter. Frömter (1982) perfused the kidney tubule with physiological saline containing 1 mM HPO_4^{2-}; thus with a coupling ratio of 3 Na^+:1HPO_4^{2-}, it is unlikely that this transporter accounts for the relatively very large conductance of 4 mS/cm^2, which leaves a Na^+ channel as the most likely candidate for the Na^+ conductance of the apical membrane. This goes along with the study by Morel and Murayama (1970), who obtained isosmotic reabsorption in microperfused rat proximal tubule in the absence of phosphate ions in the luminal perfusion solution. Added to this, a sodium ion channel was disclosed by patch clamp of rabbit proximal straight tubule (Gögelein and Greger 1986). The Goldman-Hodgkin-Katz (GHK) constant field equations are applied for handling this as well as electrodiffusion fluxes in the other ion channels including tight junction and interspace basement membrane (Goldman 1943; Hodgkin and Katz 1949; Sten-Knudsen 2002):

$$J_j = \left(\frac{z_j FV}{RT} P_j\right) \frac{C_j^{(I)} \exp\left[z_j FV/(RT)\right] - C_j^{(II)}}{\exp\left[z_j FV/(RT)\right] - 1} \tag{1a}$$

The associated chord conductance is:

$$G_j = \left(\frac{\left(z_j F\right)^2 V}{RT} P_j\right) \frac{C_j^{(I)} \exp\left[z_j FV/(RT)\right] - C_j^{(II)}}{\left(\exp\left[z_j FV/(RT)\right] - 1\right)\left(V - V_j^{eq}\right)} \tag{1b}$$

P_j is the ion permeability and V potential difference across the membrane. I = *lumen* and II = *cell* for the apical membrane, I = *cell* and II = *lis* for the lateral membrane, and I = *cell* and II = *serosa* for the serosal membrane. The proximal tubule reabsorbs 50–70% of the filtered K^+ load. Wilson et al. (1997) showed that cyanide caused a reduction in net potassium flux over the entire range of fluid fluxes in their double-perfusion experiments. Subsequent single-perfusion experiments (tubule lumen only) using the specific K^+-H^+-ATPase inhibitor, SCH28080, did not reveal evidence for primary active K^+ absorption. The authors discussed the possibility that tubular absorption of K^+ is accomplished by paracellular solvent drag. This mechanism is included in our model and will be quantitatively evaluated in Results for concluding that solvent drag cannot account for transtubular absorption of K^+. The principal importance of active K^+ absorption is independent of the molecular design of the transporter. It is of importance, however, that the transepithelial active flux of potassium ions results in a K^+ concentration of the absorbate that is close to the concentration of K^+ in serosal fluid. The K^+ absorption against the prevailing small transepithelial electrochemical potential difference shall be accounted for by assuming (1Na^+, 1K^+, 2Cl^-) cotransport across the apical membrane:

$$J_j^{NaK2Cl,m} = r \cdot K^{NaK2Cl,m}\left[C_{Na}^{(I)} \cdot C_K^{(I)} \cdot \left(C_{Cl}^{(I)}\right)^2 - C_{Na}^{(II)} \cdot C_K^{(II)} \cdot \left(C_{Cl}^{(II)}\right)^2\right] \quad (2a)$$

Here, $r = 1$ for Na^+ and K^+ and $r = 2$ for Cl^-. In agreement with cellular Cl^- accumulation via a Na^+ -dependent cotransporter in Necturus (Spring and Kimura 1978, 1979) and rat (Karniski and Aronson 1987; Warnock and Lucci 1979), we assume that a ($1Na^+$, $1Cl^-$) cotransporter is present in the apical membrane:

$$J_j^{NaCl,m} = K^{NaCl,m}\left[C_{Na}^{(I)} \cdot \left(C_{Cl}^{(I)}\right) - C_{Na}^{(II)} \cdot \left(C_{Cl}^{(II)}\right)\right] \quad (2b)$$

For generalizing the description, apical Cl^- and K^+ channels are included, but in the present calculations, they do not carry significant fluxes because they are largely quiescent under normal conditions (Boron and Boulpaep 2017).

In 1976, a sodium ion/proton antiporter was discovered in vesicles isolated from renal brush-border membranes of rat by Murer et al. (1976); it was cloned and named NHE3 (Sardet et al. 1989). As recently reviewed by Zhuo and Li (2013), subsequent studies confirmed its function as pathway for eliminating protons in exchange for luminal sodium ions in kidney proximal nephron. The NHE3 antiporter operates in series with a lateral electrogenic cotransporter of stoichiometry 1 Na^+:3 HCO_3^-. Bicarbonate is regenerated from OH^- and CO_2 catalyzed by a cytoplasmic carbonic anhydrase (Boron and Boulpaep 2017). The operation of this enzyme together with the NHE3 antiporter is assumed to recover quantitatively HCO_3^-, which is transported together with sodium ions into the interstitial fluid (Boron and Boulpaep 1983a, b; Yoshitomi et al. 1985). At this stage of our studies, we aim at transport features that are independent of acid-base transporters. As shall be demonstrated below, this "minimalistic" model is excellently suited for analysis of general features of isosmotic transport, e.g., none of our conclusions are being affected by this simplification.

Driving forces for glucose uptake across the luminal membrane of rat convoluted proximal tubule are the transmembrane Na^+ concentration gradient, the transmembrane glucose concentration gradient, and the membrane potential. The transporter saturates with luminal Na^+ concentration as well as with luminal glucose concentration (Samarzija et al. 1982). Glucose is coupled to Na^+ uptake by the Na^+/D-glucose cotransporter-2 (SGLT2) with a stoichiometry of 1 Na^+:1 glucose in tubule segments S1 and S2 and Na^+/D-glucose cotransporter-1 (SGLT1) with a stoichiometry of 2 Na^+:1 glucose in tubule segments S3 (Ghezzi et al. 2018; Hummel et al. 2011; Parent et al. 1992; Turner and Moran 1982; Turner and Silverman 1977). SGLT2 is rheogenic, and with 150 mM external Na^+ concentration, the transporter generates a nonlinear current-voltage relationship reflecting voltage dependence of the Na^+ current (Hummel et al. 2011; Parent et al. 1992). With sign conventions in epithelial studies, inward Na^+ currents are positive and $V^{am} = \psi^o - \psi^{cell}$ with the associated current-voltage relationship being upward concave. This corresponds to the downward concave current-voltage relationship obtained with SGLT2 expressed in *Xenopus* oocyte (Parent et al. 1992) or HEK293T cells (Hummel et al. 2011) where inward Na^+ currents are given a negative sign, and membrane potential is defined as $V = \psi^{cell} - \psi^o$. The last mentioned studies reported zero

SGLT2-current in the absence of external glucose or in the absence of external Na^+. Thus, in the absence of luminal glucose, the Na^+ conductance of SGLT2 is zero. Finally, the reversal potential of the SGLT2-cotransporter $E_{rev}^{am,Glu\cdot Na}$ would have to fulfill the requirement that Gibbs free energy remains constant following one transport cycle as expressed by (Schultz 1980):

$$E_{rev}^{am,Glu\cdot Na} = \frac{RT}{F} \ln \frac{C_{Glu}^{o} \cdot C_{Na}^{o}}{C_{Glu}^{cell} \cdot C_{Na}^{cell}}$$

The abovementioned requirements are fulfilled by the following set of equations:

$$J_{Na}^{am,Glu\cdot Na} = \left(\frac{P^{Glu\cdot Na} F V^{am}}{RT}\right)\left(\frac{C_{Glu}^{o}}{K_{Glu}^{Glu\cdot Na} + C_{Glu}^{o}}\right)\left(\frac{C_{Na}^{o}}{K_{Na}^{Glu\cdot Na} + C_{Na}^{o}}\right) \times \frac{C_{Glu}^{o} C_{Na}^{o} \exp\{FV^{am}/(RT)\} - C_{Glu}^{cell} C_{Na}^{cell}}{\exp\{FV^{am}/(RT)\} - 1}$$

$$J_{Glu}^{am,Glu\cdot Na} = J_{Na}^{am,Glu\cdot Na}$$

$$V^{am} = \psi^{o} - \psi^{cell} \tag{3a}$$

$P^{Glu\cdot Na^+}$ is the maximal turnover of SGLT2, where $K_{Glu}^{Glu\cdot Na^+} \approx 5$ mM and $K_{Na^+}^{Glu\cdot Na^+} \approx 25$ mM are apparent dissociation constants of the transporter's binding sites (Hummel et al. 2011). For obtaining the associated chord (integral) conductance, the current carried by SGLT2 is introduced and multiplied by unity expressed as $\left(V^{am} - E_{rev}^{am,Glu}\right)/\left(V^{am} - E_{rev}^{am,Glu}\right)$:

$$I_{Na}^{am,Glu\cdot Na} = \frac{P' F^2 V^{am}\left[C_{Glu}^{o} C_{Na}^{o} \exp\{FV^{am}/(RT)\} - C_{Glu}^{cell} C_{Na}^{cell}\right]}{RT\left[\exp\{FV^{am}/(RT)\} - 1\right]\left(V^{am} - E_{rev}^{am,Glu}\right)}\left(V^{am} - E_{rev}^{am,Glu}\right) \tag{3b}$$

By having the form $I_j = G_j\,(V_m - E_j)$, the integral conductance is calculated from:

$$G_{Na}^{am,Glu\cdot Na} = \frac{P' F^2 V^{am}\left[C_{Glu}^{o} C_{Na}^{o} - C_{Glu}^{cell} C_{Na}^{cell} \exp\{FV^{am}/(RT)\}\right]}{RT\left[\exp\{FV^{am}/(RT)\} - 1\right]\left(V^{am} - E_{rev}^{am,Glu}\right)} \tag{3c}$$

where $E_{rev}^{am,Glu\cdot Na}$ is given by Eq. (3b) and P' by:

$$P' = P^{Glu\cdot Na}\left(\frac{C_{Glu}^{o}}{K_{Glu}^{Glu\cdot Na} + C_{Glu}^{o}}\right)\left(\frac{C_{Na}^{o}}{K_{Na^+}^{Glu\cdot Na} + C_{Na}^{o}}\right) \tag{3d}$$

Other SGLT2-models also handle saturation kinetics and substrate interactions, e.g., Layton et al. (2015) and Weinstein (1985). Unlike these previous treatments, Eqs. (3a–3d) cover the transporter's contributions to membrane potential and

membrane conductance; in the present study, this is required for its validation by comparing computations with experiments.

Immuno-labeling has shown that Na^+/K^+-ATPase (Skou 1965) is expressed exclusively in lateral plasma membrane (Kashgarian et al. 1985). The active cation fluxes are saturating function of cell Na^+ (C_{Na}^{cell}) and concentration of K^+ in lateral intercellular space (C_K^{lis}) (Garay and Garrahan 1973; Goldin 1977; Jørgensen 1980). The pump rate is also a function of the electrical work done in moving one charge across the membrane per pump cycle (Thomas 1972), which is a function of lateral membrane potential, V^{lm}, and the electrical work contributed by the pump-ATPase, here denoted E^{pump}. The above properties are fulfilled by the following set of equations (Larsen et al. 2009):

$$\begin{aligned} J_{Na}^{lm,pump} &= \frac{P_{Na,K}^{lm,pump}}{F}\left(\frac{C_{Na}^{cell}}{K_{Na}^{lm,pump}+C_{Na}^{cell}}\right)^3\left(\frac{C_K^{lis}}{K_K^{lm,pump}+C_K^{lis}}\right)^2\left[V^{lm}+E^{pump}\right] \\ J_K^{lm,pump} &= -\frac{2}{3}J_{Na}^{lm,pump} \\ V^{lm} &= \psi^{cell}-\psi^{lis} \end{aligned} \tag{4a}$$

$\frac{P_{Na,K}^{lm,pump}}{F}$ of dimension of mol s^{-1} V^{-1} per unit area of plasma membrane represents the Na^+ efflux through the sodium pump saturated with internal Na^+ and external K^+ at normal cytoplasmic ATP levels. With a 3 Na^+:2 K^+ stoichiometry, the expression for the pump current is:

$$I^{lm,pump} = \frac{P_{Na,K}^{lm,pump}}{3}\left(\frac{C_{Na}^{cell}}{K_{Na}^{lm,pump}+C_{Na}^{cell}}\right)^3\left(\frac{C_K^{lis}}{K_K^{lm,pump}+C_K^{lis}}\right)^2\left[V^{lm}+E^{pump}\right] \tag{4b}$$

Eq. (4b) gives pump currents that are linearly dependent on membrane potential, which is an acceptable approximation for the interval, $-110\ \text{mV} < V^{lm} < -5\ \text{mV}$ (Gadsby and Nakao 1989; Läuger 1991; Wu and Civan 1991) that covers computations of the present study. The reversal potential of pump currents is $E_{rev}^{pump} = -E^{pump}$ with free energy of ATP hydrolysis, $\Delta G_{ATP} \approx -60$ kJ/mol and stoichiometry of 3 Na^+:2 K^+:1 ATP, E^{pump} is about 200 mV which is within the range discussed by de Weer et al. (1988) and used in all our computations independently of the rate of pump flux. Unlike the reversal potential of the Na^+ pump of a tight epithelium, e.g., frog skin (Larsen 1973; Eskesen and Ussing 1985), the last mentioned assumption is plausible for proximal tubule cells of high density of mitochondria in remarkably close contact with pump sites that would minimize the diffusion distance between sites of dephosphorylation of ATP and rephosphorylation of ADP, respectively (Dørup and Maunsbach 1997). Following Läuger (1991), by inspection of Eq. (4b) in the range indicated where $P_{Na,K}^{lm,pump}$ is considered constant, the integral conductance of the pump would be:

$$G^{lm,pump} = \frac{P^{lm,pump}_{Na,K}}{3}\left(\frac{C^{cell}_{Na}}{K^{lm,pump}_{Na} + C^{cell}_{Na}}\right)^3\left(\frac{C^{lis}_{K}}{K^{lm,pump}_{K} + C^{lis}_{K}}\right)^2 \tag{4c}$$

Early mathematical models of proximal tubule by Sackin and Boulpaep (1975) and Weinstein (1986, 1992) did not include membrane potential as driving force for pump currents. Other studies included the membrane conductance-dependent electrogenic contribution of the pump to membrane potential (Lew et al. 1979 and Larsen 1991). The above Eq. (4a) is an expansion of previous treatments by acknowledging that potential *per se* is driving force for pump currents. The advantage of this new treatment shall be underscored in Results.

The expression for convection-diffusion of glucose across tight junction and interspace basement membrane obeys the Smoluchowski equation (Smoluchowski 1915). It was derived by Hertz (1922), and when applied to a membrane of reflection coefficient indicated by σ, the expression reads (Larsen et al. 2000):

$$J_{Glu} = J_V(1-\sigma_{Glu})\frac{C^{(I)}_{Glu}\exp[J_V(1-\sigma_{Glu})/P_{Glu}] - C^{(II)}_{Glu}}{\exp[J_V(1-\sigma_{Glu})/P_{Glu}] - 1} \tag{5}$$

The equation was expanded for covering the convection-electrodiffusion regime (Larsen et al. 2002),

$$J_j = \left(\frac{z_j FV}{RT}P_j + J_V(1-\sigma_j)\right)\frac{C^{(I)}_j \exp\left[z_j FV/(RT)\right]\exp\left[J_V(1-\sigma_j)/P_j\right] - C^{(II)}_j}{\exp\left[z_j FV/(RT)\right]\exp\left[J_V(1-\sigma_j)/P_j\right] - 1} \tag{6}$$

Here, it is assumed that the pore is symmetrical such that reflection coefficient and partition coefficient (β) are related by $\sigma = (1-\beta)$ as shown by Finkelstein (1987). J_V is the volume flux from compartment I (lumen or *lis*) to II (*lis* or serosa), and σ_j is the reflection coefficient of ion j of the membrane. Exit of glucose across lateral membrane is governed by saturation kinetics of a symmetrical carrier (Stein 1967),

$$J^{lm}_{Glu} = J^{lm,\max}_{Glu}\frac{K^{lm}_{Glu}\left(C^{c}_{Glu} - C^{lis}_{Glu}\right)}{\left(K^{lm}_{Glu} + C^{c}_{Glu}\right)\left(K^{lm}_{Glu} + C^{lis}_{Glu}\right)} \tag{7}$$

2.3 Water Flux Equations

In agreement with cloned aquaporins of proximal tubule (Borgnia et al. 1999), we assume reflection coefficient of unity for water flow through all plasma membranes. Thus, equations for the respective volume fluxes per unit area of apical plasma membrane are,

$$J_V^{am} = L_p^{am}\left\{RT\left(C_{Na}^{cell} + C_K^{cell} + C_{Cl}^{cell} + C_A^{cell} + C_{Glu}^{cell} - C_{Na}^{lumen} - C_K^{lumen} - C_{Cl}^{lumen} - C_{Glu}^{lumen}\right) + \left(p^{lumen} - p^{cell}\right)\right\} \tag{8a}$$

$$J_V^{lm} = L_p^{lm}\left\{RT\left(C_{Na}^{lis} + C_K^{lis} + C_{Cl}^{lis} + C_{Glu}^{lis} - C_{Na}^{cell} - C_K^{cell} - C_{Cl}^{cell} - C_A^{cell} - C_{Glu}^{cell}\right) + \left(p^{cell} - p^{lis}\right)\right\} \tag{8b}$$

$$J_V^{sm} = L_p^{sm}\left\{RT\left(C_{Na}^{serosa} + C_K^{serosa} + C_{Cl}^{serosa} + C_{Glu}^{serosa} - C_{Na}^{cell} - C_K^{cell} - C_{Cl}^{cell} - C_A^{cell} - C_{Glu}^{cell}\right) + \left(p^{cell} - p^{serosa}\right)\right\} \tag{8c}$$

Water fluxes through membranes delimiting the lateral intercellular space from external solutions have to include reflection coefficients,

$$J_V^{tj} = L_p^{tj}\left\{RT\left[\sigma_{Na}^{tj}\left(C_{Na}^{lis} - C_{Na}^{lumen}\right) + \sigma_K^{tj}\left(C_K^{lis} - C_K^{lumen}\right) + \sigma_{Cl}^{tj}\left(C_{Cl}^{lis} - C_{Cl}^{lumen}\right) + \sigma_{Glu}^{tj}\left(C_{Glu}^{lis} + C_{Glu}^{lumen}\right)\right] + \left(p^{lumen} - p^{lis}\right)\right\} \tag{9a}$$

$$J_V^{ibm} = L_p^{ibm}\left\{RT\left[\sigma_{Na}^{ibm}\left(C_{Na}^{serosa} - C_{Na}^{lis}\right) + \sigma_K^{ibm}\left(C_K^{serosa} - C_K^{lis}\right) + \sigma_{Cl}^{ibm}\left(C_{Cl}^{serosa} - C_{Cl}^{lis}\right) + \sigma_{Glu}^{ibm}\left(C_{Glu}^{serosa} + C_{Glu}^{lis}\right)\right] + \left(p^{lis} - p^{serosa}\right)\right\} \tag{9b}$$

Rather than hydraulic conductance, L_p, in the text, we refer to osmotic permeability, P_f. With molar volume of water indicated by $\bar{V}_W$, L_p and P_f are related by Finkelstein (1987),

$$P_f = \frac{RTL_p}{\bar{V}_W} \tag{10}$$

Mean valence of nondiffusible anions in the cell with concentration, C_A^{cell}, is denoted by z_A. Thus, the two electroneutrality conditions are given by:

$$C_A^{cell} = -\left(C_{Na}^{cell} + C_K^{cell} - C_{Cl}^{cell}\right)/z_A \tag{14}$$

$$C_{Cl}^{lis} = C_{Na}^{lis} + C_K^{lis} \tag{15}$$

If I^{clamp} is the transepithelial clamping current and I_j is the current carried by j through the membrane indicated by superscript ($j = Na^+$, K^+, or Cl^-), the mathematical solution would have to obey the requirement:

$$I^{clamp} = I_{Na}^{am} + I_{Na}^{tj} + I_K^{am} + I_K^{tj} + I_{Cl}^{am} + I_{Cl}^{tj} \tag{16}$$

where $I^{clamp} = 0$ ("open circuit") defines the mathematical solution containing the transepithelial potential difference.

2.4 Compliant Model and Volumes of Intraepithelial Compartments

For obtaining the hydrostatic pressure of the cell, we followed Weinstein and Stephenson (1979, 1981) and introduce a compliance model that assumes linear relationship between cell volume and cell pressure. If it is further assumed that the hydrostatic pressure of the cell adjusts itself to a value between ambient pressures weighted relative to the local compliant constants that are given the symbol μ^m, we can write (Larsen et al. 2000),

$$p^{cell} = \frac{\mu^{am}}{\mu^{am} + \mu^{lm} + \mu^{sm}} p^{lumen} + \frac{\mu^{lm}}{\mu^{am} + \mu^{lm} + \mu^{sm}} p^{lis} + \frac{\mu^{sm}}{\mu^{am} + \mu^{lm} + \mu^{sm}} p^{serosa} \tag{17a}$$

Introducing relative compliance constants,

$$p^{cell} = \overline{\mu}^{am} p^{lumen} + \overline{\mu}^{lm} p^{lis} + \overline{\mu}^{sm} p^{serosa} \tag{17b}$$

With the volume of *lis* in the absence of fluid transport denoted, $Vol^{lis,ref}$, we have (Larsen et al. 2002):

$$Vol^{lis} = Vol^{lis,ref}\left[1 + \mu^{lm}\left(p^{lis} - p^{cell}\right)\right] \tag{18}$$

D^{cell} and M_A are number of cells per unit area of apical membrane and amount of nondiffusible anions per cell, respectively. Hence, cell volume is:

$$Vol^{cell} = D^{cell} M_A / C_A^{cell} \tag{19}$$

Here, C_A^{cell} belongs to dependent variables.

2.5 Electrical-Circuit Analysis

Shown in Fig. 1c, the five epithelial membranes constitute a bridge circuit. For convenience, in the Mathematica© equations below, the five membranes are indicated by $am = 1$, $sm = 2$, $lm = 3$, $tj = 4$, and $ibm = 5$. The method used for calculating the transepithelial conductance (resistance) is as follows. Having chosen values for independent variables, the numerical solution provides all primary dependent variables. Integral conductances calculated as specified above are used to calculate the resistance of each of the five membranes, $R_1 \ldots R_5$. Simulating a step change of the current ΔI^{trans} through the circuit, Kirchhoff's rules are applied for setting up five simultaneous linear equations,

$$
\begin{aligned}
I_1R_1 + I_3R_3 - I_4R_4 &= 0\\
I_3R_3 + I_5R_5 - I_2R_2 &= 0\\
I_2 + I_5 - \Delta I^{trans} &= 0\\
I_1 - I_2 - I_3 &= 0\\
I_4 - I_3 - I_5 &= 0
\end{aligned}
$$

The currents flowing through the five resistors were obtained by using the solve routine of *Mathematica*©:

$$I_1 = -\frac{-(R_2R_4 + R_3R_4 + R_3R_5 + R_4R_5)}{R_1R_2 + R_1R_3 + R_2R_3 + R_2R_4 + R_3R_4 + R_1R_5 + R_3R_5 + R_4R_5}\Delta I^{trans}$$

$$I_2 = \Delta I^{trans} + \frac{(R_1R_3 + R_2(R_1 + R_3 + R_4))}{-R_1R_3 - R_1R_4 - R_2(R_1 + R_3 + R_4) - R_5(R_1 + R_3 + R_4)}\Delta I^{trans}$$

$$I_3 = -\frac{(R_2R_4 + R_1R_5)}{R_1R_2 + R_1R_3 + R_2R_3 + R_2R_4 + R_3R_4 + R_1R_5 + R_3R_5 + R_4R_5}\Delta I^{trans}$$

$$I_4 = -\frac{-(R_1R_2 - R_1R_3 - R_2R_3 - R_1R_5)}{R_1R_2 + R_1R_3 + R_2R_3 + R_2R_4 + R_3R_4 + R_1R_5 + R_3R_5}\Delta I^{trans}$$

$$I_5 = -\frac{(R_1R_3 + R_2(R_1 + R_3 + R_4))}{-R_1R_3 - R_3R_4 - R_2(R_1 + R_3 + R_4) - R_5(R_1 + R_3 + R_4)}\Delta I^{trans}$$

The transepithelial electrical potential displacement ΔV^{trans} and the resistance of the apical (luminal) membrane relative to the transcellular resistance are given by the relations,

$$
\begin{aligned}
\Delta V^{trans} &= I_1R_1 + I_2R_2\\
FR^{apical} &= I_1R_1/\Delta V^{trans}
\end{aligned}
$$

Finally, the transepithelial conductance is calculated as $G_t = \Delta I^{trans}/\Delta V^{trans}$.

2.6 Nomenclature and Sign Conventions

Nomenclature is indicated in Fig. 1b and Appendix 1. The model comprises four well-stirred compartments: outside (luminal-) compartment (*o*), cell compartment (*cell*), lateral intercellular space (*lis*), and inside (serosal-, interstitial-) compartment (*i*). These are confined by five membranes: apical (*am*), serosal (*sm*), lateral (*lm*), tight junction (*tj*), and intercellular basement membrane (*ibm*). The primary

unknowns include cellular and paracellular concentrations of Na^+, K^+, and Cl^-, glucose and nondiffusible intracellular anions, hydrostatic pressures in cell and *lis*, and electrical potentials in cell, *lis*, and outside compartment. Fluxes directed from lumen to cell and *lis*, from cell to serosa and *lis*, and from *lis* to serosa are positive. Electrical potentials are indicated with reference to serosal compartment ($\psi^i \equiv 0$) so that the individual membrane potentials are given by $V^{sm} = \psi^{cell} - \psi^i$, $V^{lm} = \psi^{cell} - \psi^{lis}$, $V^{am} = \psi^o - \psi^{cell}$, $V^{tj} = \psi^o - \psi^{lis}$, and $V^{ibm} = \psi^{lis} - \psi^i$.

2.7 Numerical Methods

The set of equations can be solved for both steady states and time-dependent states. In the general case, the transport equations for water and solutes are written as (Larsen et al. 2009):

$$\frac{d\bar{V}}{dt} = \sum_m J_{\bar{V}} \tag{20}$$

$$\frac{d\left(\bar{V} \cdot C_S\right)}{dt} = \sum_m J_S \tag{21}$$

where $\bar{V}$ denotes the volume of cell or lateral intercellular space, and $J_{\bar{V}}$ and J_S denote water and solute fluxes, respectively, through the various membranes, with m indicating membrane (m = 1–5). In steady state, left hand side is zero. When transients are studied, time-dependent behavior of Eqs. (20) and (21) needs to be simulated. To solve the equations in time, we utilize second-order accurate, three-point backward difference schemes (Taylor expansion) as follows:

$$\frac{1}{2\Delta t}\left[3\bar{V}^{(n)} - 4\bar{V}^{(n-1)} + \bar{V}^{(n-2)}\right] = \sum_j J_{\bar{V}}^{(n)} \tag{22}$$

$$\frac{1}{2\Delta t}\left[3\left(\bar{V} \cdot C_S\right)^{(n)} - 4\left(\bar{V} \cdot C_S\right)^{(n-1)} + \left(\bar{V} \cdot C_S\right)^{(n-2)}\right] = \sum_m J_S^{(n)} \tag{23}$$

where index n refers to time t^n and Δt is the time step, such that $t^n = t^{n-1} + \Delta t$. Thus, the equations are solved for all variables with index n at time $t = t^n$, leaving the remaining terms as known from the former time steps. The equations are solved together with the above equations for electroneutrality and the compliance model. The strongly coupled nonlinear equations were solved to machine accuracy by a conventional iterative Newton-Raphson method. In forming the Jacobian matrix, the equations were not differentiated analytically as a simple difference scheme was employed. For analyses of transient states, the term "sampling frequency" refers to frequency of time steps. With a single time step, we jump directly from one steady state to another – skipping transient states.

2.8 Choice of Independent Variables

Appendix 2 lists independent variables of the model displayed in Fig. 1b. Ion permeabilities and maximum pump rates were chosen to obtain a net uptake of Na^+ of about 5,000 pmol cm^{-2} s^{-1} with associated volume absorption of 30–40 nL cm^{-2} s^{-1} together with intracellular concentrations and serosa-membrane potential in reasonable agreement with measured quantities (Windhager 1979). From measurements, $C_{Na}^{cell} = 17.5$, $C_K^{cell} = 113$, and $C_{Cl}^{cell} = 18$ mM at a serosal membrane potential of −76 mV (Cassola et al. 1983; Edelman et al. 1978; Yoshitomi and Fromter 1985). The corresponding model values are given in Fig. 2. For simulating the somewhat low C_K^{cell}, we assumed a mean net charge of intracellular nondiffusible anions less than unity ($z_A = -0.75$). In the model, the Na^+/K^+ pump in the serosal plasma membrane is "silent" so that the active Na^+ uptake is due entirely to the activity of lateral pumps (Kashgarian et al. 1985). The major electro-diffusive K^+ exit from cells is through the K^+ channels of *lm*. Both apical and "basolateral" plasma membrane domains contain water channels (Nielsen et al. 1996). The osmotic permeabilities were taken from experiments on rabbit proximal tubule (Carpi-Medina et al. 1984; Gonzáles et al. 1984). Solvent drag on sucrose indicated that the paracellular pathway of the kidney proximal tubule contributes to water transport across the epithelium (Whittembury et al. 1988), but the hydraulic conductance of tight junctions, which constitutes the rate limiting structure along the pathway, is not easy to determine. One would think that one way of doing this would be to block water channels of the apical membrane and measure the residual transepithelial water flux. This method was applied by Whittembury's laboratory (Carpi-Medina and Whittembury 1988), and we have used the value thus estimated, $P_{osm}^{tj} = 2.5 \times 10^3$ μm s^{-1}. As we shall see below, blocking the osmotic permeability of the apical membrane will lead to an increase in the osmolarity of *lis*, forcing an increased water flow along the paracellular pathway. Thus, our osmotic permeability of tight junctions is overestimated. However, as none of the conclusions, generally of semiquantitative nature, are affected by this choice, it is applied here in lack of better estimate. As emphasized above, the serosal plasma membrane contacting the epithelium's basement membrane and the lateral plasma membrane constitute two separate domains. The model is born with similar transport systems in the two domains. The serosal-membrane fluxes governing the majority of computations were obtained by choosing small values of associated independent variables.

Molecular biological and biophysical studies indicated that paracellular fluxes are mediated both by cation and anion selective tight junction pores, recently reviewed by Fromm et al. (2017). Claudin-2 is selectively permeable for small cations like Na^+ and K^+ and permeable for water. Claudin-10a (and perhaps claudin-17) is selectively permeable for small anions like Cl^-. Reflection coefficients of tight junctions were taken from literature $\sigma_{Na}^{tj} = \sigma_K^{tj} = 0.7$ and $\sigma_{Cl}^{tj} = 0.45$ (Ullrich 1973). The interspace basement membrane is governed by physical properties of the basement membrane, and a morphometric study of rabbit proximal

tubule indicating that *ibm* constitutes 10% of the basement membrane area of the entire tubule (Welling and Grantham 1972; Welling et al. 1987a, b). Ion permeability of convection pores was selected to obtain the paracellular electrical resistance estimated by Frömter (1979) of about 5 Ω cm^2, which requires a relatively high Cl^- permeability of delimiting membranes. The cation "selectivity" of the interspace basement membrane is that of free diffusion in water.

2.9 Geometrical Dimensions and Units of Physical Quantities

A stereological study of S1 segment of rabbit proximal tubule indicated an outer and inner diameter of 38 and 24 μm, respectively, corresponding to a cell height of 7 μm. Referring to 1 mm of tubule length, the following numbers were obtained: an epithelial volume of 6.8×10^5 μm^3, an apical membrane area of 2.20×10^6 μm^2, and a lateral membrane area of 2.29×10^6 μm^2 (Welling and Welling 1988). With 300 cells per mm (Welling et al. 1987a), single-cell volume is about 2,267 fL. With gap junctions between cells, we assume that the epithelium constitutes a continuous functional syncytium.

Physical constants, independent variables, and computed dependent variables are in MKSA units. In the text, however, all variables are presented in units commonly used in physiological literature.

3 Results

3.1 General Features

Kidney proximal tubule accomplishes isosmotic transport in absence of glucose in luminal perfusion solution (Windhager et al. 1959; Morel and Murayama 1970). Figure 2 contains values given by the model for the reference state exposed to symmetrical external glucose-free solutions. With respect to cellular ion concentrations, it is noted that C_K^{cell} of 117 mM is fairly low, which is in agreement with measurements, recently reviewed by Weinstein (2013): 70 mM (Necturus), 113 mM (rat), and 68 mM (rabbit). The intracellular electrical potential, $V^{cell} = -82$ mV, agrees with values measured in rat ranging between −64 and − 85 mV (Frömter 1979). The lumen-negative transepithelial potential difference is no more than $V^{trans} = -1.78$ mV, governed by high paracellular electrical conductance and the following transepithelial ion fluxes (pmol cm^{-2} s^{-1}): $J_{Na} = 5{,}197$, $J_K = 187$, and $J_{Cl} = 5{,}384$. Fluxes through the apical membrane are associated with an apical membrane resistance of 313 Ω cm^2, which is 57 times larger than the shunt resistance of 5.5 Ω cm^2. The corresponding values for rat are 260 and 5 Ω cm^2, respectively (Frömter 1982). At transepithelial osmotic equilibrium, water uptake would have

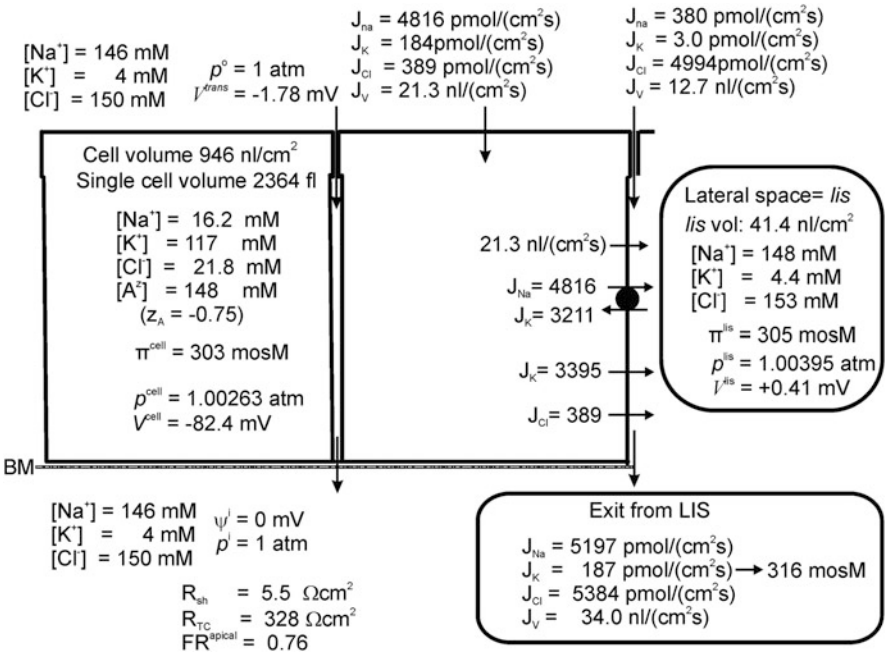

Fig. 2 Reference state of the minimalistic model epithelium. With the large osmotic permeabilities estimated experimentally (Carpi-Medina et al. 1984; Gonzáles et al. 1984) is the fluid exiting the lateral intercellular space predicted to be hyperosmotic to bath: 316 mosM versus 300 mosM. Electrical resistances given by the model: $R^{am} = 313\ \Omega\ \mathrm{cm}^2$, $R^{lm} = 15.9\ \Omega\ \mathrm{cm}^2$, $R^{tj} = 4.43\ \Omega\ \mathrm{cm}^2$, and $R^{ibm} = 1.10\ \Omega\ \mathrm{cm}^2$. $\mathrm{FR}^{\mathrm{apical}}$ is the ratio of apical (luminal) membrane resistance to transepithelial resistance

to be translateral, and with osmotic permeabilities obtained in experiments by Carpi-Medina and Whittembury (1988), the water uptake via apical membrane is 21.3 nL $\mathrm{cm}^{-2}\ \mathrm{s}^{-1}$. This is about twice the water flux of 12.7 nL $\mathrm{cm}^{-2}\ \mathrm{s}^{-1}$ through tight junctions, which is driven by $\Delta\pi = 5$ mosM. Convection fluxes energized by paracellular water absorption are discussed in detail below. Here it suffices to point out that paracellular solvent drag on potassium ions cannot account for transtubular K^+ absorption which provides a K^+ concentration of the absorbate that is significantly less than 1 mM; an estimate using numbers of Fig. 2 would give 3.0 pmol $\mathrm{cm}^{-2}\ \mathrm{s}^{-1}$/22.7 nl $\mathrm{cm}^{-2}\ \mathrm{s}^{-1} = 0.24$ mM. This should be compared to the total K^+ absorption that gives a K^+ concentration of the absorbate of 187/34.0 = 5.5 mM (Fig. 2), that is, a value much closer to the 4 mM of the serosal bath. When glucose absorption is included, this number drops to $[K^+]_{\mathrm{absorbate}} = 190$ pmol cm^{-2} nl/46 nl $\mathrm{cm}^{-2} = 4.1$ mM, see Fig. 4. Exit of water through the interspace basement membrane of low reflection coefficients is driven by a small hydrostatic pressure difference ($p^{lis} - p^i$) of 3.95×10^{-3} atm. With a total apical water uptake of $J_V = 34.0$ nL $\mathrm{cm}^{-2}\ \mathrm{s}^{-1}$ at steady state, this is also the volume flux across *ibm*. The lateral intercellular space of an osmolarity of 305 mosM is no

more than 1.7% hyperosmotic relative to the symmetrical bathing solutions of 300 mosM. Nevertheless, the fluid exiting the lateral space of 316 mosM is 5.3% hyperosmotic with respect to bath. The difference in osmolarity between *lis* and the fluid emerging from *lis*, in this example 11 mosM, shows that exit fluxes are governed by relatively large electrodiffusion permeabilities of *ibm* (conf. Eq. 6), which exposes the unavoidable diffusion-convection problem of the exit pathway in isosmotic transport.

3.2 A Component of Na^+ Uptake Bypasses the Pump

Although the electrical driving force for Na^+ movement through tight junctions is −2.19 mV, the flux of Na^+ of 380 pmol cm^{-2} s^{-1} is inward showing that solvent drag overrules the electrochemical driving force of opposite direction. Formally, the Na^+ current through tight junctions can be written,

$$I_{Na}^{tj} = G_{Na}^{tj}\left(V^{tj} - E_{Na}^{tj} + \Phi_{Na}^{tj}\right) \tag{24}$$

G_{Na}^{tj} is the Na^+ conductance of tight junctions, E_{Na}^{tj} the Na^+ equilibrium potential across tight junctions, V^{tj} the transjunctional potential difference, and Φ_{Na}^{tj} the driving force due to convection, which Ussing has given the expressive term "solvent drag." In the electrodiffusion-convection regime, the term denoted Φ_{Na}^{tj} of Eq. (24) is the driving force resulting from the convection process. Because we here consider an ion current, it follows that its dimension is "volt." Ussing's original mathematical treatment of solvent drag concerned unidirectional isotope fluxes of electroneutral molecules that included a hydrostatic pressure gradient as driving force for the net water flux. With this in mind, it should be evident that our treatment of solvent drag agrees with the original definition. Aiming at solvent drag:

$$\Phi_{Na}^{tj} = \frac{I_{Na}^{tj} - G_{Na}^{tj}\left(V^{tj} - E_{Na}^{tj}\right)}{G_{Na}^{tj}}$$

There is strong dependence of Φ_{Na}^{tj} on P_{Na}^{tj} (see Table 1). However, unlike paracellular transport, the overall tubule function is insensitive to a 10× decrease in P_{Na}^{tj}, which on the other hand leads to 11.3 times increase in paracellular solvent drag. Thus, even though the transepithelial potential difference is negative, our quantitative analysis predicts that solvent drag in tight junctions prevents passive back leak of Na^+ to tubule lumen, which is contrary to information given in medical textbooks (Boron and Boulpaep 2017).

Table 1 Solvent drag on sodium ions in tight junction

P_{Na}^{tj} (cm s^{-1})	V^{trans} (mV)	J_{Na}^{trans} (pmol cm^{-2} s^{-1})	J_V^{trans} (nL cm^{-2} s^{-1})	I_{Na}^{tj} (μA cm^{-2})	G_{Na}^{tj} (mS cm^{-2})	V^{tj} (mV)	E_{Na}^{tj} (mV)	Φ_{Na} (mV)
1.25×10^{-3}	−1.78	5,195	34.0	36.70	6.65	−2.19	−0.40	7.3
7.50×10^{-4}	−1.81	5,276	34.5	44.21	3.99	−2.23	−0.41	12.9
3.75×10^{-4}	−1.83	5,336	34.9	49.99	1.99	−2.25	−0.42	27.0
1.25×10^{-4}	−1.85	5,377	35.2	53.80	0.67	−2.28	−0.42	82.8

Independent model variables, except P_{Na}^{tj} (column 1), were kept at their standard value. The computed paracellular solvent drag on sodium ions is listed in last column. It shows that there is a strong inverse dependence of Φ_{Na}^{tm} on P_{Na}^{tj}. On the other hand, this has little effect on the overall tubule function as exemplified by the transepithelial Na^+ and water fluxes and the transepithelial potential difference.

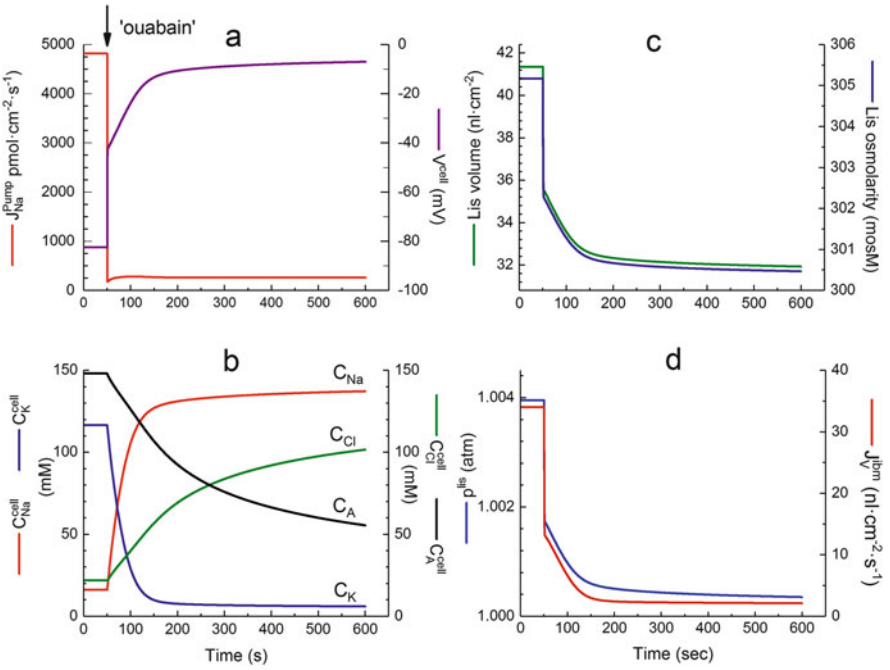

Fig. 3 (**a**–**d**) Effects of inhibition of the Na^+-K^+-ATPase of lateral membrane. (**a**) at time = 50 s, maximum pump flux (Eq. 4a) was reduced exponentially ($\tau = 0.1$ s, Eq. 25) by a factor of 50×. This resulted in fast drop of $J_{Na}^{pump,lm}$ and an associated fast cell depolarization of 40 mV. The further slow depolarization owes to dissipation of ion gradients at rates given by respective membrane permeabilities and cellular ion pool sizes. (**b**) Cation-gradient dissipations lead to Na^+ and Cl^- accumulation and K^+ loss. The net effect is cell swelling as indicated by the decrease in concentration of nondiffusible intracellular anions (C_A). (**c**) As consequence of the arrest of lateral active Na^+ flux and subsequent slow ion-gradient dissipations, volume and osmolarity of *lis* decrease accordingly. (**d**) The associated drop in hydrostatic pressure directs reduced exit of fluid across the interspace basement membrane

3.3 *Inhibition of the Na^+/K^+ Pump*

The lateral Na^+/K^+-ATPase energizes ion and water fluxes through the epithelium (Garg et al. 1981; Gyory and Kinne 1971), and owing to the very high expression of the enzyme in proximal tubule (Jørgensen 1986), pump currents may have significant electrophysiological and hydrodynamic effects. Inhibiting the Na^+/K^+ pump by a 50× reduction of $P_{Na^+,K^+}^{lm,pump}$ (Eq. 4a) is shown in Fig. 3. The time course of inhibition is given by,

$$c(t) = c(\infty) - (c(0) - c(\infty))\exp(-t/\tau), \tag{25}$$

Here, $c(0)/c(\infty) = 50$ and $\tau = 0.1$ s. Due to the voltage dependence of the pump current, the instantaneous membrane depolarization is fast and large. Computations

given by the model (Fig. 3a) predict an ouabain-induced cell depolarization of 40 mV for a pump current of 155 μA cm^{-2}. This is to be compared to a pump-generated hyperpolarization of 15–20 mV of the inward facing membrane of frog skin for pump currents of 40–50 μA cm^{-2} (Nagel 1980), and a 1.8 mV hyperpolarization of giant axon caused by a pump current of 1.8 μA cm^{-2} (Hodgkin and Keynes 1955). Our conclusion here is that the contribution of the pump current to the membrane potential has evolved for serving tissue specific functions of the Na^+/K^+ pump; in proximal tubule, the pump serves the returning of a large volume of isosmotic fluid to the extracellular fluid which requires high activity of the Na^+/K^+-ATPase. In the skin of frogs on land the function of the sodium pump is to return Na^+ (and Cl^-) to the body fluids during evaporative water loss from the cutaneous surface fluid generated by subepidermal mucous glands (Larsen 2011). Finally, electrical signalling in excitable cells relies on the membrane potential being uniquely given by the ratio of the membrane's Na^+ and K^+ permeabilities (Hodgkin 1958), which presupposes relatively very low activity of the Na^+/K^+-ATPase. Secondary to the voltage dependent sudden decrease, the pump flux decreases further but with a longer time constant caused by the relatively slow redistribution of cellular cation pools (Fig. 3b). With negatively charged intracellular macroions, the working of the pump keeps the cell from swelling and bursting, which otherwise would take place due to the continuous inflow of Na^+ (and Cl^-), conf. the theory of Gibbs-Donnan equilibrium (Sten-Knudsen 2002). Thus, concomitant with accumulation of cellular Na^+ and Cl^-, the cell swells (Fig. 3b). The sudden reduction in pumping of Na^+ into the lateral intercellular space and the slow cellular ion gradient dissipations result in reduction in osmolarity and volume of *lis* that takes place with similar fast and slow time courses (Fig. 3c). The coupling of the pump flux and the water flow across the lateral membrane as indicated in Fig. 3c is discussed in detail in Sect. 3.5. The rate of exit of fluid into the serosal compartment is governed by the hydrostatic pressure difference between the lateral intercellular space, p^{lis}, and serosal compartment, p^{i} of 1 atm (Fig. 3d).

3.4 *Effect of Adding Glucose*

Sodium and water absorption increase significantly together with apical membrane depolarization if organic solutes are added to the tubular perfusion solution (Lapointe and Duplain 1991). In rabbit and rat proximal convoluted tubules, significant effects on the rate of fluid absorption were observed upon removal of luminal glucose and other metabolites (Burg et al. 1976; Frömter 1982). We have chosen values of independent variables governing apical Na^+ uptake (Eqs. 1a–3a) for reproducing studies simulating the abovementioned significant effects of glucose. Thus, in the following, fluxes carried by Eq. (3a) are significant as compared to fluxes generated by Eqs. (1a) and (2a). The computed steady state with the physiological concentration of 5 mM glucose is shown in Fig. 4. The pertinent findings can be summarized. In steady state, the cellular glucose concentration is about twice that of the external concentration. Compared to Fig. 2 with no glucose, C_{Na}^{cell} is increased while C_{K}^{cell} is decreased, leading to 3% cell swelling from 2,366 to 2,436 fL. Such a

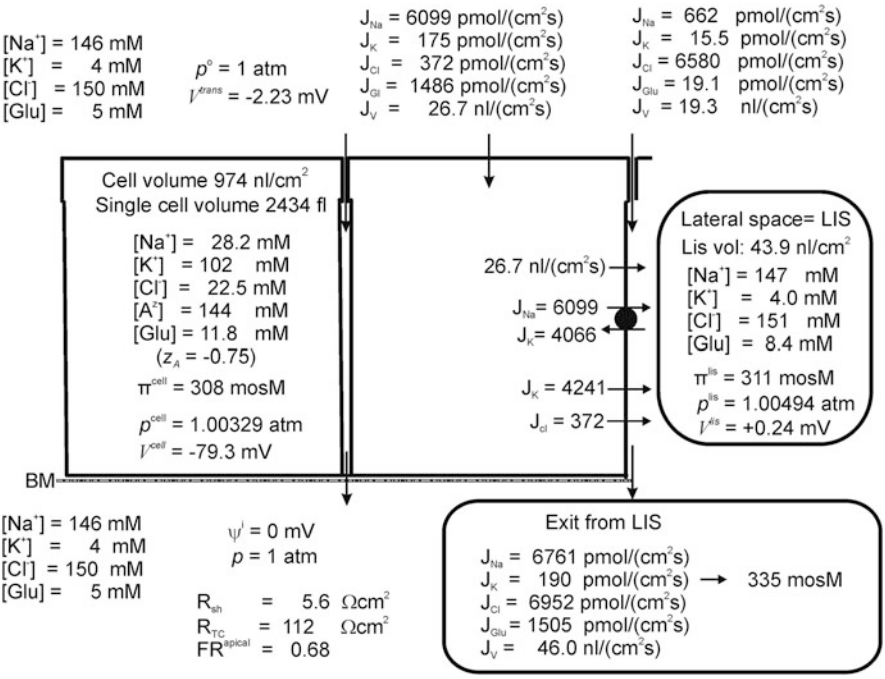

Fig. 4 The model epithelium engaged in glucose absorption. The glucose uptake across the luminal membrane is coupled to uptake of sodium ions and driven by the electrochemical gradient for Na^+ (SGLT2, Eq. 3a). Therefore, addition of glucose to external baths results in stimulation of the active Na^+ flux across the lateral membrane from 4,816 (Fig. 2) to 6,099 pmol cm^{-2} s^{-1}. The enhanced lateral Na^+ pump flux increases the Na^+ concentration and osmolarity of the lateral intercellular space, which in turn increases transepithelial fluid uptake, from 30 to 46 nL cm^{-2} s^{-1}. Importantly, this results in an increase in the hyperosmolarity of transported fluid, from 316 to 335 mosM. Electrical resistances given by the model: $R^{am} = 96.5\ \Omega\ cm^2$, $R^{lm} = 17.3\ \Omega\ cm^2$, $R^{tj} = 4.45\ \Omega\ cm^2$, and $R^{ibm} = 1.10\ \Omega\ cm^2$

small cell volume change indicates a priori an insignificant increase in intracellular chloride concentration, which is confirmed quantitatively by numbers given by the model, $C_{Cl}^{cell} = 21.8$ and 22.5 mM, respectively. The glucose-induced hyperpolarization of the transepithelial potential difference of −0.45 mV from −1.78 to −2.23 mV, compare Fig. 2 with Fig. 4, is comparable in absolute magnitude to that of rat proximal tubule, -0.36 ± 0.22 mV, mean ± S.D. (Frömter 1982). In the same study, Frömter perfused rat tubule in situ with Ringer's solution containing 30 mM bicarbonate in the perfusion solution. Prior to glucose, the transepithelial potential difference was lumen positive but becoming lumen negative, as predicted by model computation, when perfused with 3 mM glucose. The stimulated sodium pump flux results in increased osmolarity of *lis* together with an increased water uptake from 34 to 46 nL cm^{-2} s^{-1}. The deviation (Δ) from isosmotic transport becomes significantly larger following addition of glucose, i.e., $\Delta = 16$ mosM and $\Delta = 29$ mosM as indicated in Figs. 2 and 4. The increased fluid uptake discussed above includes an increased flow of fluid in tight junctions, from 12.7 to

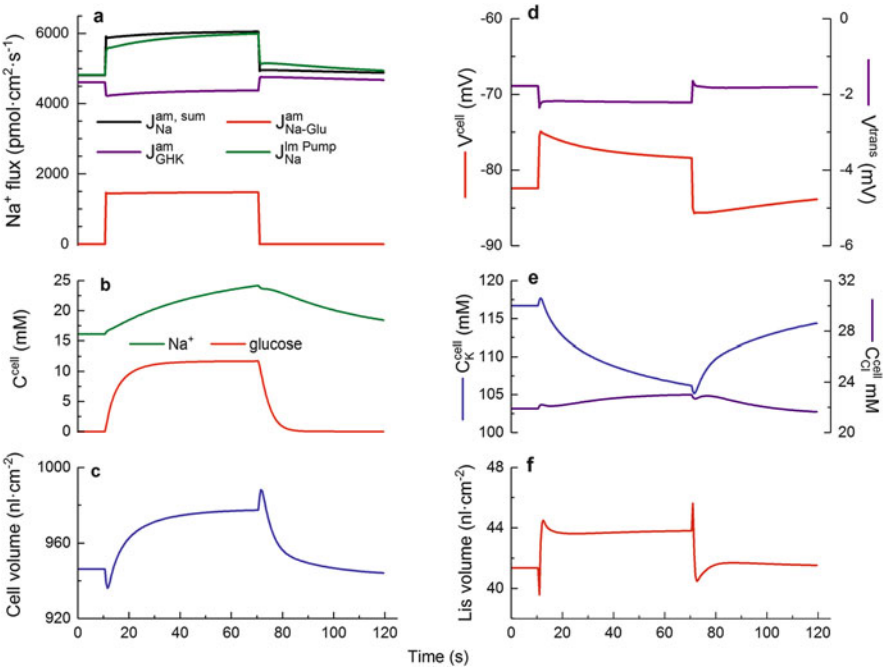

Fig. 5 (**a**–**f**) Effects of reversible bilateral exposure of 5 mM glucose of 60 s duration. (**a**) Fluxes carried by electrogenic Na^+ pathways $J_{Na}^{am,sum} = J_{GHK}^{am} + J_{Na-Glu}^{am}$. Note initial decrease in GHK-flux caused by depolarization of apical membrane. $J_{Na}^{pump,lm}$ is stimulated "instantly" and secondarily as a consequence of a slow increase in C_{Na}^{cell}. See text for discussion. (**b**) Inflow of Na^+ and glucose results in cellular accumulation of the two solutes, but steady state is not achieved for Na^+ within the 60-s glucose pulse. (**c**) Cell swelling due to accumulation of Na^+ and glucose is preceded by fast volume decrease caused by the osmotic effect of adding glucose. (**d**) The electrogenic nature of the apical Na-glucose transporter is reflected in significant membrane depolarization and associated small hyperpolarization of V^{trans}. (**e**) C_K^{cell} decreases with long time constant, e.g., at steady state is $C_K^{cell} = 102$ mM (Fig. 4), while increase in C_{Cl}^{cell} is modest. (**f**) The relatively small *lis* volume responds near instantly to adding/removing glucose to external compartments that embrace the steady volume increase caused by an increase in $C_{glucose}^{lis}$ to 8.4 mM (Fig. 4)

19.3 nL cm^{-2} s^{-1}, which results from increased osmolarity of *lis* from 305 to 311 mosM. Due to convection, this has direct effect on cation fluxes in tight junctions; e.g., for $P_{Na}^{tj} = 1.25 \times 10^{-3}$ cm s^{-1} is J_{Na}^{tj} increased from 380 to 662 pmol cm^{-2} s^{-1}. The number of 662 pmol cm^{-2} s^{-1} obtained with glucose in luminal solution is probably the better estimate of the paracellular Na^+ reabsorption driven by solvent drag in proximal convoluted tubule.

In Fig. 5 are shown time-dependent states induced by 60-s bilateral exposure to 5 mM-glucose. By choosing $\tau = 0.1$ s (Eq. 25), the time course of cell variables given in Fig. 5 is reflecting characteristic times of intracellular pools of the "functional syncytium." Due to the electrogenic nature of the apical Na^+-glucose transporter (Eq. 3a), the cell membrane potential depolarizes by 7 mV (Fig. 5d), which is comparable to 5.7 mV ± 2.0 in rat (Frömter 1982). In the same study,

Frömter found that the resistance of the brush border membrane decreased to 52.8 ± 12% (mean ± SD) of its control value. In the model, apical membrane resistance dropped from 313 to 96 Ω cm^2, i.e., to 31% of the control value. A plausible reason for the difference between experiment and computation is that Frömter had 3 mM glucose in the luminal perfusion solution as compared to our 5 mM glucose (Eq. 3a). Thus, with 3 mM glucose, the computed apical membrane resistance dropped to 46% of the control value which is within the abovementioned experimental range (details not shown). As a novel result, it should be noted that the addition of glucose also leads to "instantaneous" increase in $J_{Na}^{lm,pump}$ (Fig. 5a, green graph) which is the consequence of the pump current being an instantaneous function of lateral membrane potential (Eq. 4a). The effect of activating rheogenic Na^+ uptake across the apical membranes on Na^+ pumping rate at the lateral membrane and the associated enhanced rate of fluid uptake constitute a mechanism of "cross-talk" that is not described before. The depolarization is about the same for apical and lateral membranes, because the cell is "short-circuited" by the low-resistance paracellular shunt, cf. time course of V^{trans} shown in Fig. 5d. Subsequently, $J_{Na}^{lm,pump}$ increases slowly governed by slow increase in C_{Na}^{cell} (Fig. 5b).

The cell depolarization indicated in Fig. 5d decreases the Na^+ flux in apical GHK-rectifying Na^+ channels, conf. Eq. (1a) (Fig. 5a purple graph). In recordings of the total membrane current, this would be masked by the larger Na^+ flux via the Na^+-glucose transporter (Fig. 5a). The decrease in C_K^{cell} from 116 to 106 mM (Fig. 5e), concomitant with the increase in C_{Na}^{cell}, should be compared with the small cell swelling mentioned above, which by and large is caused by the accumulated electroneutral glucose (Fig. 5b, e). This conclusion is in agreement with microscopically observed cell volume changes in microperfused proximal convoluted tubule of rabbit kidney (Burg et al. 1976).

In conclusion, the model reproduces measured glucose effects on Na^+ fluxes, electrophysiology, and cell volume. Besides stimulated transepithelial Na^+ and glucose fluxes fluid uptake as well is increased. It is noteworthy that the solute-coupled fluid flux is predicted to become more hyperosmotic when the proximal kidney tubule is engaged in glucose reabsorption, i.e., 316 mosM versus 335 mosM, which should be compared to "bath" osmolarities of 300 and 305 mosM, respectively.

3.5 *Blocking Water Channels of Apical Membrane*

Reducing the osmotic permeability of the apical membrane from 0.449×10^4 to 0.449 μm s^{-1} results in elimination of translateral water flow with hardly detectable effects on rate of active Na^+ uptake and overall transepithelial water absorption, the latter being 34.0 and 35.5 nL cm^{-2} s^{-1}, respectively (Figs. 2 and 6). At the new steady state with little change in apical flux of sodium ions, the pumping of Na^+ into *lis* is also changed by a small amount by the above maneuver, $J_{Na}^{lm,pump} = 4{,}816$ and 4,837 pmol $cm^{-2} \cdot s^{-1}$, respectively (Figs. 2 and 6). Water is now forced to take the paracellular route. Osmolarity and hydrostatic pressure of *lis*, governing entrance

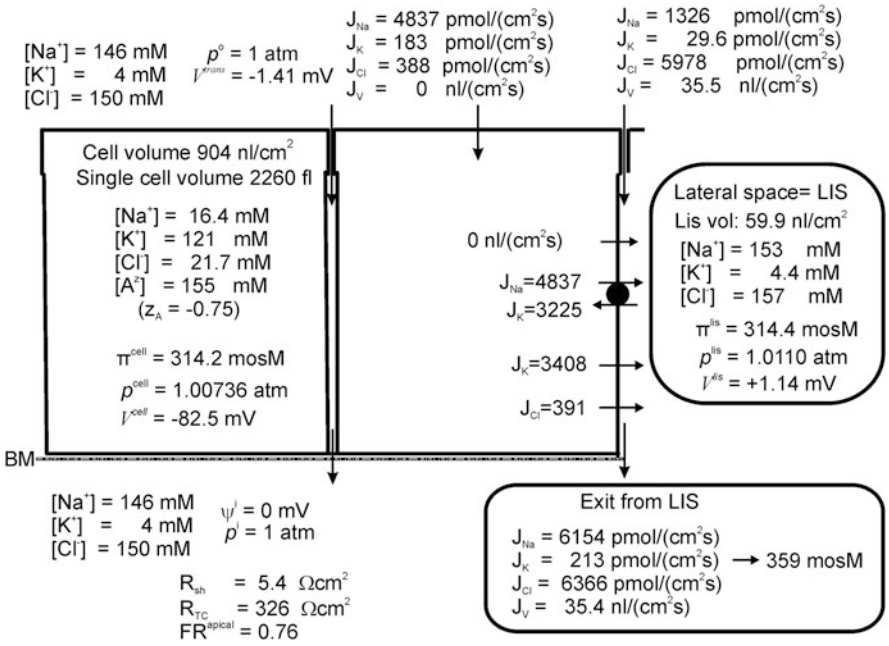

Fig. 6 Steady-state solution with eliminated apical osmotic permeability. Apical P_f was reduced by a factor of 10^4 from 0.449 × 10^4 to 0.449 μm s^{-1}. At transepithelial osmotic equilibrium, this eliminates cellular water transport, thus simulating AQP-1 (− /−). Electrical resistances given by the following models: R^{am} = 312 Ω cm^2, R^{lm} = 14.3 Ω cm^2, R^{tj} = 4.37 Ω cm^2, and R^{ibm} = 1.08 Ω cm^2. It is important to note that the transepithelial water flux is not significantly reduced by eliminating the apical membrane's water channels, J_V^{ibm} = 34.0 and 35.4 nL cm^{-2} s^{-1}, respectively (Figs. 2 and 5)

and exit of water across tight junction and interspace basement membrane, respectively, energize the significantly increased water flux along the paracellular route. The larger ion concentrations of *lis* result in increased convection-electrodiffusion fluxes through *ibm* as reflected in the increased osmolarity to 359 mosM of the fluid emerging from *lis* (Fig. 6).

The relationships described above can be analyzed in detail by inspecting time-dependent states following a mono-exponential reduction of P_f^{am} from 0.449 × 10^4 to 0.449 μm/s governed by τ = 1 s (Eq. 25); see Fig. 7a–f. The initial response to "eliminating" the apical water permeability is a shift of water volume from cells to *lis* driven by the difference in osmolarity between the two compartments, which is maintained by pumping of Na^+ into *lis* (Fig. 7a). In the beginning, where volume shift is fast, C_{Na}^{cell} increases rapidly, whereby the Na^+ pump flux is transiently stimulated (Fig. 7b). This lasts for about 20 s, where the osmolarity of *lis* of a relatively small volume increases toward its new steady-state value. While C_{Cl}^{cell} increases transiently, the concentration of nondiffusible anions increases in parallel with loss of cell volume (Fig. 7c). The increase in osmolarity of *lis* drives fluid into *lis* from the luminal solution (Fig. 7d), which brings ions into the compartment by solvent drag (Eq. 6). At the beginning of *lis*-volume expansion, p^{lis} is too low for

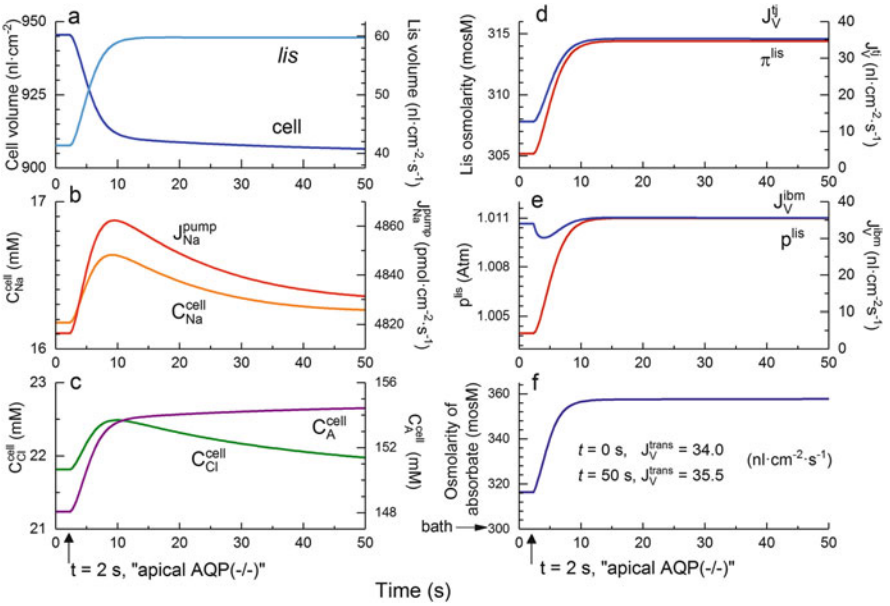

Fig. 7 (**a**–**f**) Time course of physiological variables in response to "eliminating" osmotic permeability of apical membrane. At time = 2 s and governed by $\tau = 1$ s, P_f^{am} was reduced exponentially from 4,490 to 0.449 μm s^{-1}. (**a**) this results in a fast shift of water volume from cells to *lis*. (**b**) C_{Na}^{cell} increases transiently, which stimulates Na^+ pump flux, $J_{Na}^{pump,lm}$. (**c**) While the transient increase in C_{Cl}^{cell} parallels the transient increase in C_{Na}^{cell}, the increase in concentration of nondiffusible anions is closely following the loss of cell volume. (**d**) The water flux is redirected from being translateral to being paracellular driven by the increased osmolarity of *lis* governed by the C_{Na}^{cell}-stimulated increase in $J_{Na}^{pump,lm}$. (**e**) Due to inflow of water, the hydrostatic pressure of *lis* increases, which drives the volume flux across the interspace basement membrane J_V^{ibm}. (**f**) The final result is a significant increase in osmolarity of the fluid emerging from *lis* due to convection-electrodiffusion of solutes across the interspace basement membrane (Eq. 6). Notably, at the new steady state, the transepithelial water flux is about the same as the water flux prior to eliminating P_f^{am} (35.5 versus 34.0 nL cm^{-2} s^{-1})

preventing a decrease in the flux of fluid across *ibm*, J_V^{ibm}, conf. Eq. (9b) (Fig. 7e). This is transient, however; the continued influx of fluid across tight junction causes p^{lis} to increase, which enhances the fluid efflux across *ibm* into the serosal compartment. The new steady state is reached when J_V^{ibm} matches J_V^{tm} (Fig. 7e, $J_V^{lm} = 0$ at all times). The significantly increased solute concentrations of *lis* combined with relatively large ion diffusion permeabilities of *ibm* (Eq. 6) causes the osmolarity of the fluid exiting the epithelium to increase to 359 mosM, which now becomes hyperosmotic by 59 mosM.

With isosmotic luminal perfusate and bath solutions, Schnermann et al. (1998) found that the fluid absorption rate in the S2 portion was halved in AQP-1 knock-out [−/−] mice; expressed in nL per mm tubule length, the rate dropped from 0.64 ± 0.15 (wild type, $n = 8$) to 0.31 ± 0.12 (−/−, $n = 5$). Our analysis presented

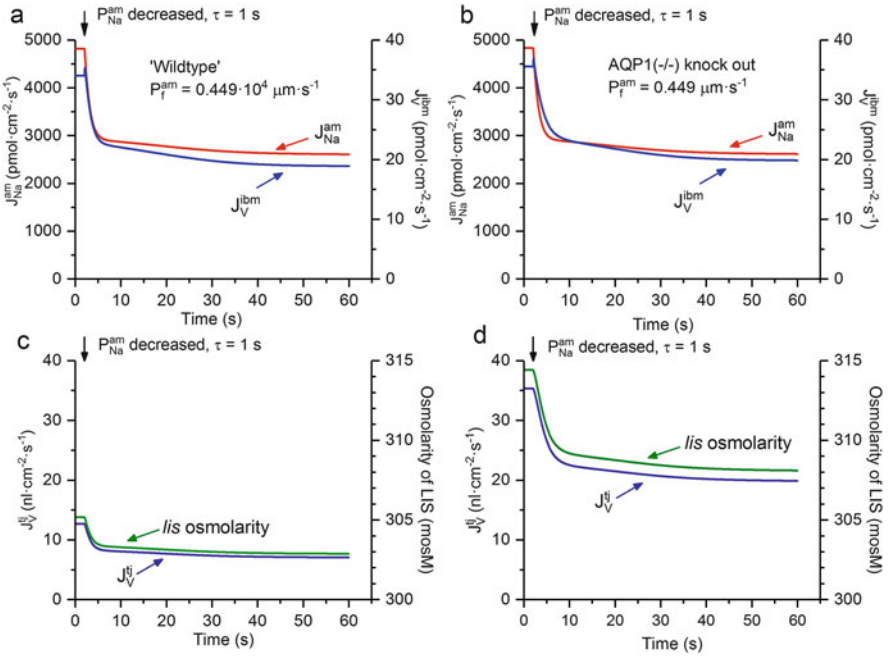

Fig. 8 (**a**–**d**) Effects of reducing apical P_{Na} on water fluxes. Reducing apical entrance permeability of sodium ions ($\tau = 1$ s, text Eq. 25) results in parallel decreases in Na^+ flux and rate of transepithelial water absorption. This response is independent of the pathway taken by water. (**a**) Water absorption is both translateral and transjunctional. (**b**) About similar responses are seen after having reduced apical osmotic permeability. (**c**) In "wild type" with intact osmotic permeability of the apical membrane, the small paracellular water uptake is driven by a relatively small difference in osmolarity between surrounding solutions of 300 mosM and *lis*. (**d**) With the translateral water uptake eliminated, all of the water enters the epithelium through tight junctions, which requires larger osmotic driving force

above showed that a very significant reduction in the number of water channels of the luminal membrane effectively eliminated cellular water fluxes but did not per se reduce the transepithelial absorption of water when studied at transepithelial osmotic equilibrium, where the rate of transepithelial water uptake as found by Solomon's group (Windhager et al. 1959) is being directed by the rate of active Na^+ uptake. Therefore, it might well be that the observed significant reduction in fluid absorption in AQP-1(−/−) mice observed by Schnermann et al. (1998) would have to be ascribed to the authors' concomitantly reported reduction in active Na^+ absorption. For testing this hypothesis, we studied the effect of reducing the rate of Na^+ absorption on transtubular water absorption; see Fig. 8. Wild type and AQP-1 knock-out show similar reduction in rate of fluid uptake in response to reduction in the rate of transepithelial Na^+ uptake, here expressed as volume flow out of *lis*, cf. the time course of J_V^{ibm} in Fig. 8a, b. The transepithelial water flow in Fig. 8b is entirely paracellular so the lack of translateral water uptake is reflected in an increased transjunctional water flux and osmolarity of *lis*, compare Fig. 8d with Fig. 8c.

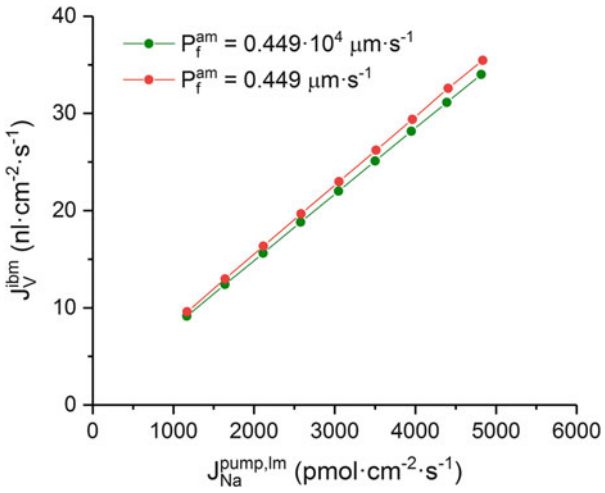

Fig. 9 The fundamental dependence of rate of water absorption on lateral active Na^+ flux. The rate of water absorption is governed by the rate at which Na^+ ions are pumped into the lateral intercellular space independently of the pathway taken by water, mostly translateral (red) or purely transjunctional (green)

The decisive influence on water absorption of the rate of active Na^+ flux across the lateral membrane is well documented by the computed relationships between transepithelial water uptake and the rate of pumping of Na^+ into the lateral space in wild type and apical AQP-1 knock-out, respectively; see Fig. 9.

3.6 Volume Response of the Epithelium to a Luminal Osmotic Pulse

Exposure of the epithelium to a luminal hyperosmotic pulse results in reversible cell shrinkage (Fig. 10a, b). This is similar to rabbit proximal straight tubule, which does not exhibit volume regulatory increase (Kirk et al. 1987). Volume of the lateral intercellular space increases (Fig. 10c), reflecting that the influx of water from cells to *lis* exceeds the efflux of water to luminal bath through tight junctions. The explanation for this is obvious: the osmotic water permeability of apical and lateral plasma membranes is larger than that of tight junctions; there is, therefore, a flow of water from cells to *lis*, which swells. The loss of cell volume is quantitatively reflected in the increase in concentration of nondiffusible anions (Fig. 10d), a principle that was applied by Reuss (1985) for real-time monitoring of volume changes of epithelial cells in studies of cell volume regulation. The transient increase in osmolarity of cells and *lis* follows the external osmotic pulse in such a way that *lis* remains hyperosmotic to cells at all times maintained by lateral Na^+/K^+ pump (Fig. 10e, f).

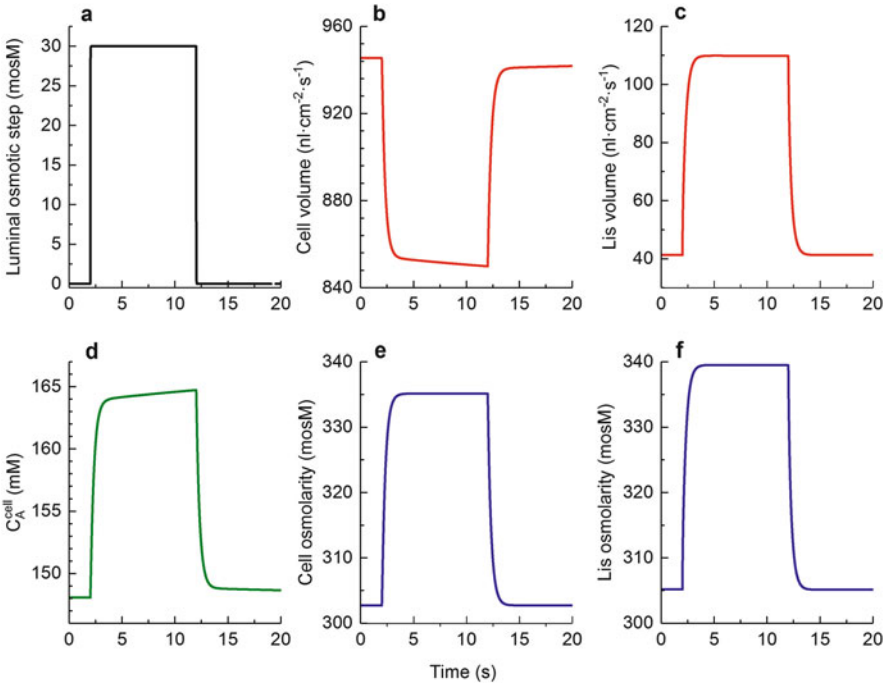

Fig. 10 (**a**–**f**) Time-dependent responses to reversible luminal osmotic step. (**a**) Pulse of 30-mosM of an electroneutral, non-permeable solute applied to outside (luminal) solution. (**b**, **c**) Time course of change in the two intraepithelial water volumes; cell volume decreases, while *lis* volume increases. (**d**) The loss of cell water results in concentration increase in the non-permeable negatively charged intracellular electrolyte with a time course similar to that of change in cell volume. (**e**, **f**) Cell and *lis* osmolarity increase. At all times is osmolarity of *lis* larger than osmolarity of cell

3.7 Uphill Water Transport and Intraepithelial Water Fluxes

In Fig. 11, a non-permeable electroneutral solute is added in steps of 5 mosM to the luminal compartment. The two examples are with and without 5 mM glucose, respectively. In both cases, the relationship between water fluxes emerging from the lateral intercellular space and osmotic driving force is near-linear, displaying x-axis intercepts of −27 and −37 mosM, respectively. Thus, the model reproduces "uphill" water transport as observed in proximal tubule of rat (Green et al. 1991) and mice (Schnermann et al. 1998) and generated by previous models of leaky epithelia (Weinstein and Stephenson 1981; Larsen et al. 2000, 2009). In the literature, an (apparent) osmotic permeability of the epithelium is calculated by:

$$P_f^{epit} = \Delta J_V^{trans} / \left(\Delta \pi^o \cdot \bar{V}_W \right),$$

where $\bar{V}_W = 18.1$ cm^3/mol is the molar volume of water at 310 K. From the slope of linear fits, $P_f^{epit} = 680$ μm s^{-1}. This is significantly smaller than

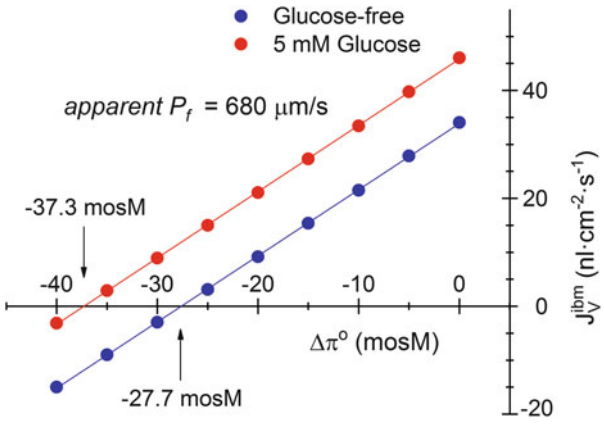

Fig. 11 The model epithelium transports water against an adverse osmotic gradient ("uphill"). A ramp of increasing outside concentration of a non-permeable electroneutral solute, $\Delta\pi^o$, was imposed on the model epithelium. The graph shows computed *steady-state* water fluxes emerging from the lateral intercellular space at each ramp step of 5 mosM. The enhanced water flux following addition of glucose owes to the coupling of Na^+ and glucose in apical SGLT2 which depolarizes the cell membranes. As a result, the Na^+ pumps in the lateral membrane are stimulated ("cross-talk") which directs an enhanced rate of transepithelial water uptake. Full lines are linear fits to computed points. The slope of the linear relationships denoted *apparent* P_f has physical dimension of osmotic permeability. In the literature, it is used as measure of the osmotic permeability of the epithelium. As discussed in the text, its physical significance is ambiguous with no relationship to an osmotic permeability and should be abandoned

the rate-limiting osmotic permeabilities of apical entrance pathways, $P_f^{am} + P_f^{tj} = 4{,}490 + 2{,}500 = 6{,}990$ μm s^{-1}. To explain this discrepancy, we will study non-stationary water fluxes between intraepithelial compartments by model computations, which cannot be studied by experiment. Figure 12 depicts the response of the apical membrane water flux to a 30 mosM pulse applied to luminal compartment. Prior to the pulse, the water flux is 21.3 nL cm^{-2} s^{-1}. The "instantaneous" response is a fast reversal of the water flux to −197 nL cm^{-2} s^{-1}, driven by the imposed osmotic pulse, followed by relaxation toward an inward stationary flux of 35.1 nL cm^{-2} s^{-1} at the end of the pulse. While this inward water flux is energized by ATP hydrolysis at the lateral Na^+/K^+ pumps, the time course of the relaxation depends on the compliance of the lateral plasma membrane; the more resilient the membrane, the longer it takes to achieve the new stationary flux, and for large μ^{lm}, the water flux response is heavily attenuated as compared to the squared shape of the osmotic pulse. The standard compliance constant of the lateral membrane, $\mu^{lm} = 2.5 \times 10^{-3}$ Pa^{-1}, is taken from experiments on Necturus gallbladder (Spring and Hope 1978). As seen, this gives rise to transients of a few seconds duration. At the prevailing sampling rate of 300 Hz, the amplitude of the "instantaneous" response is 21.3 + 197 = 218 nL cm^{-2} s^{-1} corresponding to an apparent osmotic permeability, $P_f^{am} = 4{,}037$ μm s^{-1}. This is significantly larger than the estimate

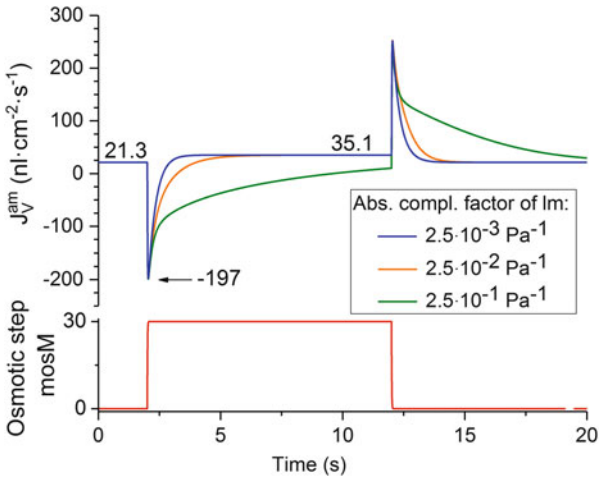

Fig. 12 Dependence of transient states of intraepithelial water fluxes on compliance factors of lateral intercellular membrane. *Bottom panel* applied luminal 10-s pulse of 30 mosM of non-permeable electroneutral solute. Time constant of rise time, $\tau = 0.01$ s, sampling rate = 300 Hz. *Upper panel*, compliance factor-dependent relaxation of water flux redistribution between cells and *lis* with $Vol^{lis} = Vol^{lis,\ ref}[1 + \mu^{lm}(p^{lis} - p^{cell})]$ (Eq. 18). Blue graph is given by standard input variables. Due to the very fast redirection of intraepithelial water fluxes, the peak response at the onset of the pulse of, −197 nL cm^{-2} s^{-1}, is underestimating the apical membrane's water permeability. Thus, the amplitude of the "instantaneous" response is −197–21.3 = ~218 nL cm^{-2} s^{-1} corresponding to an apparent osmotic permeability of apical membrane, $P_f^{am} = 4{,}037$ μm s^{-1}, as compared to the true $P_f^{am} = 4{,}490$ μm s^{-1}

provided by the method of Fig. 11, and much closer to, but not identical with the model's permeability of, $P_f^{am} = 4{,}490$ μm s^{-1}. This is not due to the sampling rate of 300 Hz being too slow (not shown), but because the osmotic permeability of the "network" of epithelial membranes distributes "instantaneously" water fluxes between intraepithelial compartments. This is illustrated in Fig. 13a–d, where the analysis is extended for covering all intraepithelial water fluxes. Quasi-stationary states are achieved for all fluxes within the pulse length of 10 s; the numbers given in the four panels verify consistency of intraepithelial fluxes.

3.8 Isosmotic Transport

The present study shows that a physiological variation of the rate of fluid absorption by proximal tubule of constant osmotic membrane permeabilities results in predictable variation in osmolarity of transported fluid. For example, an osmolarity of transported fluid of 316 mosM becomes 335 mosM when the rate of fluid absorption is increased by adding glucose to the external solutions (Figs. 2 and 4). Decreasing the osmotic permeability of the luminal membrane also increased the hyperosmolarity, e.g., from 316 to 359 mosM (Figs. 6 and 7). In vitro, the proximal

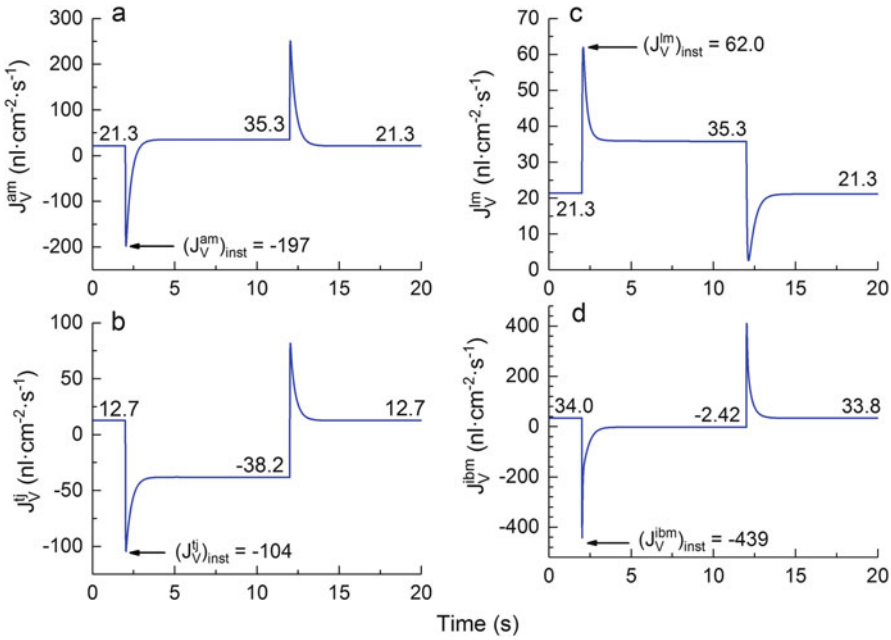

Fig. 13 (**a**–**d**) Response of intraepithelial water fluxes to luminaly applied 30-mosM pulse. The pulse applied is defined in Fig. 10a. (**a**) Water flux across apical membrane; graph is that of Fig. 10 with $\mu^{lm} = 2.5 \times 10^{-3}$ Pa^{-1}. (**b**) Water flux in tight junction is directed toward hyperosmotic luminal bath. In quasi-stationary state, $J_V^{tj} = -38.2$ nL cm^{-2} s^{-1}, illustrating that it is energized by the hyperosmotic pulse. (**c**) Water flux across plasma membrane lining the lateral intercellular space is positive from cell to *lis*. J_V^{lm} added to the tight junction flux (J_V^{tj}) leaves the epithelium across *ibm* to the serosal bath. (**d**) Water flux across the intercellular basement membrane into serosal compartment. The small difference in water fluxes at $t = 0$ s and $t = 20$ s, respectively, reflects that intraepithelial ion and volume redistributions are too slow for bringing the epithelium back to its initial steady state (details not shown)

tubule accomplishes isosmotic transport independent of the presence of glucose in luminal perfusion solution. Thus, the above computations show that our model cannot provide an isosmotic absorbate for a given set of osmotic permeabilities. This is an important finding because it indicates that isosmotic absorption is achieved by regulation at epithelial cell level. In an experimental study designed by Ussing of the mechanism of isosmotic transport by the small intestine, Nedergaard et al. (1999) observed that sodium ions are recirculated from the serosal solution via cells back into the lateral intercellular space, which suggested a mechanism for regulating the osmolarity of the transported fluid. In the small intestine (Larsen et al. 2002) and amphibian skin (Larsen et al. 2009), the recirculation pathway would be the 1Na:2Cl:1K cotransporter studied by Frizzell et al. (1979), Ferreira and Ferreira (1981), and Ussing (1985), respectively. In the heterocellular proximal tubule with absorption of Na^+, Cl^-, and HCO_3^-, one would expect that different segments handle recirculation by different cotransporters depending on whether Cl^- or HCO_3^- are transported together with Na^+. For illustrating the

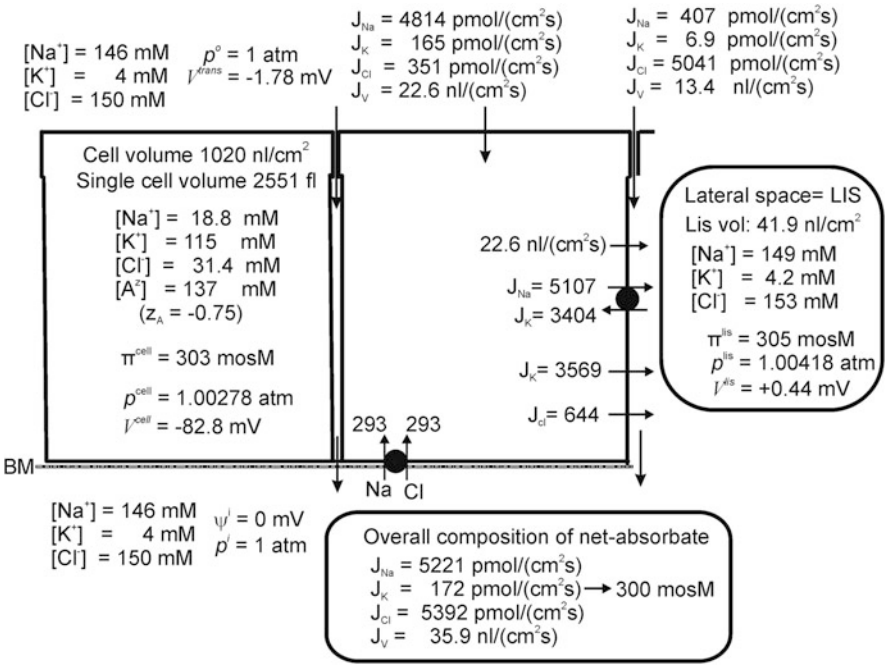

Fig. 14 The Na^+ recirculation theory applied to the kidney proximal tubule. Model solution illustrating how truly isosmotic transport is achieved by recirculating Na^+ and Cl^- from the serosal compartment back into the lateral intercellular coupling compartment energized by lateral $3Na^+/2K^+$-pumps. Independent variables of all membrane pathways are similar to those used in computations of Fig. 2 in which the serosal 1Na:1Cl cotransporter is quiescent. Turning on regulated 1Na:1Cl cotransport corrected the hyperosmotic absorbate emerging from the lateral space to an overall osmolarity of the absorbate of 300 mosM. It should be noted that the 1Na:1Cl cotransporter is considered here just for the purpose of illustration

significance of regulated ion recirculation in the minimalistic model of the proximal tubule, we introduced a 1Na:1Cl cotransporter of the serosal membrane and adjusted the fluxes carried by this transporter until an overall isosmotic fluid transport was achieved. The result is shown in Fig. 14. It can be seen that a recirculation of $J^{sm}_{NaCl} = -293$ pmol cm^{-2} s^{-1} results in truly isosmotic transport of 300 mosM; this is associated with an increase of C^{cell}_{Na} from 16.2 to 18.8 mM and an increase of C^{cell}_{Cl} from 21.8 to 31.4 mM. The concomitant increase in active Na^+ pump flux from 4,816 to 5,107 pmol cm^{-2} s^{-1} indicates that the extra metabolic load of generating truly isosmotic transport would be modest, 100 (5,107 − 4,816)/4,816 = 6.0%, compared to the results of Fig. 2 obtained with no recirculation.

4 Discussion

Our previously published analytical model of transporting epithelia (Larsen et al. 2002) is here extended for analyzing transient states evoked by perturbing independent variables for simulating commonly applied experimental protocols. This has allowed us to deal with time-dependent dynamic interactions of ion and water fluxes through the epithelium and, for the first time, between subepithelial compartments. The updated model also contains equations for the Na^+/K^+ pump and the Na^+-glucose transporter (SGLT2) with new equations for these transport systems' contribution to the electrical conductance of the plasma membranes. The model was shown to be quite sufficient for giving answers to a number of pertinent problems in kidney physiology that presupposes quantitative biophysical analysis. The check on these points was provided by comparing published experimental observations with predictions given by the model.

4.1 The Coupling Between Active Sodium Transport and Fluid Uptake

The model reproduces a large number of observations based on a physiologically plausible set of input variables such as intracellular ion composition, membrane potentials and resistances, cell volumes, and transepithelial fluxes of water and ions all in agreement with proximal convoluted tubule in situ and microperfused tubule segments (Figs. 2 and 4). Ion composition, hydrostatic pressure, and volume of the lateral intercellular space, inaccessible to measurements in a transporting epithelium, are obtained at any physiological condition. The convection-electrodiffusion equation for tight junction transport provides basis for discussion of leak fluxes associated the reabsorption of the major fraction of the ultrafiltrate. Interestingly, based upon the convection-electrodiffusion equation (Eq. 6), calculations shown in Figs. 4 and 6 and in Table 1 predict as a novel result that passive back leaks would be prevented by solvent drag in tight junctions in the initial segment of proximal tubule, where the electrochemical driving force otherwise would return a component of the Na^+ flux to the tubule lumen.

This seems to be a suitable point at which to emphasize that absorption by proximal tubule of K^+ requires active uptake mechanism, here given by Eq. (2a), because paracellular solvent drag turned out to be quite insufficient, see Sect. 3.1, underscoring the importance of the experimental study by Wilson et al. (1997). By choosing appropriate value of the intrinsic parameter, $K^{NaK2Cl,\ am}$ of Eq. (2a) we could direct the overall transepithelial K^+ absorption so that the potassium ion concentration of the absorbate becoming close to that of the interstitial fluid. [Results of such a use of the model are independent of the molecular mechanism of active K^+ uptake]. Thus, governed by the same value of $K^{NaK2Cl,\ am}$ in Figs. 2 and 4, the K^+ concentration of the absorbate calculates to be 5.2 and 4.1 mM, respectively. With a

fluid absorption rate of 120 l/day by proximal tubule of human kidney the extracellular K^+ concentration could possibly not be maintained within physiological values unless the $[K^+]$ of the absorbate is regulated at epithelial cell level to be within a range not much different from the physiological range stated to be between 3.8 and 5.0 mM (Hall 2016). By emphasizing the necessity of active K^+ absorption by proximal tubule and the significance of achieving a $[K^+]$ of the absorbate that is not much different from that of the serosal fluid our analysis has pointed out two important questions for future studies: (1) identification of the molecular mechanism of active transport across the apical membrane, and (2) disclosure of the nature of coordination of the *rate* of fluid absorption and the *flux* of K^+ absorption, respectively, for securing near-extracellular $[K^+]$ of the absorbate.

The model predicts the well-established stimulation of Na^+- and fluid absorption by glucose (Figs. 4 and 5). Of particular interest, the new kinetics- and conductance-equations for SGLT2 (Eqs. 3a, 3c) predict the membrane depolarization and decrease in apical membrane resistance caused by glucose absorption, as observed in a microelectrode study by Frömter (1982). With reference to Fig. 4, computed for 5 mM external glucose, the reversal potential of the SGLT2 transporter is given by the expression (cf. Methods),

$$
\begin{aligned}
E_{rev}^{Glu\cdot Na,am} &= \frac{RT}{F}\ln\frac{C_{Glu}^{o}\cdot C_{Na^+}^{o}}{C_{Glu}^{cell}\cdot C_{Na^+}^{cell}} \\
&= 10^3\times\frac{8.31\cdot 310}{96485}\ln\frac{5\cdot 146}{11.8\cdot 28.2} \\
&= 21.0\ \text{mV}
\end{aligned}
$$

This is 100 mV above the membrane potential of −79 mV indicating that our conclusion of glucose absorption by the reversible SGLT2 is robust. It is a new and physiologically significant finding of our study that the voltage dependence of the active Na^+ flux (Eq. 4a) predicts an overlooked "cross-talk" mechanism between apical rheogenic Na^+ uptake and active Na^+/K^+ pump fluxes across the lateral membrane. The physiological implication of this mechanism is indicated by the secondary effect on rate of fluid uptake and a higher osmolarity of the fluid exiting the epithelium via the lateral intercellular space (Fig. 4).

4.2 *Eliminating the Osmotic Permeability of Apical Membrane*

An intriguing result was obtained when a simulation of aquaporin knock-out showed that water uptake at transepithelial osmotic equilibrium is not significantly changed after elimination of the osmotic permeability of the apical membrane: $J_V = 34.0$ nL cm^{-2} s^{-1} for $P_f^{am} = 4{,}490$ μm s^{-1} and $J_V = 35.4$ nL cm^{-2} s^{-1} for

$P_f^{am} = 0.449\ \mu m\ s^{-1}$, respectively (Figs. 2 and 6). This maneuver effectively blocked the translateral water flux and forced the water absorption to be entirely paracellular (Fig. 6). This response was analyzed in detail by following the development of nonstationary states toward the new steady state. By predicting an increase in the osmolarity of the lateral intercellular space, the analysis provided the biophysical mechanism for the large increase in osmolarity of the absorbate (Fig. 7). The experimental study by Schnermann et al. (1998) showed that AQP-1-null mice exhibited a tubular fluid absorption that is 50% of that of AQP-1(+/+) mice. In our analysis of this finding, we showed that the rate of fluid absorption is given by the rate at which sodium ions are pumped into the lateral intercellular space, independent of the pathway taken by water (Figs. 8 and 9). Therefore, we can conclude that the observed significant decrease in rate of fluid absorption in AQP-1(−/−) mice has to be ascribed solely to the authors' concomitantly reported reduction in active Na^+ absorption. The computed relationship between transepithelial water uptake and active flux of sodium ions (Fig. 9) is a general and fundamental feature of fluid transporting epithelia.

The general applicability of the present study is underscored by pointing out that our analysis eliminates the paradox discussed by Wittekindt and Dietl (2019) that aquaporins in the lung facilitate osmotic water transport, whereas their contribution to water fluxes at near-isosmotic conditions was concluded "elusive." Our analysis of this problem leads to the conclusion that also in the lung are aquaporins of physiological importance for isosmotic transport with the rate of water transport given by the active sodium flux, that is, not by expression of aquaporins. This applies to AQP-1(−/−) engineered lung epithelia as well where the water flow is redirected to the paracellular pathway at a rate given by the active Na^+ flux (conf. Figs. 2 and 6).

4.3 Transepithelial Osmotic Permeability Versus Osmotic Permeability of Individual Membranes

The substantial discrepancy between the osmotic permeability of the epithelium obtained by transepithelial osmotic step experiments and the significantly larger experimentally estimated osmotic permeabilities of individual plasma membranes (Carpi-Medina et al. 1984; Gonzáles et al. 1984; Schafer et al. 1978) was characterized by Weinstein (2013) as "one of the confusing features" of epithelia specialized for isosmotic transport. Our analysis provided the mechanistic explanation for this "confusing feature" by revealing how lateral Na^+/K^+ pumps on a time scale of about 1 s energize redistribution of water flows between intraepithelial compartments that in the end results in relatively small changes in transepithelial water fluxes and uphill water transport across the epithelium (Figs. 11, 12 and 13). This result illustrates the advantage of our dynamic model over and above the steady-state model of Weinstein (2013) which requires a hypotonic luminal space for generating an absorbed fluid that is "isosmotic to plasma." Our computational analytical method providing time-dependent states of physical variables enabled us to study the time course of

intraepithelial water redistributions that result from an imposed external osmotic pulse. Obviously, a "transepithelial osmotic permeability" calculated from this type of experimental protocol is inadequate for functional characterization of the transporting epithelium (Figs. 9 and 12). Furthermore, the result of our analysis shows that Weinstein's concept of "intraepithelial solute polarization" cannot be ascribed physical significance. In conclusion, it is a result of significant physiological implications that the osmotic permeability of the whole epithelium P_f^{epit} has ambiguous biophysical meaning and should be abandoned in studies of water fluxes across intact epithelia.

4.4 Truly Isosmotic Transport

In the standing gradient theory of isosmotic transport by Diamond and Bossert (1967), sodium pumps are located in the closed apical end of the lateral intercellular space. It was hypothesized that for a particular set of independent variables such as active pumping rate, diffusion coefficients in *lis* of unstirred fluid, and physical dimensions of the space, this model would have capacity to generate isosmotic transport. The theory directed fresh approaches to the problem of solute-coupled fluid transport and broadened the field by including epithelia of a larger number of animal species adapted to a variety of habitats as reviewed in Berridge and Oschmann (1972). The theory is now abandoned because pumps are uniformly distributed in the lateral membrane or concentrated near the basal end, tight junctions are permeable to both ions and water, and the lateral space cannot be assumed unstirred. Importantly, however, Diamond and Bossert's theoretical approach gave rise to a clear formulation of the fundamental problem of isosmotic transport. In the authors' own words (loc. cit. page 2077), "two forces are responsible for carrying solute out the open mouth of the system: the diffusion of solute down its concentration gradient, and the sweeping effect of water flow upon solute. Any factor that increases the relative importance of diffusion will make the emergent fluid more hypertonic, while factors increasing the relative importance of water flow are associated with a more nearly isotonic emergent fluid."

Mathematical models of today are significantly different from the Diamond and Bossert model; the fluid of the lateral intercellular space is assumed well stirred, tight junctions are ion- and water permeable, a basement membrane is separating lis and serosal compartment, and hydrostatic pressures and membrane potentials constitute driving forces for water and ion flows. Furthermore, in our treatment of convection-electrodiffusion at the interfaces limiting the lateral intercellular space from outside and inside compartments, respectively, we introduced an expanded version of Hertz' equation (Larsen et al. 2002). Nevertheless, in general terms, our computations underscored the above conclusion of the Diamond-Bossert paper.

A study applying the pre-steady-state theorem (Sten-Knudsen and Ussing 1981) for separating paracellular and transcellular radioactive Na^+ fluxes in small intestine

indicated recirculation of sodium ions from serosal solution bath back into lateral space via the transporting epithelial cells (Nedergaard et al. 1999). Our subsequent theoretical analysis (Larsen et al. 2002) indicated that the fairly large recirculation fluxes of the above study follow logically from the relatively small osmotic permeability of small intestine. The present study indicates that in the highly water permeable proximal tubule the putative Na^+ recirculation flux necessary for isosmotic transport would be small and probably too small for being measured. This prediction focuses future research on the precise nature and operation of the serosal Na^+ cotransporters that may mediate Na^+ recirculation in the different segments of proximal tubule.

5 Additional Information

Competing Interests
None declared.

Author Contributions
EHL contributed to the conception of the work. JNS developed the FORTRAN program including the numerical methods. EHL provided mathematical equations, performed most of the computations, and wrote the first draft of the manuscript that was further edited by both authors. Both authors have approved the final version of the manuscript and agree to be accountable for all aspects of the work and qualify for authorship. No one else qualify for authorship.

Funding
This work was supported by grant CF17-0186 from the Carlsberg Foundation.

Appendix 1: Nomenclature

See also overview in Fig. 1b.

Variables or constants and their definition	Symbol
Concentration of j (Na^+, K^+, Cl^-, A^-, or *glucose*) in compartment *comp* (*o*, *cell*, *lis*, or *i*)	C_j^{comp}
Osmolarity of compartment indicated by superscript (*o*, *cell*, *lis*, or *i*)	π^{comp}
Hydrostatic pressure of compartment indicated (*o*, *cell*, *lis*, or *i*)	p^{comp}
Electrical potential of compartment indicated (*o*, *cell*, *lis*, or *i*) with $\psi^i \equiv 0$	ψ^{comp}
Transepithelial potential difference, $\psi^o - \psi^i$	V^{trans}
Electrical potential difference between *o* and *cell*, $\psi^o - \psi^{cell}$	V^{am}
Electrical potential difference between *cell* and *lis*, $\psi^{cell} - \psi^{lis}$	V^{lm}
Electrical potential difference between *cell* and *i*, $\psi^{cell} - \psi^i$	V^{sm}

(continued)

Variables or constants and their definition	Symbol
Passive permeability of *j* in membrane *m* (*am*, *lm*, *sm*, *tj*, *ibm*)	P_j^m
Reflection coefficient of *j* (Na^+, K^+, Cl^-, glucose) in *m* (*tj*, *ibm)*	σ_j^m
Flux of *j* (= Na^+, K^+, Cl^-, glucose) across *m* (*am*, *lm*, *sm*, *tj*, *ibm*)	J_j^m
Electrical current carried by *j* (Na^+, K^+, Cl^-) across *m* (*am*, *lm*, *sm*, *tj*, *ibm*)	I_j^m
Integral ion (*j*) conductance of membrane *m*	G_j^m
Water volume flux across *m* (*am*, *lm*, *sm*, *tj*, *ibm*)	J_V^m
Hydraulic conductance of membrane *m* (*am*, *lm*, *sm*, *tj*, *ibm*)	L^m
Osmotic permeability of *m* (*am*, *lm*, *sm*, *tj*, *ibm*)	P_f^m
Relative compliance constant of membrane *m* (*am*, *lm*, *sm*)	μ^m
Absolute compliance constant of *lm*	$\overline{\mu}^{lm}$
Empirical constant of 1Na:1K:2Cl cotransporter of membrane *m*	$K^{NaK2Cl,\ m}$
Empirical constant of 1Na:1Cl cotransporter of membrane *m*	$K^{NaCl,\ m}$
Apparent dissociation constants of Na^+ binding of Na^+/K^+ pump at *lm*	$K_{Na^+}^{pump,lm}$
Apparent dissociation constants of K^+ binding of Na^+/K^+ pump at *lm*	$K_{K^+}^{pump,lm}$
Turnover constant of Na^+:glucose transporter at *am*	$P^{Glu\cdot Na^+}$
Empirical apparent dissociation constant of Na^+:glucose transporter at *am*	$K_{Glu}^{Glu\cdot Na}$
Empirical apparent dissociation constant for glucose of Na^+:glucose transporter at *am*	$K_{Na^+}^{Glu\cdot Na}$
Maximum turnover of glucose exchanger at *lm*	$J_{Glu}^{\max,lm}$
App dissociation const. of symmetrical carrier at *lm*	K_{Glu}^{lm}
Turnover constant of Na^+:glucose transporter at *am*	$P^{Glu\cdot Na^+}$
Temperature in K	T
Faraday	F
Universal gas constant	R

Appendix 2: Independent Variables

Name	Symbol	Value	MKSA unit
Hydraulic conductance of *am*	L^{am}	3.1370d−11	$m^3\ s^{-1}\ N^{-1}$
Hydraulic conductance of *sm*	L^{sm}	3.5000d−14	$m^3\ s^{-1}\ N^{-1}$
Hydraulic conductance of *lm*	L^{lm}	3.4980d−11	$m^3\ s^{-1}\ N^{-1}$
Hydraulic conductance of *tj*	L^{tj}	3.1370d−11	$m^3\ s^{-1}\ N^{-1}$
Hydraulic conductance of *ibm*	L^{ibm}	2.3100d−07	$m^3\ s^{-1}\ N^{-1}$
Na^+ concentration of outside compartment	C_{Na}^o	146	mol m^{-3}
K^+ concentration of outside compartment	C_K^o	4	mol m^{-3}
Cl^- concentration of outside compartment	C_{Cl}^o	150	mol m^{-3}
Concentration of non-diffusible solute of outside compartment	C_S^o	Protocol dependent	mol m^{-3}
Glucose concentration of outside compartment	C_{glu}^o	0, 3 or 5	mol m^{-3}

(continued)

Name	Symbol	Value	MKSA unit
Na^+ concentration of inside compartment	C^i_{Na}	146	mol m^{-3}
K^+ concentration of inside compartment	C^i_K	4	mol m^{-3}
Cl^- concentration of inside compartment	C^i_{Cl}	150	mol m^{-3}
Concentration of non-diffusible solute of inside comp.	C^i_S	0	mol m^{-3}
Glucose concentration of inside compartment	C^i_{glu}	0, 3, or 5	mol m^{-3}
Na^+ GHK permeability of *am*	P^{am}_{Na}	0.100d−6	m s^{-1}
K^+ GHK permeability of *am*	P^{am}_K	0.274d−12	m s^{-1}
Cl^- GHK permeability of *am*	P^{am}_{Cl}	0.160d−11	m s^{-1}
Na^+ GHK permeability of *sm*	P^{sm}_{Na}	0.100d−11	m s^{-1}
K^+ GHK permeability of *sm*	P^{sm}_K	0.100d−11	m s^{-1}
Cl^- GHK permeability of *sm*	P^{sm}_{Cl}	0.100d−11	m s^{-1}
Na^+ GHK permeability of *lm*	P^{lm}_{Na}	0.300d−12	m s^{-1}
K^+ GHK permeability of *lm*	P^{lm}_K	0.120d−6	m s^{-1}
Cl^- GHK permeability of *lm*	P^{lm}_{Cl}	0.800d−7	m s^{-1}
Na^+ GHK permeability of *tj*	P^{tj}_{Na}	0.125d−6	m s^{-1}
K^+ GHK permeability of *tj*	P^{tj}_K	0.180d−6	m s^{-1}
Cl^- GHK permeability of *tj*	P^{tj}_{Cl}	0.400d−5	m s^{-1}
Glucose permeability of *tj*	P^{ibm}_{glu}	0.950d−8	m s^{-1}
Na^+ GHK permeability of *ibm*	P^{ibm}_{Na}	0.750d−6	m s^{-1}
K^+ GHK permeability of *ibm*	P^{ibm}_K	0.110d−5	m s^{-1}
Cl^- GHK permeability of *ibm*	P^{ibm}_{Cl}	0.159d−4	m s^{-1}
Glucose permeability if *ibm*	P^{ibm}_{glu}	0.350d−5	m s^{-1}
1Na:1 K:2Cl co-transporter constant of *am*	$K^{NaK2Cl,\ am}$	0.150d−12	m^{10} s^{-1} mol^{-3}
1Na:1Cl co-transporter constant of *am*	$K^{NaCl,\ am}$	0.100d−10	m^4 s^{-1} mol^{-1}
Turnover constant of lateral $3Na^+/2K^+$ pump	$P^{pump,lm}_{Na^+,K^+}$	0.100d−2	mol s^{-1} m^{-2}
Electromotive force of the $3Na^+/2K^+$ pump	E^{pump}	0.2	Volt
Apparent dissociation constants of Na^+ binding	$K^{pump,lm}_{Na^+}$	3.40d0	mol m^{-3}
Apparent dissociation constants of K^+ binding	$K^{pump,lm}_{K^+}$	0.75d0	mol m^{-3}
Turnover constant of Na^+:glucose transporter of *am*	$P^{Glu\cdot Na^+}$	1.6d−8	mol s^{-1} m^{-2}
Apparent dissociation constant for Na^+	$K^{Glu\cdot Na}_{Glu}$	5.d0	mol m^{-3}
Apparent dissociation constant for glucose	$K^{Glu\cdot Na}_{Na^+}$	0.25d2	mol m^{-3}
Maximum turnover of glucose exchanger at *lm*	$J^{\max,lm}_{Glu}$	2.0d−4	mol s^{-1} m^{-2}
App dissociation const. of symmetry. carrier at *lm*	K^{lm}_{Glu}	5.0d1	mol m^{-3}
Hydrostatic pressure of outside compartment	p^o	1.01325e5	Pa

(continued)

Name	Symbol	Value	MKSA unit
Hydrostatic pressure of inside compartment	p^i	1.01325e5	Pa
Electrical potential of inside compartment	ψ^i	0	Volt
Mean valence of nondiffusible intracellular anions	z_A	−0.75	
Na^+ reflection coefficient of *tj*	σ_{Na}^{tj}	0.70	
K^+ reflection coefficient of *tj*	σ_{K}^{tj}	0.70	
Cl^- reflection coefficient of *tj*	σ_{Cl}^{tj}	0.45	
Glucose reflection coefficient of *tj*	σ_{Glu}^{tj}	0.80	
Na^+ reflection coefficient of *ibm*	σ_{Na}^{ibm}	0.03	
K^+ reflection coefficient of *ibm*	σ_{K}^{ibm}	0.03	
Cl^- reflection coefficient of *ibm*	σ_{Cl}^{ibm}	0.03	
Glucose reflection coefficient of *ibm*	σ_{Glu}^{ibm}	0.03	
Temperature	T	310	K
Faraday	F	96,485	C mol^{-1}
Absolute compliance constant of *lm*	μ^{lm}	0.250d−2	Pa^{-1}
Reference volume of *lis*	$Vol^{lis,ref}$	3.10d−7	$m^3\ m^{-2}$
Cell density	D^{cell}	4.00d+9	# cells m^{-2}
Nondiffusible anions in cell	M_A	3.50d−13	mol $cell^{-1}$

o outside (luminal) compartment, *i* inside (serosal) compartment, *am* apical membrane, *lm* lateral membrane, *sm* serosal membrane, *lm* lateral membrane, *tj* tight junctions, *ibm* interspace basement membrane

References

Agre P, Christensen EI, Smith BL, Nielsen S (1993a) Distribution of the aquaporin CHIP in secretory and resorptive epithelia and capillary endothelia. Proc Natl Acad Sci U S A 90: 7275–7279

Agre P, Knepper MA, Christensen EI, Smith BL, Nielsen S (1993b) CHIP28 water channels are localized in constitutively water-permeable segments of the nephron. J Cell Biol 120:371–383

Altenberg GA, Reuss L (2013) Mechanisms of water transport across cell membranes and epithelia. In: Alpern RJ, Caplan M, Moe OW (eds) Seldin and Giebisch's the kidney. Physiology and pathophysiology. Elsevier/Academic Press, London, pp 95–120

Amerongen HM, Mack JA, Wilson JM, Neutra MR (1989) Membrane domains of intestinal epithelial-cells – distribution of Na^+,K^+-ATPase and the membrane skeleton in adult-rat intestine during fetal development and after epithelial isolation. J Cell Biol 109:2129–2138

Andreoli TE, Schafer JA (1979) External solution driving forces for isotonic fluid absorption in proximal tubules. Fed Proc 38:154–160

Bennett CM, Clapp JR, Berliner RW (1967) Micropuncture study of proximal and distal tubule in dog. Am J Physiol 213:1254

Berridge MJ, Oschmann JL (1972) Transporting epithelia. Academic Press, New York/London, pp 1–91

Borgnia M, Nielsen S, Engel A, Agre P (1999) Cellular and molecular biology of the aquaporin water channels. Annu Rev Biochem 68:425–458

Boron WF, Boulpaep EL (1983a) Intracellular pH regulation in the renal proximal tubule of the salamander. Basolateral HCO_3^- transport. J Gen Physiol 81:53–94

Boron WF, Boulpaep EL (1983b) Intracellular pH regulation in the renal proximal tubule of the salamander. Na-H exchange. J Gen Physiol 81:29–52
Boron WF, Boulpaep EL (2017) Medical physiology, 3rd edn. Elsevier, Philadelphia
Burg M, Patlak C, Green N, Villey D (1976) Organic solutes in fluid absorption by renal proximal convoluted tubules. Am J Physiol 231:627–637
Carpi-Medina P, Whittembury G (1988) Comparison of transcellular and transepithelial water osmotic permeabilities (P_{os}) in the isolated proximal straight tubule (PST) of the rabbit kidney. Pflugers Arch 412:66–74
Carpi-Medina P, Gonzáles E, Whittembury G (1983) Cell osmotic water permeability of isolated rabbit proximal convoluted tubules. Am J Physiol 244:F554–F563
Carpi-Medina P, Lindemann B, Gonzáles E, Whittembury G (1984) The continuous measurement of tubular volume changes in response to step changes in contraluminal osmolarity. Pflugers Arch 400:343–348
Cassola AC, Mollenhauer M, Frömter E (1983) The intracellular chloride activity of rat kidney proximal tubular cells. Pflugers Arch 399:259–265
Curran PF (1960) Na, Cl, and water transport by rat ileum *in vitro*. J Gen Physiol 43:1137–1148
De Weer P, Gadsby DC, Rakowski RF (1988) Voltage dependence of the Na-K pump. Annu Rev Physiol 50:225–241
Diamond JM (1964) Transport of salt and water in rabbit and guinea pig gallbladder. J Gen Physiol 48:1–14
Diamond JM, Bossert WH (1967) Standing-gradient osmotic flow. A mechanism for coupling of water and solute transport in epithelia. J Gen Physiol 50:2061–2083
DiBona DR, Mills JW (1979) Distribution of Na^+ −pump sites in transporting epithelia. Fed Proc 38:134–143
Dørup J, Maunsbach AB (1997) Three-dimensional organization and segmental ultrastructure of the rat proximal tubules. Exp Nephrol 5:305–317
Edelman A, Curci S, Samarzija I, Fromter E (1978) Determination of intracellular K^+ activity in rat-kidney proximal tubular cells. Pflugers Arch 378(1):37–45
Eskesen K, Ussing HH (1985) Determination of the electromotive force of active sodium transport in frog skin epithelium (*Rana temporaria*) from presteady-state flux ratio experiments. J Membr Biol 86:105–111
Ferreira KTG, Ferreira HG (1981) The regulation of volume and ion composition in frog skin. Biochim Biophys Acta 646:193–202
Finkelstein A (1987) Water movement through lipid bilayer, pores, and plasma membranes. Theory and reality. Wiley, New York/Chisester/Brisbane/Toronto/Singapore, pp 1–228
Fischbarg J (2010) Fluid transport across leaky epithelia: central role of the tight junction and supporting role of aquaporins. Physiol Rev 90:1271–1290
Frizzell RA, Field M, Schultz SG (1979) Sodium-coupled chloride transport by epithelial tissues. Am J Physiol 236:F1–F8
Fromm M, Piontek J, Rosenthal R, Gunzel D, Krug SM (2017) Tight junctions of the proximal tubule and their channel proteins. Pflugers Arch 469:877–887
Frömter E (1979) The Feldberg lecture 176: solute transport across epithelia: what can we learn from micropuncture studies on kidney tubules? J Physiol 288:1–31
Frömter E (1982) Electrophysiological analysis of rat renal sugar and amino acid transport. I. Basic phenomena. Pflugers Arch 393:179–189
Gadsby DC, Nakao M (1989) Steady-state current-voltage relationship of the Na/K pump in guinea-pig ventricular myocytes. J Gen Physiol 94:511–537
Gaeggeler HP, Guillod Y, Loffing-Cueni D, Loffing J, Rossier BC (2011) Vasopressin-dependent coupling between sodium transport and water flow in a mouse cortical collecting duct cell line. Kidney Int 79:843–852
Garay RP, Garrahan PJ (1973) The interaction of sodium and potassium with the sodium pump in red cells. J Physiol 231:297–325
Garg LC, Knepper MA, Burg MB (1981) Mineralocorticoid effects on Na-K-ATPase in individual nephron segments. Am J Physiol 240:F536–F544

Ghezzi C, Loo DDF, Wright EM (2018) Physiology of renal glucose handling via SGLT1, SGLT2 and GLUT2. Diabetologia 61:2087–2097

Gögelein H, Greger R (1986) Na^+ selective channels in the apical membrane of rabbit late proximal tubules (pars recta). Pflugers Arch 406:198–203

Goldin SM (1977) Active transport of sodium and potassium ions by the sodium and potassium ion-activated adenosine triphosphatase from renal medulla. Reconstitution of the purified enzyme into a well defined in vitro transport system. J Biol Chem 252:5630–5642

Goldman DE (1943) Potential, impedance, and rectification in membranes. J Gen Physiol 27:37–60

Gonzáles E, Carpi-Medina P, Linares H, Whittembury G (1984) Osmotic water permeability of the apical membrane of proximal straight tubular (PST) cells. Pflugers Arch 402:337–339

Gottschalk CW (1963) Renal tubular function – lessons from micropuncture. Harvey Lect 58: 99–124

Green R, Giebisch G, Unwin R, Weinstein AM (1991) Coupled water transport by rat proximal tubule. Am J Physiol 261:F1046–F1054

Gyory AZ, Kinne R (1971) Energy source for transepithelial sodium transport in rat renal proximal tubules. Pflugers Arch 327:234–260

Hall JE (2016) Guyton and Hall textbook of medical physiology. Philadelphia, PA, Elsevier

Hertz G (1922) Ein neues Verfahren zur Trennung von Gasgemischen durch Diffusion. Phys Z 23:433–434

Hodgkin AL (1958) The Croonian lecture: ionic movements and electrical activity in giant nerve fibres. Proc R Soc Lond B Biol Sci 148:1–37

Hodgkin AL, Katz B (1949) The effect of sodium ions on the electrical activity of the giant axon of the squid. J Physiol 108:37–77

Hodgkin AL, Keynes RD (1955) Active transport of cations in giant axons from Sepia and Loligo. J Physiol 128:28–66

Hummel CS, Lu C, Loo DD, Hirayama BA, Voss AA, Wright EM (2011) Glucose transport by human renal Na^+/D-glucose cotransporters SGLT1 and SGLT2. Am J Physiol 300:C14–C21

Jørgensen PL (1980) Sodium and potassium ion pump in kidney tubules. Physiol Rev 60:864–917

Jørgensen PL (1986) Structure, function and regulation of Na,K-ATPase in the kidney. Kidney Int 29:10–20

Karniski LP, Aronson PS (1987) Anion-exchange pathways for Cl^- transport in rabbit renal microvillus membranes. Am J Physiol 253:F513–F521

Kashgarian M, Biemesderfer D, Caplan M, Forbush B III (1985) Monoclonal antibody to Na, K-ATPase: immunocytochemical localization along nephron segments. Kidney Int 28:899–913

Kirk KL, Schafer JA, DiBona DR (1987) Cell volume regulation in rabbit proximal straight tubule perfused in vitro. Am J Physiol 252:F922–F932

Kokko JP, Burg MB, Orloff J (1971) Characteristics of NaCl and water transport in renal proximal tubule. J Clin Investig 50:69

Lapointe JY, Duplain M (1991) Regulation of basolateral membrane potential after stimulation of Na^+ transport in proximal tubules. J Membr Biol 120:165–172

Larsen EH (1973) Effect of amiloride, cyanide and ouabain on the active transport pathway in toad skin. In: Transport Mechanisms in Epithelia, Proc Alfred Benzon Symp, vol V. Munksgaard, Copenhagen, pp 131–147

Larsen EH (1991) Chloride transport by high-resistance heterocellular epithelia. Physiol Rev 71: 235–283

Larsen EH (2011) Reconciling the Krogh and Ussing interpretations of epithelial chloride transport – presenting a novel hypothesis for the physiological significance of the passive cellular chloride uptake. Acta Physiol 202:435–464

Larsen EH, Sørensen JB, Sørensen JN (2000) A mathematical model of solute coupled water transport in toad intestine incorporating recirculation of the actively transported solute. J Gen Physiol 116:101–124

Larsen EH, Sørensen JB, Sørensen JN (2002) Analysis of the sodium recirculation theory of solute-coupled water transport in small intestine. J Physiol 542:33–50

Larsen EH, Willumsen NJ, Møbjerg N, Sørensen JN (2009) The lateral intercellular space as osmotic coupling compartment in isotonic transport. Acta Physiol 195:171–186

Läuger P (1991) Electrogenic ion pumps. Sinauer Associates, Sunderland, pp 1–313
Layton AT, Vallon V, Edwards A (2015) Modeling oxygen consumption in the proximal tubule: effects of NHE and SGLT2 inhibition. Am J Physiol 308:F1343–F1357
Lew VL, Ferreira HG, Moura T (1979) The behavior of transporting epithelial cells. I. Computer analysis of a basic model. Proc R Soc Lond B Biol Sci 206:53–83
Maunsbach AB (1966) Observations on the segmentation of the proximal tubule in the rat kidney. Comparison of results from phase contrast, fluorescence and electron microscopy. J Ultrastruct Res 16:239–258
Maunsbach AB (1973) Ultrastructure of the proximal tubule. In: Orloff J, Berliner RW (eds) Handbook of physiology. American Physiological Society, Washington, DC, pp 31–79
Maunsbach AB, Boulpaep EL (1991) Immunoelectron microscope localization of Na,K-ATPase in transport pathways in proximal tubule epithelium. Micron Microsc Acta 22:55–56
Mills JW, DiBona DR (1977) On the distribution of Na^+-pump sites in the frog skin. J Cell Biol 75: 968–973
Mills JW, DiBona DR (1978) Distribution of Na^+-pump sites in the frog gallbladder. Nature 271: 273–275
Mills JW, Ernst SA, DiBona DR (1977) Localization of Na^+-pump sites in frog skin. J Cell Biol 73: 88–110
Morel F, Murayama Y (1970) Simultaneous measurement of undirectional and net sodium fluxes in microperfused rat proximal tubules. Pflügers Arch 320:1–23
Murer H, Hopfer U, Kinne R (1976) Sodium/proton antiport in brush-border-membrane vesicles isolated from rat small intestine and kidney. Biochem J 154:597–604
Nagel W (1980) Rheogenic sodium transport in a tight epithelium, the amphibian skin. J Physiol 302:281–295
Nedergaard S, Larsen EH, Ussing HH (1999) Sodium recirculation and isotonic transport in toad small intestine. J Membr Biol 168:241–251
Nielsen R, Larsen EH (2007) Beta-adrenergic activation of solute coupled water uptake by toad skin epithelium results in near-isosmotic transport. Comp Biochem Physiol A Mol Integr Physiol 148A:64–71
Nielsen S, Kishore BK, Chou C-L, Mandon B, Marples D, Ecelbarger A, Terris J, Wade JB, Knepper MA (1996) Renal aquaporins. Kidney Int 49:1712–1717
Padilla-Benavides T, Roldán ML, Larre I, Flores-Benitez D, Villegas-Sepúlveda N, Contreras RG, Cereijido M, Shoshani L (2010) The polarized distribution of Na^+,K^+-ATPase: role of the interaction between β subunits. Mol Biol Cell 21(13):2217–2225
Parent L, Supplisson S, Loo DDF, Wright EM (1992) Electrogenic properties of the cloned Na^+/glucose cotransporter: I. Voltage-clamp studies. J Membr Biol 125:49–62
Parsons DS, Wingate DL (1958) Fluid movements across the wall of rat small intestine *in vitro*. Biochim Biophys Acta 30:666–667
Reuss L (1985) Changes in cell volume measured with an electrophysiologic technique. Proc Natl Acad Sci U S A 82:6014–6018
Sackin H, Boulpaep EL (1975) Models for coupling of salt and water transport. Proximal tubular reabsorption in necturus kidney. J Gen Physiol 66:671–733
Samarzija I, Hinton BT, Fromter E (1982) Electrophysiological analysis of rat renal sugar and amino acid transport II. Dependence on various transport parameters and inhibitors. Pflugers Arch 393(2):190–197
Sardet C, Franchi A, Pouyssegur J (1989) Molecular cloning, primary structure, and expression of the human growth factor-activatable Na^+/H^+ antiporter. Cell 56:271–280
Schafer JA (1990) Transepithelial osmolality differences, hydraulic conductivities, and volume absorption in the proximal tubule. Annu Rev Physiol 52:709–726
Schafer JA (1993) The rat collecting duct as an isosmotic volume reabsorber. In: Ussing HH, Fischbarg J, Sten-Knudsen O, Larsen EH, Willumsen NJ (eds) Proceeding of alfred benzon symposium 34. Isotonic transport in leaky epithelia. Munksgaard, Copenhagen, pp 339–354
Schafer JA, Troutman SL, Andreoli TE (1974) Volume reabsorption, transepithelial potential differences, and ionic permeability properties in mammalian superficial proximal straight tubules. J Gen Physiol 64:582–607

Schafer JA, Patlak CS, Troutman SL, Andreoli TE (1978) Volume absorption in the parts recta. II. Hydraulic conductivity coefficient. Am J Physiol 234:F340–F348
Schatzmann HJ, Windhager EE, Solomon AK (1958) Single proximal tubules of the Necturus kidney. II. Effect of 2, 4-dinitro-phenol and ouabain on water reabsorption. Am J Physiol 195(3):570–574
Schnermann J, Chou C-L, Ma T, Traynor T, Knepper MA, Verkman AS (1998) Defective proximal tubular fluid reabsorption in transgenic aquaporin-1 null mice. Proc Natl Acad Sci U S A 95: 9660–9664
Schultz SG (1980) The electrochemical potential. In: Hutchinson F, Fuller W, Mullins LJ (eds) Basic principles of membrane transport. Cambridge University Press, Cambridge, pp 8–13
Skou JC (1965) Enzymatic basis for active transport of Na^+ and K^+ across cell membrane. Physiol Rev 45:596–617
Smoluchowski MV (1915) Über Brownsche Molekularbewegung unter Einwirkung äusserer Kräfte und derem Zusammenhang mit der verallgemeinerten Diffusionsgleichung. Ann Phys 48:1103–1112
Spring KR (1999) Epithelial fluid transport – a century of investigation. News Physiol Sci 14:92–98
Spring KR, Hope A (1978) Size and shape of the lateral intercellular spaces in a living epithelium. Science 200:54–57
Spring KR, Kimura G (1978) Chloride reabsorption by renal proximal tubules of *Necturus*. J Membr Biol 38:233–254
Spring KR, Kimura G (1979) Intracellular ion activities in *Necturus* proximal tubule. Fed Proc 38:2729–2732
Stein WD (1967) The movement of molecules across cell membranes. Academic Press, New York, pp 1–369
Sten-Knudsen O (2002) Biological membranes. Theory of transport, potentials and electric impulses. Cambridge University Press, Cambridge, pp 1–671
Sten-Knudsen O, Ussing HH (1981) The flux ratio equation under nonstationary conditions. J Membr Biol 63:233–242
Stirling CE (1972) Radioautographic localization of sodium pump sites in rabbit intestine. J Cell Biol 53:704–714
Thomas RC (1972) Electrogenic sodium pump in nerve and muscle cells. Physiol Rev 52:563–594
Tripathi S, Boulpaep EL (1989) Mechanisms of water transport by epithelial cells. Q J Exp Physiol 74:385–417
Turner RJ, Moran A (1982) Heterogeneity of sodium-dependent D-glucose transport sites along the proximal tubule – evidence from vesicle studies. Am J Physiol 242:F406–F414
Turner RJ, Silverman M (1977) Sugar uptake into brush-border vesicles from normal human kidney. Proc Natl Acad Sci U S A 74:2825–2829
Ullrich KJ (ed) (1973) Permeability characteristics of the mammalian nephron. American Physiological Society, Bethesda
Ussing HH (1985) Volume regulation and basolateral co-transport of sodium, potassium, and chloride ion in frog skin epithelium. Pflugers Arch 405(suppl 1):S2–S7
Warnock DG, Lucci MS (1979) Effect of anion-transport inhibitors on NaCl reabsorption in the rat superficial proximal convoluted tubule. J Clin Investig 64:570–579
Weinstein AM (1985) Glucose-transport in a model of the rat proximal tubule epithelium. Math Biosci 76:87–115
Weinstein AM (1986) A mathematical model of the rat proximal tubule. Am J Physiol 250: F860–F873
Weinstein AM (1992) Chloride transport in a mathematical model of the rat proximal tubule. Am J Physiol 263:F784–F798
Weinstein AM (2013) Sodium and chloride transport: proximal nephron. In: Alpern RJ, Moe OW, Caplan MJ (eds) Seldin and Giebisch's the kidney. Elsevier, Amsterdam, pp 1081–1141
Weinstein AM, Stephenson JL (1979) Electrolyte transport across a simple epithelium. Steady-state and transient analysis. Biophys J 27:165–186
Weinstein AM, Stephenson JL (1981) Models of coupled salt and water transport across leaky epithelia. J Membr Biol 60:1–20

Welling LW, Grantham JJ (1972) Physical properties of isolated perfused renal tubules and tubular basement membranes. J Clin Investig 51:1063–1075
Welling LW, Welling DJ (1975) Surface areas of brush border and lateral cell walls in the rabbit proximal nephron. Kidney Int 8:343–348
Welling LW, Welling DJ (1988) Relationship between structure and function in renal proximal tubule. J Electron Microsc Tech 9:171–185
Welling LW, Welling DJ, Holsapple JW, Evan AP (1987a) Morphometric analysis of distinct microanatomy near the base of proximal tubule cells. Am J Physiol 253:F126–F140
Welling LW, Welling DJ, Ochs TJ (1987b) Video measurement of basolateral NaCl reflection coefficient in proximal tubule. Am J Physiol 253:F290–F298
Whittembury G, Reuss L (1992) Mechanisms of coupling of solute and solvent transport in epithelia. In: Seldin DW, Giebisch G (eds) Kidney: physiology and pathophysiology. Raven Press, New York, pp 317–360
Whittembury G, Malnic G, Mello-Aires M, Amorena C (1988) Solvent drag of sucrose during absorption indicates paracellular water flow in the rat kidney proximal tubule. Pflugers Arch 412:541–547
Wilson RW, Wareing M, Green R (1997) The role of active transport in potassium reabsorption in the proximal convoluted tubule of the anaesthetized rat. J Physiol 500:155–164
Windhager EE (1979) Sodium chloride transport. In: Giebisch G, Tosteson DC, Ussing HH (eds) Membrane transport in biology, Transport organs, vol IVA. Springer, Berlin, pp 145–213
Windhager EE, Whittembury G, Oken DE, Schatzmann HJ, Solomon AK (1959) Single proximal tubules of the Necturus kidney. III. Dependence of H_2O movement on NaCl concentration. Am J Physiol 197:313–318
Wittekindt OH, Dietl P (2019) Aquaporins in the lung. Pflugers Arch 471(4):519–532
Wu MM, Civan MM (1991) Voltage dependence of current through the Na,K-exchange pump of Rana oocytes. J Membr Biol 121:23–36
Yoshitomi K, Fromter E (1985) How big is the electrochemical potential difference of Na+ across rat renal proximal tubular cell membranes in vivo? Pflugers Arch 405(Suppl 1):S121–S126
Yoshitomi K, Burckhardt BC, Fromter E (1985) Rheogenic sodium-bicarbonate cotransport in the peritubular cell membrane of rat renal proximal tubule. Pflugers Arch 405:360–366
Zeuthen T (2000) Molecular water pumps. Rev Physiol Biochem Pharmacol 141:97–151
Zeuthen T, Meinild AK, Loo DD, Wright EM, Klaerke DA (2001) Isotonic transport by the Na^+-glucose cotransporter SGLT1 from humans and rabbit. J Physiol 531:631–644
Zhuo JL, Li XC (2013) Proximal nephron. Compr Physiol 3:1079–1123
Zurzolo C, Rodriguezboulan E (1993) Delivery of Na^+,K^+-ATPase in polarized epithelial-cells. Science 260:550–552

Rev Physiol Biochem Pharmacol (2020) 177: 149–150
https://doi.org/10.1007/112_2020_40

Published online: 19 August 2020

Correction to: Stationary and Nonstationary Ion and Water Flux Interactions in Kidney Proximal Tubule: Mathematical Analysis of Isosmotic Transport by a Minimalistic Model

Erik Hviid Larsen and Jens Nørkær Sørensen

Correction to: Chapter "Stationary and Nonstationary Ion and Water Flux Interactions in Kidney Proximal Tubule: Mathematical Analysis of Isosmotic Transport by a Minimalistic Model" E. H. Larsen and J. N. Sørensen, Rev Physiol Biochem Pharmacol, DOI: 10.1007/112_2019_16

The chapter 'Stationary and Nonstationary Ion and Water Flux Interactions in Kidney Proximal Tubule: Mathematical Analysis of Isosmotic Transport by a Minimalistic Model' has now been made available open access under a CC BY 4.0 license and the copyright holder has been updated to 'The Author(s)'.

Further, in Fig. 7e the left-hand side axis label was published incorrectly as being p^{cell} (Atm) instead of the correct label of p^{lis} (Atm). This has now been corrected.

The updated Fig. 7 is shown below.

The updated online version of this chapter can be found at
DOI: 10.1007/112_2019_16

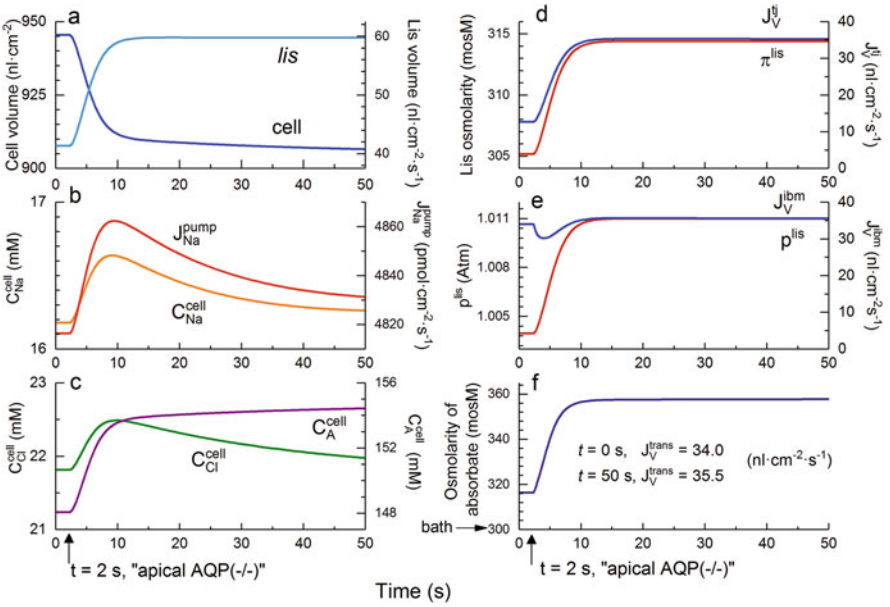

Fig. 7 (**a**–**f**) Time course of physiological variables in response to "eliminating" osmotic permeability of apical membrane. At time = 2 s and governed by $\tau = 1$ s, P_f^{am} was reduced exponentially from 4,490 to 0.449 μm s^{-1}. (**a**) this results in a fast shift of water volume from cells to *lis*. (**b**) C_{Na}^{cell} increases transiently, which stimulates Na^+ pump flux, $J_{Na}^{pump,lm}$. (**c**) While the transient increase in C_{Cl}^{cell} parallels the transient increase in C_{Na}^{cell}, the increase in concentration of nondiffusible anions is closely following the loss of cell volume. (**d**) The water flux is redirected from being translateral to being paracellular driven by the increased osmolarity of *lis* governed by the C_{Na}^{cell}-stimulated increase in $J_{Na}^{pump,lm}$. (**e**) Due to inflow of water, the hydrostatic pressure of *lis* increases, which drives the volume flux across the interspace basement membrane J_V^{ibm}. (**f**) The final result is a significant increase in osmolarity of the fluid emerging from *lis* due to convection-electrodiffusion of solutes across the interspace basement membrane (Eq. 6). Notably, at the new steady state, the transepithelial water flux is about the same as the water flux prior to eliminating P_f^{am} (35.5 versus 34.0 nL cm^{-2} s^{-1})